THE UNIVERSITY OF HULL

Evaporation Rates from Emulsions Stabilised by Surfactants and Nanoparticles

being a Thesis submitted for the Degree of
Doctor of Philosophy in the University of Hull

by

Ibon Aranberri Askargorta, BSc, MSc

September 2003

Thus, the task is, not so much to see what no one has yet seen; but to think what nobody has yet thought, about that which everybody sees.

Erwin Schrödinger (Nobel Prize 1933)

Acknowledgements

I would like to thank my supervisors, Prof. Bernard P. Binks, Dr. John H. Clint and Prof. Paul D. I. Fletcher for their high standard of supervision, guidance and being always fully encouraging and enthusiastic.

I thank Dow AgroSciences (Indianapolis, USA) for the studentship and Dr. Eric Paterson and Dr. Andrew Fowles (King's Lynn, UK) for their interest in the project and very useful discussions and suggestions throughout the thesis.

I show my gratitude to Tony Sinclair for the great SEM images.

I thank the glass, electronic and mechanical workshops members for their help and specially the porters for the efficient delivery of the gas cylinders.

I also thank all members of the Surfactant & Colloid Group, past and present for making my time in the group so enjoyable.

I would like to thank Shabs and Allan, for the good time we had out of the lab.

I thank Dr. Alexander Bismarck for being always so encouraging.

Finally I thank my family and Idurre for their support and encouragement all through this time.

Publications and presentations

The work contained in this thesis has given rise to the following publications and presentations:

1 *How do emulsions evaporate?* I. Aranberri, K.J. Beverley, B.P. Binks, J.H. Clint and P.D.I. Fletcher, *Langmuir*, 2002, **18**, 3471.

2 *Retardation of oil drop evaporation from oil-in-water emulsions*, I. Aranberri, B.P. Binks, J.H. Clint and P.D.I. Fletcher, *Chem. Commun.* 2003, 2538,

3 *Evaporation rates of water from high internal phase emulsions,* I. Aranberri, B.P. Binks, J.H. Clint and P.D.I. Fletcher, submitted to *Langmuir.*

4 *Evaporation rates of Pickering emulsions,* I. Aranberri, B.P. Binks, J.H. Clint and P.D.I. Fletcher, in preparation.

5 Poster entitled "*Evaporation studies of surfactant-stabilised and particle-stabilised emulsions*" at the 14th Surfactants in Solution Symposium, Barcelona, 9th –14th June 2002.

6 Oral presentation "*Evaporation of liquids, liquids crystals, microemulsions and emulsions*", at the 14th Surfactants in Solution Symposium, Barcelona, 9th –14th June 2002.

7 Oral presentation "Multiple emulsions stabilised by nanoparticles", Trieste 2002.

8 Oral presentation "Evaporation rates of emulsions", at the University of Hull, Department of Chemistry, 2nd April 2003.

9 Oral presentation "Evaporation of volatiles from complex formulation mixtures", at "New developments in the formulation of dispersions", Manchester, 30th Sept. - 1st Oct. 2003.

List of symbols

Some of the symbols and abbreviations used in this thesis are given here; others are defined locally in the text.

A	Cross section area of the sample tube
a	Average drop radius
A_V	Cross section area of the vessel
cmc	Critical micelle concentration
CTAB	Cetyltrimethyl ammonium bromide
d	Distance between two particles
DBG	n-Decyl-β-D-glucopyranoside
ΔG	Change in Gibbs free energy
D_L	Diffusion coefficient of liquid in liquid
DP	Degree of polymerisation
D_v	Diffusion coefficient of liquid in vapour
E_n	Entry coefficient
F	Gas flux
g	Acceleration due to gravity
Γ	Surface excess concentration
γ	Surface tension
γ_{ov}	Interfacial tension of oil-vapour surface
γ_{ow}	Interfacial tension of oil-water interface
γ_{wv}	Interfacial tension of water-vapour surface
h	Vapour space thickness

η	Viscosity
HLB	Hydrophilic-lipohilic balance
HMDS	Hexamethyldisiloxane
h_t	Total height of the sample tube
J	Matter flux
k	Boltzmann's constant 1.381×10^{-23} J K^{-1}
m	Mass
M	Molecular weight
MCH	Methylcyclohexane
Π	Disjoining pressure
P	Vapour pressure
PDMS	Polydimethylsiloxane
PVA	Polyvinyl alcohol
θ	Contact angle
ρ	Density
R	Gas constant, 8.314 J mol^{-1} K^{-1}
s	Solubility
S	Spreading coefficient
SDS	Sodium dodecyl sulphate
T	Absolute temperature
V	Volume
z	Correction factor

Abstract

This thesis is concerned with the evaporation rates of emulsions stabilised by either surfactant molecules or nm-size solid particles. Understanding of the mechanisms of the evaporation process plus the control of the rate limiting step of each mechanism involved in such processes is important for a number of practical applications which include cosmetics, paints and agrochemicals.

The work of this thesis deals with three main aspects. Firstly the evaporation rates of pure liquids have been determined. Secondly, evaporation rates of surfactant-stabilised creamed, gelled and high internal phase emulsions have been investigated. Lastly, evaporation rates of emulsions stabilised by solid particles will be discussed.

The study concerned with the pure liquids was mainly to verify the set-up of the evaporation rig, to compare our results with those obtained by K.J. Beverley (Thesis in preparation, University of Hull) and determine the diffusion coefficients of different liquids in the vapour phase.

For creamed emulsions stabilised by surfactants it was found that the evaporation rate of the continuous phase is as that of bulk phase and the evaporation rate of the dispersed phase is slowed down up to 20 times. The retardation in the evaporation rate of the dispersed droplets depends mainly on the solubility of the dispersed phase in the continuous phase. In the case of gelled emulsions, the mass loss of the emulsions gelled by different gelling agents (colloidal particles and water-soluble polymers) show that the evaporation rates depend on the gelling agent. For

high internal phase emulsions, evaporation rates of water from emulsions containing involatile oils have been studied. Depending on the geometrical properties of the initial conditions, the mass loss rate is controlled by either diffusion of the liquid in the vapour (large emulsion/sample tube volume ratio) or diffusion of the liquid in the nm-thin films which separate the close-packed oil drops (small emulsion/sample tube volume ratio). The nature of the colloidal forces acting between the dispersed droplets also plays an important role during the evaporation.

For emulsions stabilised solely by nm-size silica particles (Pickering emulsions), the evaporation rate is slower compared with that stabilised by surfactants under the same conditions. Moreover, we have found that the solid residues left behind after the total evaporation of the volatile species (oil and water) from Pickering emulsions show macroporous structures. The type of the microstructure is related to that of the parent emulsion and the vapour pressure of the oil. These results may lead to the production of novel macroporous inorganic materials.

EVAPORATION RATES FROM EMULSIONS STABILISED BY SURFACTANTS AND NANOPARTICLES

Contents **Page**

Chapter 1

CHAPTER 1

INTRODUCTION

1.1 Introduction: Evaporation rates from emulsions and relevance to industry

The study of evaporation rates is important for many reasons in our everyday lives. Assessment of hazards arising from the spillage of volatile liquids, drying processes and release of volatile active components from commercial products such as cosmetics (perfumes, skin care lotions, lipsticks etc.), food aromas, paints and agrochemical formulations are only a few examples where evaporation rates should be well understood. Many agrochemicals for example, cover a wide range of systems, from simple aqueous solutions (for water-soluble actives) to disperse systems of suspensions and emulsions, which often are used in sprays e.g., fungicides or insecticides. When deposited onto the leaves of the plants differential evaporation of the components of complex agrochemical formulations are likely to affect the product performance. The flavour of a food is determined largely by their aromas, which are small molecules with sufficient vapour pressure to be present in the air above the food. This thesis, sponsored by Dow AgroSciences, is concerned with understanding the rate and mechanism of the evaporation of a wide range of emulsions (stabilised by either surfactants or nm size solid particles) very often used in some of the industrial applications mentioned above. This

work is also concerned with the study of the microstructures left behind after the evaporation of particle-stabilised emulsions. We have found a novel method to make inorganic porous materials using silica particle-stabilised emulsions as templates. The pore size of the macroporous material ranges from 10 to 60 μm and can be controlled depending on the condition used to prepare the initial emulsions.

In this first Chapter, a brief review about emulsions and emulsion stability is presented. Moreover some relevant aspects of surfactant behaviour and of nm size silica particles at the interfaces will be considered. A literature review related to evaporation of emulsions is given and the structure of the present thesis will be outlined.

1.2 Emulsions and emulsion stability

1.2.1 Introduction to emulsions

An emulsion is a thermodynamically unstable dispersion of two or more immiscible or partially miscible liquids. The diameters of the dispersed liquid drops are usually in the range between 0.1 and 20 μm. Although thermodynamically-unstable, emulsions may be made kinetically-stable by the presence of a suitable surfactant which adsorbs at the drop surfaces. In most emulsions, one of the phases is aqueous and the other is oil. If the oil is the dispersed phase, the emulsion is termed an *oil-in-water* (o/w) emulsion and if the aqueous phase is the dispersed phase, the emulsion is termed a *water-in-oil* (w/o) emulsion. The type of emulsion which tends to form depends on the balance

between the hydrophilic and hydrophobic properties of the emulsifier. The generalisation that "the phase in which the emulsifying agent is more soluble tends to be the continuous phase" is knows as Bancroft's rule[1]. The amphiphilic nature of the surfactants (mainly for non-ionic) can be expressed in terms of an empirical scale based on so-called HLB (hydrophile-lipophile balance) numbers[1]. Several equations have been established for calculating the HLB values and the least hydrophilic surfactants are assigned with the lowest HLB values. However, the HLB number is assigned to the neat surfactant alone and does not apply to its behaviour when it is adsorbed at the oil-water interface. The HLB can be varied by electrolyte, temperature, oil type and co-surfactant concentration which modify the geometry of the surfactant monolayer at an interface[2] and thus changes the preferred curvature of the surfactant monolayer, which in some way affects the preferred emulsion type.

1.2.2 Stability of emulsions

Four mechanisms may contribute to the overall emulsion breaking process[3]. Figure 1.1 shows a schematic representation of each process. Notice that creaming and sedimentation are explained in a similar manner.

i) Creaming/sedimentation is caused by the action of gravity and produces a vertical gradient in concentration of the droplets without changing the droplet size distribution. For the o/w emulsions considered here, the oil drops are less dense than the aqueous continuous phase and creaming occurs. For an isolated emulsion drop, the velocity of creaming/sedimentation (v) is given by[4]

$$v = 2a^2 \frac{(\rho_o - \rho)g}{9\eta} \qquad [1.1]$$

Figure 1.1 Mechanisms that contribute to emulsion instability.

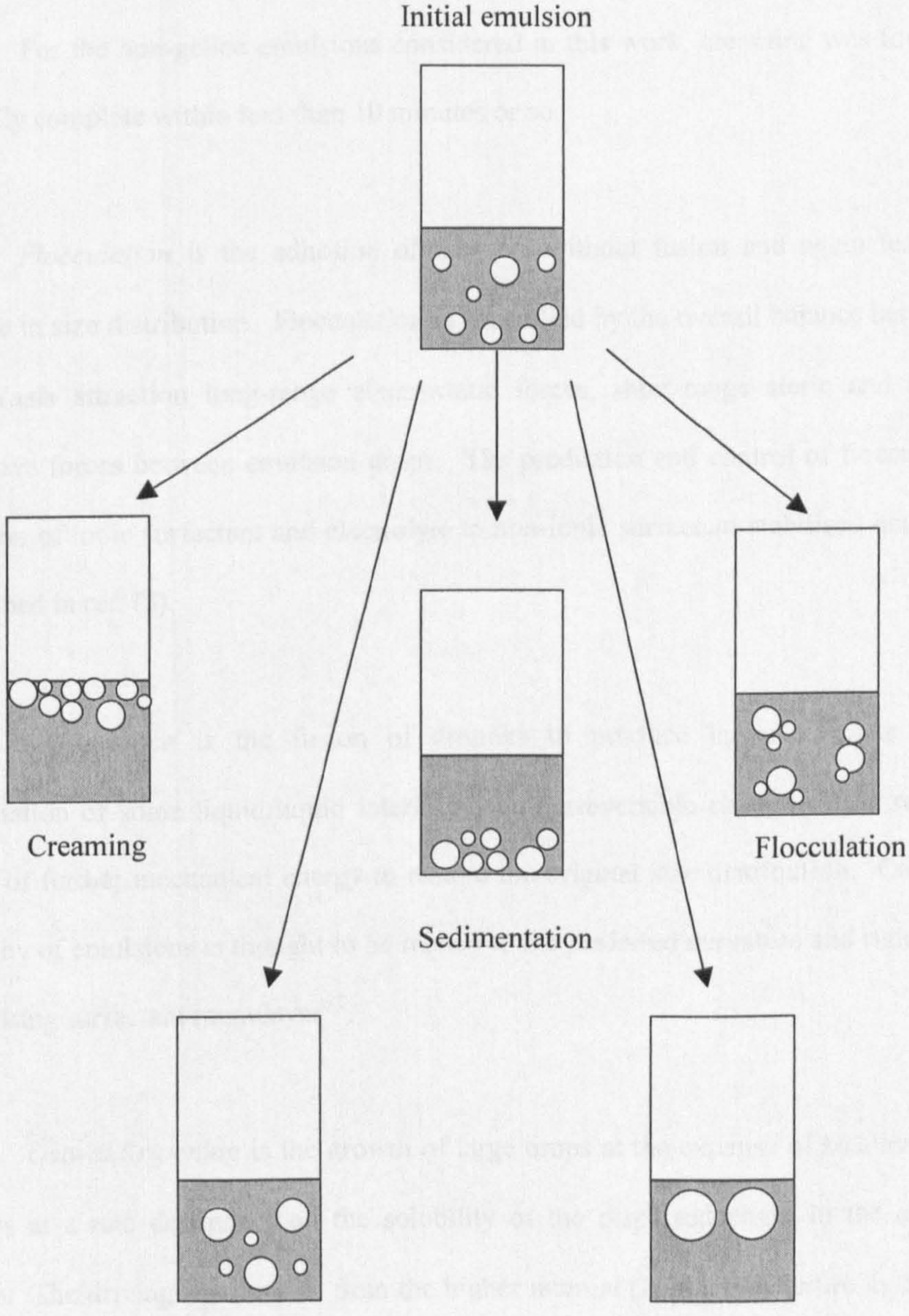

where a is the drop radius, ρ_0 and ρ are the densities of the continuous phase and drops respectively, g is acceleration due to gravity and η is the viscosity of the continuous phase. For the non-gelled emulsions considered in this work, creaming was found to be virtually complete within less than 10 minutes or so.

ii) *Flocculation* is the adhesion of droplets without fusion and again leads to no change in size distribution. Flocculation is controlled by the overall balance between van der Waals attraction long-range electrostatic forces, short-range steric and hydration repulsive forces between emulsion drops. The prediction and control of flocculation by addition of ionic surfactant and electrolyte to non-ionic surfactant stabilised emulsions is described in ref. (5).

iii) *Coalescence* is the fusion of droplets to produce larger droplets with the elimination of some liquid/liquid interface. This irreversible change would require the input of further mechanical energy to restore the original size distribution. Coalescence stability of emulsions is thought to be related to the preferred curvature and rigidity of the stabilising surfactant monolayer[6,7].

iv) *Ostwald ripening* is the growth of large drops at the expense of smaller ones and occurs at a rate dependent on the solubility of the dispersed phase in the continuous phase. The driving force arises from the higher internal (Laplace) pressure in the smaller drops relative to that in larger drops. Lifshitz and Slezov[8,9] and Wagner[10] derived the following equation for the rate of ripening,

$$\omega = \frac{da_c^3}{dt} = \frac{8c(\infty)\gamma DV_m}{9RT} f(\phi) \qquad [1.2]$$

where t is time, a_c is the critical drop radius for which the radius is neither growing or shrinking (approximately equal to the number average radius), D is the diffusion coefficient of the dissolved species in the aqueous phase, γ is the interfacial tension at the oil-water interface, V_m is the molar volume of the oil, $c(\infty)$ is the molecular solubility of the dispersed phase in the continuous phase oil and $f(\phi)$ is the correction factor accounting for the increase in the rate with dispersed phase volume fraction, ϕ, and is equal to 1 in the limit as $\phi \rightarrow 0$, R is the gas constant and T is the absolute temperature. Experimentally, ω is obtained from the slope of a linear plot of a_c^3 versus t.

In general, the overall process of emulsion breakdown can occur via a combination of all four processes which may proceed simultaneously at different rates. The situation is further complicated by the fact that the rates of the different processes are highly coupled. For example, creaming rates in dilute emulsions are faster in flocculated systems than in non-flocculated systems since the size of the creaming particle (an aggregate of drops in the flocculated case) is increased.

1.2.3 Introduction to DLVO theory

A number of microscopic events contribute to the destabilisation of a colloidal dispersion (emulsions in this case). The general DLVO theory (after Derjaguin, Landau, Verwey and Overbeek) can be used to describe the qualitative features of the droplet-droplet interaction[11]. The DLVO theory assumes that more long ranged drop interactions

mainly control colloidal stability. Two type of forces are considered here; long range van der Waals attractive (V_A) forces and electrostatic repulsive forces due to either charged surface groups (adsorbed surfactants) or by specific ion adsorption from the solution. For similar drops this charge leads to a repulsive double-layer interaction energy (V_R). The total interaction potential V is written as

$$V = V_A + V_R \qquad [1.3]$$

V_A and V_R are functions of the distance (d) between the drops. Depending on the relative strengths and ranges of the attractive and repulsive terms, we can generate the curve of interaction potential versus distance as shown schematically in Figure 1.2. The attractive term V_A may dominate the repulsive term V_R when d is very large or very small.

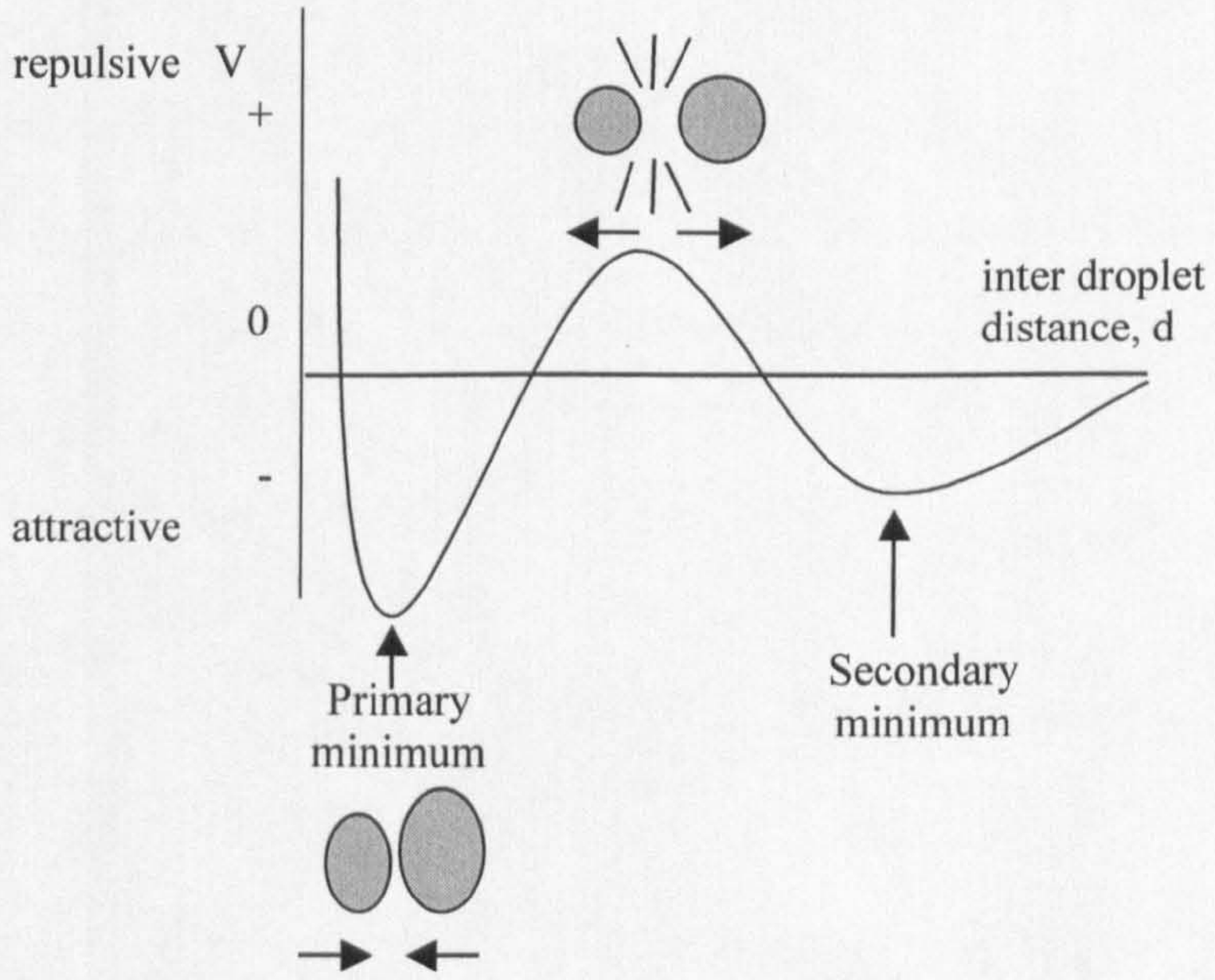

Figure 1.2 **Plot of interactions potential as a function of the distance between particles showing both primary and secondary minima.**

At intermediate separations, the double-layer repulsion gives rise to a potential energy barrier to drop coagulation if the surface is charged and if the electrolyte ions do not screen the charge completely. Generally, the primary minimum is so deep that once the drops have passed over it, aggregation becomes irreversible.

In an emulsion, if the mean distance between the drops is larger than the distance corresponding to the secondary minimum, the system gains energy by bringing drops together and flocculation occurs. Once drops have been brought into proximity by flocculation and/or creaming, they can coagulate into a primary minimum while still keeping their identity as separate droplets. If the surfactant film surrounding the drops breaks, coalescence occurs. This is the final stage in the life of an emulsion drop.

1.3 Surfactants and solid particles as stabilisers

1.3.1 Introduction to surfactants

The word surfactant is an acronym for surface active agent. Surfactants are molecules that have a characteristic molecular structure which enables them to adsorb at interfaces and aggregate or self-associate in aqueous solutions. They are characterised by the possession of both polar and non-polar regions on the same molecule. The polar or hydrophilic region of the molecule may carry a positive or negative charge, giving rise to cationic or anionic surfactants respectively (ionic in general), or may not carry any charge (non-ionic surfactants). The non polar or hydrophobic portion of the molecule is most

commonly a flexible hydrocarbon backbone. Figure 1.3 shows a schematic representation of a surfactant molecule.

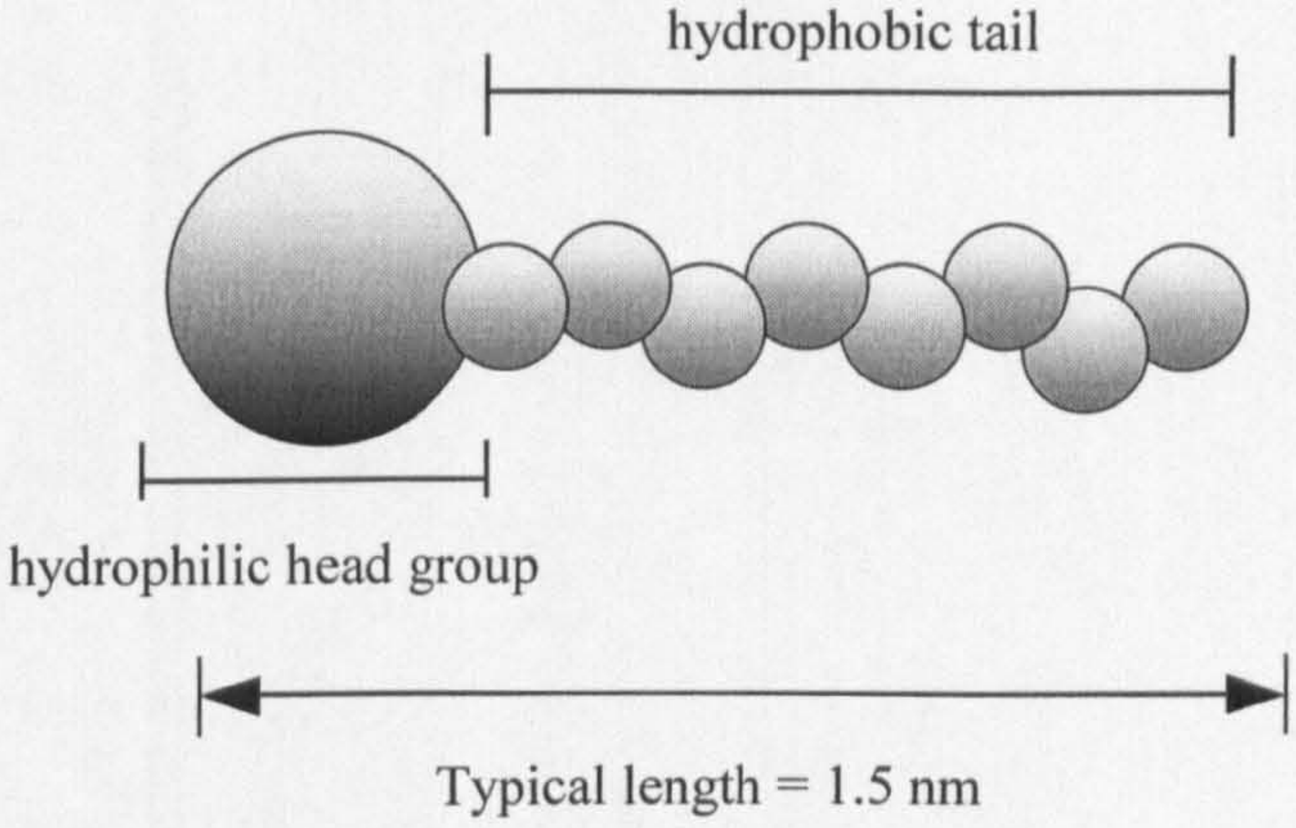

Figure 1.3 Scheme of a typical surfactant molecule.

1.3.2 Classes of Surfactants

Depending on the type of the head group, surfactants can be classified in four groups.

i) Anionic: All surfactants in which the hydrophilic head of the molecule carries a negative charge are classified as anionics. They all possess a positively charged counter-ion which is often Na^+.

ii) Cationic: They possess a positively charged head group, e.g., the trimethyl-ammonium ion ($-N(CH_3)_3^+$) and a negatively charged counter ion, e.g., Br^-.

iii) Zwitterionic: These surfactants contain both positive and negative charges in the molecule making the surfactant neutral, with no free counter-ions.

iv) Non-ionic: They have no charged polar groups, but contain groups such as the ethoxylates, -(O CH_2-$CH_2)_m$ OH, and these have a strong affinity for water due to the strong dipole-dipole interactions arising from hydrogen bonding.

The hydrophobic part of the surfactant is commonly a single chain hydrocarbon which may contain alkyl branches and aryl or olefin groups.

1.3.3 Surfactants at interfaces

As evidenced by the very small solubility of the hydrocarbon chains in water, there is a tendency for these molecules to minimise their hydrocarbon-water contact in aqueous solution and this may be done in two ways. At low concentration the molecules accumulate at the interface so the hydrophobic part can escape the aqueous environment whilst the hydrophilic head group remain immersed in water. However, above a well defined concentration known as the critical micelle concentration (CMC), the interface does not accommodate further surfactant molecules and the maximum concentration of free monomers in the bulk is reached. The hydrocarbon-water interaction for the surfactant molecules in the bulk solution can be minimised with the hydrophobic parts tending to aggregate together with exclusion of water. These aggregates are termed micelles and may take on many shapes and sizes depending on the nature and concentration of the surfactant. Figure 1.4 shows a typical spherical micelle.

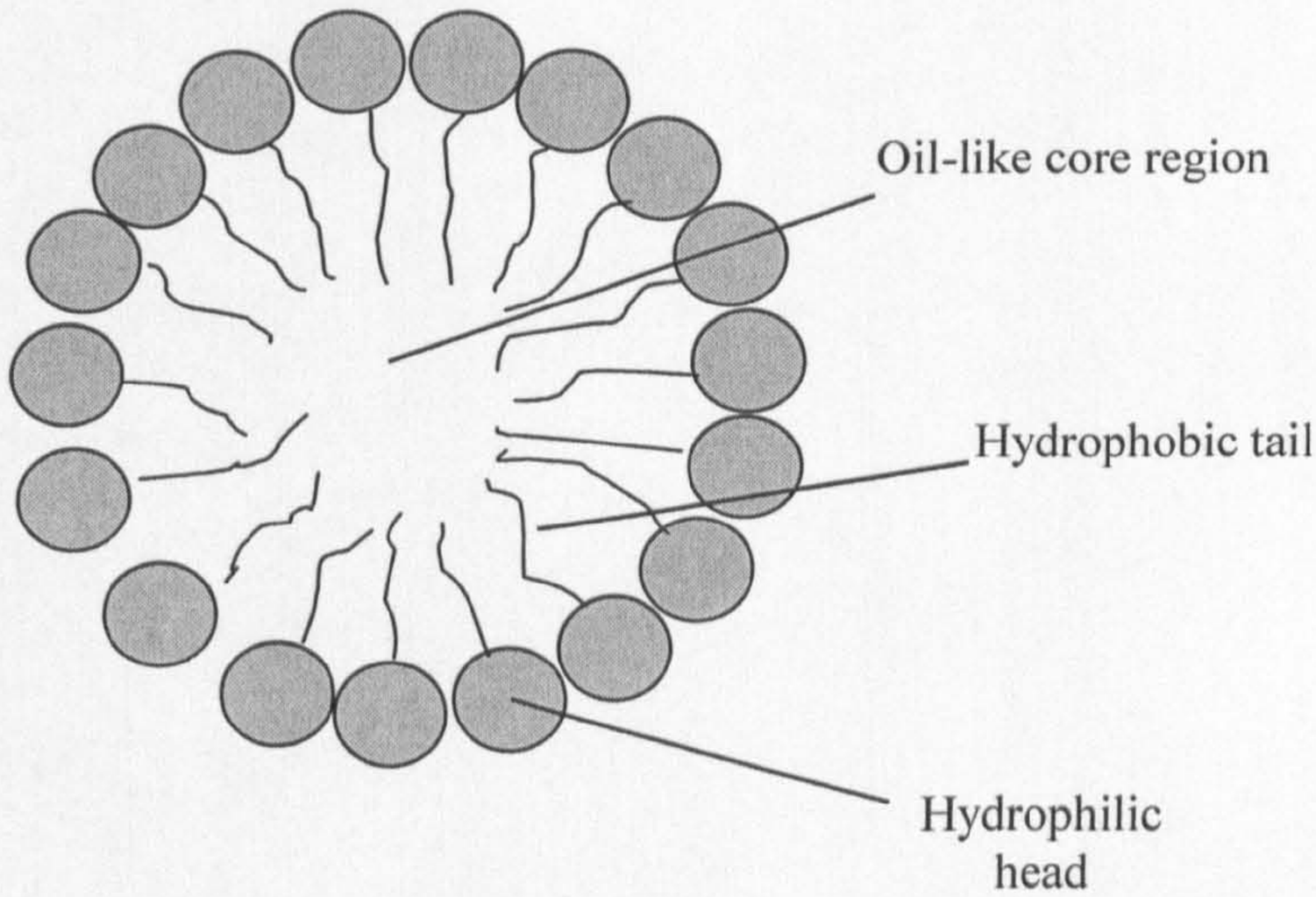

Figure 1.4 Schema of a spherical micelle.

In surfactant adsorption and micellisation, the hydrocarbon aggregation allows the polar head groups to remain in contact with the water. Interaction between the hydrophobic tail and the surrounding water molecules is entropically unfavourable. The attractive interaction between hydrocarbon groups that are segregated from water is called the hydrophobic effect[12]. Figure 1.5 shows a schematic representation of the surfactant's conformation in bulk and at the interface.

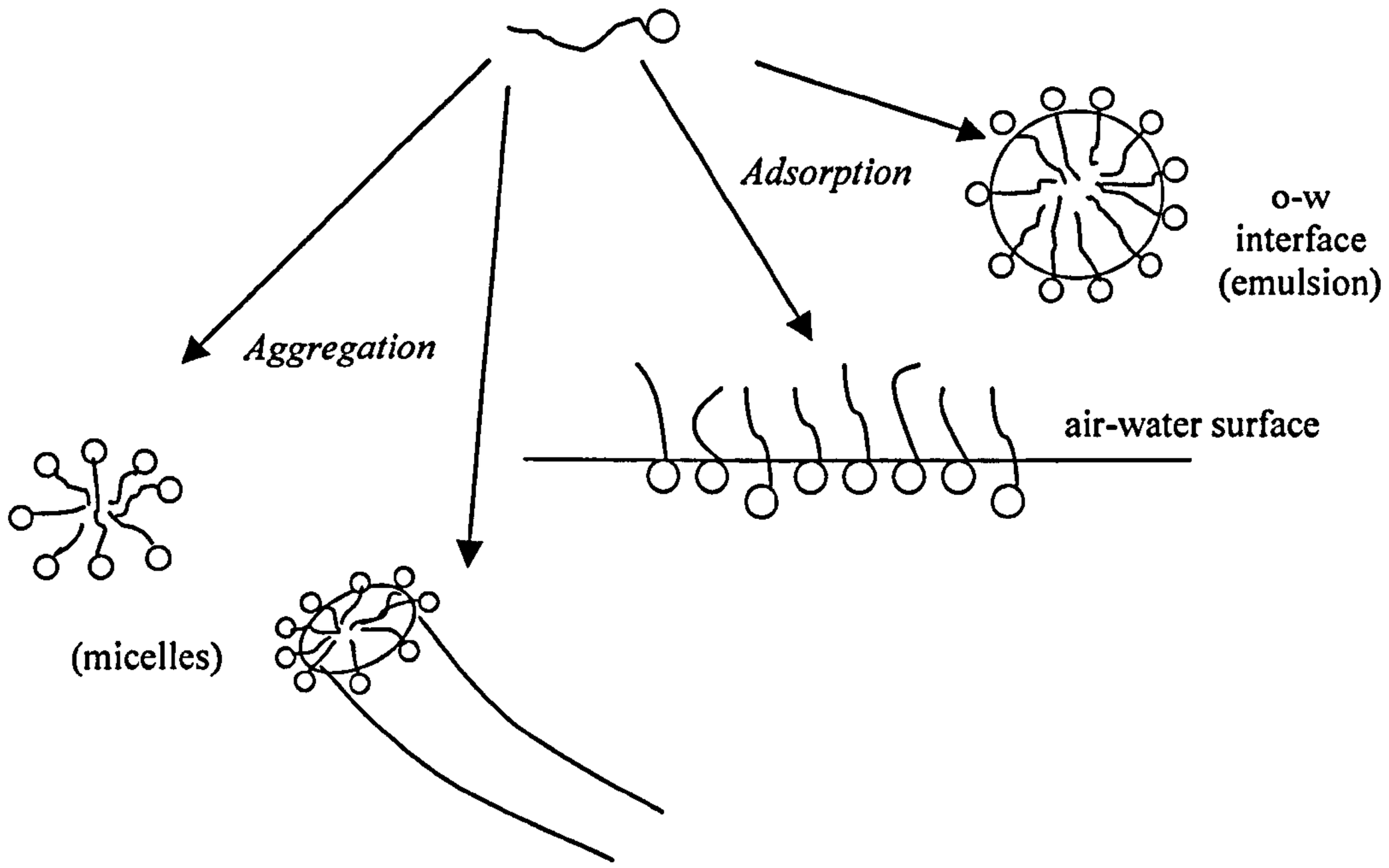

Figure 1.5 Schematic representations of the fundamental properties of the surfactants in aqueous solution: adsorption and aggregation.

At the surface, the molecules experience fewer interactions with other molecules and thus moving a molecule from the bulk to the surface (i.e., creating a surface) requires energy. The amount of free energy, ΔG, required to create a unit area of surface is called the surface free energy and can be expressed in terms of the Gibbs free energy as:

$$\Delta G = \gamma \Delta A \qquad [1.4]$$

where γ is the surface tension. The surface free energy is equal to the surface tension for a liquid, and thus can be expressed as either energy per unit area (J/m^2) or a force per unit length (N/m).

Liquids with strongly attractive intermolecular forces have large surface tensions. As an example of the role that intermolecular forces play in the surface tension we can look at three liquids at 20 °C; mercury (mainly metallic bonding) has a surface tension of 485 mN/m, water (mainly hydrogen bonding) has a surface tension of 73 mN/m, and heptane (solely dispersion forces) has a surface tension of 20 mN/m. The surface tension of liquids may be affected by the addition of surfactants which lower the surface tension of a liquid and concentrate at the surface of the liquid.

As mentioned above, surfactants tend to concentrate at the surface in comparison to the bulk liquid. Thus, the concentration of surfactant at the surface is larger than the concentration of surfactant in the bulk. The excess concentration of surfactant at the surface is called the Gibbs surface excess concentration and is denoted by the symbol Γ. The surface excess concentration is named after Gibbs who developed a model for describing the interfacial region between two bulk phases. From this model a relationship (the Gibbs adsorption isotherm) was developed between the surface excess concentration (Γ), the bulk concentration of surfactant (c), and the surface tension (γ). For non-ionic surfactants the following equation is given:

$$\Gamma = -\frac{1}{RT}\frac{d\gamma}{d\ln c} \qquad [1.5]$$

which is valid for low surfactant concentration where the activity is equal to the concentration. Thus the surface excess concentration can be determined by measuring the surface tension for different bulk concentrations of surfactant.

1.3.4 Introduction to solid particles

In the early 1900's Ramsden[13]and Pickering[14] found that finely divided solid particles adsorb at o/w interfaces and may stabilise emulsions. However, it was not until the work of Finkle et al.[15] that the relationship between the type of solid, the nature of the liquid and emulsion type (o/w or w/o) was recognised. These authors stated that in an emulsion containing solid particles, one of the liquids will probably wet the solid more than the other liquid, with the more poorly wetting liquid becoming the dispersed phase. This is similar to Bancroft's rule for surfactants. The wettability of the particles at oil-water interface is quantified by the contact angle θ that the particle makes with it. If θ (measured through the water phase) is less than 90° the particles are preferentially water wetted and tend to stabilise o/w emulsions. If the particle is preferentially wetted by the oil phase, the contact angle will be greater than 90° and w/o emulsions will be favoured. However, if the particles are too hydrophilic (low θ) or too hydrophobic (high θ), they tend to remain dispersed in either the aqueous or oil phase respectively, giving rise to unstable emulsions. Figure 1.6 shows a schematic representation of particles with different wettability adsorbed at an o-w interface.

Why do the solid particles adsorb to the interface? Consider a particle (p) adsorbed to an oil (o) -water (w) interface with their respective interfacial tensions γ_{ow} (interfacial tension of oil-water interface), γ_{op} (interfacial tension of oil-particle surface) and γ_{pw} (interfacial tension of particle-water surface). The adsorption of a particle from the oil phase to the interface results in an area of the op interface being lost but being replaced by an equal area of the pw interface. Importantly however, an area of the planar

ow interface (normally of high tension) is also lost due to the presence of the particle and this is the main origin of the high adsorption energy.

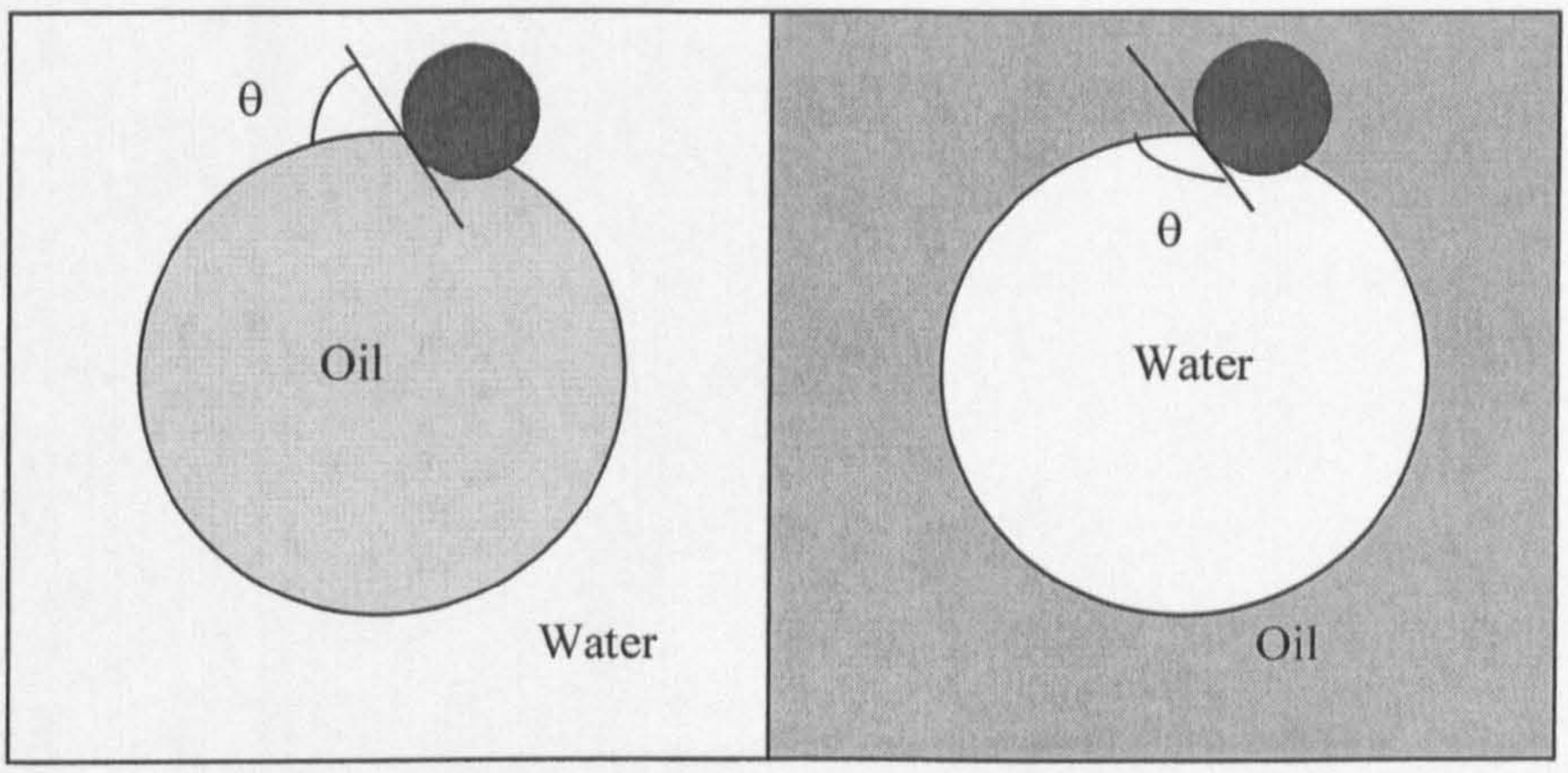

Figure 1.6 Schematic representation of hydrophilic and hydrophobic particles at the oil-water interface of solid-stabilised emulsions.

The energy of attachment of a particle to a fluid-fluid interface is related to the contact angle and the tension of the interface γ_{ow}. For a particle with radius R, small enough to neglect the effect of gravity, the energy E required to remove the particle from the interface is given by[16]:

$$E = \pi R^2 \gamma_{ow} (1 \pm \cos\theta)^2 \qquad [1.6]$$

in which the sign inside the brackets is negative for removal into the water phase and positive for removal into the air or oil phase (for the convention used here in which θ is measured through the water phase). Figure 1.7 shows the variation of E with θ at constant R and γ_{ow} for a silica particle of radius 10 nm at the toluene-water interface (γ_{ow} = 36 x 10^{-3} N m^{-1}). It can be seen that the particle is strongly held in the interface for

$\theta = 90°$. Either side of 90° the energy of attachment falls rapidly such that for θ between 0 and 20° or between 160 and 180°, the energy is only 10 kT or less.

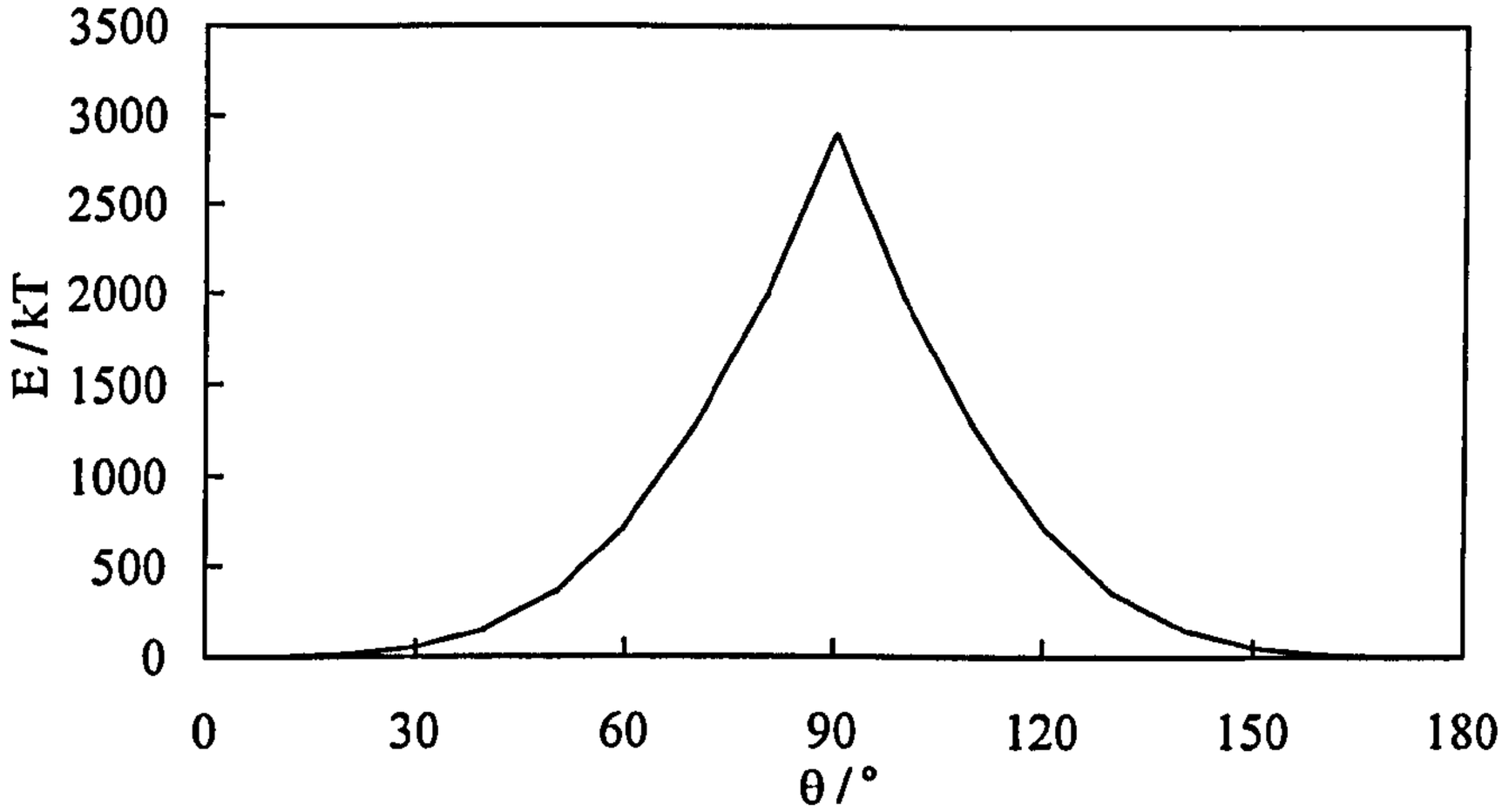

Figure 1.7 Variation of the energy of attachment, E with the contact angle θ for a particle of R = 10 nm at a planar oil-toluene interface. The energy scale is expressed in units of the thermal energy kT (Boltzmann constant x absolute temperature).

A consequence of the high energy of the attachment of particles at interfaces is that the particles adsorb irreversibly, in significant contrast with surfactants which typically adsorb and desorb rather easily from oil-water interfaces. As seen in equation [1.6], E is proportional to R^2. Figure 1.8 shows the variation in the detachment energy for spherical particles of different radius for $\theta = 90°$ and $\gamma_{ow} = 50$ mN m^{-1} (typical of an alkane-water interface). Clearly, very small particles ($R < 0.5$ nm) of the size comparable to most surfactant molecules are easily detached (i.e. $E \approx kT$) and may not be too effective as stabilisers. The average radius of silica particles that have been used in this work is

20 nm, which give an E around 3 x 10^3 kT, i.e., E >> kT and particle adsorption is expected to be irreversible.

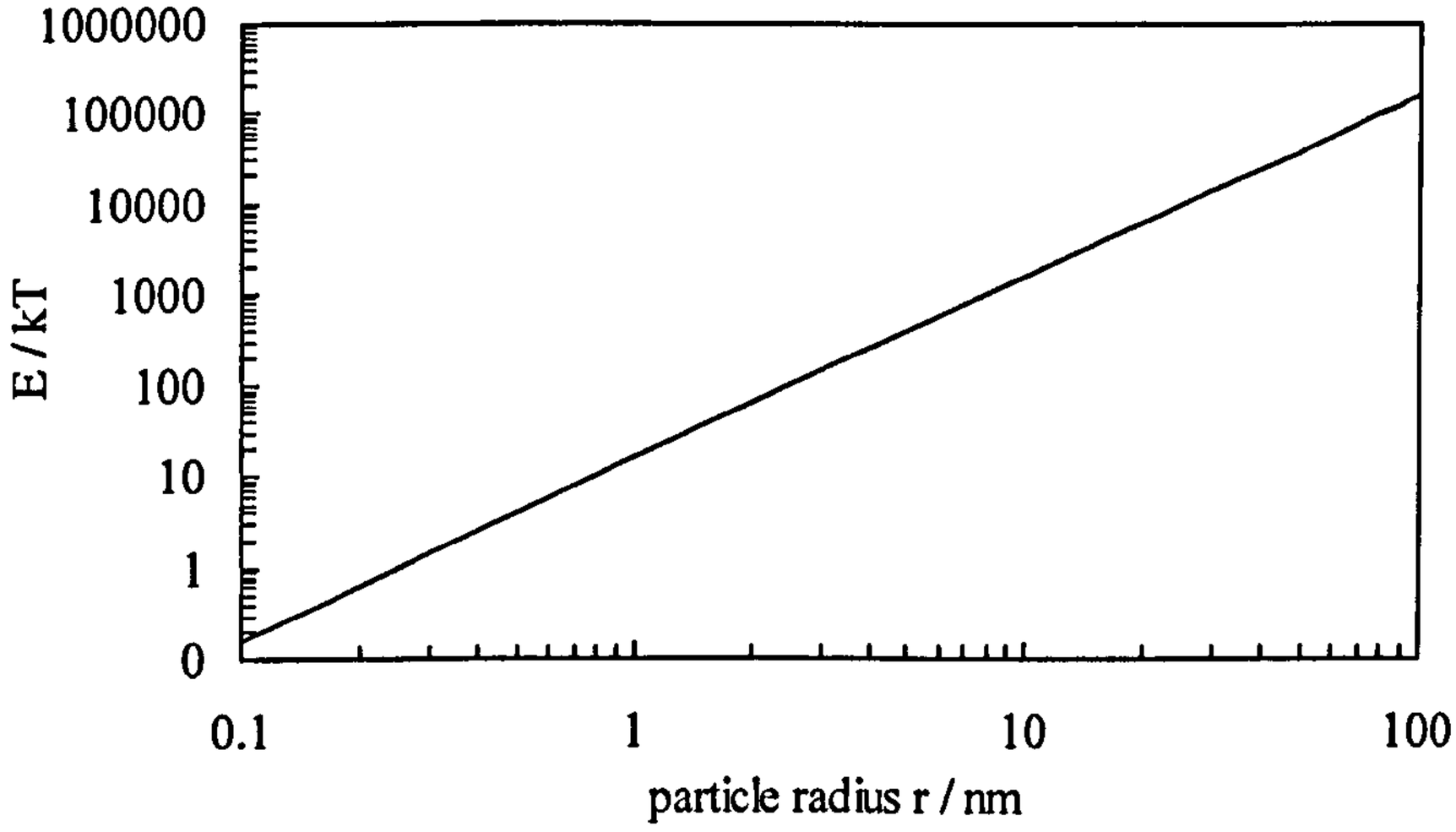

Figure 1.8 **Variation of the energy required to detach a single spherical particle from a planar water-alkane interface (γ_{ow} = 50 mN m^{-1}), $\theta = 90^{\circ}$ with particle radius.**

1.4 Literature review on evaporation

The apparatus to determine evaporation rates used in this work was designed in the Surfactant and Colloid group at Hull University. Previous studies from our laboratory have shown that accurate evaporation rates of pure liquids[17], liquids contained within porous solids[18], w/o microemulsions[19] and structured and non-structured liquid mixtures[20] can be obtained and quantitatively modelled.

In addition to the Hull work, the group of Friberg *et al.* have studied evaporation from a range of emulsions and surfactant systems including model layered structures of *stratum Corneum* lipids with 32% water[21], skin lotion systems containing water, decane, triethanolamine and isostearic acid[22], phenethyl alcohol + limonene + decane mixtures[23] and o/w and w/o emulsions containing either cyclohexane, decane or hexadecane as oil[24]. This latter study showed that phase inversion of the emulsions could be induced by differential evaporation rates of the different components. In general, the methods used in these studies were rather uncontrolled (particularly in relation to the gas flow driving the evaporation) and the results are not easily amenable to quantitative modelling and analysis.

Regarding the evaporation of water it is a well established fact that insoluble monolayers when close-packed may produce distinct effects of hindrance with respect to the evaporation of the bulk water phase[25]. For example the evaporation rate of water can be reduced by a monolayer of a long-chain alcohol such as hexadecanol or octadecanol[26]. Water-soluble surfactants such as sodium myristate and sodium palmitate also may retard the evaporation rate of water but only when very densely packed adsorption layers are formed at concentrations close to the solubility limit[27].

1.5 Aims of this study and the structure of the thesis

The main aim of the present work is to understand the mechanisms by which the oil and water phases of emulsions evaporate and are transported to the vapour phase.

Different emulsions show different mechanisms during the evaporation and understanding such physical processes will help to control the rate limiting step and hence the loss of volatile species. Moreover we are interested in the study of the microstructures left behind after the total evaporation of particle-stabilised emulsions.

Chapter 2 will describe the materials used in this work and the experimental procedures which were carried out throughout it. Chapter 3 will introduce the model proposed and the basic equations that explain the evaporation rate of pure liquids. Parts of the experiments that correspond to this Chapter were repeated after K.J. Beverley's work[28] in order to set up the evaporation rig again and estimate the experimental errors related to this work. Chapter 4 is concerned with the evaporation rate of creamed emulsions. In the introduction, possible mechanisms of oil transport to the vapour phase will be discussed and results for both o/w and w/o emulsions will be examined. In Chapter 5, evaporation rates of o/w emulsions gelled by thickening agents will be shown. Initially, the way in which the creaming rate is affected by such additives will be discussed and then the mass loss of o/w emulsions stabilised by surfactants and gelled by either polymers or colloidal particles will be studied. Chapter 6 is concerned with the evaporation of the water continuous phase from high internal phase emulsions (HIPEs) stabilised by surfactants. Interestingly, the rate limiting step of water transport from the HIPEs to the vapour phase depends on the ratio between the volume of the sample tube and initial sample volume. Chapter 7 is about the evaporation rates of nanometer size particle-stabilised emulsions. Results for the mass loss of particle dispersions will be shown and compared to that of pure water. Results of the evaporation rates of solid-

stabilised emulsions will be compared with results obtained from evaporation rates of surfactant-stabilised emulsions measured under the same conditions. The solid residues obtained after the evaporation of such emulsions show interesting microstructures. The correlation between the microstructure and the properties and preparation conditions of the emulsions will be thoroughly discussed. Finally, in Chapter 8, a summary of the main conclusions will be reported.

1.6 References

1 W. C. Griffin, *J. Soc. Cosmetic Chemists*, 1946, **1**, 311.

2 R. Aveyard, B. P. Binks and J. Mead, *J. Chem. Soc. Faraday Trans. I*, 1986, **82**, 1755.

3 J. H. Clint, *Surfactant Aggregation*, Chapman and Hall, New York, 1991.

4 E. Dickinson, *An Introduction to Food Colloids*, Oxford University Press, Oxford, 1992, p83.

5 R. Aveyard, B. P. Binks, J. Esquena and P. D. I. Fletcher, *Langmuir*, 1999, **15**, 970.

6 P. D. I. Fletcher and D. I. Horsup, *J. Chem. Soc. Faraday Trans.*, 1992, **88**, 855.

7 A. S. Kabalnov, Coalescence in Emulsions in *Modern Aspects of Emulsions Science*, Ed. B. P. Binks, RSC, Cambridge, 1998, pp. 205-260.

8 I. M Lifshitz, V. V. Slezov, *Zh. Ex. Teor. Fiz.*, 1958, **35**, 479.

9 P. J. Voorhees, *J. Stat. Phys.*, 1985, **38**, 231.

10 C. Z. Wagner, *Electrochem*, 1961, **35**, 581.

11 R. J. Hunter, Foundations of Colloid Science, Vol. 2, Clarendon Press, Oxford, 1995.

12 C. Tanford, *The hydrophobic effect. Formation of Micelles and Biological Membranes (2nd edition),* Wildey, New York, 1980.

13 W. Ramsden, *Proc R Soc*, 1903, **72**, 156.

14 S. U. Pickering, *J. Chem Soc.*, 1907, **91**, 2001.

15 P. Finkle, H. D. Draper and J.H. Hildebrand, *J. Am. Chem. Soc.*, 1923, **45**, 2780.

16 S. Levine, B. D. Bowen and S. J. Partridge, *Colloid Surf.* 1998, **38**, 325.

17 K. J. Beverley, J. H. Clint and P. D. I. Fletcher, *Phys. Chem. Chem. Phys.* 1999, **1**, 149.

18 K. J. Beverley, J. H. Clint, P. D. I. Fletcher and S. Thubron, *Phys. Chem. Chem. Phys.* 1999, **1**, 909.

19 J. H. Clint, P. D. I. Fletcher and I. T. Todorov, *Phys. Chem. Chem. Phys.* 1999, **1**, 5005.

20 K. J. Beverley, J. H. Clint and P. D. I. Fletcher, *Phys. Chem. Chem. Phys.*, 2000, **2**, 4173.

21 S. E. Friberg and I. Kayali, *J. Pharm. Sci.,* 1989, **78**, 639.

22 B. R. C. Langlois and S. E. Friberg, *J. Soc. Cosmet. Chem.,* 1993, **44**, 23.

23 S. E. Friberg and Q. Yin, *J. Disp. Sci. Technol.,* 1999, **20**, 395.

24 S. E. Friberg and B. Langlois, *J. Disp. Sci. Technol.,* 1992, **13**, 223.

25 G. T. Barnes, *Adv. Colloid Interface Sci.*, 1986, **25**, 89.

26 V. K La Mer (Ed.), "Retardation of evaporation by monolayers: Transport processes." Academic Press, New York, 1962.

27 K. Lunkenheimer and M. Zembala, *J. Colloid Interface Sci.*, 1997, **188**, 363.

28 K. J. Beverley, Thesis in preparation, University of Hull.

Chapter 2

CHAPTER 2

EXPERIMENTAL

2.1 Materials

2.1.1 Water

Water was purified by reverse osmosis and by passage through a Milli-Q reagent water system. Surface tension measurements showed typically a value of 71.9 mN m^{-1} at 25 °C, which is in good agreement with literature values[1]. The resistivity was always above 18 mΩ cm.

2.1.2 Organic liquids

The organic solvents used in this study are summarised in Table 2.1, together with their purity and source. All solvents were used as received.

Solvent	Purity	Source
benzene	99.8%	Fisons
o-xylene	99%	Avocado
toluene	99.9%	Fischer
n-pentane	>99%	Sigma-Aldrich

n-hexane	99%	Prime Chemicals
n-heptane	99%	Fischer
n-octane	>99%	Fluka
n-decane	99%	Lancaster
n-dodecane	>99%	Avocado
methylcyclohexane	99%	Aldrich
cyclopentane	99%	Lancaster
HMDS[a]	99.7%	Lancaster
PDMS[b]	unknown	Dow Corning
1-bromobutane	>98%	Avocado
squalane	99%	Aldrich
chlorobenzene	>99%	Acros
1,2 dicholobenzene	99%	Acros
perfluoropentane	97%	Fluorochem
perfluoroheptane	98%	Fluorochem

Table 2.1 **Summary of organic solvents used, source and purity. [a] refers to hexamethyldisiloxane (η = 0.65 cS) and [b] to polydimethylsiloxane (η = 300 cS)**

2.1.3 Surfactants

The surfactants used in this work are listed in Table 2.2 with the formula, purity, supplier, cmc at 25°C and the type. All surfactants were used without further treatment.

Surfactant	Formula	Purity	Supplier	cmc/M	Type
Sodium dodecyl sulphate (SDS)	$C_{12}H_{25}O_4S^-Na^+$	pure	BDH	8.10^{-3}	anionic
Cetyltrimethylammonium bromide (CTAB)	$C_{19}H_{42}N^+Br^-$	99%	BDH	1.10^{-3}	cationic
Dodecyl β–D glucopyranosyde (DBG)	$C_{18}H_{36}O_6$	98%	Sigma	2.10^{-3}	non-ionic
Sorbitan monooleate (Span 80)	$C_{24}H_{44}O_6$	unknown	Koch lab	33.10^{-3}	non-ionic
PVA (DP = 600)	$[CH_2\text{-}CH]_n$- O C = O CH_3	unknown	Nippon Gohsei	-	Polymeric (non-ionic)
PVA (DP = 2350)	$[CH_2\text{-}CH]_n$- O C = O CH_3	unknown	Nippon Gohsei	-	Polymeric (non-ionic)

Table 2.2 Summary of the surfactants used including the purity, supplier, c.m.c. (at 25 °C) and type.

2.1.4 Gelling agents

Carrageenan (see Figure 2.1) is a collective term for polysaccharides prepared by alkaline extraction and modification from seaweed (*Rhodophycae*). In this work κ–,

ι–, and λ–carrageenan (supplied by Sigma) have been used. The molecular weight of κ-carrageenan is approximately 154,000 g/mol.

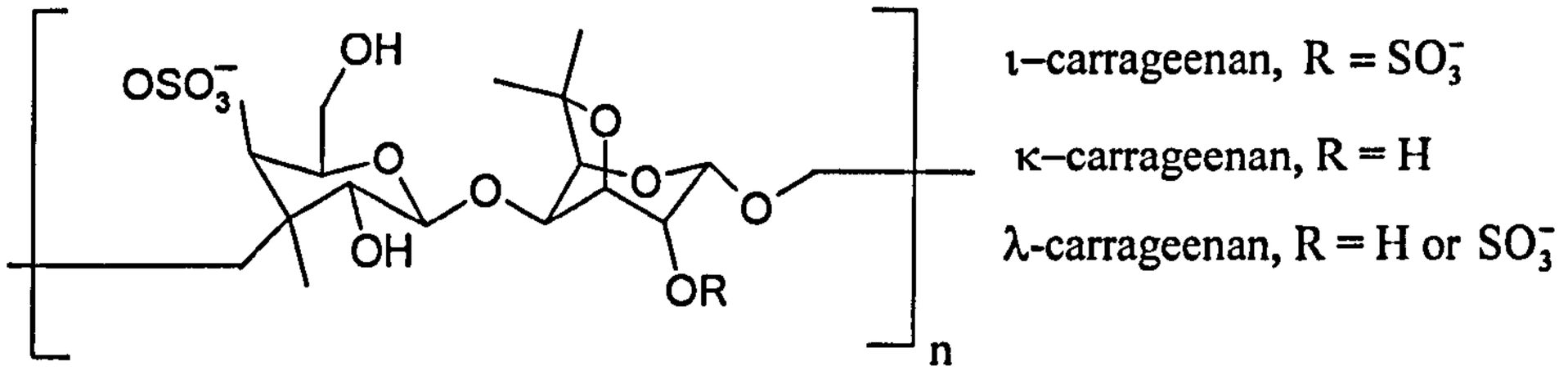

Figure 2.1 Molecular structure of carrageenan.

Avicel® CL611 is a mixture of microcrystalline cellulose (isolated from wood pulp) and sodium carboxymethyl cellulose (see Figure 2.2 for details). It was supplied by FMC Biopolymer.

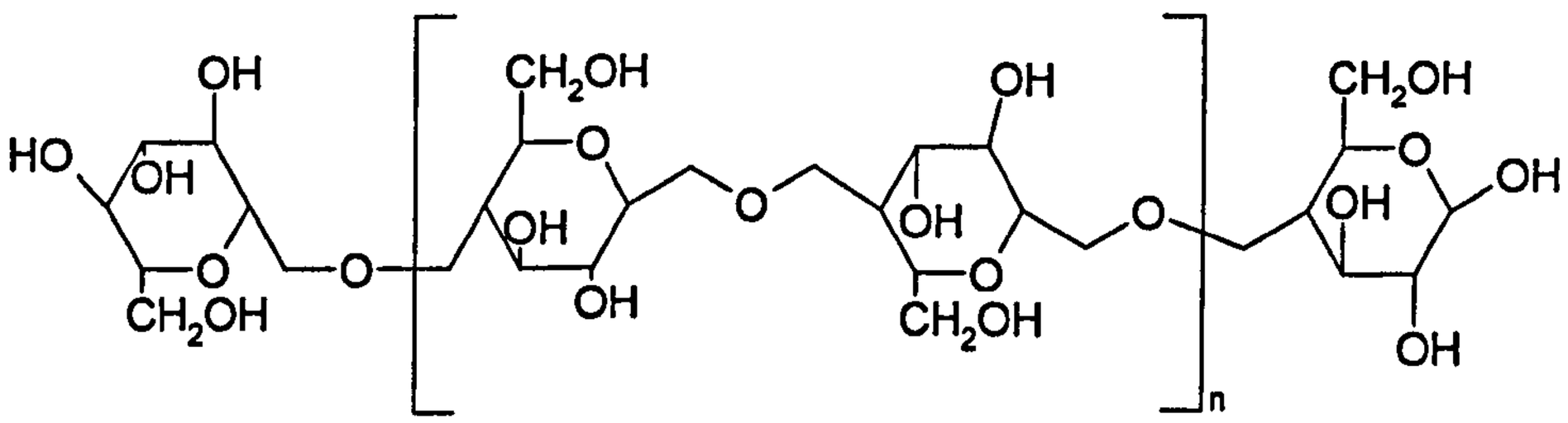

Figure 2.2 Molecular structure of microcrystalline cellulose.

Kelzan® S, an industrial and dispersed grade of xanthan gum, is a natural high-molecular weight branched polysaccharide and it contains glucose, mannose and glucuronic acid (as a mixed potassium, sodium and calcium salt). Kelzan is a trademark

of Merck & Co., Inc. USA. The repeating unit structure of xanthan gum is detailed in Figure 2.3. The molecular weight of the polymer is probably on the order of 2 x 10^6 g/mol [2].

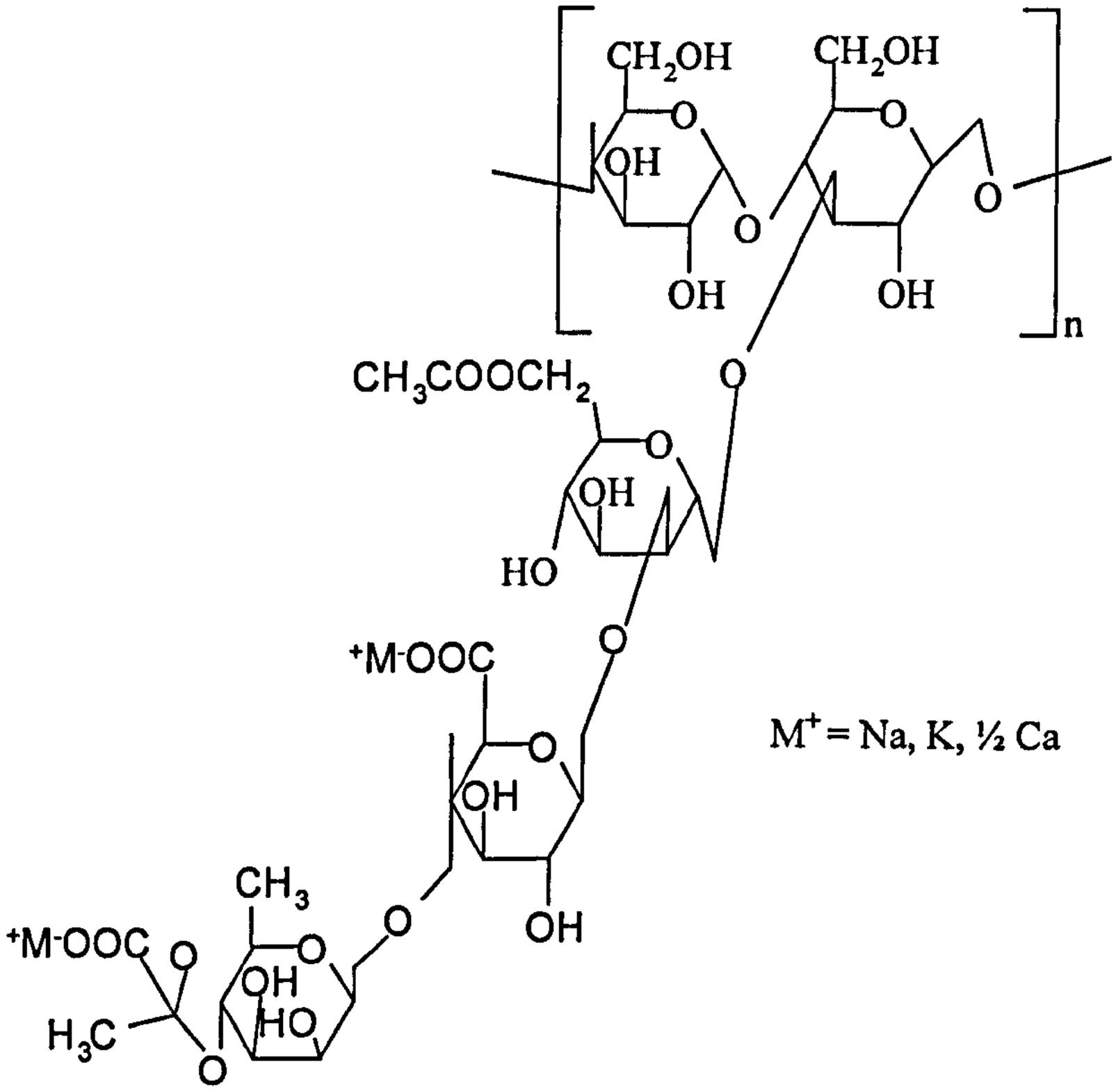

Figure 2.3 Molecular structure of Kelzan (xanthan gum).

Veegum® R is an inorganic, complex, colloidal, magnesium aluminium silicate and it was supplied by Vanderbilt. The typical analysis of Veegum, conventionally expressed as oxides, is as follows:

Oxide	%
SiO_2	63.05
MgO_2	10.5
Al_2O_3	10.5
Na_2O	2.4
CaO	2.3
K_2O	1.2
Fe_2O_3	0.9
Ignition loss	7.5

Table 2.3 Typical analysis of Veegum R[3].

All gelling agents were used as received.

2.1.5 Nano-size silica particles

The silica primary particles used in this work have diameters between 5 and 30 nm and can aggregate into larger units. Production of fumed hydrophilic silica (100 % Si-OH) uses a continuous flame hydrolysis technique. It involves the conversion of silicon tetra chloride ($SiCl_4$) to the gas phase using an oxygen/hydrogen flame. It then reacts with hydrogen and oxygen at about 1200 °C to yield silica (SiO_2) and hydrochloric acid according to

$$SiCl_4 + 2H_2 + O_2 \rightarrow SiO_2 + 4HCl$$

Under the reaction conditions in the flame, SiO_2 primary particles of the order of about 10 nm (diameter) are first produced. The silica is hydrophilic due to the silanol groups (Si-OH) present on its surface. The surface may also contain siloxane bridges

(Si-O-Si). Fuji et al.[4] define hydrophilic silica when the surface coating by hydrophobic groups represents less than 20%. Therefore, as the surfaces of all particles used in this work have been modified, they will be referred as partially hydrophobic particles. In Figure 2.4 a schema of a 100% hydrophilic silica particle and a partially hydrophobic particle are shown. Hydrophobic silica is prepared by reacting hydrophilic silica with dimethyl-dichlorosilane reagent to various extents in the presence of water followed by drying at 300 °C for 2 hours[5].

$$-SiOH + SiCl_2(CH_3)_2 \rightarrow -Si\text{-}(OSiCl(CH_3)_2)$$

This reaction produces covalent siloxane bonds between the silica atoms of the organosilane molecules and the silica atoms of the solid surface. For untreated hydrophilic particles there are usually about 2 Si-OH per 1 nm^2. Coated particles have surface concentrations of unreacted Si-OH groups in the range from 2-0.5 Si-OH per nm^2.

Silica particle	Mole% of unreacted surface Si-OH groups
SLM 1469	18
SLM 091	36
H30	47
SLM 957	57
SLM 1471	65.7
SLM 135	71
SLM 079	76
SLM 1466	79.9
SLM 160	87

Table 2.4 **Summary of silica particles with their respective silanol group content.**

Figure 2.4 **Schematic of a hydrophilic (a) and partially hydrophobic (b) silica particle**

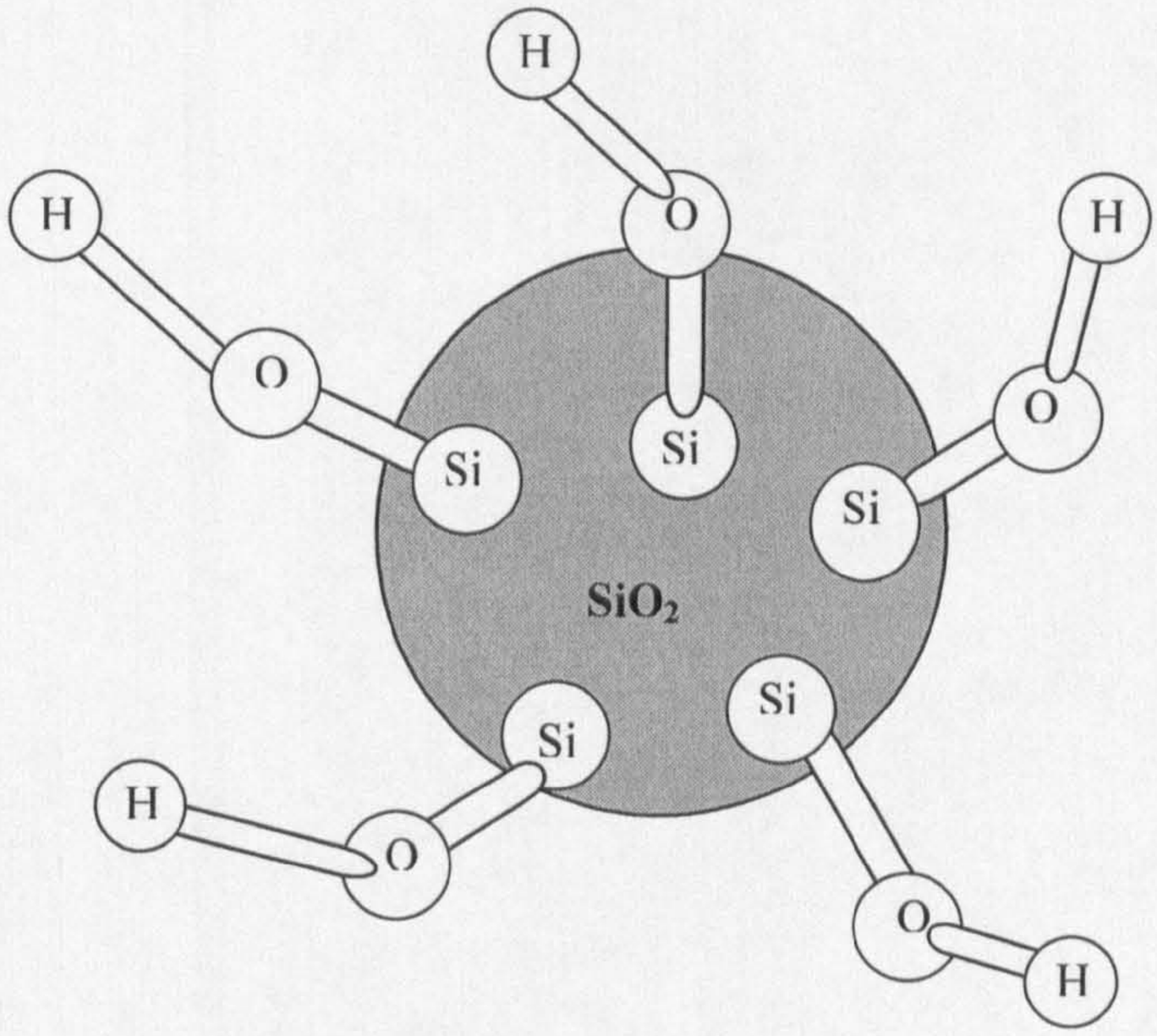

a) Hydrophilic silica particle

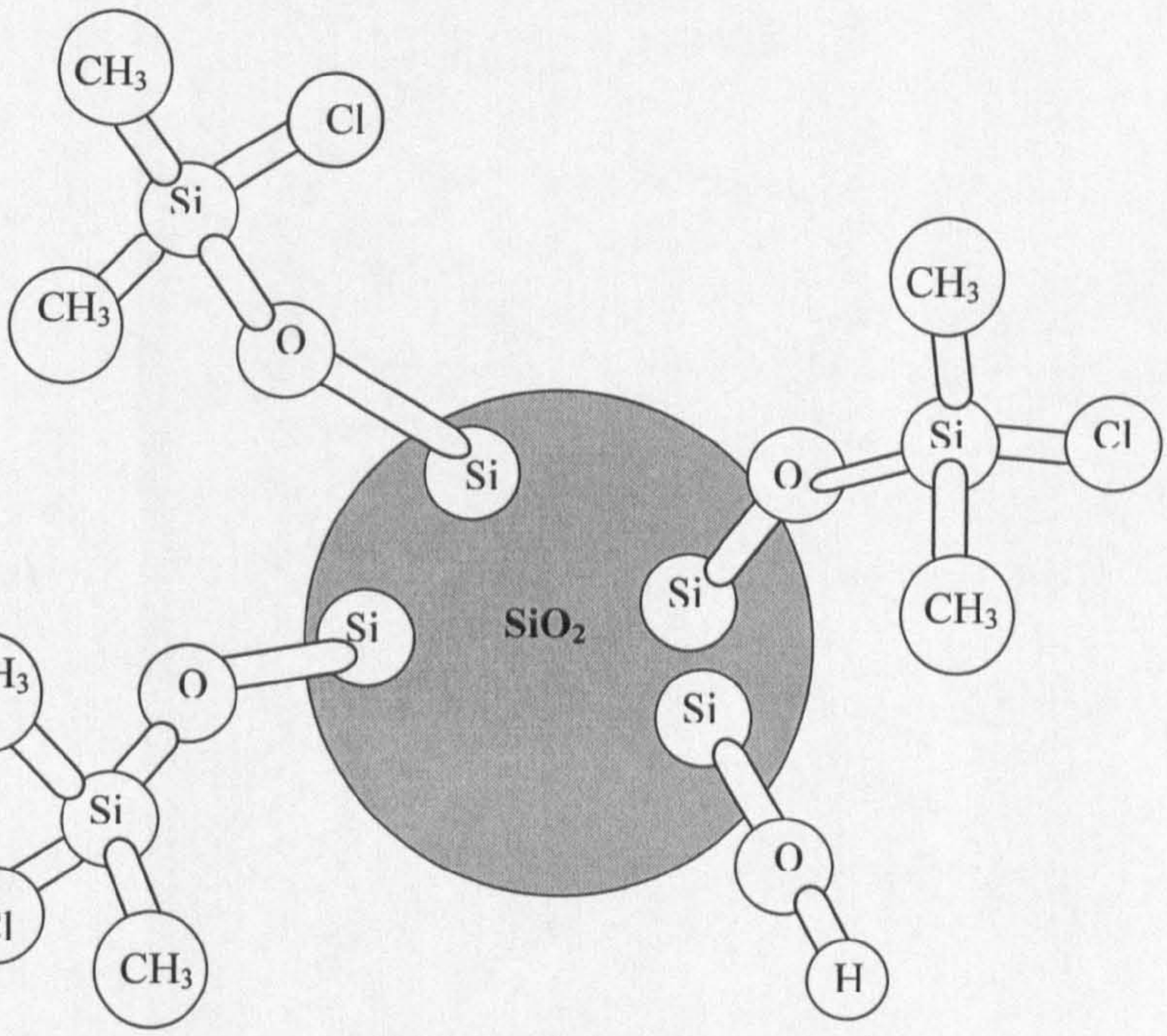

b) Hydrophobic silica particle

All silica particle samples were prepared, characterised and supplied by Wäcker-Chemie, Germany.

2.1.6 Others

Nitrogen gas (Energas, 99.9%) was passed through a Puritube (supplied by Phase Sep) containing activated charcoal to remove impurities. NaBr (99%) was supplied by BDH.

2.2 Methods

2.2.1 Evaporation rate measurements

The apparatus for measurement of the evaporation rates is shown in Figure 2.5. The liquid or emulsion sample is contained in a cylindrical glass sample tube suspended from a Precisa 125 A balance. The gas (nitrogen) is passed through a column of activated charcoal and through a flow meter to record the gas flow rate, F. The purified nitrogen stream flows through a thermostatting coil and enters the measurement vessel through an annular opening of approximately 1 mm gap. The gas then flows vertically upwards around the sample tube and emerges from the top of the vessel. The vessel containing the suspended sample tube is contained within a stirred, thermostatted outer vessel. The evaporation rate of the sample is determined from the sample mass loss ($\pm$ 0.0001 g) recorded on the Precisa balance. The data is logged automatically into an EXCEL spreadsheet using a PC equipped with TAL technologies WinWedge software which allows data transfer from the balance.

Figure 2.5 Schematic diagram of the evaporation rate apparatus.

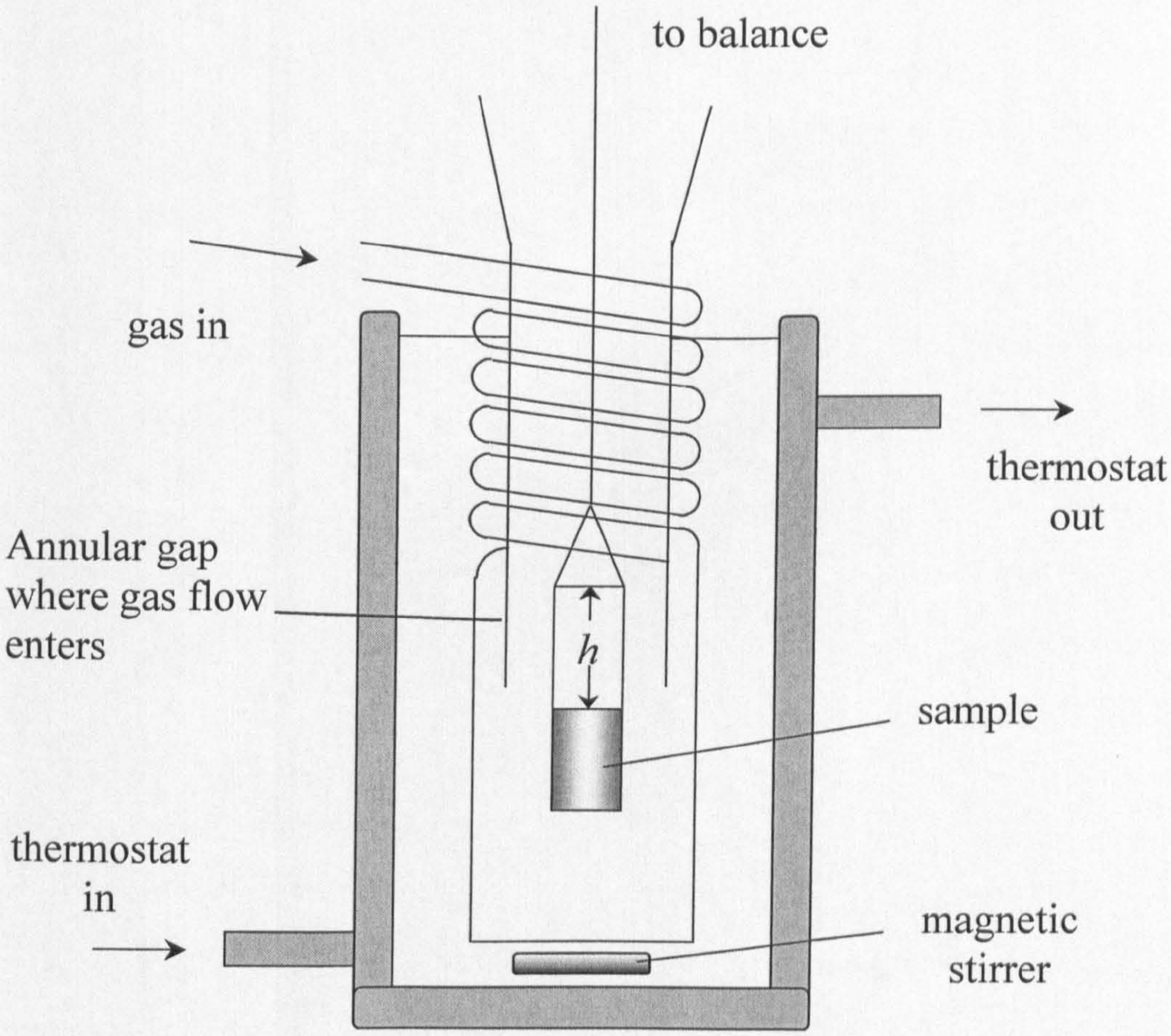

For the evaporation rate measurements, the nitrogen gas flow rate was kept constant at 1700 cm^3 min^{-1} for the two identical experimental rigs constructed and used in this work.

2.2.2 Determination of sample tube dimensions

Several different methods were used to measure the sample tube dimensions. Firstly, an analogue and a digital calliper gauge were used to measure them directly. Secondly, a travelling microscope (equipped with a digital clock gauge) was used to measure the liquid heights for the tubes fully and partially filled with different, accurately known volumes of squalane (selected for its lack of volatility). Using the measured heights and known volumes (by direct weight), we calculated the inner radii and inner heights of the tubes. Table 2.5 shows the summary of the dimensions (average from repeat measurements using the different methods) of the sample tubes used in this work.

Sample tube	Inner radius/mm	Inner height/mm
1	8.97 ± 0.06	38.5 ± 0.2
2	9.16 ± 0.06	38.9 ± 0.4
3	9.17 ± 0.07	37.3 ± 0.2
4	9.14 ± 0.05	37.3 ± 0.2
5	9.15 ± 0.07	37.3 ± 0.1
6	8.97 ± 0.04	38.5 ± 0.1
7	9.01 ± 0.01	38.5 ± 0.2

Table 2.5 **Summary of the dimensions of the sample tubes used in the evaporation rate measurements. Tubes 1-5 were made from glass and 6 and 7 made from Teflon (PTFE).**

2.2.3 Emulsion sample

High internal phase emulsions (HIPEs) and creamed emulsion samples, always of 20 cm^3 total volume, were prepared as follows. A known amount of oil was added to a known value of aqueous surfactant solution in a cylindrical vessel of 160 mm inner height and 32 mm internal diameter. Emulsification of the mixtures was done using a Janke and Kunkel Ultra Turrax fitted with an 18 mm head and operated at 11000 rpm for 1 minute at room temperature. Depending on the effect to be studied, NaBr was added either to the aqueous surfactant solution or directly to the emulsion.

Gelled emulsions were prepared as follows. Initially an emulsion was prepared as above and then a known mass of polymer was added to it. The samples were stirred using a magnetic stirrer slowly for up to ten hours until the emulsion appeared homogeneously gelled and thick.

In order to study the evaporation rates of the emulsions, except for experiments where the effect of sample volume was studied, approximately 4 cm^3 of the final emulsions were pipetted into the sample tube. Before that, all samples (where air bubbles were present) were left approximately 15 minutes until air bubbles disappeared.

A wide range of both o/w and w/o emulsions stabilised by either hydrophilic or hydrophobic silica particles with oils of different volatility were left in open tubes at room temperature until the volatile species were completely evaporated (1 to 6 weeks). SEM images were obtained from the dry solid residues (see *2.2.11* for details).

Figure 2.6 **Calibration plots of measured gas flow rate versus flow meter reading for flowmeter 1 (a) and 2 (b).**

a) Flowmeter 1

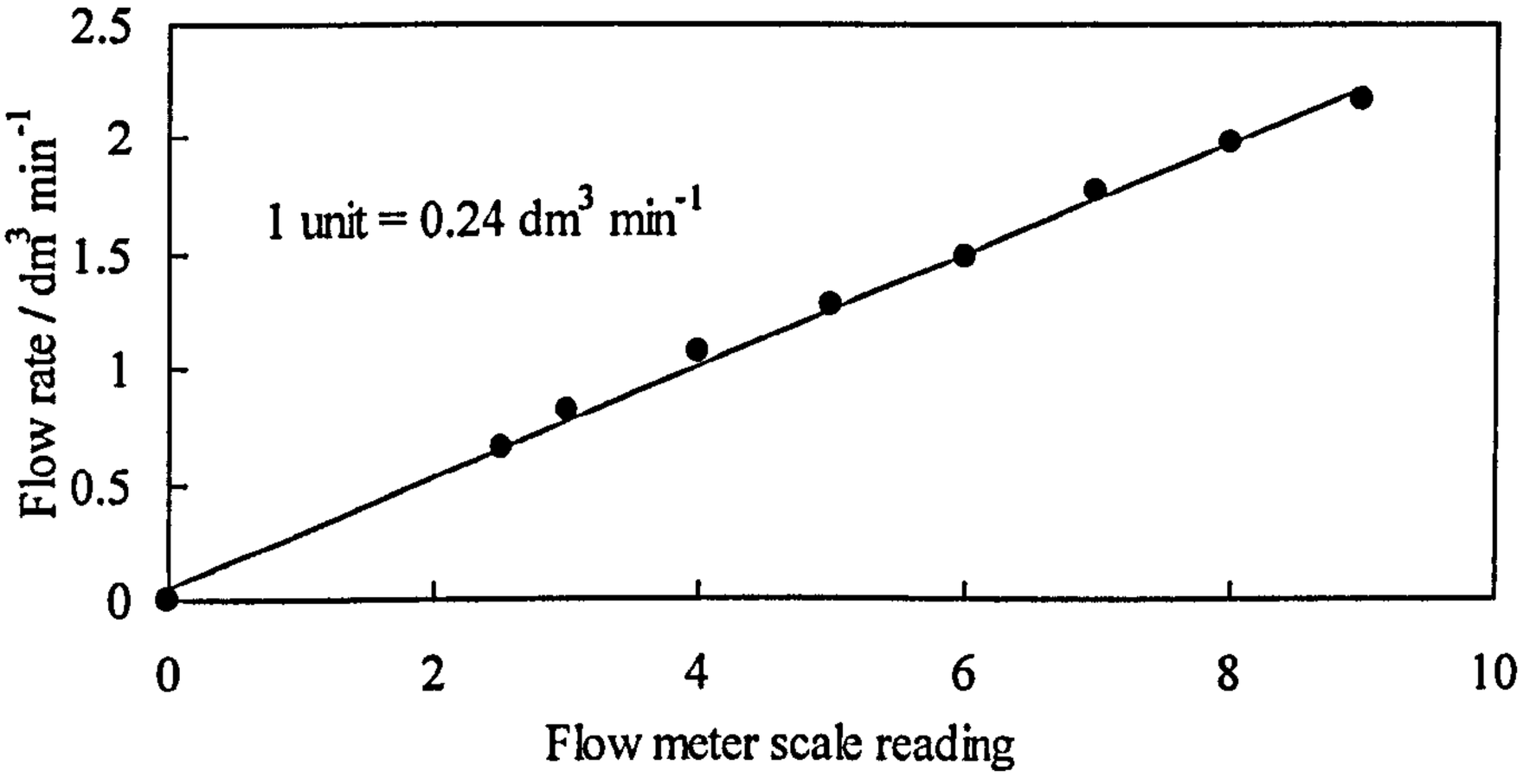

b) Flow meter 2

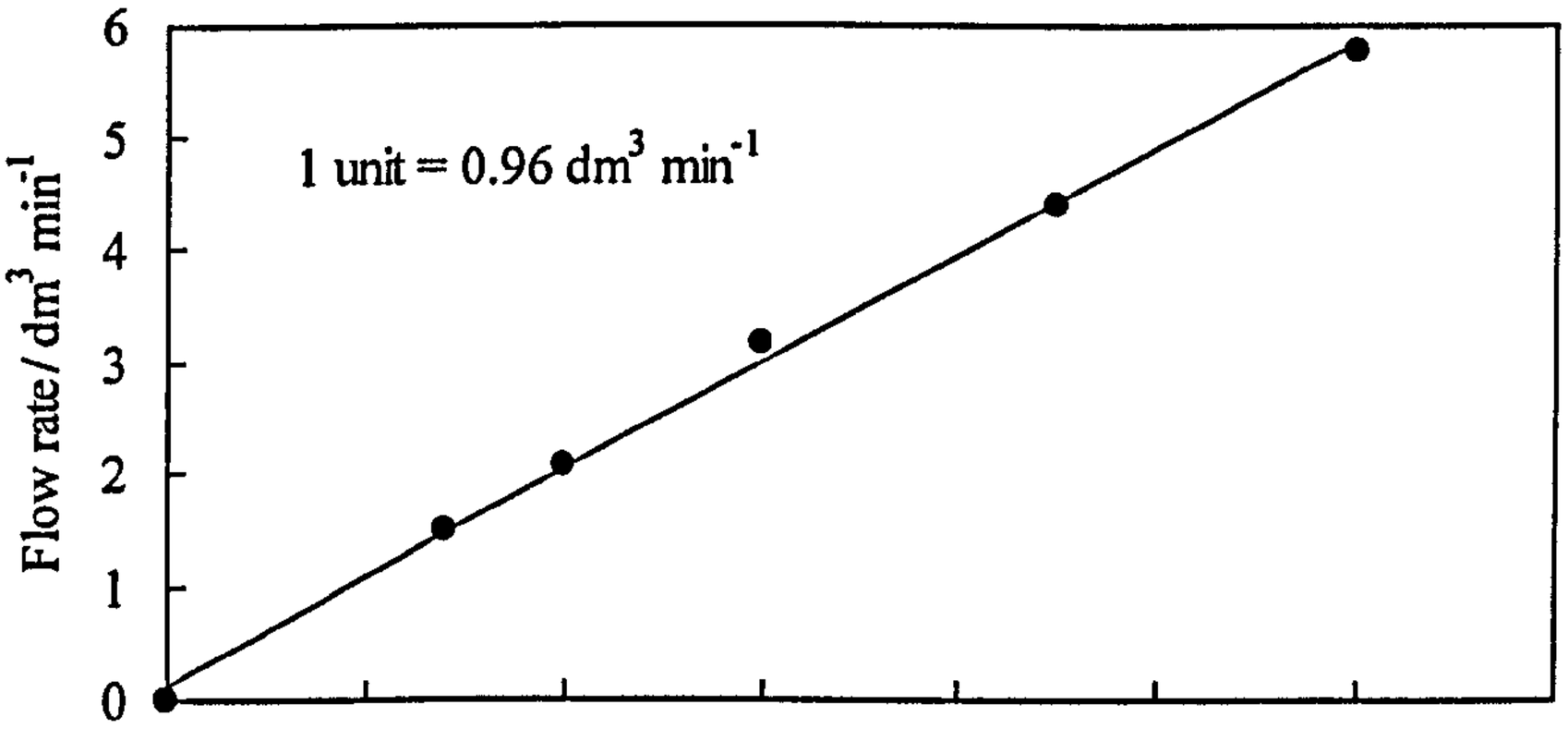

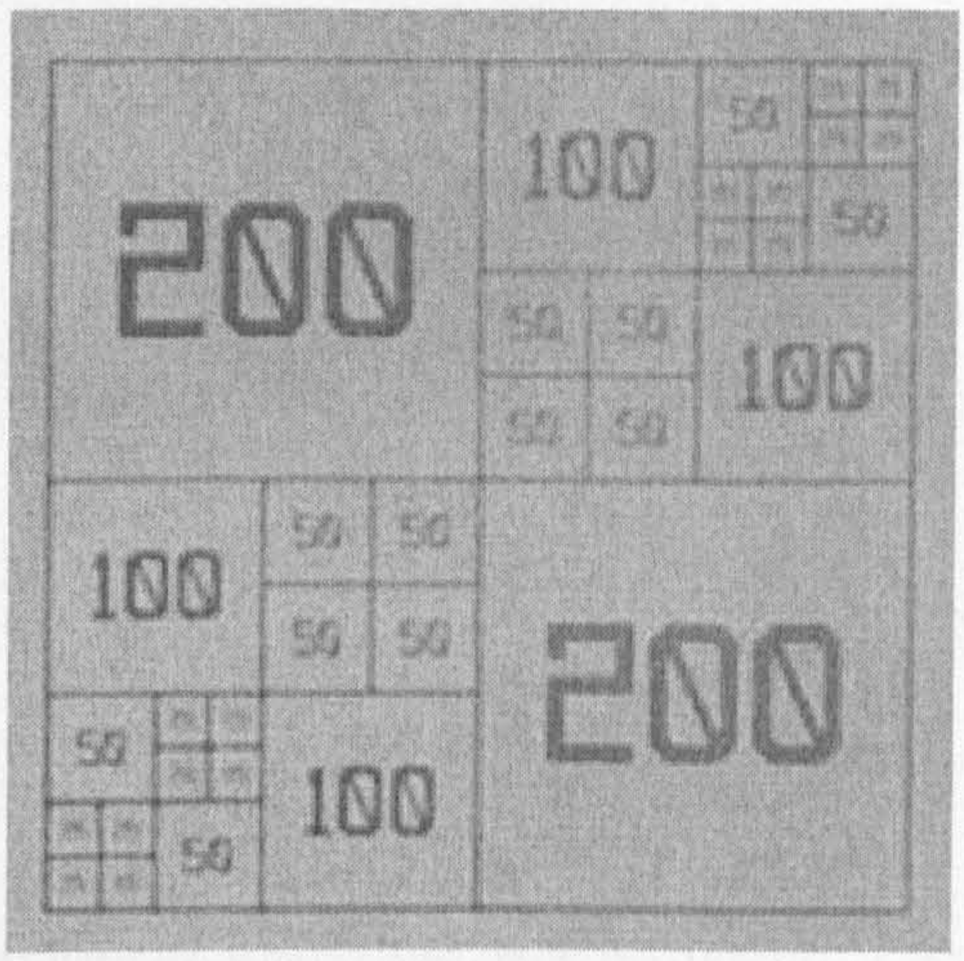

Figure 2.7 **Graticule used to scale images taken with the optical microscope. The numbers represents length in μm.**

2.2.6 Emulsion drop test

To determine whether an emulsion was oil-in-water (o/w) or water-in-oil (w/o), a simple observational experiment called the "drop-test" was used. A couple of drops of emulsion were added to sample tubes containing a volume of either pure oil or pure water. If the emulsion drops dispersed in water and remained intact in the oil phase, then the emulsion was characterised as o/w type. Similarly, a w/o type of emulsion was apparent if the emulsion drops were observed to disperse in oil and remain as drops in water.

2.2.7 Ultrasonic dispersion

Dispersions of the silica particles in either pure water (of pH around 6) or in oil were prepared by dispersing a known mass of powder into the continuous phase using a high-intensity ultrasonic vibracell processor (Sonics & Materials), tip diameter 3 mm, operating at 20 kHz and up to 10 W for 1 min. During sonification, it was necessary to cool the vessel in an ice bath. The resulting dispersions were generally bluish in appearance.

2.2.8 Drop size distribution measurements

A Malvern Mastersizer (Malvern Instruments Ltd) was used to measure the particle size distribution of emulsion samples[6]. Figure 2.8 shows a schema of a laser diffractometer. The light from a low power Helium-Neon laser is used to form a collimated and monochromatic beam of light typically 18 mm in diameter. This beam is called the analyser beam and drops passing through it in the sample presentation cell will scatter the laser light. Large drops scatter at small angles and small drops at large angles. The scattered light is incident on the receiver lens. This operates as a Fourier Transform lens forming the far field diffraction pattern of the scattered light at its focal plane. The receiver lens has a special configuration, which means that regardless of the position or movement of the drops its diffraction pattern is stationary and focuses onto the multi-element photoelectric detector plane.

Prior to measurements, a number of experimental parameters must be entered on the software used to run the instrument. The focal length of the lens determines the

effective drop size range to be used. For example, the 45 mm lens can only be used for drops between 0.1 and 80 μm. The presentation code is dependent on the type of the emulsion to be studied and is calculated from the refractive indices of the two liquids.

The important optical properties are the refractive index of both the dispersed drops (n_D) and the continuous phase (n_C) and the sample absorption. The differential refractive index (DRI) is defined as

$$DRI = \frac{n_D}{n_C} \qquad [2.1]$$

and is marked on the Y co-ordinate of the optical properties grid in the Malvern manual. The absorption parameter is marked on the X co-ordinate. This constitutes the presentation code for the sample and the code needs to be input before each run.

Experimentally for o/w emulsions, a few drops of the sample were extracted from the emulsion with a Pasteur pipette and then diluted into ~200 cm^3 of aqueous solution of the same surfactant as in the emulsion at a concentration equal to its critical micelle concentration (cmc). This dilution procedure ensured that no desorption of the surfactant from the emulsion drop surface occurred in the dilution procedure. Drop size distribution measurements were made using the 16 cm^3 of emulsion sample remaining after removal of 4 cm^3 for the evaporation rate measurements.

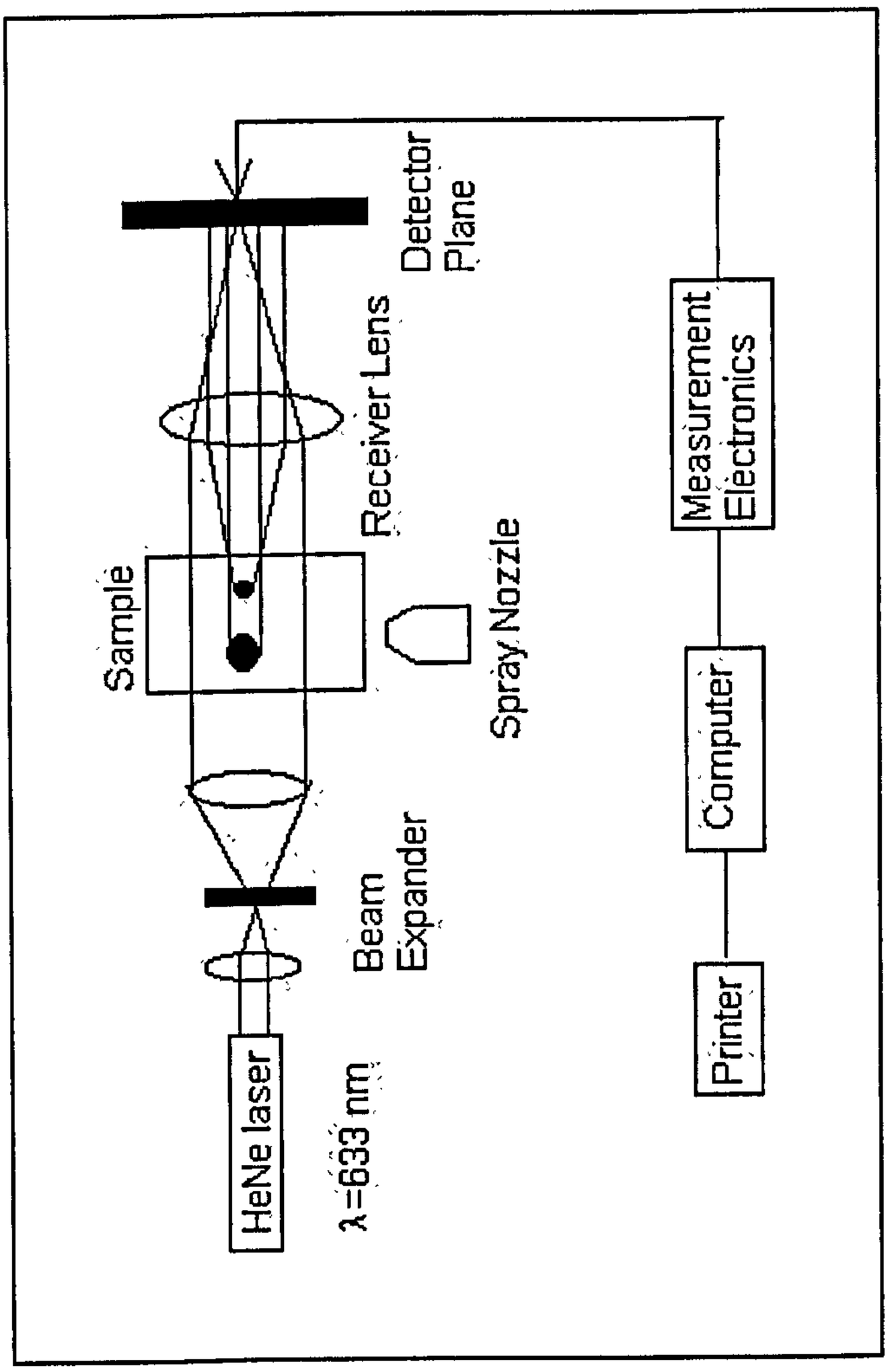

Figure 2.8 Schematic configuration of the 2600 laser diffractometer

The emulsion samples, stored in stoppered vessels at room temperature, were sized immediately after homogenisation and at selected time intervals up to the total time of the corresponding evaporation rate measurement. The results are presented as a histogram of volume frequency and the cumulative volume under the size on a log scale. The volume mean diameter is defined as the emulsion drop size such that 50% of the volume distribution of the droplets is $\leq$ this value.

2.2.9 Conductivity measurements

The conductivity of the emulsions was measured using a Jenway 4310 digital conductivity meter at 20°C using Pt electrodes. Before the measurements the conductivity meter was calibrated (for 0.01 M KCl solution $\kappa = 1413$ $\mu S\ cm^{-1}$). The measurements were carried out a short time after the preparation of the emulsions.

2.2.10 pH-measurements

The pH was measured using a Jenway PHM 6 meter with a combined glass/calomel reference electrode. The meter was calibrated before use with buffer solutions of pH = 4, 7 and 10. The pH of the aqueous dispersion was varied by addition of hydrochloric acid or sodium hydroxide.

2.2.11 Scanning Electron Microscopy (SEM)

Solid residues obtained after the evaporation of particle-stabilised emulsions were attached to standard 12 mm diameter aluminium sample mounts using quick drying two-

part epoxy resin. Since most of the samples were extremely fragile, the selection and mounting of reasonable sized (approximately 2-4 mm) agglomerates using tweezers was very difficult; even using extreme care, most fragments just desintegrated into powder during handling. The method used was to apply a film (approximately 1 mm thick) of freshly mixed epoxy resin to the sample mount and then to sprinkle on to this a layer of sample material. Excess sample material not adhering to the mount was collected and returned to the sample bottle. Samples were prepared in batches of five due to the limited time the epoxy was "workable". When the epoxy resin was fully hardened, each sample was gently and carefully scraped with the edge of a clean piece of paper. This action removed the tops of the sample fragments in order to expose fresh fracture surfaces for SEM examination. Any loose sample material was removed with compressed air. The samples were coated with a thin (approximately 20 nm) layer of spec-pure carbon using an Edwards High Vacuum E12E Vacuum Evaporator, fitted with a planetary-motion sample rotation device.

A LEO Electron microscopy (formerly Cambridge Instruments) model S360 SEM was used to examine the samples. Many areas of each sample were examined prior to recording representative images. A PC connected to the SEM was used to digitally acquire the images. The hardware interface and driving software were designed and constructed in-house. The images were stored in both raw bmp and edited in (brightness and contrast corrected) pdf formats. Results were presented on CD ROM and as inkjet prints on coated paper.

2.3 References

1 Handbook of Chemistry and Physics, CRC Press, Boca Raton, Florida, 62nd Ed., (1981).

2 Kelzan (Xanthan Gum), Technical Bulletin DB-15.

3 Vanderbilt products database.

4 M. Fuji, K. Machida, T. Takei, T. Watanabe and M. Chicazawa, *Langmuir*, 2000, **16**, 3281.

5 H. Balard, E. Papirer, A. Khalfi and H. Barthel, *Composites Interfaces*, 1999, **6**, 19.

6. www.Malvern.co.uk and Malvern Manual, Malvern Instruments UK.

Chapter 3

CHAPTER 3

EVAPORATION RATES OF PURE LIQUIDS

3.1 Introduction and theory

When a pure liquid is in equilibrium with its vapour, there is no net transfer of molecules between both phases. Among all the liquid molecules, a finite number may be near the surface of the liquid and possess kinetic energy great enough to overcome attractive forces and escape into the gas phase (see Figure 3.1a). If the vapour space is limited, the molecules will steadily accumulate in it, and there will be a tendency for them to return to the liquid phase (see Figure 3.1b).

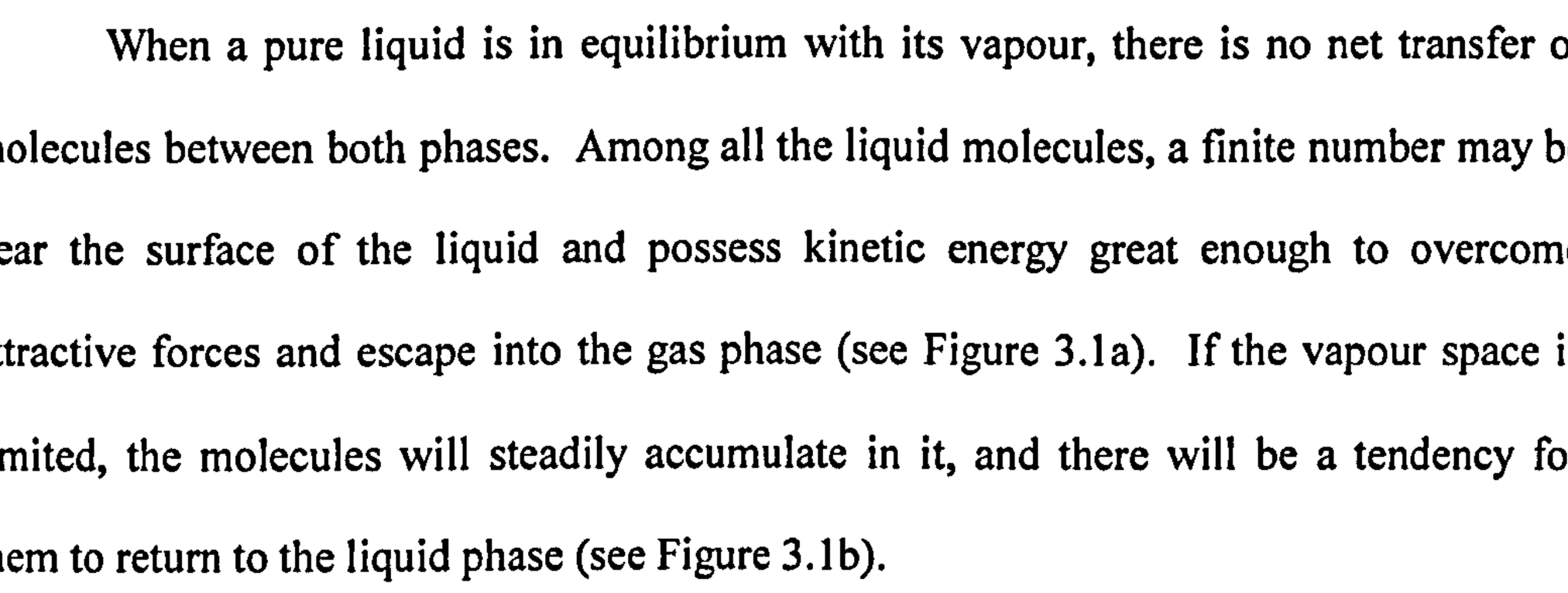

Figure 3.1 Schema of the evaporation process and the meaning of the vapour pressure.

A condition of equilibrium will be attained, when the number of molecules leaving the liquid to enter the space above is equal to the number returning in a given time (see Figure 3.1c). The space over the liquid is now saturated with vapour and the pressure it exerts will be the vapour pressure of the liquid at the given temperature.

In order to determine the maximum rate of evaporation for a pure liquid, the kinetic molecular theory of gases will be used[1]. Consider a wall of area A perpendicular to the x-axis. Let v_x be the component of a molecule's velocity in the x direction. If a molecule has $v_x > 0$, then it will strike the wall within an interval Δt if it lies within a distance $\Delta t.v_x$ of the wall. Therefore, all molecules in the volume $A.\Delta t.v_x$, will strike the wall in the interval Δt. The total number of collisions in the interval is therefore the volume $A.\Delta t.v_x$ multiplied by the number density, N, of molecules. However, to take account of the presence of a range of velocities in the sample, we must sum the result over all the positive values of v_x weighted by the probability distribution of velocities $f(v_x)$:

$$\text{Number of collisions} = N \cdot A \cdot \Delta t \int_0^\infty v_x f(v_x) dv_x \qquad [3.1]$$

The collision flux, Z, expressed per unit area and per unit time, is therefore, the number of collisions divided by A and Δt, so

$$Z = N \int_0^\infty v_x f(v_x) dv_v \qquad [3.2]$$

The integral can be evaluated using the Maxwell distribution to give:

$$\int_0^\infty v_v f(v_v) dv_x = \left(\frac{kT}{2\pi m}\right)^{1/2} \qquad [3.3]$$

where k is the Boltzmann constant, T is the absolute temperature and m is the mass of the molecule.

Let n be the number of moles of gas in volume V at pressure P. Since $N = nN_A/V = P/kT$, where N_A is Avogadro's constant, a final expression relating the collision flux to the pressure and temperature of the gas can be obtained:

$$Z = \frac{P}{\sqrt{2\pi mkT}} \qquad [3.4]$$

The amount (in moles) transported through unit area in unit time is defined by the mass transfer flux, J. For evaporation into a perfect vacuum, if it is assumed that all molecules striking the surface will condense. Then the maximum possible evaporation flux J_{max} (mol s^{-1} m^{-2}) is given by the following expression:

$$J_{max} = \frac{P}{\sqrt{2\pi MRT}} \qquad [3.5]$$

where P is the vapour pressure at the liquid surface (assumed to be the equilibrium vapour pressure), M is the molecular weight, R is the gas constant and T is the absolute temperature. For pure water at 25°C, P is 3167 Pa, M is 0.018 kg mol^{-1} and J_{max} is therefore 188 mol s^{-1} m^{-2}. This theoretical maximum rate corresponds to a rate of loss of water depth by evaporation of approximately 3.4 mm s^{-1}. Experimentally, it is observed that evaporation is much slower than this limit since vapour molecules must diffuse through a stagnant (i.e. unstirred) layer of gas above the liquid surface.

In the theoretical analysis that will be used here, it is assumed that the only resistance to evaporation of a pure liquid arises from the presence of the stagnant layer of

gas between the liquid surface and the sample vessel mouth (thickness h in Figure 2.5 and Figure 3.2). The liquid vapour diffuses through this and is carried away by the gas stream at the sample tube mouth. It is possible to calculate the evaporation flux J (i.e. the flow of vapour per unit time and area) from a liquid surface with cross-sectional area A across the stagnant layer using Fick's laws[2]. Fick's first law gives the instantaneous flux J at any point,

$$J = -D\frac{\partial c}{\partial x} \qquad [3.6]$$

where D is the diffusion coefficient of the vapour through the stagnant gas layer and c is the concentration of the diffusing vapour at vertical position x above the surface. Fick's second law describes the time dependence.

$$\frac{\partial c}{\partial t} = -D\frac{\partial^2 c}{\partial x^2} \qquad [3.7]$$

Experimentally, the evaporation rate is observed to reach a constant value relatively quickly. In this steady state, dc/dt = 0 at all points within the stagnant vapour space and, from Fick's second law, dc/dx must be constant. Therefore, a linear concentration gradient of the evaporating species is established along the vertical axis through the stagnant layer. This can be represented as

$$\frac{\partial c}{\partial x} = \frac{c_0 - c_s}{h} \qquad [3.8]$$

where c_s is the concentration of vapour just above the liquid surface and c_0 is the concentration at the mouth of the open vessel.

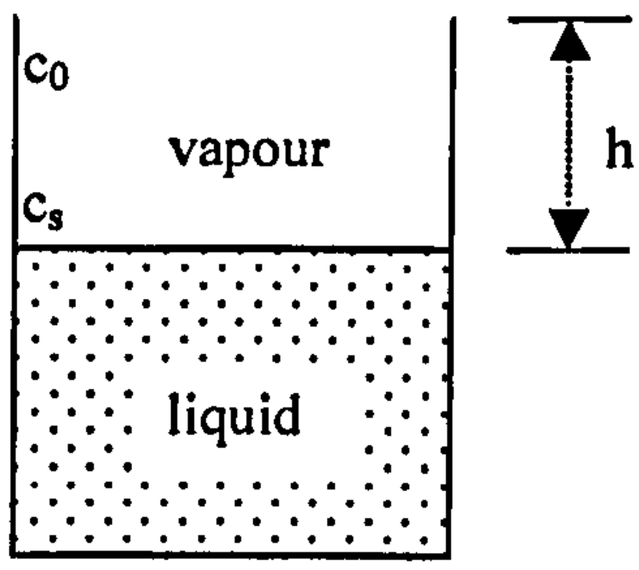

Figure 3.2 Schema of the liquid sample and some important parameters.

By combining equations [3.6] and [3.8], we obtain

$$J = -D\frac{c_0 - c_s}{h} = V_L c_0 \qquad [3.9]$$

where V_L is the mean linear velocity of the gas stream. The second relationship in equation [3.9] arises since the flux arriving from the liquid surface to the mouth of the sample vessel must be equal to that carried away by the gas stream. The mean linear velocity is calculated from the volumetric gas flow rate F using $V_L = F / A_V$, where A_v is the cross sectional area of the external vessel in the region of the mouth of the sample vessel. Solving to eliminate c_0 yields

$$J = \left\{\frac{Dc_s}{h} - \frac{D^2 c_s}{h^2 V_L + hD}\right\} \qquad [3.10]$$

Assuming the liquid vapour behaves ideally, c_s = P/RT and that the mass evaporation rate E (= -dm/dt where m is the liquid mass remaining) is given by E = JMA where M is the molecular mass of the liquid and A is the cross section surface area of the sample vessel, we obtain an equation for E,

$$E = \frac{MADP}{hRT}\left\{1 - \frac{D}{hF/(A_v + D)}\right\} \qquad [3.11]$$

For diffusing vapours of high vapour pressure, equation [3.11] must be modified to take account of the effect of the concentration gradient of the second gas component. As described by Jost[2], this creates an upward convection of the gas mixture. The effect may be accounted for by inclusion of a correction factor *z*, as follows,

$$E = \frac{MADPz}{hRT}\left\{1 - \frac{D}{hF/(A_v + D)}\right\} \qquad [3.12]$$

$$z = \left[\frac{P_{atm}}{P}\ln\left(\frac{1}{1-(P/P_{atm})}\right)\right] \qquad [3.13]$$

where P_{atm} is atmospheric pressure (equal to the sum of the pressures of vapour and gas). The correction factor z reduces to unity when $P << P_{atm}$.

At high flow rates the gas stream sweeps away the vapour from the mouth of the vessel effectively and c_0 approaches zero. In this regime, the second term on the right in equation [3.12] becomes negligible and the evaporation rate is approximately given by

$$E = \frac{MADPz}{hRT} \qquad [3.14]$$

The theoretical predictions of equations [3.12] and [3.14] have been validated[3] using measurements of the evaporation rates of heptane as a function of both the gas flow rate F and stagnant layer thickness h. For the measurements in the present work, the gas flow rate used is sufficiently high such that the approximate equation [3.14] is valid.

So far, h has been treated as a constant parameter. For initial evaporation rates the variation (increase) of h can be neglected, but for studies over long periods of time, as the sample evaporates, h increases. Under conditions of high flow rates, when $E \approx -dm/dt$, $h = (h_t - m/\rho A)$ and m is the mass of the liquid sample remaining, h_t is the total inner height of the sample tube and ρ is the liquid density, integration yields the following relation between m and t.

$$t = \frac{RTh_t}{MADPz}(m_0 - m) - \frac{RT}{2\rho A^2 DP}(m_0^2 - m^2) \qquad [3.15]$$

where m_0 is the initial mass of the liquid at time zero.

3.2 Evaporation rates of pure liquids

A range of pure liquid samples was measured, firstly to check the reproducibility of rate measurements made on the two different rigs and secondly, to determine the necessary diffusion coefficient data (of liquid vapour species in nitrogen gas, D_v) required for the emulsion studies.

A typical plot of sample mass loss versus time is shown in Figure 3.3. The rate of evaporation is taken to be the gradient of the best-fit line to the data. In this figure the mass loss of pure water is shown and the evaporation rate, i.e., the gradient is approximately 6×10^{-6} g s^{-1}. Since for pure liquids the evaporation rates were studied over a relatively short time-scale, the change in the height in the tube with time is negligible and the weight loss plots are linear over the initial period.

Figure 3.3 **Typical mass loss plot for pure water. The evaporation rate is determined as the gradient of the line of the best-fit to the data.**

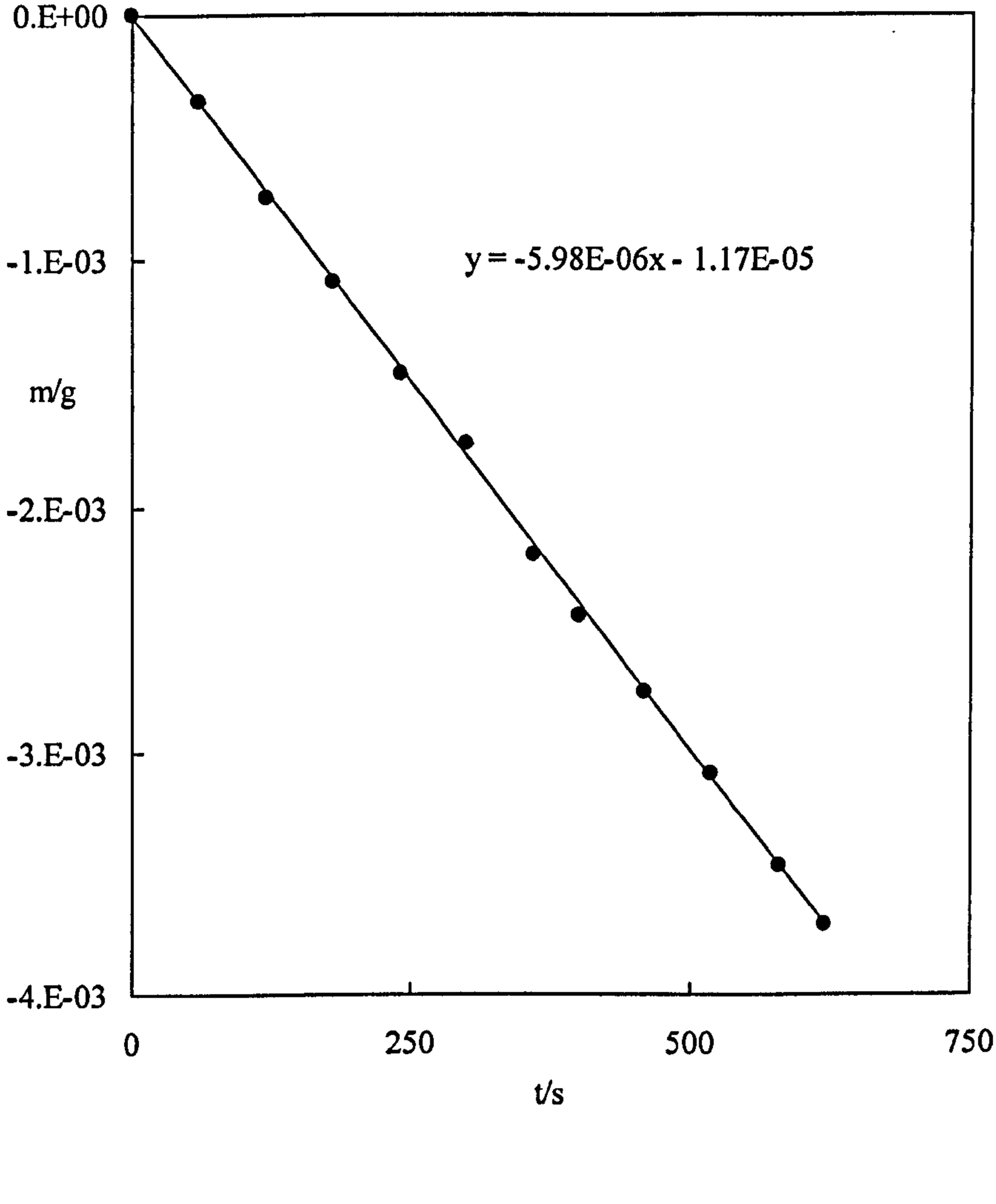

In order to determine D_v, experimental results of mass versus time were fitted to the appropriate model (equation [3.15]) using VBA routines within EXCEL spreadsheets. Figure 3.4 shows an example of a spreadsheet used to fit evaporation rate data for a pure liquid. The upper spreadsheet cells contain the measurement conditions (temperature, sample tube dimensions and the initial mass of the sample) and the physical-chemical properties (density, vapour pressure and molecular weight) of the liquid. For each value of the sample mass lost, the spreadsheet calculates the time residual, i.e. the absolute difference between calculated and experimental time values. The "best fit" to the data was obtained by adjustment of the appropriate constants such that the sum of time residuals was a minimum. In most cases, only the diffusion coefficient of the vapour species was adjusted to fit the experimental data using the SOLVER routine within EXCEL. In certain cases, some slight adjustments to the initial sample mass were made to improve the fit quality. Different evaporation runs (and in different rigs) of the same liquid provide values of D_v within an uncertainty of 5%. Figures 3.5 show examples of a series of mass loss curves of some oils used in this work together with the best fit according to the theory, described in the text.

Figure 3.4 The spreadsheet configuration used to fit data of mass versus time for a pure liquid. The results here refer to water at 25°C. The experimental data (solid) and the best-fit calculated curve (dashed) obtained by floating the value D are compared in the plot.

..\aranberri\integrated equation for evap rate Measured on RIG 2, sample tube 2, flow rate is 1700 ml min-1

WATER	RUN 17			radius/m		P/Torr				
DATA · 12 01.01				0 00916		23.75				
R/J mol^{-1} K^{-1}	T/K	ht/m	M/kg mol^{-1}	A/m^2	D/m^2 s^{-1}	P/Pa	ρ/kg m^{-3}	m_o/kg	X	B/2
8.314	298.35	0.0389	1 80E-02	2 64E-04	2.38E-05	3167.21	995 67	4 02E-03	2.70E+08	1.32E+10
		sum of resids			floated					

CALCULATED 336194.265

t/s	m/g	time resid
0	0	0
128.966551	-0.0008	67.8864731
322.447663	-0.002	200.347809
467.5831	-0.0029	284.463227
548.223011	-0.0034	304.132923
467.5831	-0.0029	162.473237
532.094508	-0.0033	166.01443
677.260406	-0.0042	250.160309
644.999495	-0.004	156.879622
741.785353	-0.0046	192.695265
838.580582	-0.0052	228.470475
806.314464	-0.005	135.234386
903.115943	-0.0056	171.015845
1129.02251	-0.007	335.892381
1032.19916	-0.0064	178.109072
1032.19916	-0.0064	117.079043
1193.57661	-0.0074	217.496536
1225.85523	-0.0076	188.745121
1403.40623	-0.0087	305.276099
1451.83469	-0.009	292.744605
1371.12188	-0.0085	151.001766
1645.57199	-0.0102	364.492157
1661.71846	-0.0103	319.608351
1580.98873	-0.0098	177.858599
1419.54879	-0.0088	44.5510656
1871.64622	-0.0116	346 52635
2017.0066	-0.0125	430.916517
2000.85441	-0.0124	353.744303
2113.92524	-0.0131	405.795115
2146.23354	-0.0133	377.133683
2291.63375	-0.0142	461.513879
2420.89609	-0.015	529.806004
2388.57895	-0.0148	436.468838
2356.26284	-0.0146	343.132712
2485.53351	-0.0154	411.433657

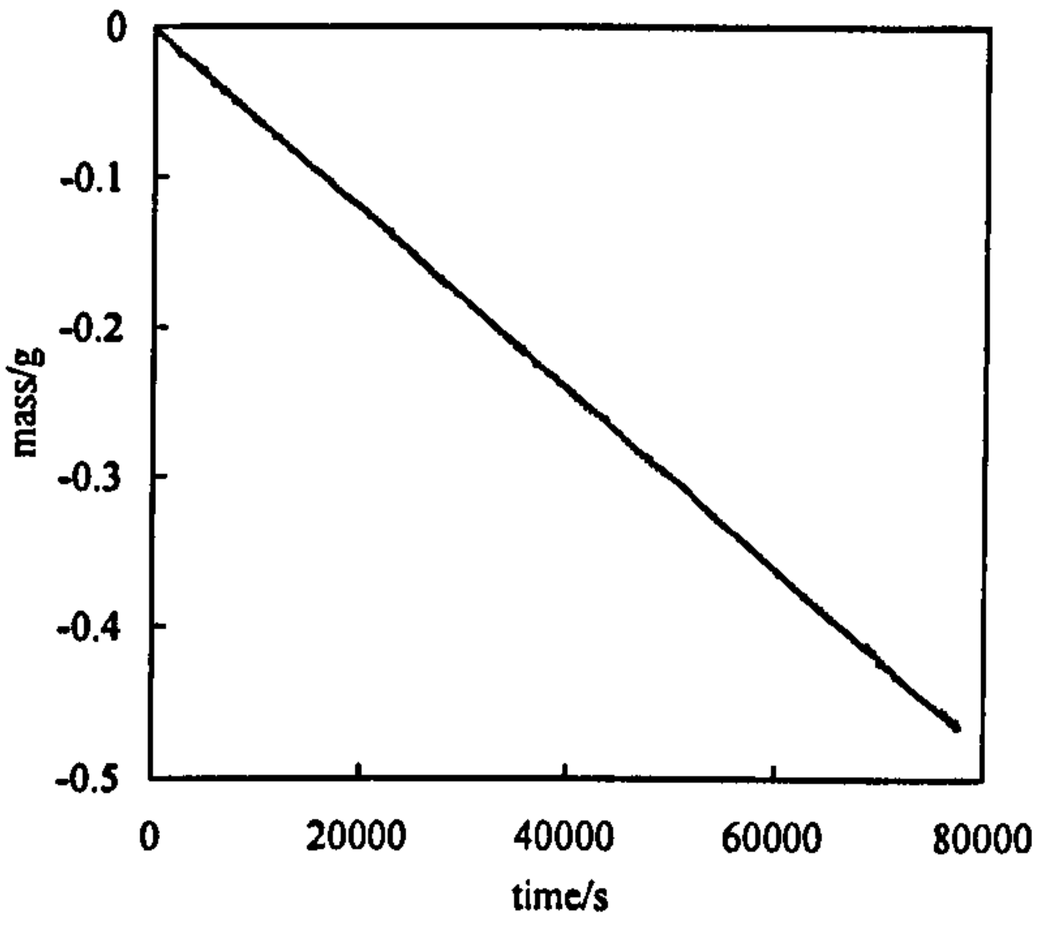

EXPERIMENTAL

t/s	m/g
0	4.0185
61.08	4.0177
122.10	4.0165
183.12	4 0156
244.09	4.0151
305.11	4.0156
366 08	4.0152
427.10	4 0143
488.12	4.0145
549 09	4 0139
610.11	4.0133
671.08	4.0135
732.10	4.0129
793.13	4.0115
854.09	4.0121
915.12	4.0121
976.08	4.0111
1037.11	4.0109
1098.13	4.0098
1159 09	4.0095
1220 12	4 01
1281.08	4.0083
1342.11	4.0082
1403.13	4.0087
1464.10	4.0097
1525.12	4 0069
1586.09	4 006
1647.11	4 0061
1708 13	4 0054
1769.10	4.0052
1830.12	4 0043
1891.09	4 0035
1952.11	4.0037
2013.13	4.0039
2074 10	4 0031

Figure 3.5 **Mass loss curves of a range of solvents used in this work at 25°C. The experimental data (solid line) are compared with the calculated (dashed line) best fit.**

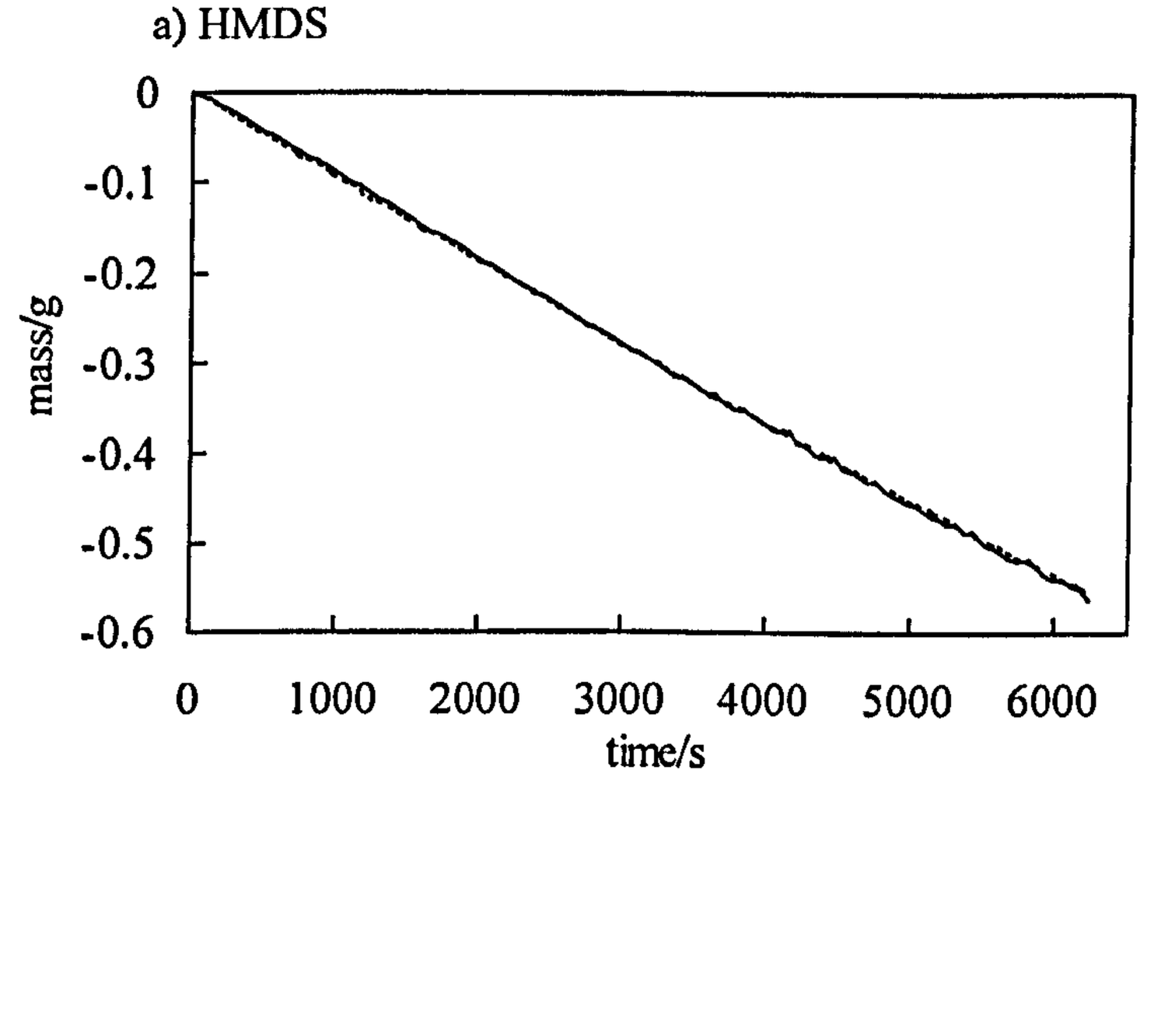

c) heptane

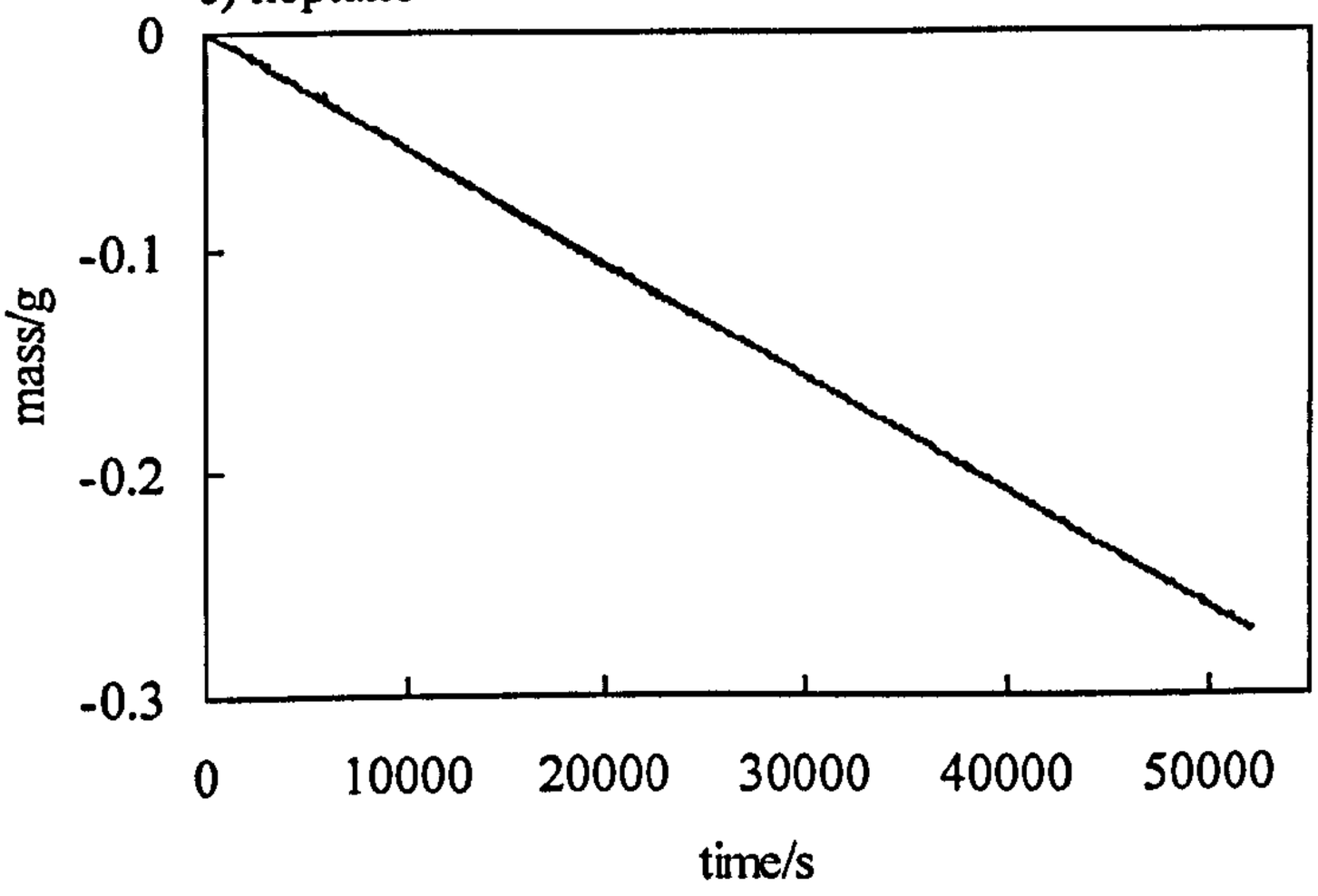

d) o-xylene

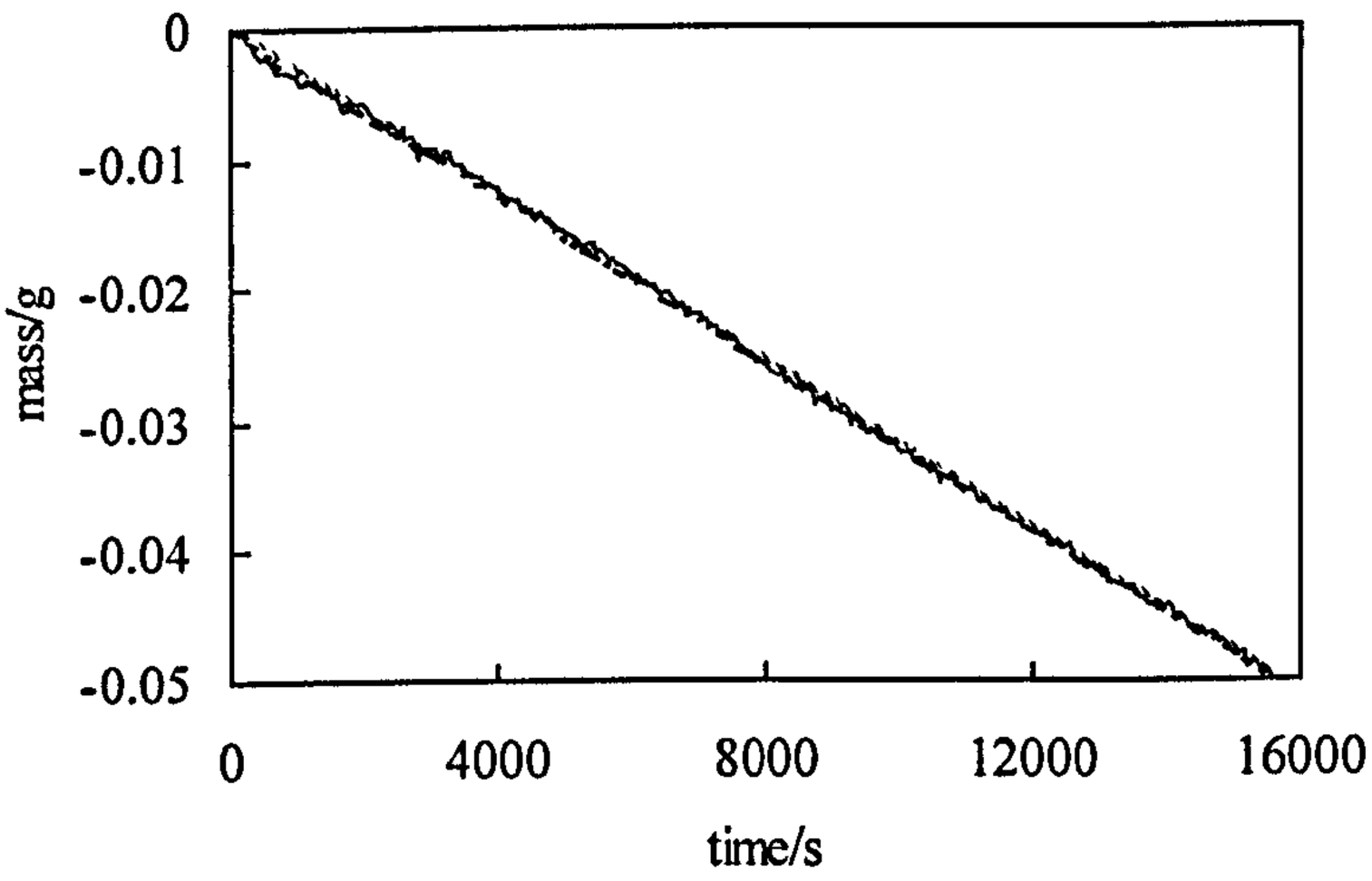

e) n-hexane

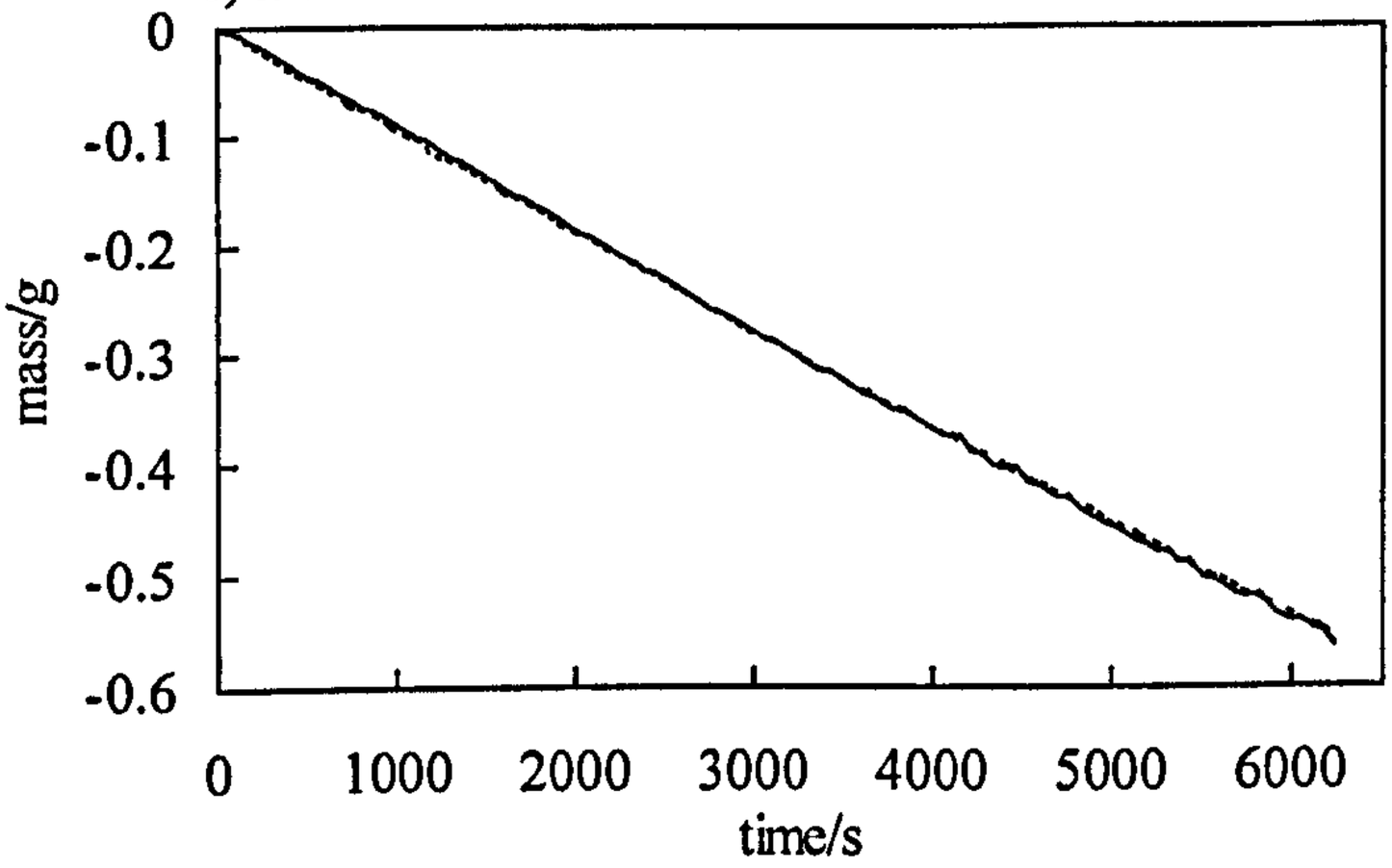

f) Methylcyclohexane

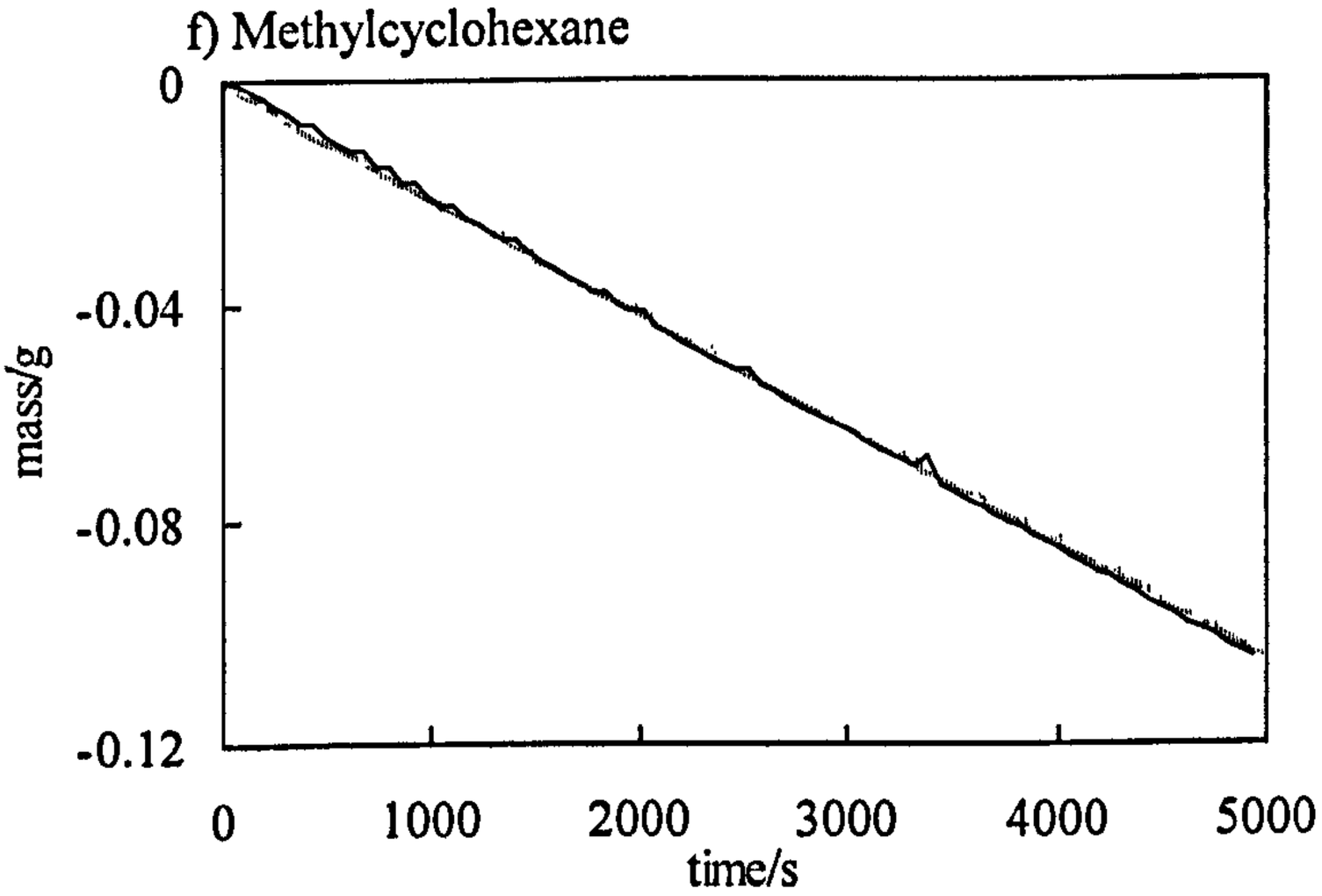

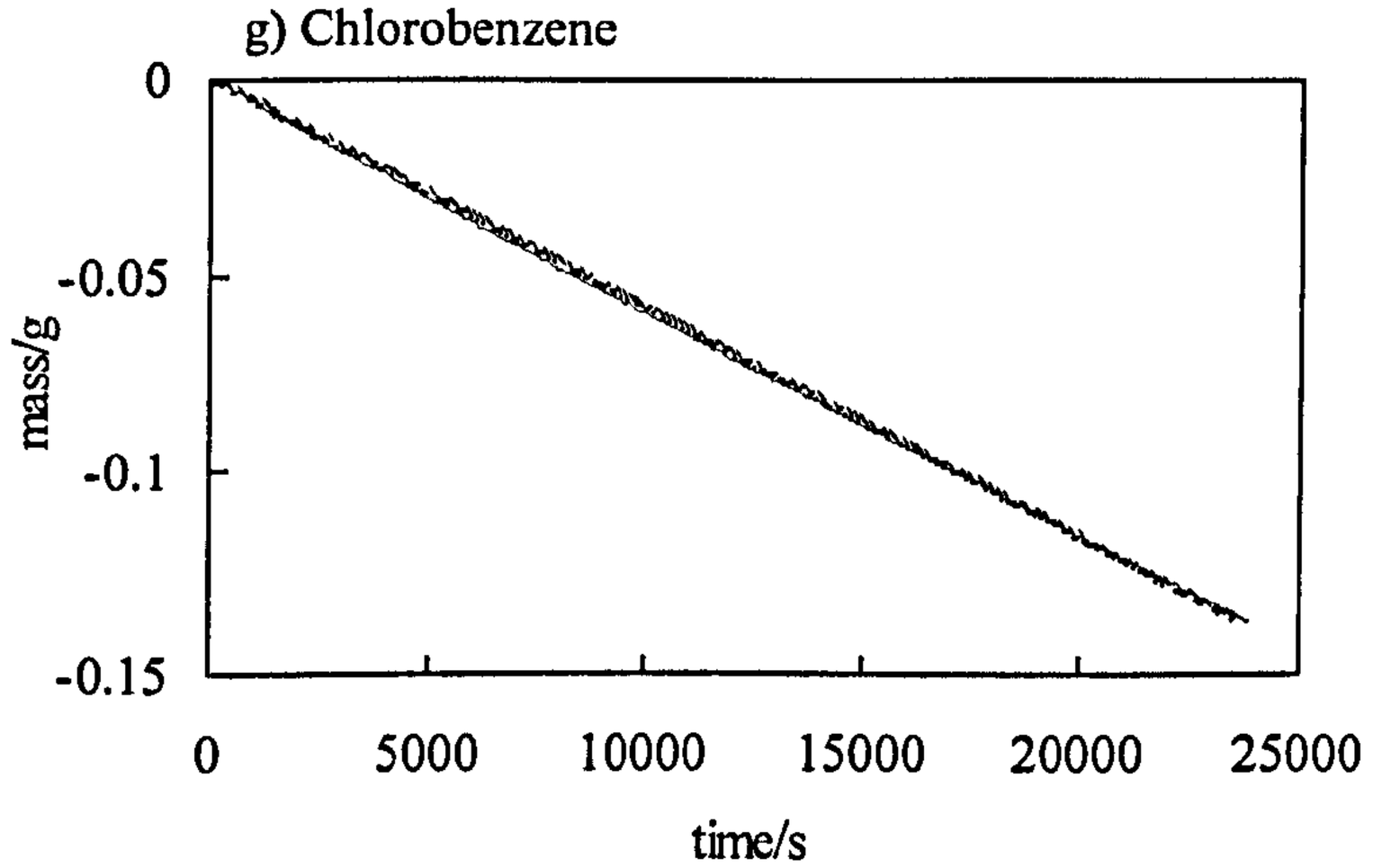
g) Chlorobenzene
0
-0.05
-0.1
-0.15
mass/g
0
5000
10000
15000
20000
25000
time/s

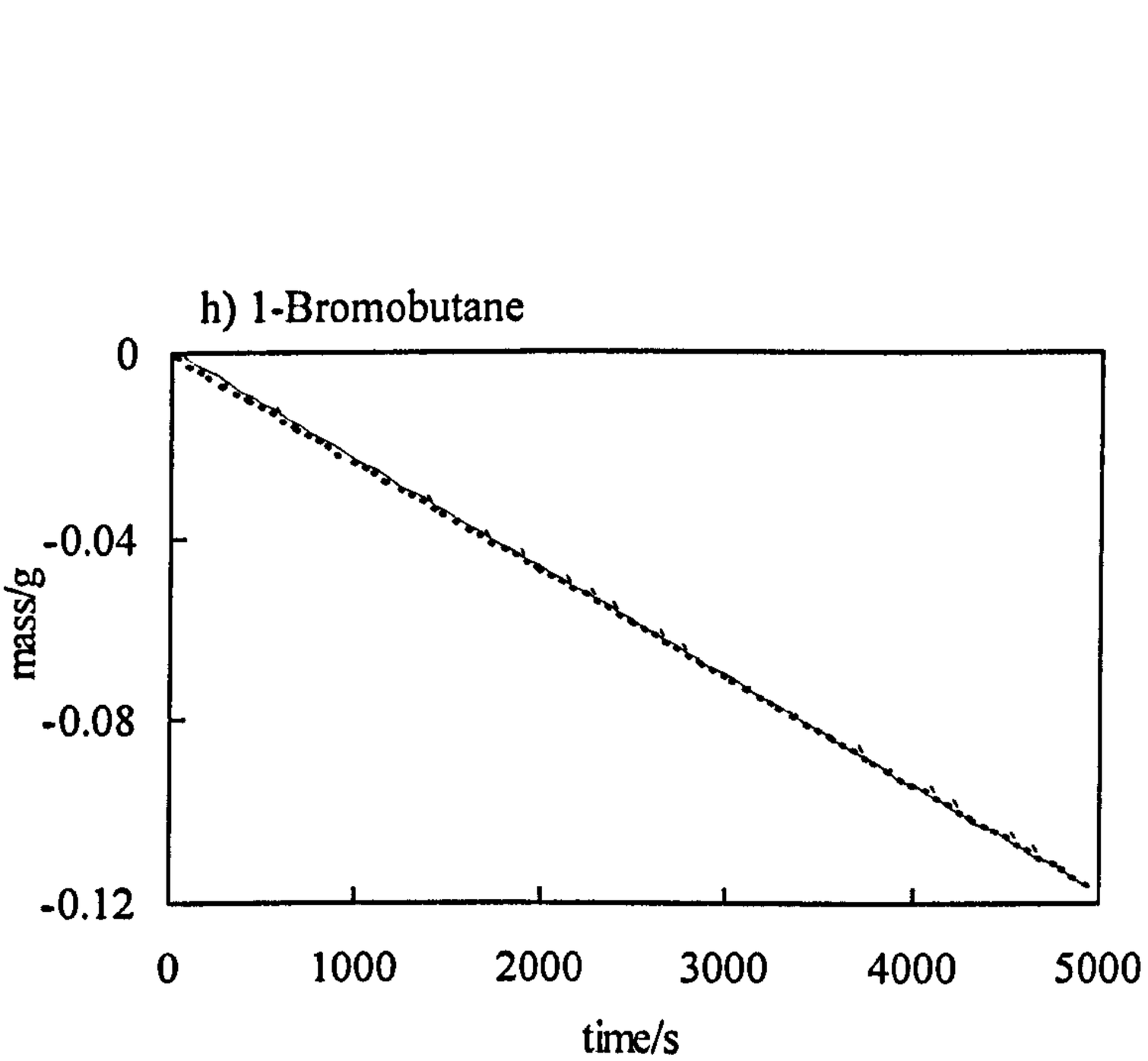
h) 1-Bromobutane
0
-0.04
-0.08
-0.12
mass/g
0
1000
2000
3000
4000
5000
time/s

i) Benzene

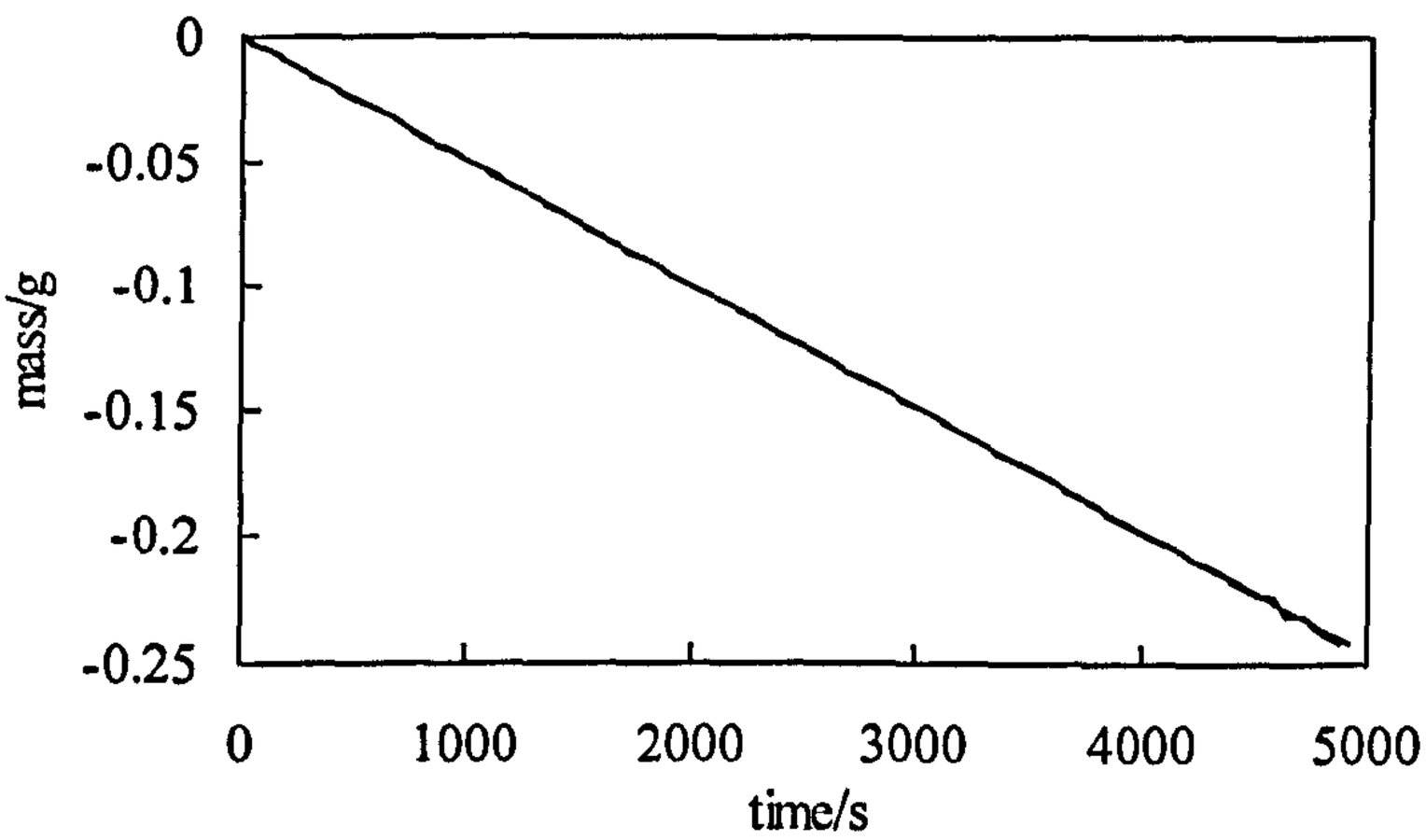

j) Toluene

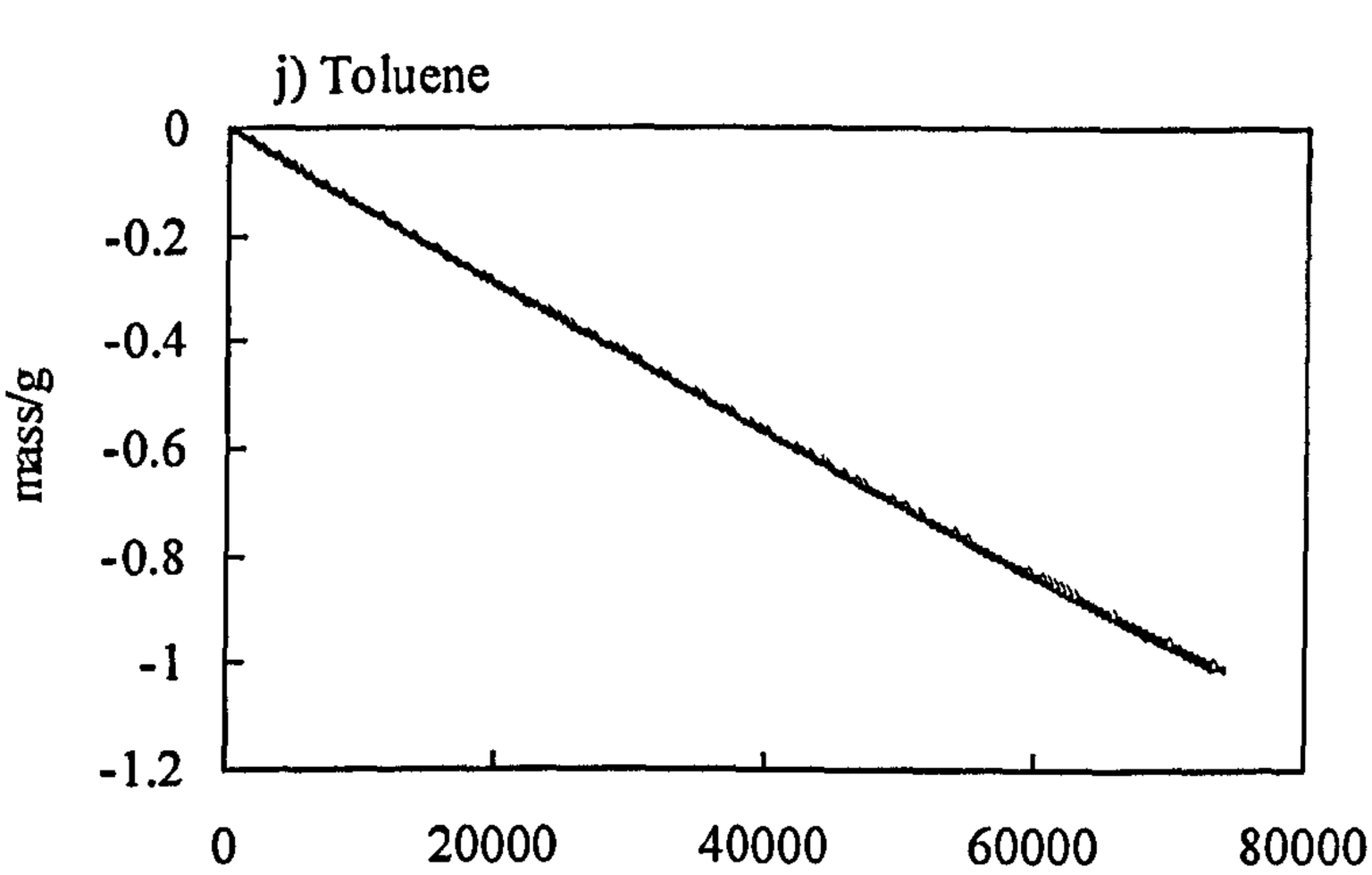

Table 3.1 shows a summary of vapour pressures, densities and diffusion coefficients for the range of liquids used in this study.

Liquid	P/Pa	ρ /kg m^{-3}	D_v/ 10^{-6} m^2 s^{-1}
squalane	0	806[4]	-
polydimethylsiloxane (PDMS)	0	998.5[5]	-
n-dodecane	18.0[6]	745.2[6]	5.0
n-decane	179.9[6]	726.4[6]	5.7
1,2 dichlorobenzene	592[7]	1300[8]	2.75
o-xylene	891[7]	867[8]	6.83
chlorobenzene	1554[7]	1100[8]	8.1
n-octane	1864[6]	698.6[6]	6.5
water	3167[6]	995.7[6]	22-24*
toluene	3786[8]	866.9[8]	7.8-8.2*
hexamethyldisiloxane (HMDS)	4887[5]	760[9]	6.51
1-bromobutane	5356[7]	1275.8[8]	7.58
n-heptane	6113[6]	679.5[6]	6.81
methylcyclohexane	6151[7]	769.4[8]	6.58
perfluoroheptane	10561.6[9]	1720.6[10]	4.83
benzene	12614[8]	876.5[8]	8.16
n-hexane	19812[6]	654.7[6]	8.27
cyclopentane	42296[8]	745.7[8]	7.9
n-pentane	77775.4[6]	621.2[6]	8.42

Table 3.1 **Summary of the densities, vapour pressures and diffusion coefficients of the liquids used in this work at 25 °C. Numbers above the data show the references from which the value was taken. The values marked with superscript* show the range of values obtained in measurements that were repeated 4 times.**

Figure 3.6 shows the mass loss curves of a range of solvents used in this work. Notice that the mass loss is related to the vapour pressure, P, of the liquids and that as P increases, the gradient of the mass loss, i.e. the evaporation rate, increases.

3.3 Conclusions

- A gravimetric method used for the determination of the evaporation rate of pure liquids and emulsions provides values of D_v within an uncertainty of 5%.
- Evaporation rates for pure liquids are consistent with the rate-limiting step being vapour diffusion across a stagnant vapour layer.

Figure 3.6 Mass loss curves of a range of pure solvents at 25°C.

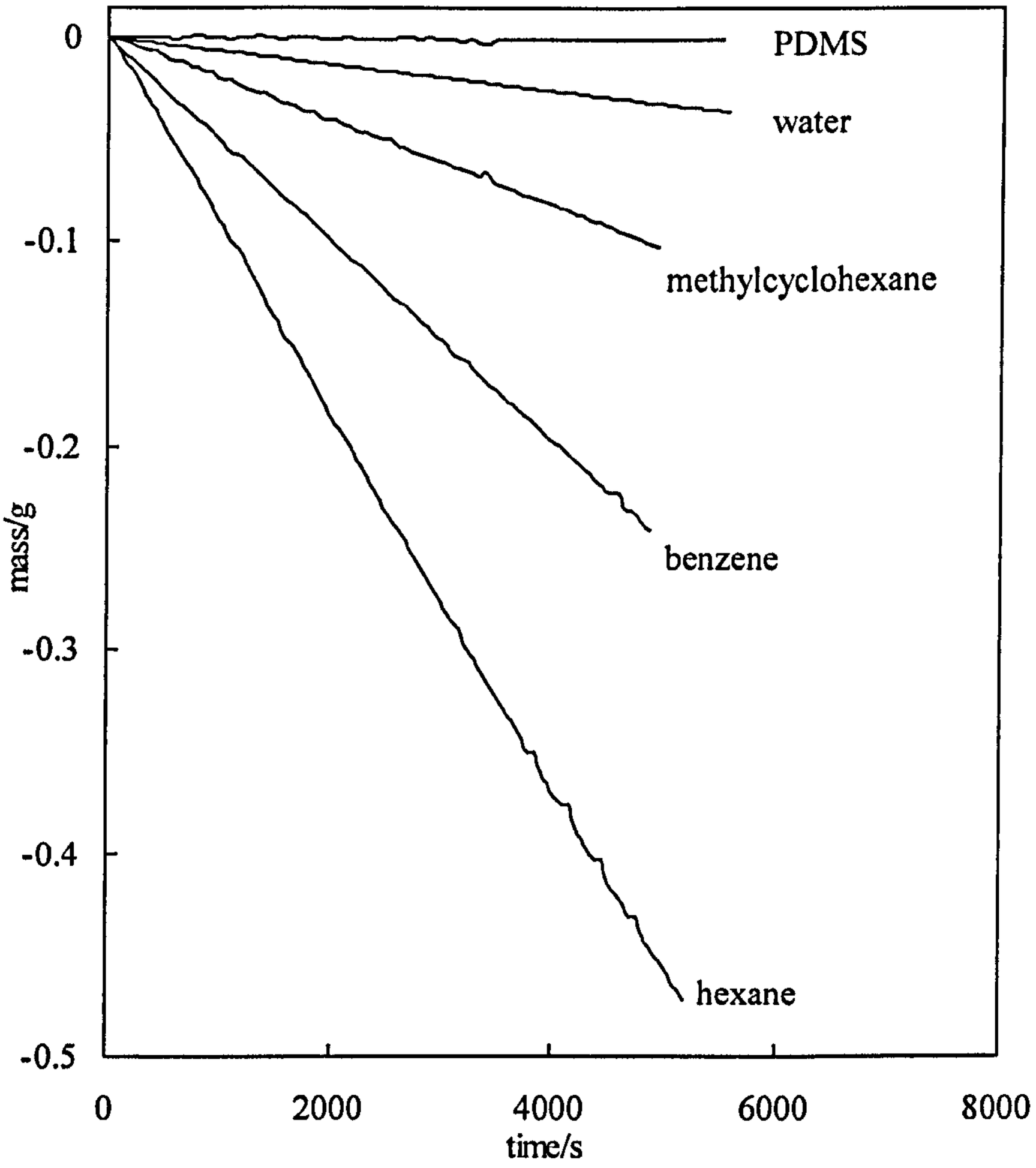

3.4 References

1 J. C. Maxwell, *Illustrations of the Dynamic Theory of Gases,* 1866. See also, *Physical Chemistry*, 6th edition, P.W. Atkins, Oxford University Press, 1998.

2 W. Jost, *Diffusion in Solids, Liquids and Gases*, Academic Press Inc., New York, 1952.

3 K. J. Beverley, J. H. Clint and P. D. I. Fletcher, *Phys. Chem. Chem. Phys.*, 1999, **1**, 149.

4 Sigma-Aldrich Database. See also www.Sigma-Aldrich.com.

5 M. J. Hunter, E. L. Warrick, J. F. Hyde and C. C. Currie, *J. Amer. Chem. Soc.*, 1946, **68**, 2284.

6 Selected Values of Properties of Hydrocarbons and related Compounds: Thermodynamics Research Center, AP 144, Texas A&M University, 1978.

7 D. R. Stull, *Ind. & Eng. Chem.*, 1947, **39**, p517.

8 RC *Handbook of Chemistry and Physics*, CRC Press Inc., Boca Raton, 62nd edn., 1981.

9 T. M. Reed, vol. V in *Fluorine Chemistry*, Ed J. H. Simons, Academic Press Inc., New York, 1964.

10 Fluorochem database.

Chapter 4

CHAPTER 4

EVAPORATION RATES OF SURFACTANT-STABILISED CREAMED EMULSIONS

4.1 Introduction

In this Chapter, evaporation rates of both the continuous phase and the dispersed phase from creamed emulsions stabilised by low molar mass surfactants and high molecular weight polymers will be discussed. As explained in Chapter 1, the emulsions contain dispersed micron-size drops of either oil (o/w), or water (w/o), within the continuous phase and although thermodynamically unstable, they may be made kinetically stable by the presence of a suitable surfactant which adsorbs at the drop surfaces. Due to the instability, emulsions may break into two separated phases. One contributing mechanism is the creaming process, where in o/w emulsions the less dense oil phase drops move up to the top forming a concentrated layer of oil drops at the surface.

The emulsions examined here were all nonflocculated and stable to coalescence of the dispersed drops. The drops creamed in typically 10-15 minutes to form a top cream layer rich in dispersed drops (oil in o/w and water in w/o) above a drop-free continuous

phase layer. The depth of the cream layer was dependent on the overall volume fraction of the dispersed phase in the emulsion, which was between 5 and 30 vol%.

For the emulsions of the type considered here, the equilibrium vapour pressures of both the continuous and dispersed phase are practically equal to the values of bulk, pure liquids. In principle, for the continuous phase, one might expect a slight vapour pressure lowering from the dissolved surfactant or polymers. However, this reduction is insignificant for the low surfactant/polymer concentrations in the continuous phase used here. For the dispersed drops, one might expect a small increase of the droplets vapour pressure due to the Kelvin effect[1]. The so-called Kelvin equation compares the equilibrium vapour pressure of a drop with the vapour pressure of the same liquid at plane surface and is given by the following expression,

$$\frac{P}{P_0} = \exp\left(\frac{2\gamma V}{RT} \cdot \frac{1}{r}\right) \qquad [4.1]$$

where P is the vapour pressure of the droplet of radius r, P_0 the vapour pressure of the flat surface and γ and V are the surface tension and the molecular volume of the pure liquid respectively, R is the gas constant and T is the absolute temperature. Figure 4.1 shows the magnitude of the drop curvature effect for pure water as a function of droplet radius. For pure water droplets with radius of 0.1 μm for example, the ratio P/P_0 is found to be 1.01. Therefore it can be concluded that the vapour pressure of the drops dispersed in the emulsions concerned in this work (with radii of 10-25 μm), is virtually the same as that of bulk liquids. The interfacial tension is also lower that the air-water tension.

The main key questions addressed in this Chapter are, whether the evaporation rate of the continuous phase (water in o/w and oil in w/o emulsions) is affected if compared to bulk liquids and how the drops get to the vapour phase during the dynamic evaporation process.

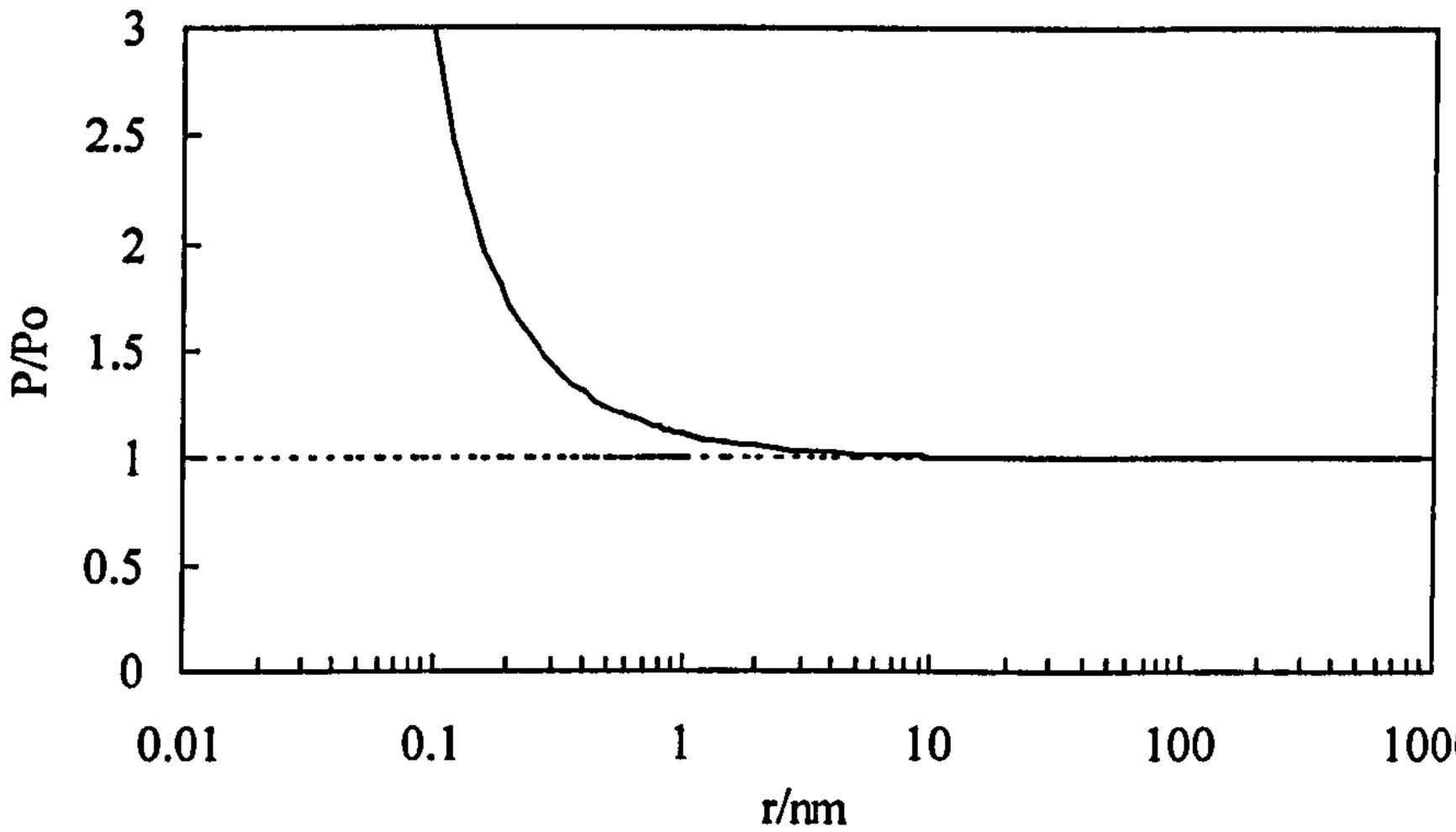

Figure 4.1 **Variation of the vapour pressure of a water drop with respect to that of bulk water determined by the Kelvin equation ($\gamma = 71.9$ mN m^{-1}).**

In discussing the evaporation of dispersed oil drops, it is relevant to consider the possible fates of the oil drops at an air-water surface. As shown in Figure 4.2, an oil drop may either enter (mechanism 1) or not enter the surface[2] (mechanism 2). If entry occurs, the drop may either spread or remain as a lens on the surface. If entry does not occur, oil transport to the vapour phase must involve passage of oil through a thin asymmetric oil-water-vapour film.

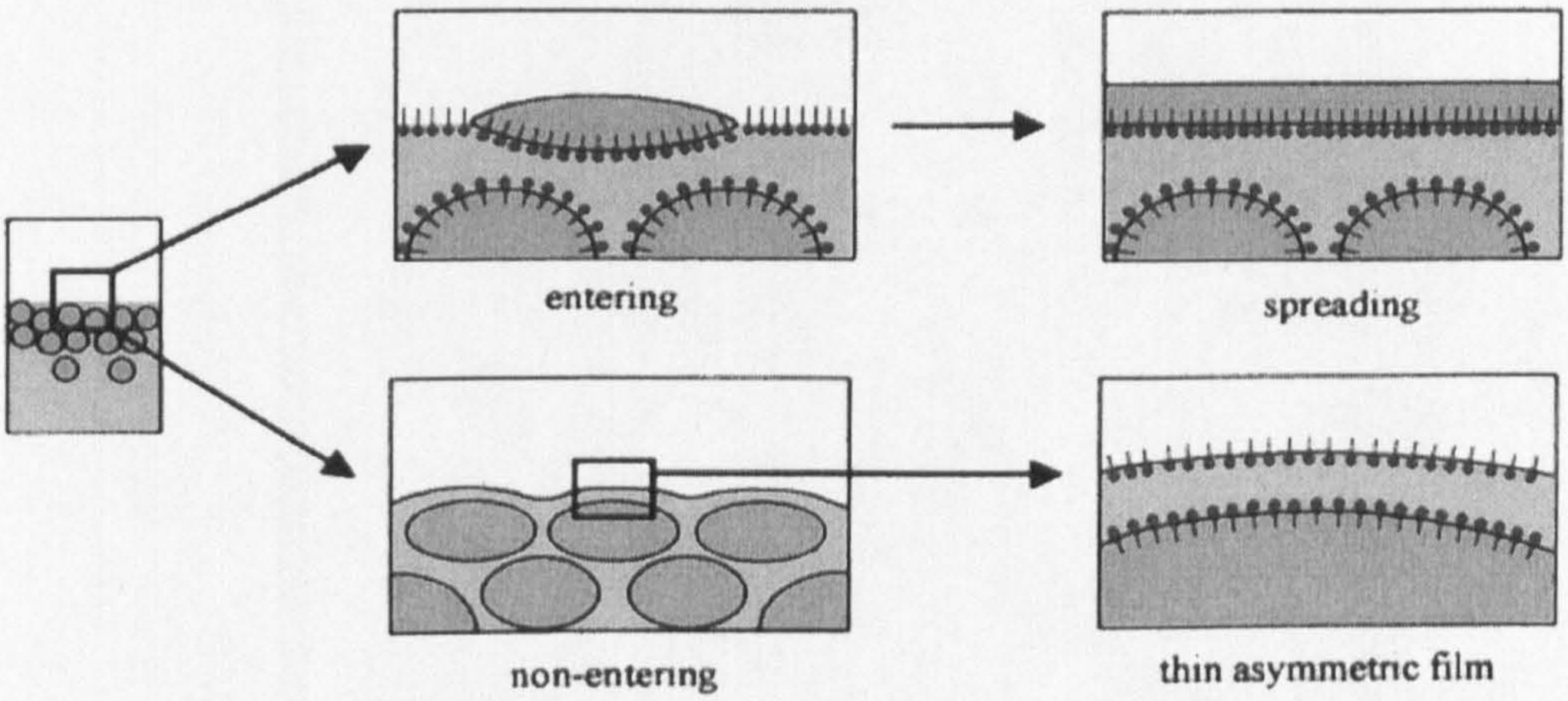

Figure 4.2 Possible fates of oil drops at the air-vapour surface.

The thermodynamic feasibility of drop entry and spreading is determined by the so-called entry and spreading coefficients, E_n and S respectively, and these depend on the three tensions involved:

$$E_n = \gamma_{wv} + \gamma_{ow} - \gamma_{ov} \qquad [4.2]$$

$$S = \gamma_{wv} - \gamma_{ow} - \gamma_{ov} \qquad [4.3]$$

where γ_{wv}, γ_{ow} and γ_{ov} are the interfacial tensions of the water-vapour, oil-water and oil-vapour interfaces respectively (see Figure 4.3). Entry of the drop is feasible if E_n is positive and the drop will spread if S is positive. In addition to their thermodynamic feasibility, the kinetics of these processes may be limited by the repulsive colloidal forces acting across the asymmetric oil-water-vapour film.

If drops must enter the surface before evaporation (mechanism 1) one would expect the evaporation rates of different systems to correlate with the values of E_n (determined by the three interfacial tensions) together with the magnitudes of the colloidal forces determining the kinetic feasibility of entry. For non-entering oils, evaporation can only occur by the transport of molecular oil across the oil-water-vapour film (mechanism 2).

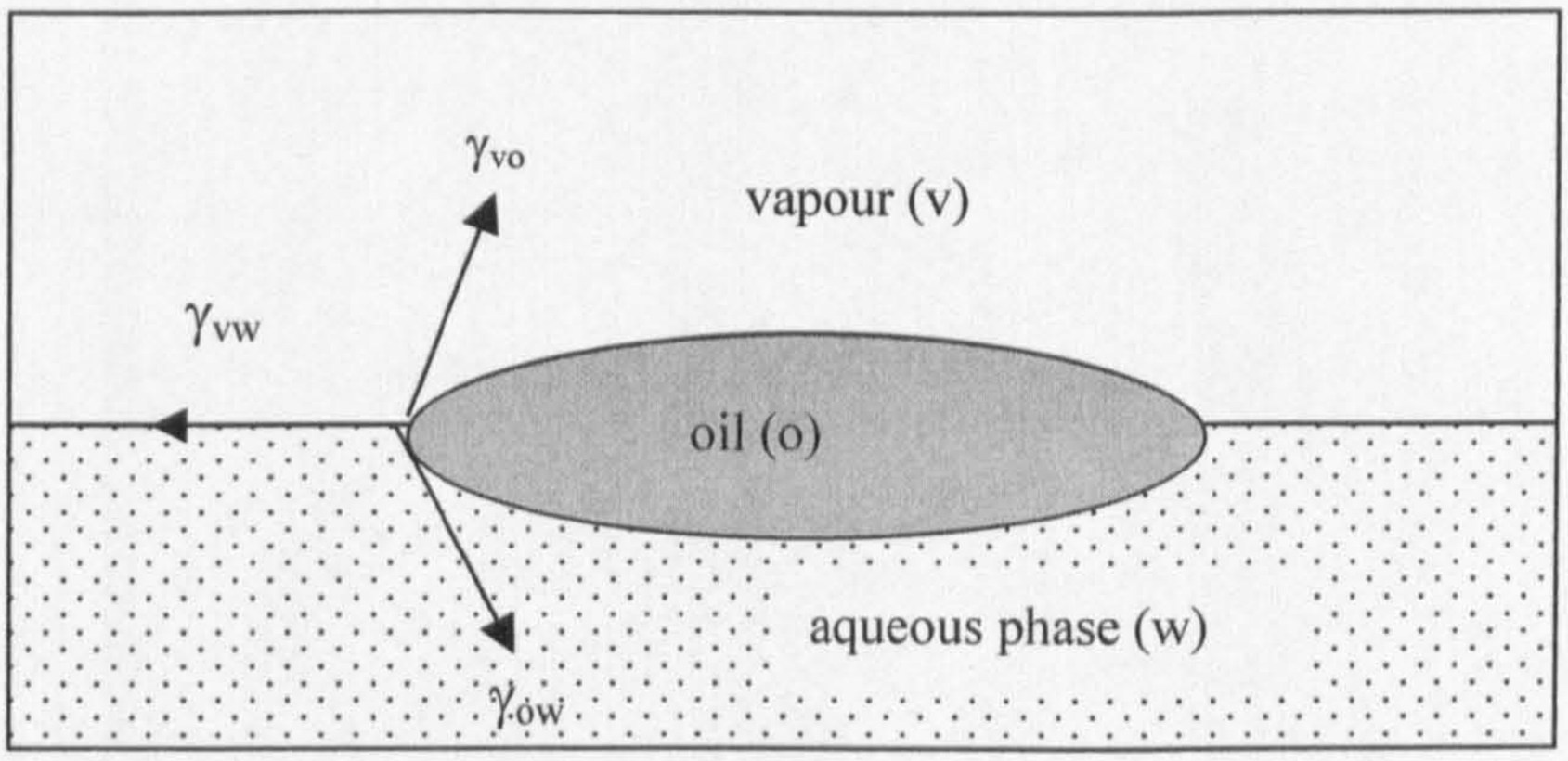

Figure 4.3 An oil lens resting at a vapour/water interface.

In the case of mechanism 2 the evaporation rate of the dispersed phase should depend on the film thickness (controlled by colloidal forces) and on the oil solubility in water. To discriminate between mechanisms 1 and 2, we have determined evaporation rates of a series of emulsion systems containing oils whose solubility in water varies over many orders of magnitude and which are stabilised by different surfactants (ionic, anionic and polymeric).

Evaporation rates of creamed o/w emulsions have been analysed according to the following model,

$$E = E_{water} + f.E_{oil} \qquad \text{when oil is present}$$

$$E = E_{water} \qquad \text{when all oil is evaporated} \qquad [4.4]$$

where E_{water} and E_{oil} are the evaporation rates of pure water and oil under the same experimental conditions. The factor f is an adjustable factor in the range of 0 to 1 which reflects the magnitude of the energy barrier to transfer oil from the emulsion drops to the vapour phase. A value of f = 1 corresponds to zero energy barrier whereas f less than 1 corresponds to a finite barrier. The differential equation for the rate of total mass loss from an emulsion sample has been derived by K. J. Beverley[3] and is given below:

$$E_{emul} = \frac{A(\alpha+\beta)}{\left(h_t - \left(\left(\frac{1}{\rho_0\rho_w A}\right)\left(\left(m_0^i\rho_w + \frac{\beta m\rho_w}{(\alpha+\beta)}\right) + \left(m_w^i\rho_0 + \frac{\alpha m\rho_0}{(\alpha+\beta)}\right)\right)\right)RT\right)} \qquad [4.5]$$

where h_t is the inner height of the sample tube, m is the total remaining mass reading from the balance, m^i and ρ are the initial mass and the density of each component, (w is with respect to the water and o is with respect to the oil), α is equal to the term MDPz for the water and β is equal to fMDPz for the oil. An integrated form of equation [4.5] was used to fit experimental curves of mass versus time. The VBA code used for this fitting is shown in Appendix (AIII.2).

Figure 4.4 shows an example of the spreadsheet used to fit emulsion evaporation rate data. In this case, measurement conditions (the same as for pure liquids plus the oil volume fraction) and the physico-chemical properties of both liquids are given in the boxed cells. In principle for emulsions, the only unknown parameter requiring fitting is f.

Figure 4.4 **The spreadsheet configuration used to fit the data of mass versus time for an emulsion. The results here refer to 20 vol% methyl-cyclohexane-in-water emulsion stabilised by 20 mM SDS at 25 °C. Experimental data (solid) and the best-fit calculated (dashed line) obtained by floating the oil volume fraction and the initial mass are compared in the plot.**

..\aranberri\emulsion evaporation fitting mch-sds1

20 vol% methylcyclohexane in 20 mM SDS emulsion in sample tube 1, rig 1, run 105, MCH-SDS1,flow rate 1743 ml min-1

GENERAL CONSTANTS TUBE CONSTANTS

R/ JK^{-1} mol^{-1}	T/K	A_{tube} / m^2	h_t / m	vol fraction oil
8 31451	298.15	2.56E-04	0 0385	0.193402042

OIL CONSTANTS methylcyclohexane floated

ρ_{oil} / kg m^{-3}	M_{oil}/ kg mol^{-1}	D_{oil}/ m^2 s^{-1}	P_{oil} / Pa	Z_{oil}	m_o^i / kg	f	time residual sum/s
769.4	0.096	6.58E-06	6151	1.031640006	0.000705779	0.59	0 00699

WATER CONSTANTS Ind&Eng floated measured

ρ_{water}/ kg m^{-3}	M_{water}/ kg mol	D_{water}/ m^2 s^{-1}	P_{water}/ Pa	Z_{water}	m_w^i / kg	total emulsion mass/ kg	total emulsion mass/ kg
995 67	0.018	2.40E-05	3167 21	1 015962464	0.003809152	0 004514931	0.00389

floated

expt *time/s*	expt *mass/g*	zero corrected *mass/g*	calc *time/s*	calc *time resid/s*
0	4.5149	0	-0	0
60.48	4.5007	-0.014231216	736.323	675.8426893
121.50	4.5002	-0.014731216	762.237	640.7369369
182.52	4.4984	-0.016531216	855.553	673.0331813
243.54	4.4977	-0.017231216	891.853	648.3133279
304.46	4.4966	-0.018331216	948.908	644.4483505
365.53	4.4956	-0.019331216	1000.79	635.2591677
426.50	4.4946	-0.020331216	1052.68	626.1819831
487.52	4.4938	-0.021131216	1094.2	606.6849587
548.55	4.4927	-0.022231216	1151.31	602.7615275
609.51	4.4918	-0.023131216	1198.05	588.5359061
670.53	4.4908	-0.024131216	1249.98	579.454481
731.50	4.4898	-0.025131216	1301.94	570.4350054
792.47	4.4898	-0.025131216	1301.94	509.4650347
853.49	4.4889	-0.026031216	1348.7	495.2108463
914.46	4.4878	-0.027131216	1405.87	491.4122247
975.48	4.4878	-0.027131216	1405.87	430.3922052
1036.50	4.4849	-0.030031216	1556.67	520.1665792
1097.47	4.4849	-0.030031216	1556.67	459.1966085
1158.55	4.4828	-0.032131216	1665.93	507.3755455
1219.51	4.4828	-0.032131216	1665.93	446.4155846
1280.48	4.4828	-0.032131216	1665.93	385.4456139
1341.50	4.4803	-0.034631216	1796.06	454.5649809
1402.47	4.4803	-0.034631216	1796.06	393.5950102
1463.55	4.4779	-0.037031216	1921.07	457.5194366
1524.52	4.4768	-0.038131216	1978.39	453.8663408
1585.48	4.4768	-0.038131216	1978.39	392.9063798

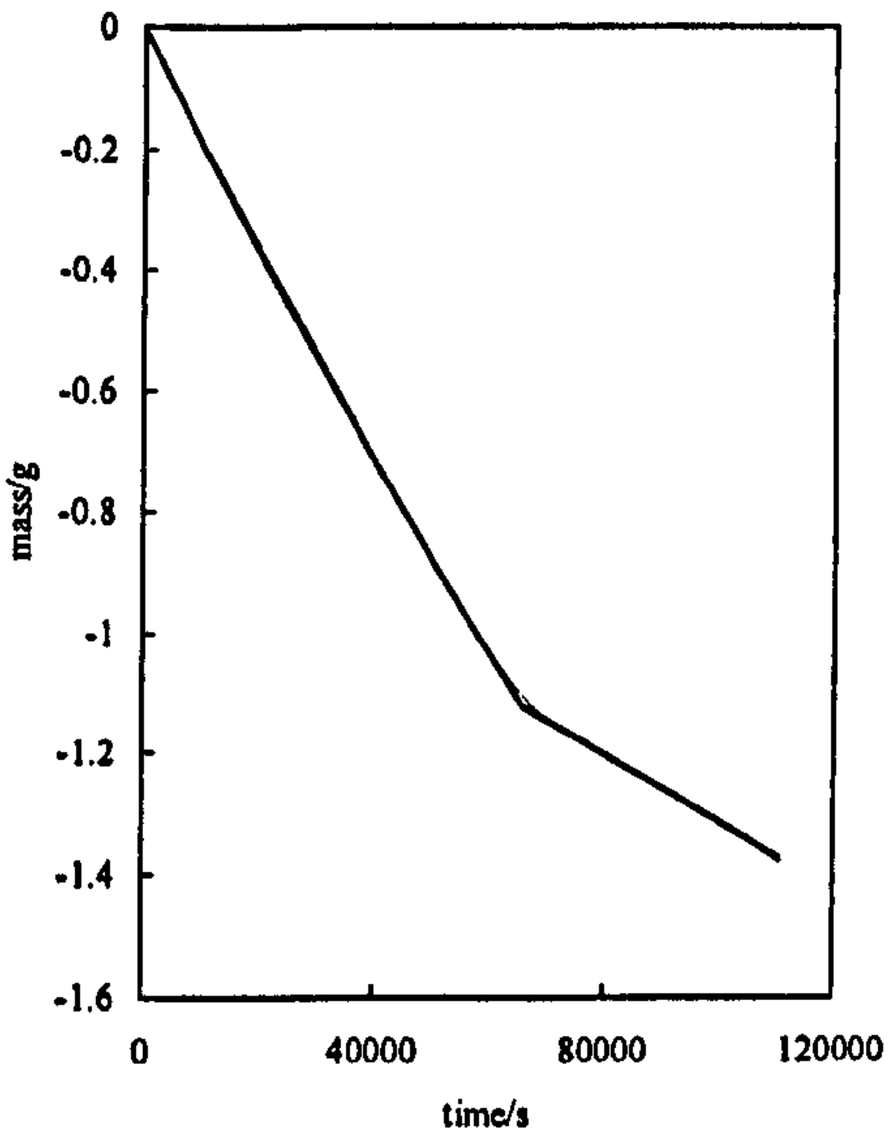

However, it was found that minor fitting adjustments were generally also required for the initial sample mass and the oil volume fraction. These adjustments were generally within the experimental uncertainties in these quantities which arise because of small mass losses from the sample during loading into the measurement apparatus.

4.2 Evaporation rates of creamed o/w emulsions

4.2.1 Evaporation rate of the continuous aqueous phase

Initially, the mass loss of an o/w emulsion containing an involatile oil was measured. In this case, the measured mass loss curve would only arise from the loss of the continuous water. For such experiment squalane was chosen. In order to confirm that squalane is involatile at 25 °C the mass loss of squalane over 12 h was measured. The experiments (see Figure 4.5) confirmed that the vapour pressure of squalane is negligible at 25 °C and no mass loss was recorded. Next, using an emulsion containing the involatile oil squalane, it was established that the evaporation rate of the water continuous phase in an emulsion is identical to that of pure water under the same conditions, that is, gas flow rate, sample tube geometry and stagnant thickness h. Figure 4.6 shows a comparison of the measured mass loss versus time curve for a squalane-in-water emulsion with a theoretical curve calculated according to equation [3.14] using the known sample masses, tube dimensions and parameter listed for water in Table 3.1. The measured curve agrees very closely with the calculated using no adjustable parameters, thereby providing strong evidence that the evaporation rate of the continuous phase is

Figure 4.5 Mass loss curve of squalane over 12 h.

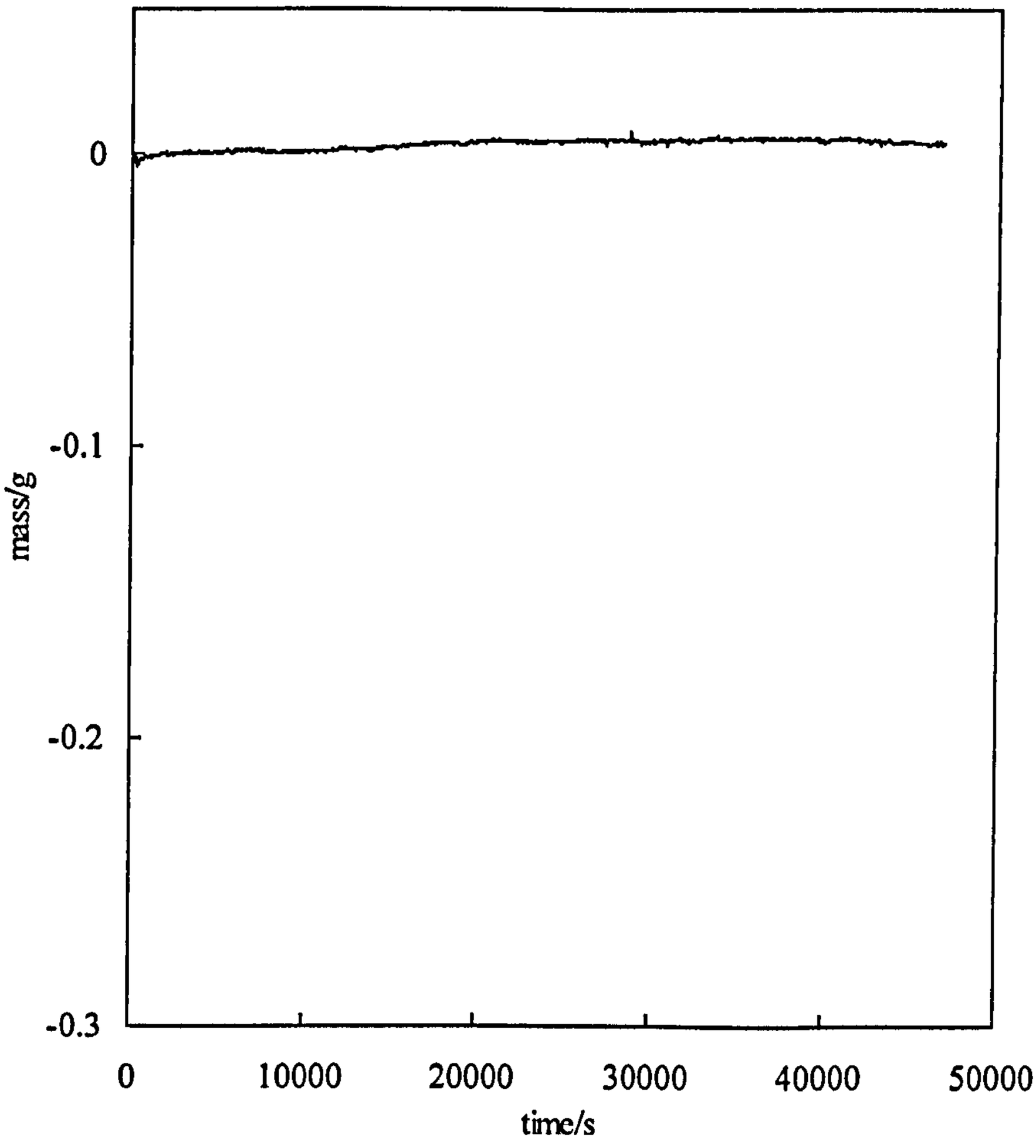

Figure 4.6 **Mass loss versus time for a squalane-in-water emulsion (20 vol%) stabilised by 20 mM SDS. The calculated curve, using a value of Dv for water of 2.31 x 10^{-5} m^2s^{-1}, corresponds to the evaporation of water alone and overlies the experimental data.**

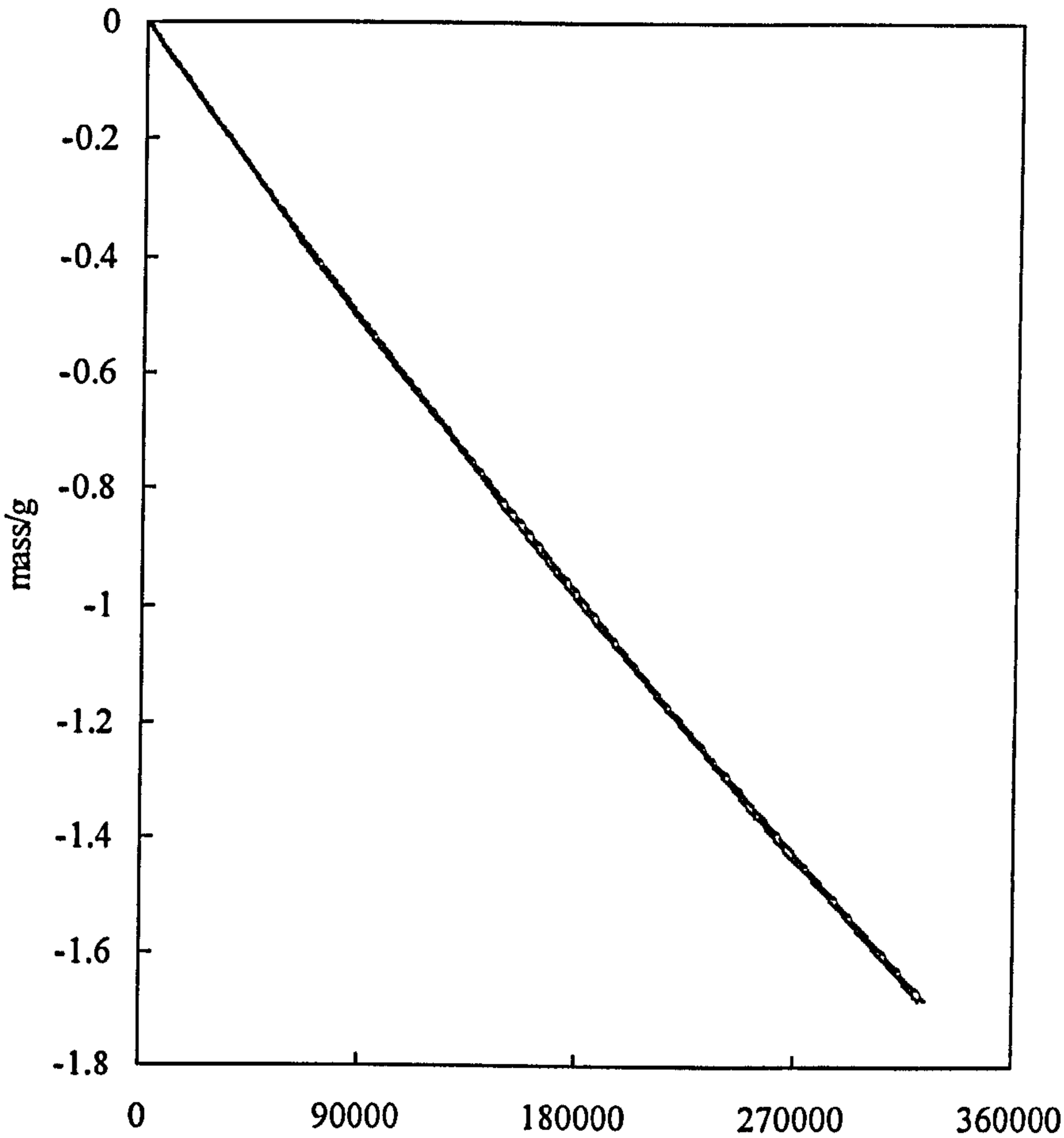

identical to that of pure water and that the evaporation rate of the water is unaffected by emulsification.

4.2.2 Effect of the surfactant type: Electrostatic and steric repulsions

For creamed emulsions containing a volatile oil, the mass loss curves show a two-stage decay. In the first stage, all the curves show an initial high slope corresponding to the sum of the evaporation rates of the water continuous phase plus the evaporation of the disperse oil phase, the latter one being slowed down by a factor equal to f. In the second stage, when all the oil has evaporated, the lower slope corresponds to the evaporation of water alone. Figure 4.7 shows an illustrative example of a two-stage mass loss curve fitted using equation [4.5] with f as the only adjustable parameter. For the calculations of the fits, values of the densities and vapour pressure were taken from Table 3.1. Diffusion coefficients were determined separately from measurements of the evaporation rate of the pure liquid components (see Chapter 3).

In order to confirm the validity of the model, the effect of variation of the volume fraction of the dispersed oil in the emulsions has been studied. Figure 4.8 shows the mass loss curves for different toluene volume fractions in 20 mM SDS stabilised emulsions and their respective best-fit curves. Within the estimated precision of f (= 10% or so) the fitted values of f (shown in Table 4.1) are not significantly affected by the oil volume fraction.

Figure 4.7 **Experimental and fitted mass loss curves for an emulsion containing 20 vol% of heptane stabilised by 20 mM SDS. The best-fit value of f is 0.26.**

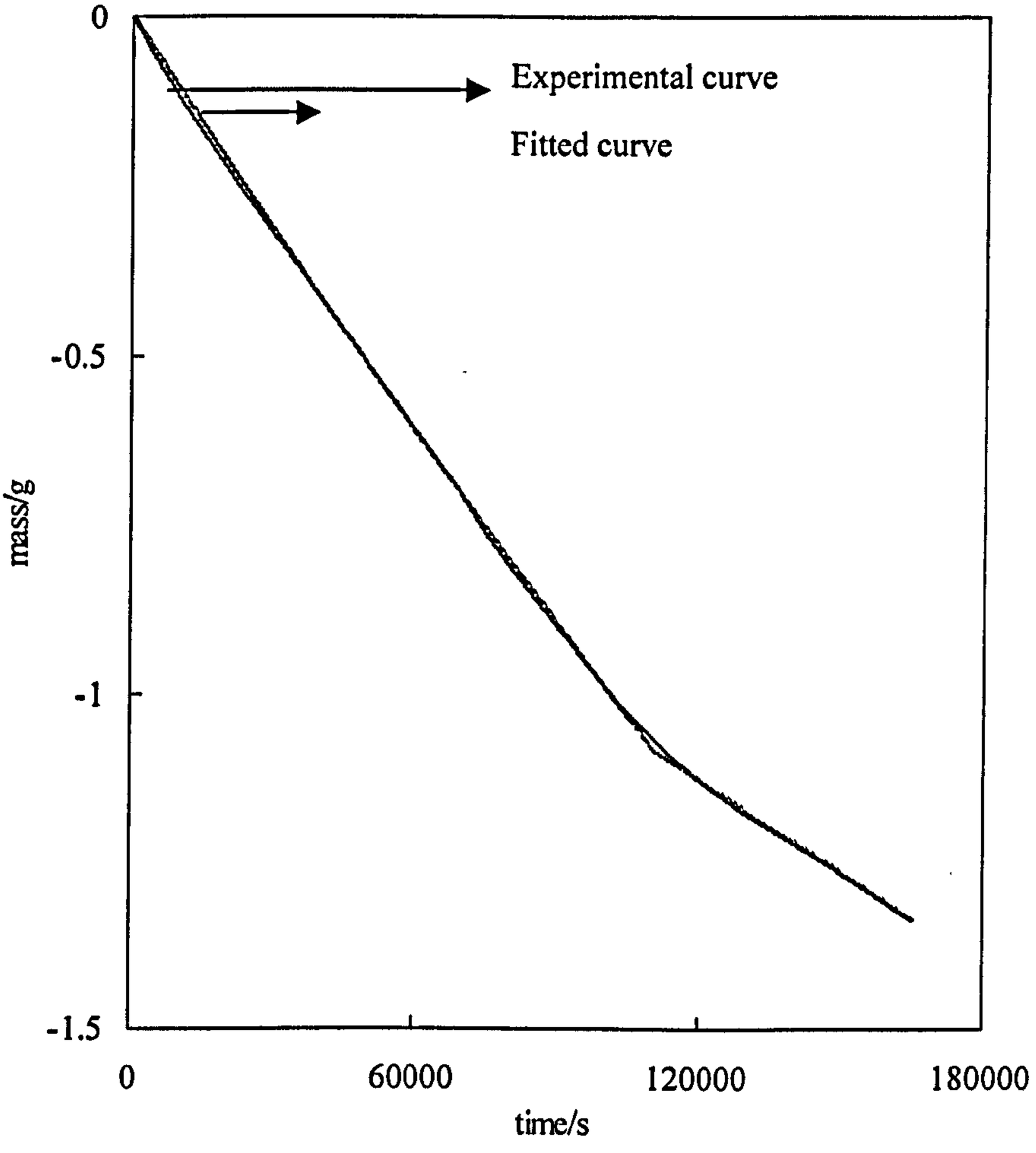

Figure 4.8 Mass loss curves for 8, 18 and 26 vol % toluene-in-water emulsions stabilised by 20 mM SDS. The experimental data and fitted curves (corresponding to the best-fit value of $f = 0.85 \pm 0.08$) are compared.

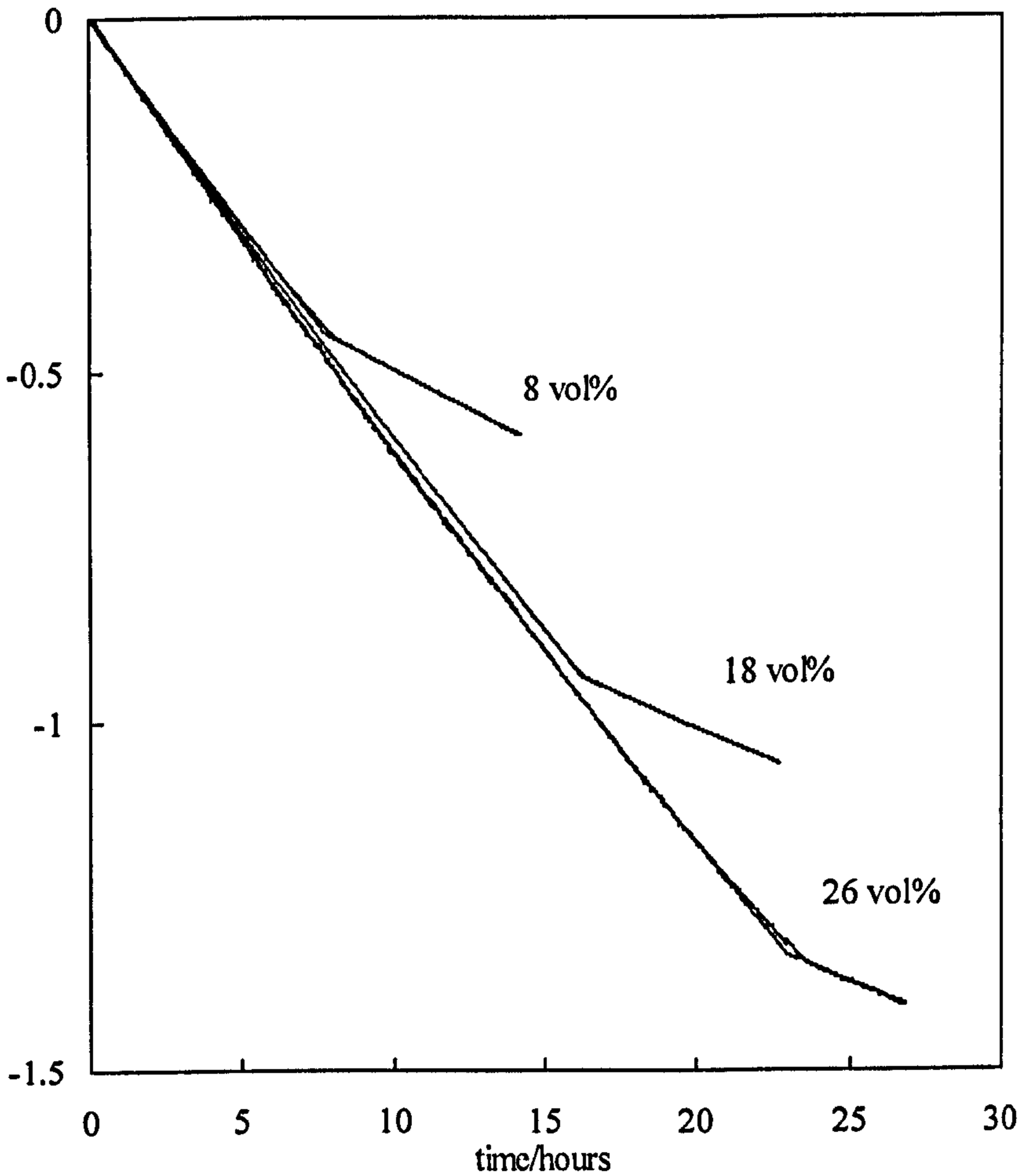

Figure 4.9 shows the mass loss curve for 20 vol% toluene-in-water emulsions stabilised by 8 mM (cmc) and 20 mM SDS (above the cmc) and their respective best fit curves. The latter concentration was selected in order to study whether the micelle formation may affect the evaporation rate of the dispersed oil drops. Table 4.1 also shows f values determined for toluene-in-water emulsions stabilised by different SDS concentrations and, as can be seen, f is hardly affected by the presence of micelles.

ϕ_o	[SDS] aq./mM	f
0.08	20	0.79
0.2	8	0.96
0.18	20	0.86
0.26	20	0.92

Table 4.1 Summary of f values determined for toluene-in-water emulsions containing different oil volume fractions and SDS concentrations.

After determining the evaporation rate of the continuous aqueous phase, and observing that the proposed model works, the next step was to study the evaporation rate of the dispersed drops (either water or oil) and the mechanism whereby the droplet material is transported to the vapour phase. As mentioned in the introduction of this Chapter the possible mechanisms by which dispersed oil may transport to the vapour phase may involve either (1) drop entry and/or spreading or (2) oil transport across the thin oil-water-vapour film for non-entering oil drops.

Figure 4.9 **Mass loss curves for toluene-in-water emulsions stabilised by SDS (8 and 20 mM). The experimental (solid line) and calculated for each curve are overlaid. m_0 (8 mM) = 3.75 g, m_0 (20 mM) = 3.85 g**

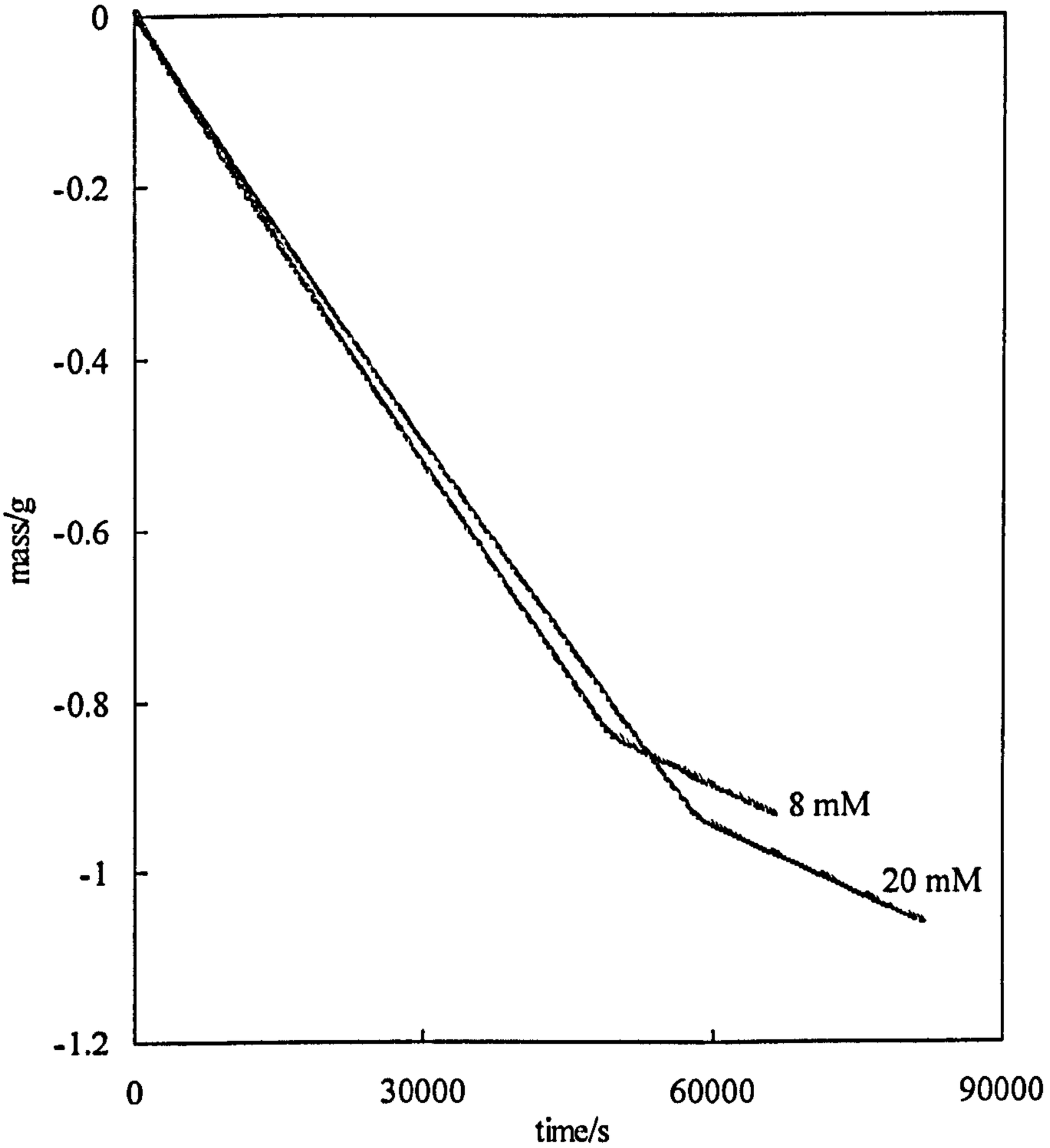

If mechanism (1) operates, the evaporation rates for different emulsions are expected to correlate with the entry coefficients and the magnitude of the colloidal forces affecting the drop entry rate. If mechanism (2) operates, the evaporation rates should correlate with the solubility of oil in the aqueous phase and with the oil-water-vapour film thickness (affected by colloidal forces). In order to attempt to distinguish between possibilities (1) and (2) and eliminate one of them, evaporation rates of emulsions containing oils with solubility in water ranging from 2.23×10^{-2} M (benzene) to 5.70×10^{-6} M (HMDS) have been measured. In addition, rates for emulsions stabilised by ionic surfactants (dodecyl sulphate (SDS) and cetyltrimetyl ammonium (CTAB), for which electrostatic repulsion is expected to produce relatively thick oil-water-vapour films), and non-anionic surfactants (decyl-β-D glucoside (DBG) and polyvinyl alcohol (PVA) for which the films should be thinner) have been measured and compared. Table 4.2 shows a summary of the oils used in this Chapter with their respective solubilities in water.

Liquid	S/M	Reference
benzene	2.28×10^{-2}	4
toluene	5.85×10^{-3}	4
cyclopentane	2.23×10^{-3}	4
o-xylene	1.65×10^{-3}	4
methylcyclohexane	1.43×10^{-4}	4
hexane	1.10×10^{-4}	4
heptane	2.93×10^{-5}	4
octane	5.79×10^{-6}	4
HMDS	5.70×10^{-6}	5

Table 4.2 Values of solubility (at 25 °C) in water for the oils used in this Chapter.

a) Electrostatic effects on the water film thickness

Figures 4.10 (a-f) show experimental and fitted mass loss curves for emulsions containing different oils and stabilised by SDS (anionic), CTAB (cationic) and DBG (non-ionic). The mass loss curves were accurately fitted using an integrated form of equation [4.5] with f the only adjustable parameter. Table 4.3 shows a summary of the f values obtained by fitting the mass loss curves. Measurements were made only for emulsion systems for which the volatilities of the oils were significant compared with that of water, thereby giving a significant change in mass loss rates with and without oil. This is necessary to ensure that f is determined reasonably accurately. The observed correlation between f and the oil solubility in water suggests that the oil evaporation involves mass transport of dissolved oil through the water film present at the emulsion surface, that is, evaporation occurs by mechanism (2).

	f		
Oil	**SDS**	**CTAB**	**DBG**
benzene	0.93	0.99	1.03
toluene	0.86	0.86	Coalescence observed
methylcyclohexane	0.58	0.6	0.93
cyclopentane	0.54	0.56	Coalescence observed
hexane	0.38	0.41	0.65
octane	0.35	0.23	0.56
heptane	0.26	0.34	0.53
HMDS	0.08	0.09	0.11

Table 4.3 Summary of f values determined for 20 vol% o/w emulsions stabilised by 20 mM surfactant.

Figure 4.10 **Mass loss curves of a range of o/w emulsions stabilised by SDS, CTAB and DBG (20 mM). The experimental data and the fitted curve are compared.**

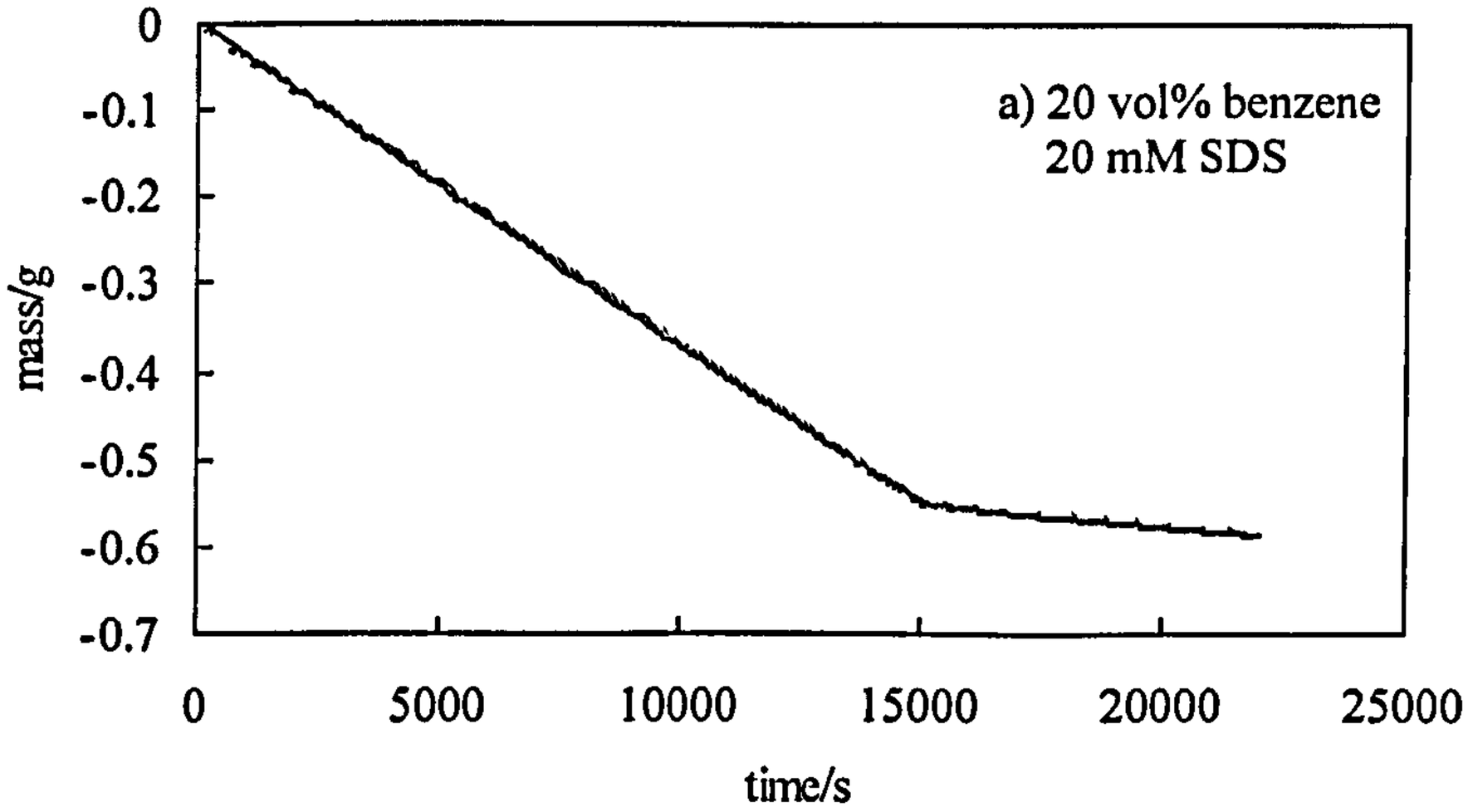

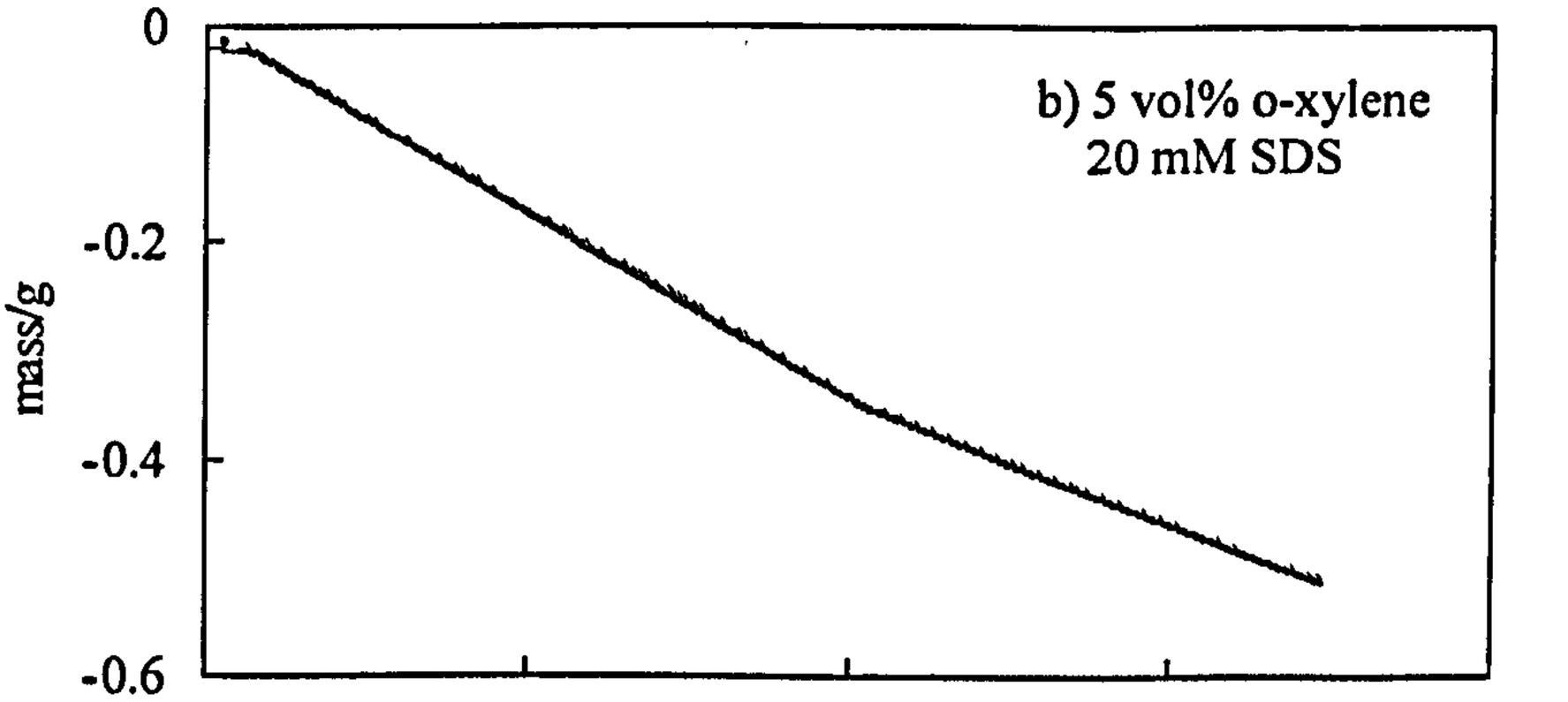

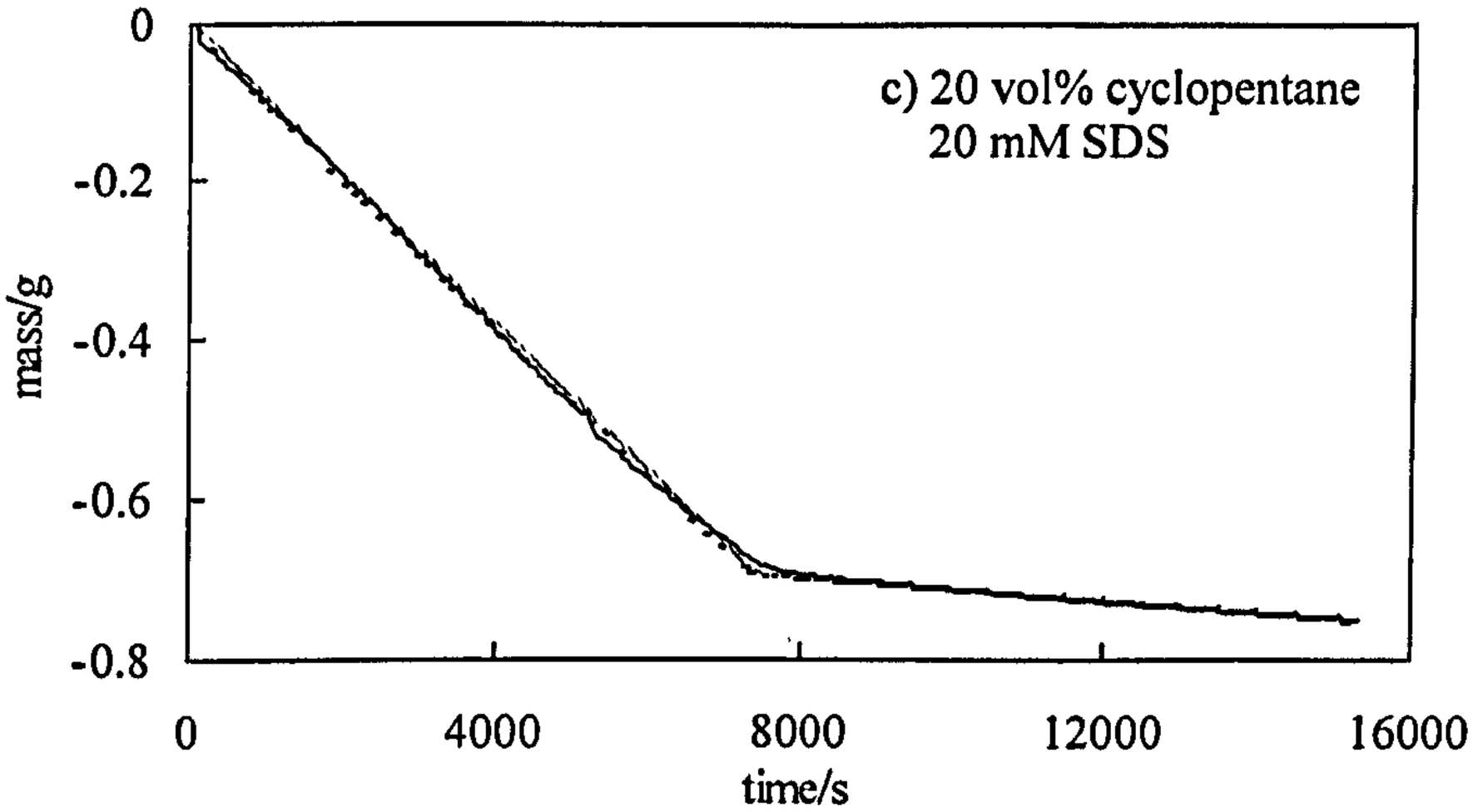
c) 20 vol% cyclopentane
20 mM SDS
mass/g
0
-0.2
-0.4
-0.6
-0.8
0
4000
8000
12000
16000
time/s

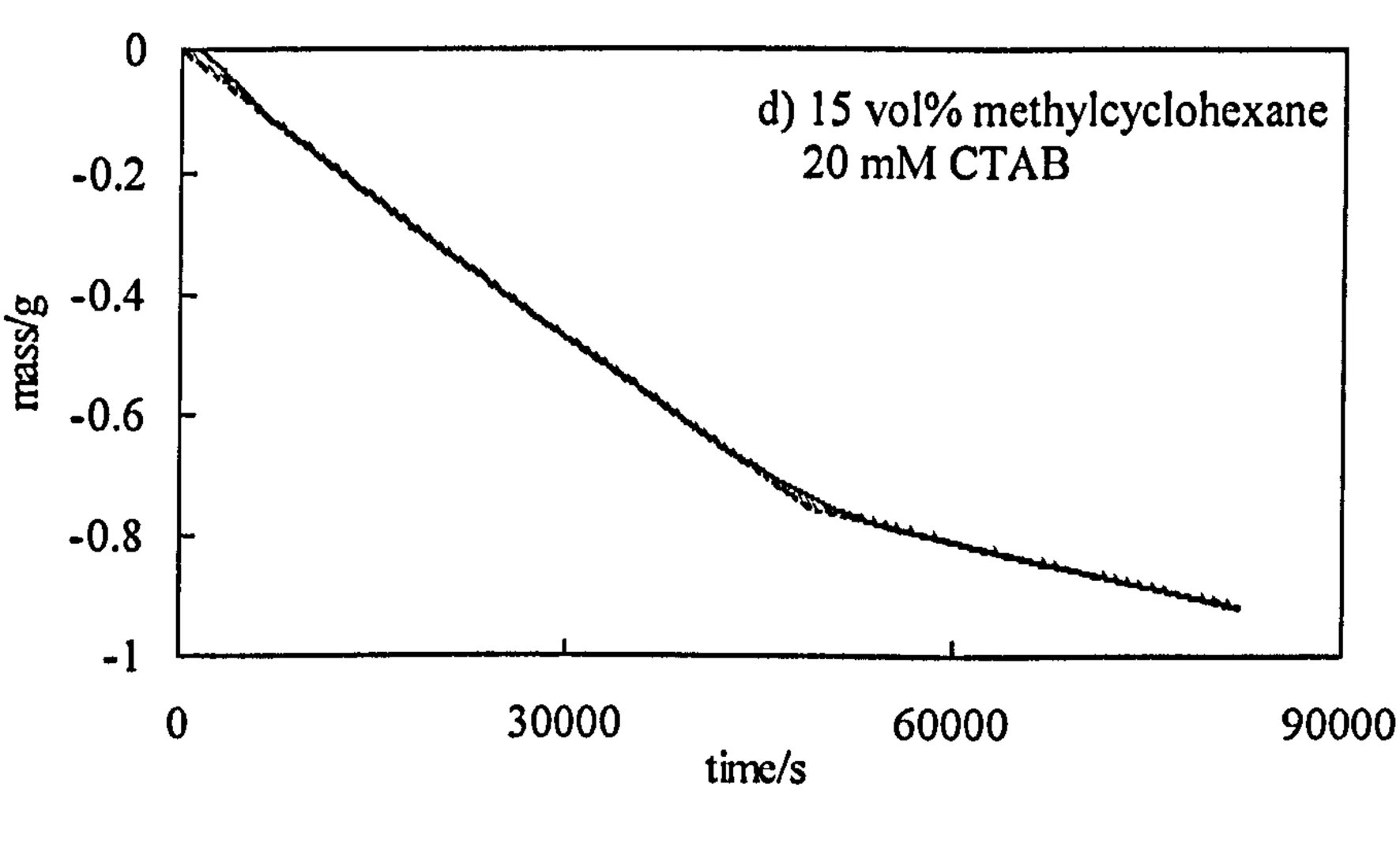
d) 15 vol% methylcyclohexane
20 mM CTAB
mass/g
0
-0.2
-0.4
-0.6
-0.8
-1
0
30000
60000
90000
time/s

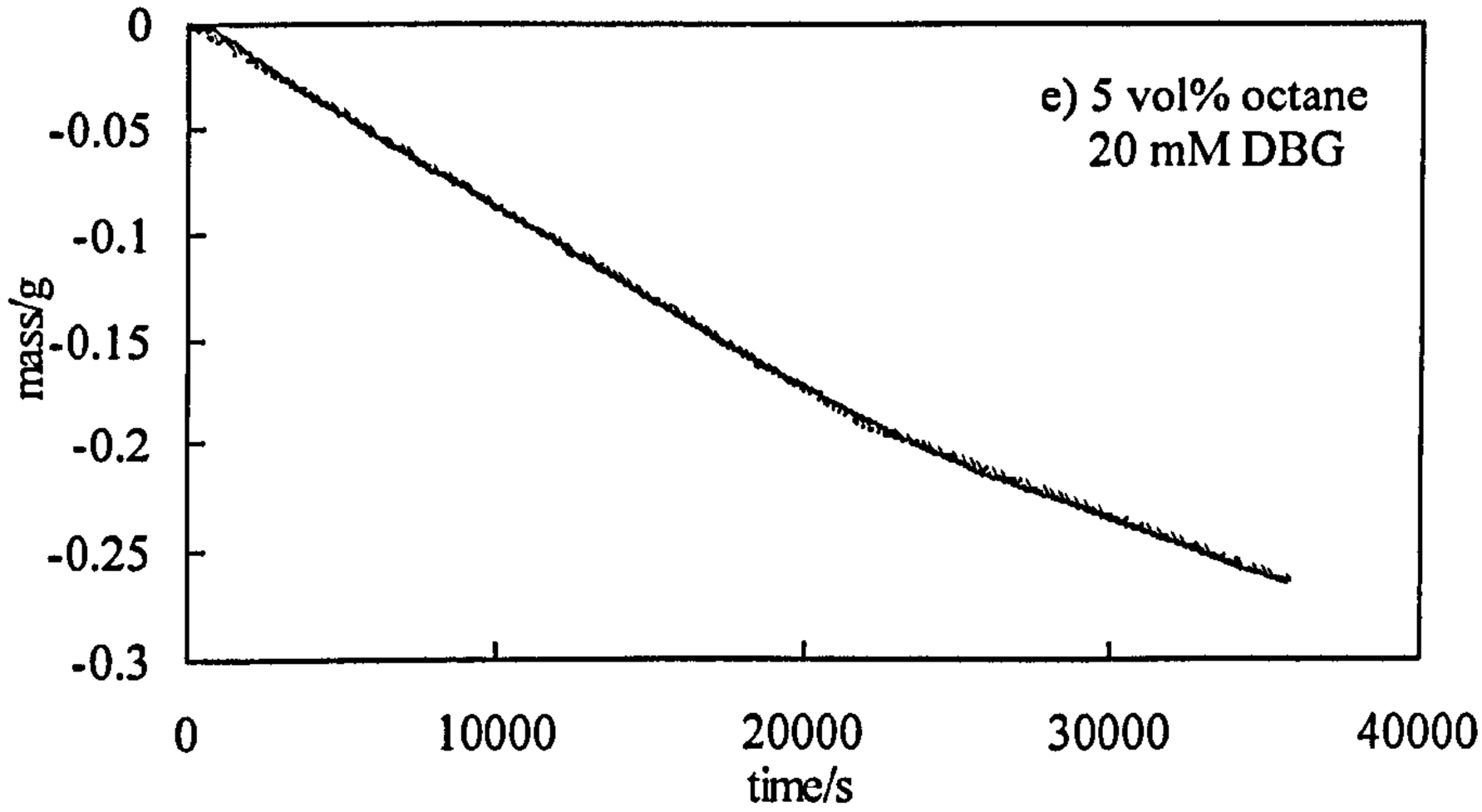
e) 5 vol% octane
20 mM DBG
mass/g
0
-0.05
-0.1
-0.15
-0.2
-0.25
-0.3
0
10000
20000
30000
40000
time/s

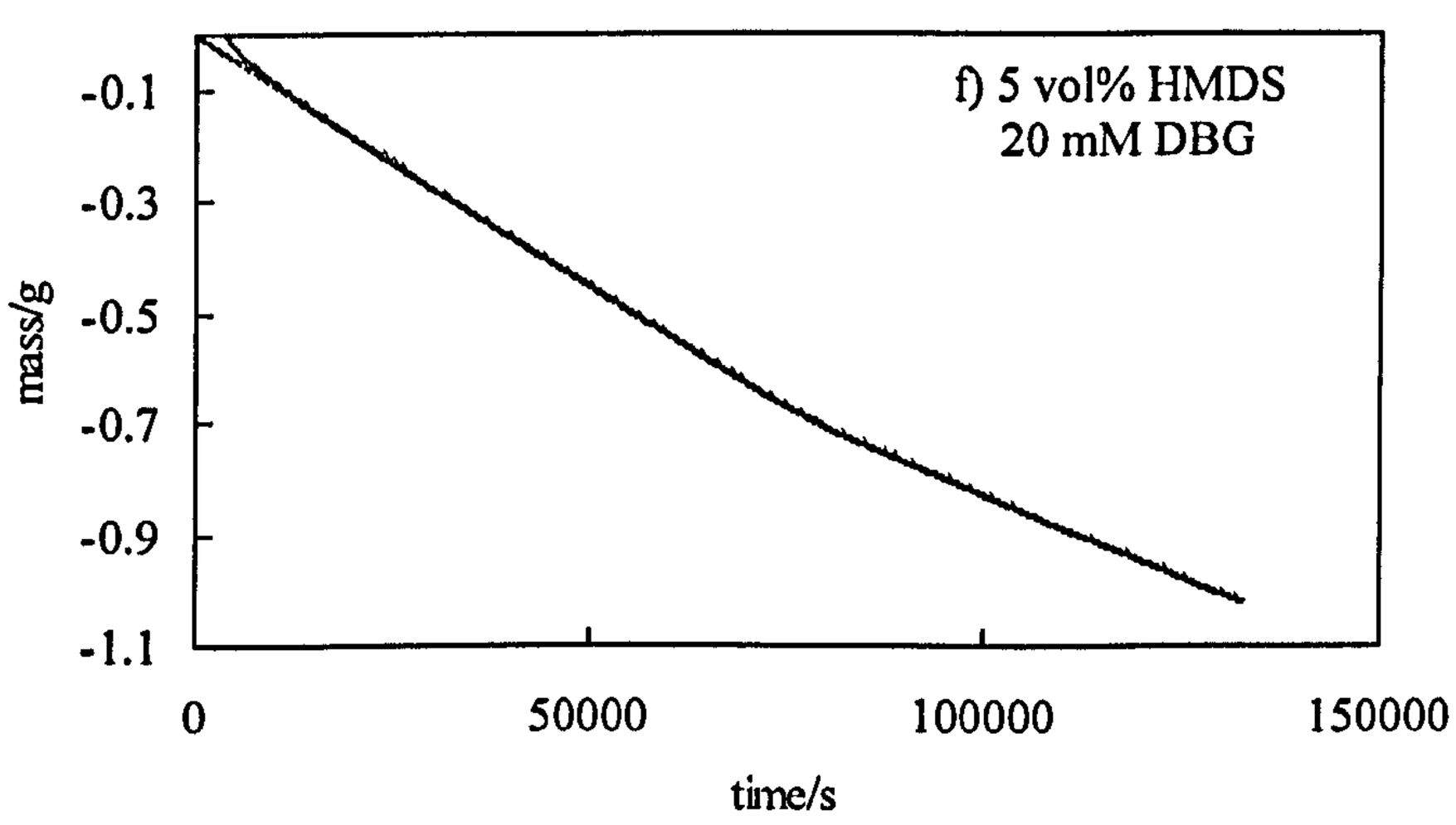
f) 5 vol% HMDS
20 mM DBG
mass/g
-0.1
-0.3
-0.5
-0.7
-0.9
-1.1
0
50000
100000
150000
time/s

Assuming that mechanism (2) operates, the relationship between oil solubility in water and the rate retardation factor f can be derived as follows. At the mouth of the sample tube, the partial pressure of oil vapour is virtually zero for the high gas flow rate used in this work[6] . Since the oil evaporation rate is f times that for pure oil, the oil vapour pressure on the vapour side of the emulsion surface must be fP. The corresponding molar concentration (mol dm^{-3}) is fP/RT. Assuming that the distribution of oil between vapour and the thin water film corresponds to local pseudoequilibria across both the water-vapour and the oil-water interfaces, the concentration of oil on the water side of the emulsion surface is fS, where S is the equilibrium aqueous solubility of the oil, and that at the oil drop surface is S. This also assumes that Henry's law applies over the range of P from fP to P and aqueous oil concentration from fS to S. This latter assumption is reasonable in view of the low solubilities of the oils in water. Fick's first law of diffusion relates the oil flux J to the linear concentration gradients across both the stagnant vapour phase and the thin water film. Figure 4.11 shows the local concentrations of oil expected during steady-state evaporation of the oil.

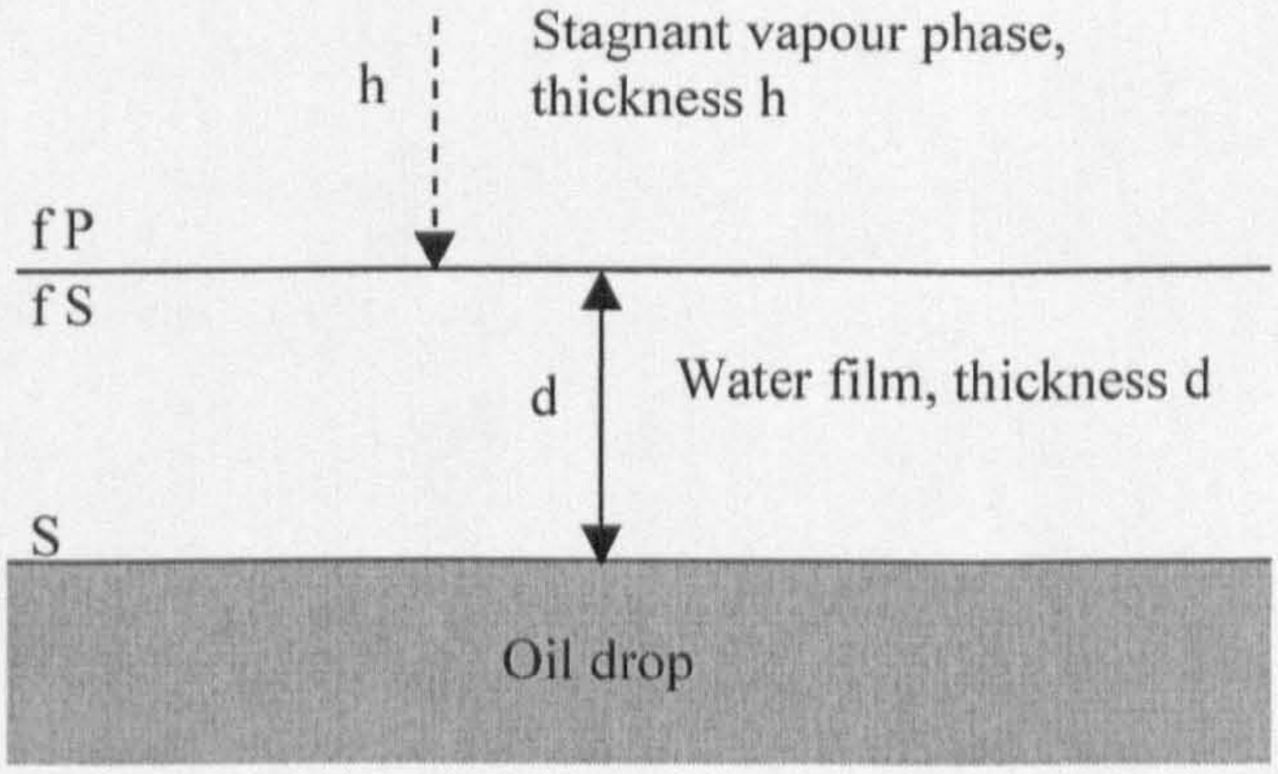

Figure 4.11 Expanded view of the thin water film separating the oil drops from the vapour at the surface of the emulsion sample.

Mass conservation requires that these fluxes be equal in the steady state, and hence

$$J = D_v \frac{(fP/RT - 0)}{h} = D_w \frac{(S - fS)}{d} \qquad [4.6]$$

where D_W is the diffusion coefficient of oil in the water film. Solving the second equality for f gives

$$f = \frac{1}{\left(\frac{D_v dP}{D_w hRTS}\right) + 1} = \frac{1}{(1/X) + 1} \qquad [4.7]$$

where X is the product of the ratios of the diffusion coefficients, saturated concentrations, and thicknesses corresponding to the stagnant vapour phase and water film, that is, $X = (D_W/D_V)(RTS/P)(h/d)$. Thus, if mechanism (2) operates, it is predicted that for $X << 1$ virtually all resistance to oil transport is located within the water film and $f \approx X$. For $X >> 1$, the resistance is located within the stagnant vapour phase and $f = 1$.

To compare experimental f values for all the different emulsions with the predictions of equation [4.7], the values of D_V, P, h (averaged over the run duration), and S required to estimate X were either known or taken from the literature (see Tables 3.1 and 4.2). D_W values were estimated using a literature value of 1.06×10^{-9} m^2 s^{-1} for pentane[7] and assuming that D_W for different oils scales as (molar volume)$^{-0.4}$, where the scaling exponent was taken to be intermediate between -1/3 (spherical molecules)[7] and -1/2 (random coil chains)[8]. The uncertainty in D_W estimated in this way is ± 30%. Thicknesses of equilibrium water films at emulsion surfaces are known to be of the order of tens of nanometres (7-16 nm)[9] but are dependent on the balance between the capillary pressures and colloidal forces across the thin film[9,10]. Films are expected to be thicker for

ionic surfactant films where electrostatic repulsions thicken the films relative to those stabilised by non-ionic surfactants. However, water film thicknesses during the dynamic evaporation process are likely to differ somewhat from equilibrium values. To proceed, we have taken d to be 147 nm for all emulsions stabilised by SDS (anionic), 89 nm for CTAB (cationic) emulsions, and 39 nm for DBG (non-ionic) emulsions, where the values have been adjusted to obtain the best correlation between the experimental f values and the predictions of equation [4.7]. The uncertainty in X for each system mainly arises from the crude approximation made here that d is constant for a particular surfactant but independent of the nature of the oil. In fact, d may depend on the magnitude of the capillary pressure exerted by the buoyant oil drops and hence might be expected to depend on the oil drop sizes and the oil-water and vapour-water interfacial tensions. Neglecting these complicating factors probably gives rise to an uncertainty in d (and hence X) of the order of a factor of 2-3. Although large, this uncertainty is tolerable because the total variation in X for the different systems (dominated by the variation of oil solubility in water) covers 4 orders of magnitude. Figure 4.12 shows the measured variation of f with X for all the emulsions stabilised by SDS, CTAB and DBG. The data all cluster around the theoretical line with almost all data falling within the boundary curves estimated assuming a factor 2 uncertainty in the absolute values of X. It is concluded that evaporation of emulsified oil drops proceeds by diffusion of dissolved oil through a thin water film at the emulsion surface. The thicknesses of the water films during evaporation are estimated to be significantly larger than those of equilibrium oil-water-vapour films reported in the literature[10].

Figure 4.12 **Variation of the oil evaporation factor f with X for o/w emulsions stabilised by DBG, CTAB and SDS. The solid line is calculated according to equation [4.7]. The dashed boundary lines correspond to a factor 2 uncertainty in X.**

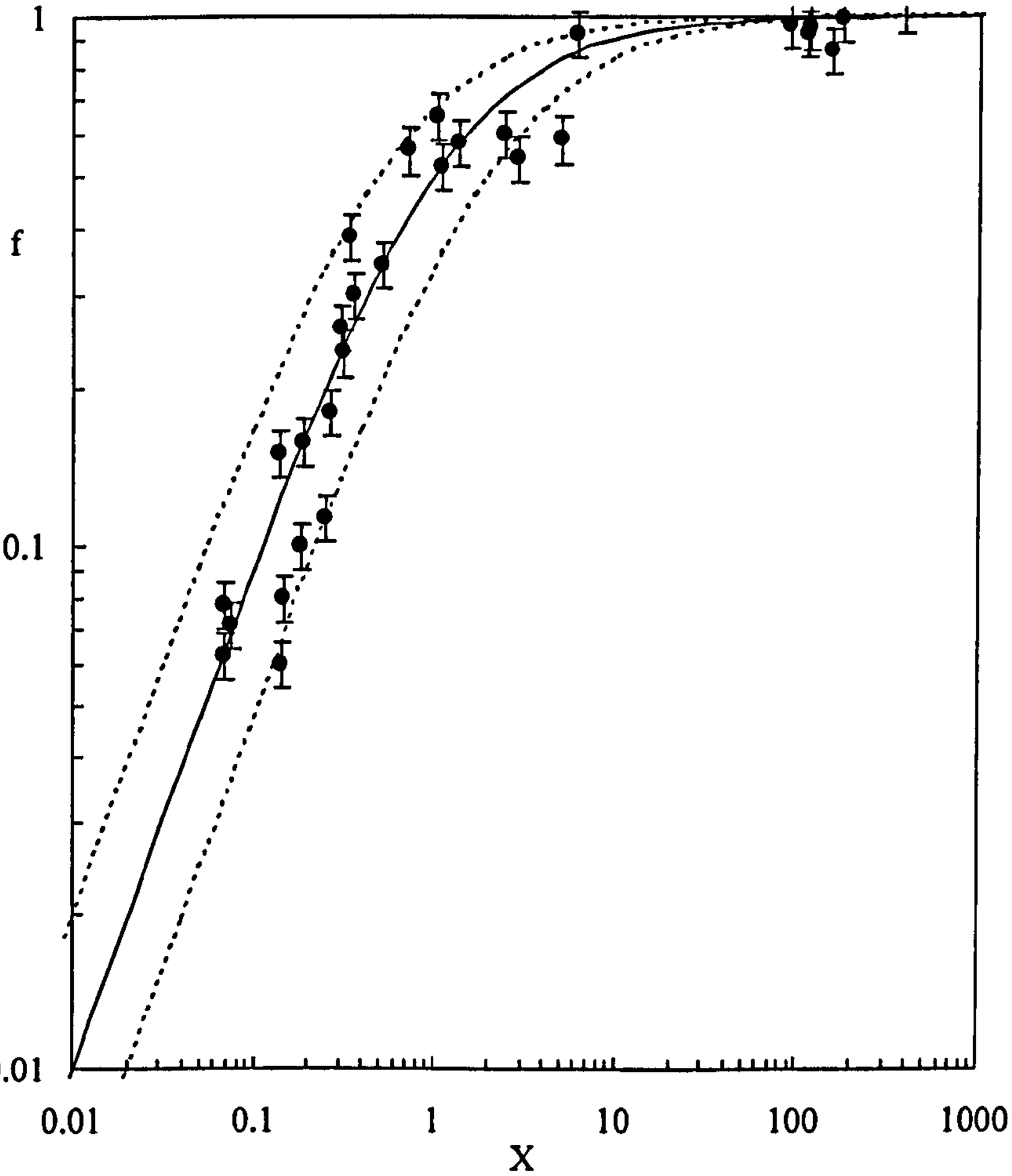

b) Effect of steric interactions between adsorbed polymer layers

In the absence of electrostatic repulsions between monolayers (i.e. for non-ionic DBG stabilisers), we have seen that the water film thickness is much smaller than in the presence of charged surfactants. Inspection of equation [4.7] shows that, for a particular oil and evaporation geometry (defined tube, gas flow rate, temperature etc.) the maximum retardation of oil evaporation (i.e. minimum f) is predicted to occur when the water film thickness d is maximum. Here we have investigated the way in which steric repulsion between polymeric stabiliser monolayers can further increase d and hence retard oil evaporation rate. For this purpose two different PVA samples with molecular weight (Mw) of 29,000 g mol^{-1} and 115,000 g mol^{-1} were used as emulsion stabilisers.

Figure 4.13 shows a mass loss curve of a 10 vol% methylcyclohexane-in-water emulsion stabilised by low Mw PVA together with the best-fit curve. The calculated curve is calculated in exactly the same way as for emulsions stabilised by low molar mass surfactants and as for low Mw surfactant stabilisers, the fit is excellent. Figure 4.14 compares the f values determined for emulsions stabilised by non-ionic surfactants (DBG and low and high Mw PVA) versus X/(h/d). As for emulsions stabilised by low molecular surfactants, the evaporation rates of the oils with relatively high water solubilities (e.g. toluene) are virtually unaffected by being emulsified, i.e., f = 1. Oils such as heptane with relatively low water solubilities show evaporation rates which are strongly retarded relative to non-emulsified oils under the same conditions. Each curve of Figure 4.14 was fitted to equation [4.7] using the water film thickness d as the only parameter to be adjusted.

Figure 4.13 **Mass loss curve for 10 vol% methylcyclohexane-in-water emulsion stabilised by 1 wt% high Mw PVA. The experimental line and the calculated best-fit are overlaid.**

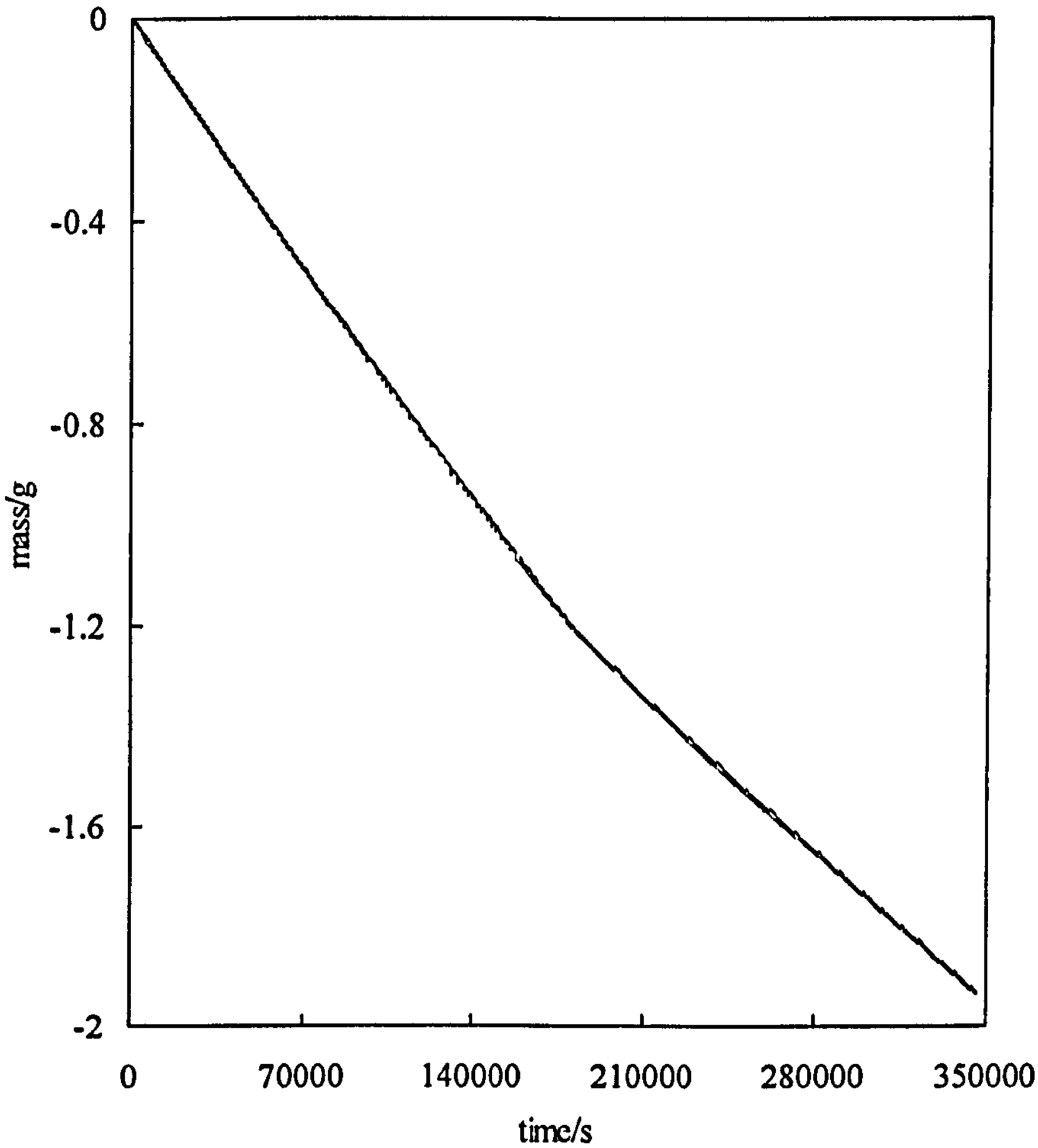

Figure 4.14 Variation of oil evaporation rate retardation factor f with X / (h/d) for DBG and low and high Mw PVA emulsion stabilisers. The curves were calculated according to equation [4.7] using best-fit values of d listed in the legend.

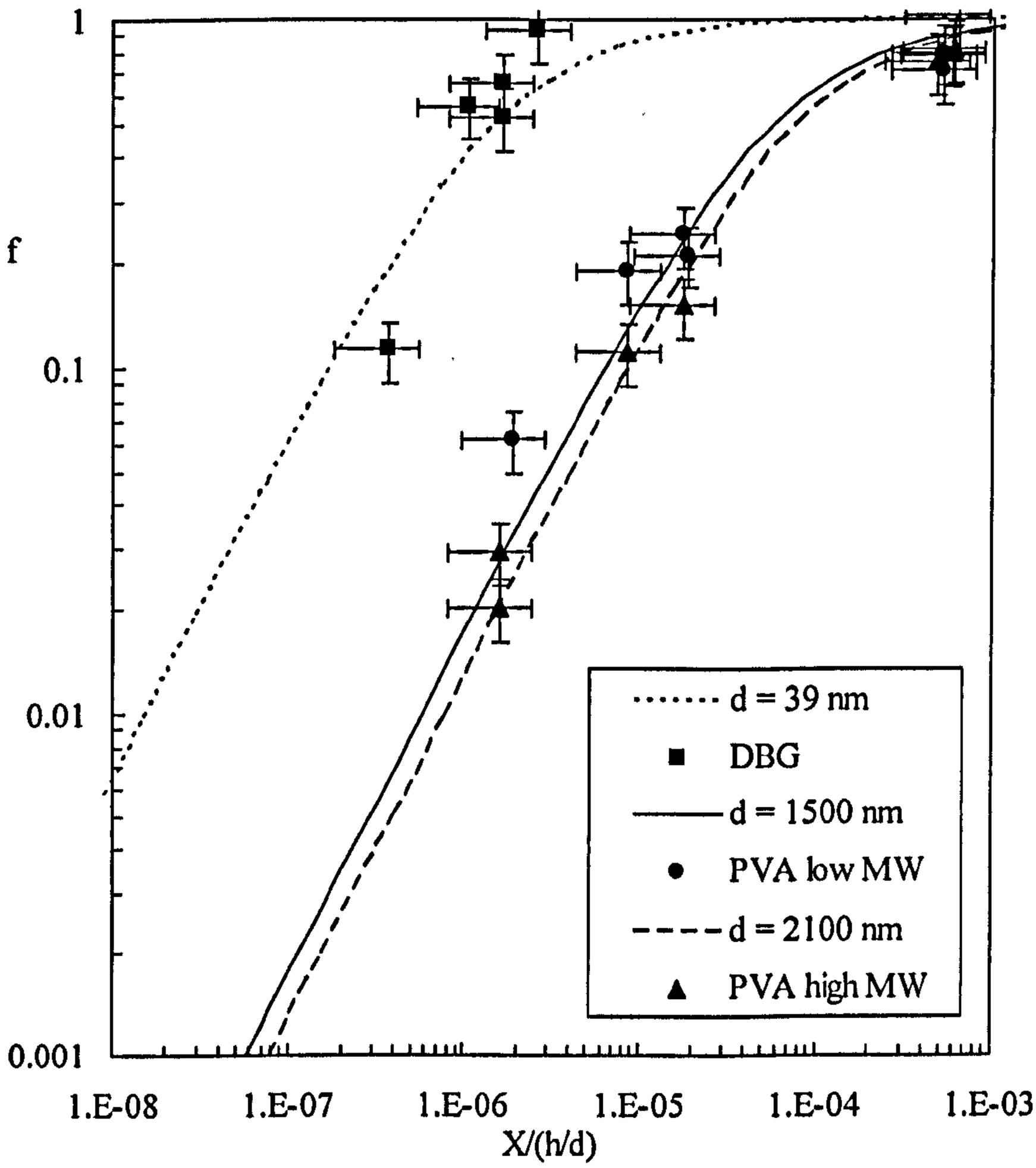

The resulting best-fit values of d provide a quantitative measure of the effectiveness of the different non-ionic emulsifiers in retarding the evaporation rates of oils of low water solubility. The progressive increase in d from 39 nm for DBG, to 1500 nm for low Mw PVA and 2100 nm for high Mw PVA presumably results from increased steric repulsion with increasing Mw of the stabiliser. As seen in Figure 4.14, the increase in water film thickness corresponds to an additional retardation of the evaporation rates of water insoluble oils by a further 10-20 fold relative to emulsions stabilised by DBG.

In Table 4.4 the f values determined for all o/w emulsions stabilised by PVA are shown. As discussed above, for the same oil and evaporation measurements conditions, the f values determined for emulsions stabilised by low Mw PVA are slightly bigger than those determined for high Mw PVA and significantly smaller than for emulsions stabilised by DBG. It can be concluded therefore that, as the Mw of the non-ionic stabiliser increases, f decreases, i.e., the evaporation rate of the oil is more retarded.

	f	
Oil	**Low Mw PVA**	**High Mw PVA**
benzene	0.79	0.8
toluene	0.8	0.75
cyclopentane	0.24	0.15
methylcyclohexane	0.19	0.11
hexane	0.06	0.02
heptane	0.015	too low to measure, ≤ 0.01

Table 4.4 **Summary of the determined f values for o/w emulsions stabilised by low and high Mw PVA.**

In parallel with the evaporation rate measurements, we have also determined the variation of the oil drop size distributions in the emulsions. Table 4.5 shows the average oil drop diameters before and after the evaporation measurements in emulsions stabilised by different surfactants. Note that, as has already been explained, these remaining samples were stoppered to avoid the evaporation of the species.

	SDS		CTAB		DBG	
Oil	d^b/μm	d^a/μm	d^b/μm	d^a/μm	d^b/μm	d^a/μm
benzene	6.52	22.54	7.16	13.31	5.68	3.51
cyclopentane	8.45	8.71	6.56	9.8		
heptane	5.13	5.55	7.93	9.12		
methylcyclohexane	9.21	11.74	9.6	11.43	9.57	12.81
HMDS	7.36	8.25	9.14	12.07	8.81	8.87
octane	10.32	10.57	10.32	10.57		
toluene	5.98	15.96	6.48	6.02		
hexane	4.86	6.15			4.82	4.25
squalane	28.55	26.05				

Table 4.5 **Summary of the average drop diameter of the oil drops in o/w emulsions stabilised by different surfactants (20 mM in aqueous phase) before and after (denoted by b and a superscripts respectively) time periods corresponding to the evaporation rate measurements.**

The emulsion drops sizes generally remain constant or increase over the time period of the evaporation rate measurements and there is no clear correlation between emulsion drop size and the evaporation rate. As noted in the introduction, oils such as toluene showing relatively high water solubility are expected to show appreciable rates of

Ostwald ripening. Figure 4.15 compares the drop size distribution of toluene and heptane drops in water measured after the emulsion formation and 24 h later. It can be observed that toluene drops grow in time whereas the size of heptane drops hardly increases. Figure 4.16 compares plots of d^3 with time for toluene-in-water and heptane-in-water emulsions stabilised by 20 mM SDS. Consistent with a drop growth mechanism by Ostwald ripening, toluene (high water solubility) shows significant drop growth whereas the drop sizes for heptane (low water solubility) remain constant. However, the non-linearity of the toluene plot suggests that the observed droplet growth may include contributions from mechanisms other than Ostwald ripening, e.g. coalescence. Table 4.6 summarises the average drop diameter of the o/w emulsions stabilised by low and high Mw PVA for different concentration. It can be seen that oil drops stabilised by high Mw PVA are smaller than drops stabilised by low Mw PVA.

	Low Mw PVA		High Mw PVA	
Oil	**d^b/μm**	**d^a/μm**	**d^b/μm**	**d^a/μm**
toluene	24.71	25.49	9.68	11.21
cyclopentane	25.77	23.6	10.95	12.35
hexane	25.89	26.01	11.54	11.34
benzene	23.28	33.92	20.71	19.73
methylcyclohexane	25.25	22.61	14.14	14.40

Table 4.6 **Summary of the average drop diameter of the oil drops in 10 vol% o/w emulsions stabilised by 0.5 wt% PVA before and after (denoted by b and a superscripts respectively) time periods corresponding to the evaporation rate measurements.**

Figure 4.15 **Variation on the heptane (upper figure) and toluene (lower figure) drop size distributions for 20 vol% o/w emulsions stabilised by 20 mM SDS. Solid line: t = 0; dashed line: t = 24h.**

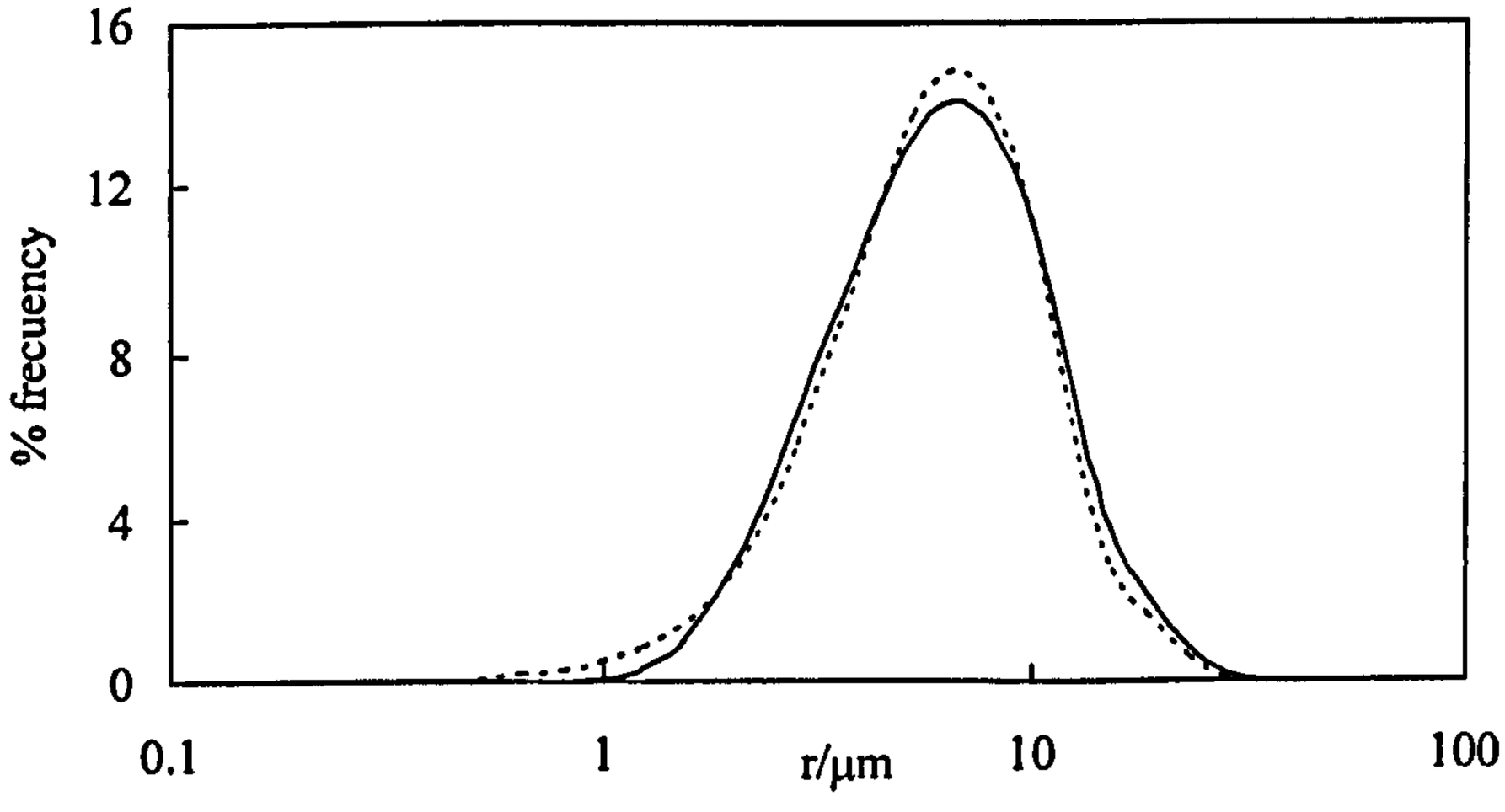

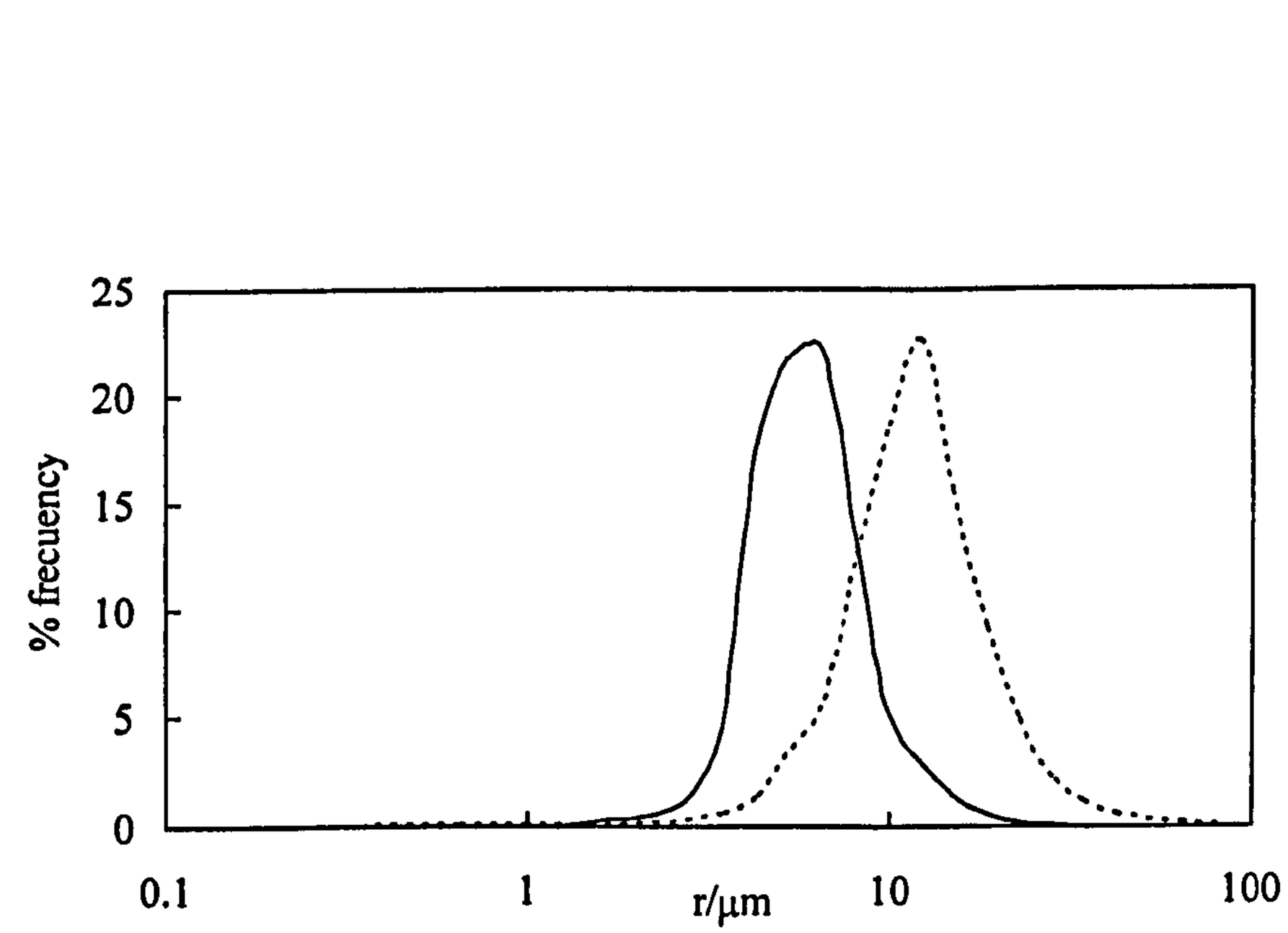

Figure 4.16 **Cube of the volume average drop diameter versus time for 20 vol% o/w emulsions containing either heptane (squares) or toluene (circles) and stabilised by 20 mM SDS.**

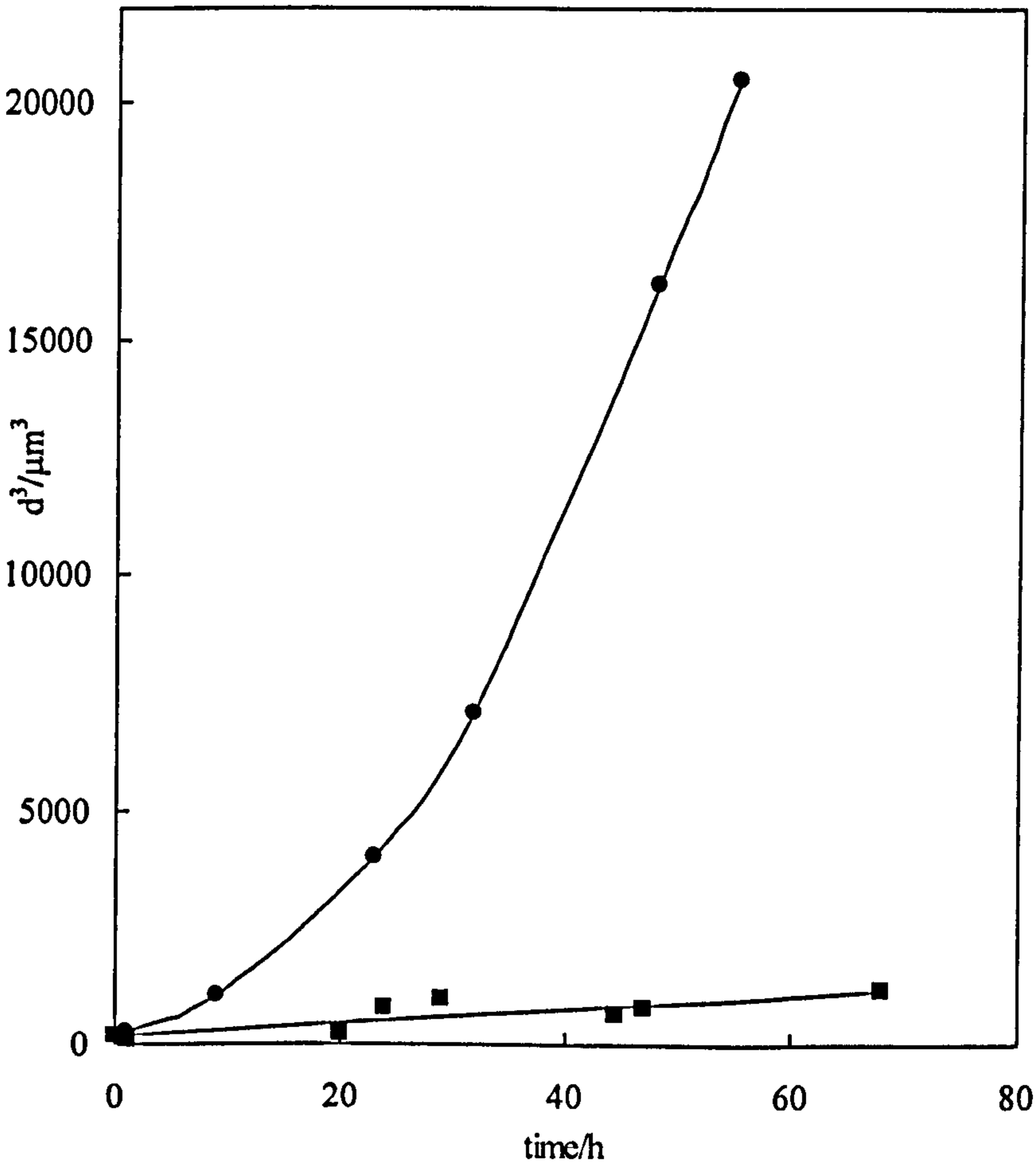

Unlike emulsions stabilised by surfactants, emulsions stabilised by high and low Mw PVA are viscous and they behave as gels. This viscosity of the continuous aqueous phase hinders the movement of the dispersed droplets (see Chapter 5) and hence the probability that two drops first approach and then "stick" together or even merge is much smaller. Figure 4.17 shows micrographs of 10 vol% methylcyclohexane-in-water emulsions stabilised by 0.5 wt% high Mw PVA. Emulsions stabilised by PVA show high stability over long period of time and no increase on the average drop diameter was observed (see also Table 4.6).

4.2.3 Effect of electrolyte concentration

Initially, the effect of the presence of NaBr on the evaporation of the aqueous continuous phase was studied. According to Raoult's Law, the presence of electrolytes in a pure liquid lowers the vapour pressure of the solvent and hence a decrease of the evaporation rate should be observed. Figure 4.18 shows mass loss curves of pure water and NaBr aqueous solutions. As was expected, the presence of salt slightly reduces the evaporation rate of the solvent. Secondly the effect of salt on the evaporation of dispersed oil drops from creamed emulsions was studied. According to equation [4.7], for oils which are highly insoluble in water ($X < 1$) the oil evaporation rate is expected to be retarded when the water film thickness d is larger. This is consistent with our observation that the evaporation rates for oils of low water solubility are slower for ionic surfactants than for non-ionic surfactants since ionic surfactants are expected to give thicker water films as a result of electrostatic repulsion between the oil-water and water-vapour surfaces. For an emulsion stabilised by an ionic surfactant, electrolyte addition is

Figure 4.17 Micrographs of a 10 vol% methylcyclohexane-in-water emulsion stabilised by 0.5 wt% high Mw PVA. Pictures taken after (a) t = 0 and (b) t = 24 h.

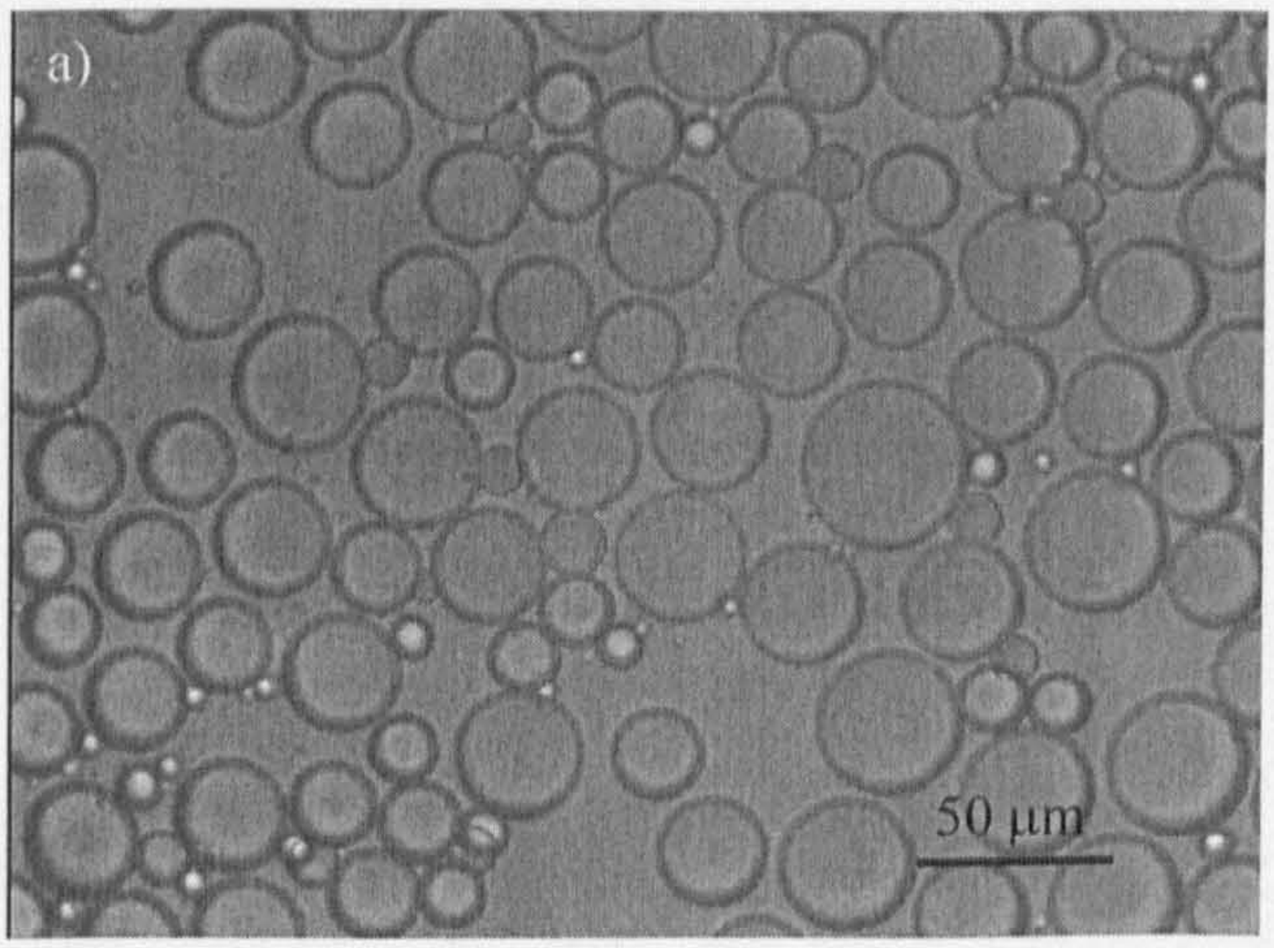

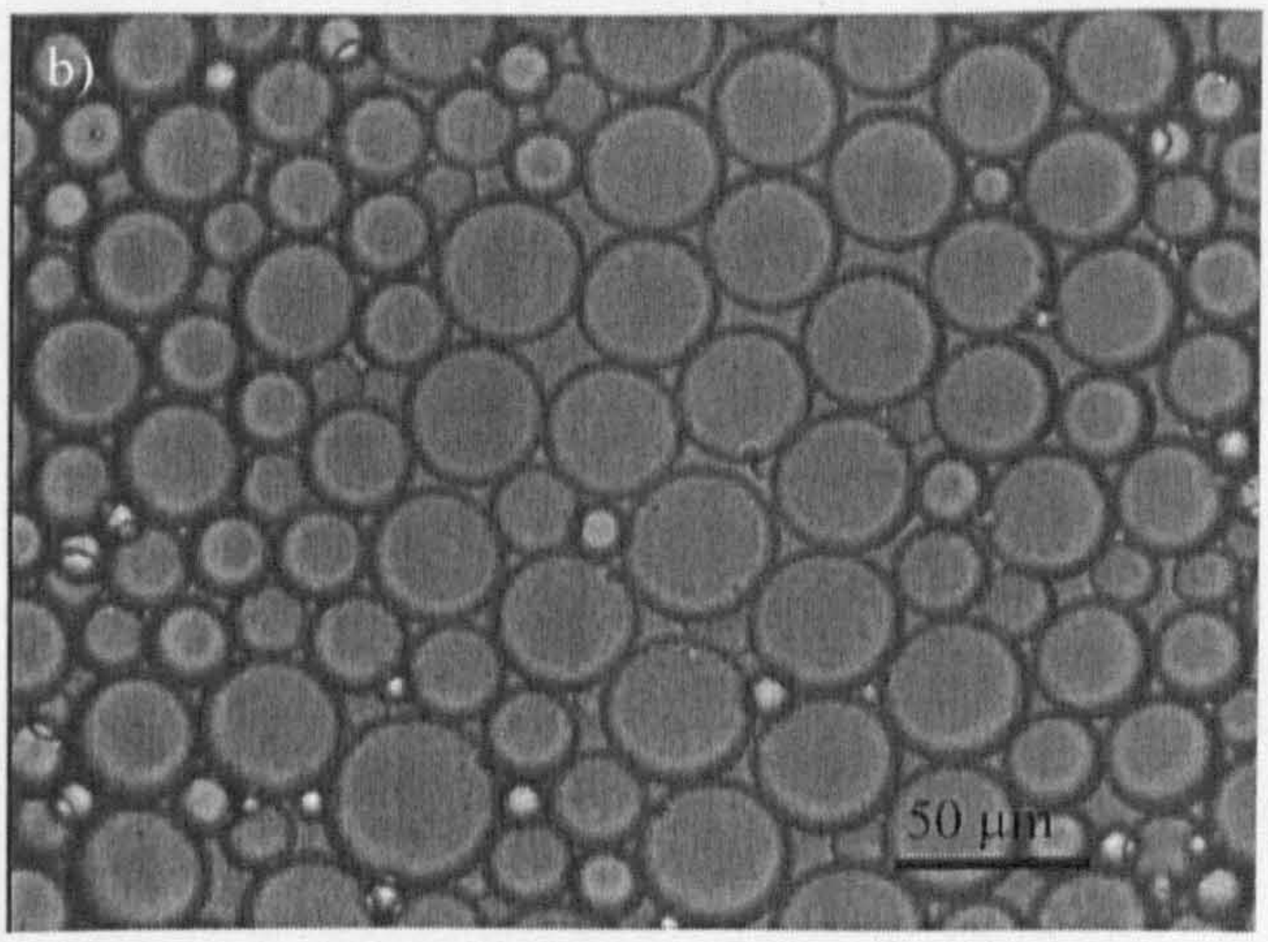

Figure 4.18 Mass loss curves of NaBr aqueous solutions.

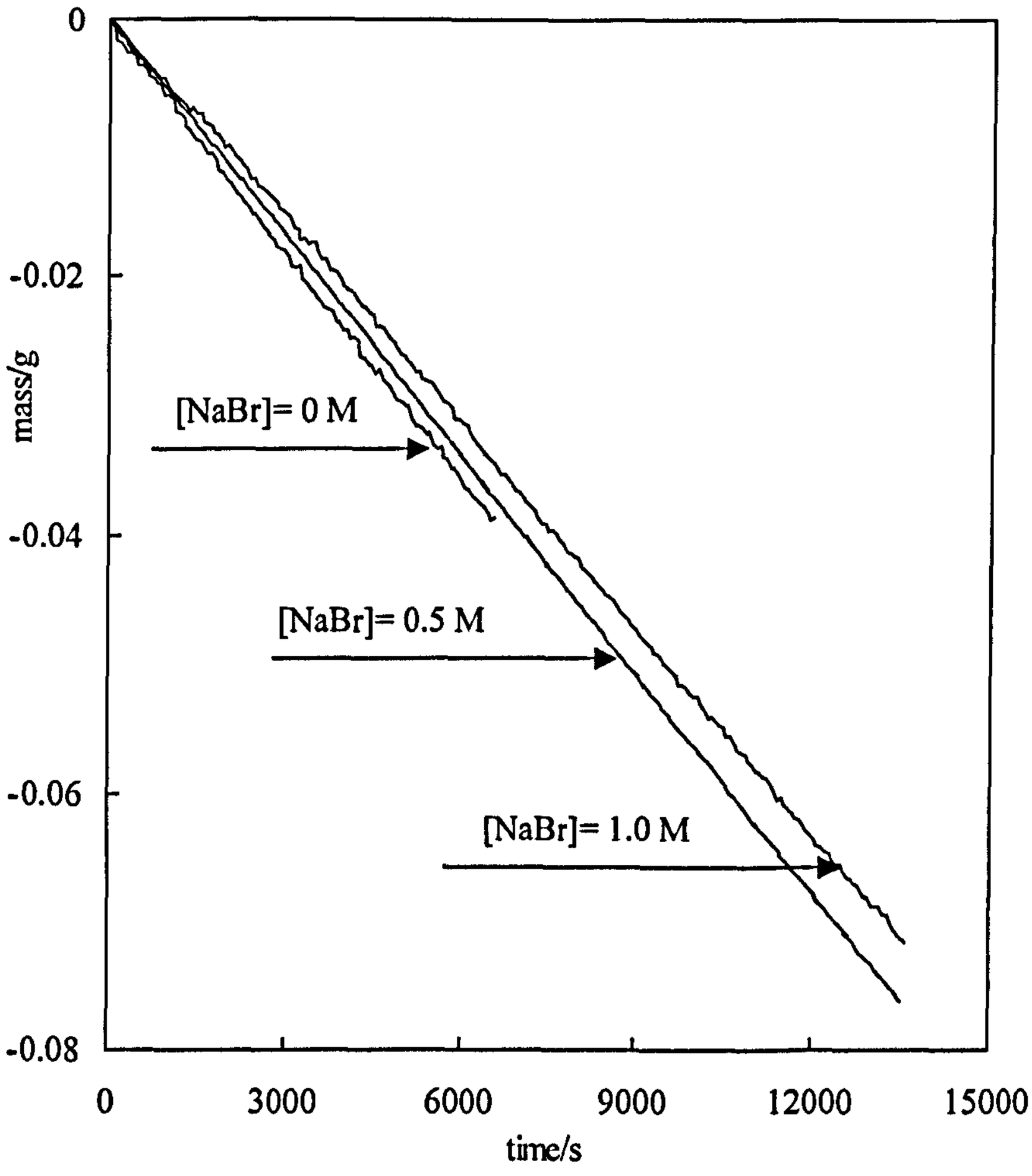

expected to thin the water film by screening the electrostatic repulsion and hence, accelerate the evaporation rate of the dispersed oil drops. Figure 4.19 shows that f does indeed increase with increased electrolyte concentration for a series of emulsions stabilised by the cationic surfactant CTAB. The effect of changing surfactant concentration was investigated for three systems, and the results are summarised in Table 4.7. For the SDS/toluene system for which f is close to 1, increasing the SDS concentration from the critical micelle concentration (cmc) to 2.5 times the cmc produces no significant change in f. For heptane as oil, f is less than 1 and increasing the surfactant concentration produces a slight increase in f for both SDS and CTAB as surfactant. A possible explanation for this increase is that the presence of micelles aids the transport of oil across the thin water film by increasing the effective oil solubility in the aqueous phase.

System	[Surf.]/mM	[Surf.]/cmc	f
SDS with 20 vol % toluene	8	1	0.96
SDS with 20 vol % toluene	20	2.5	0.86
SDS with 20 vol % heptane	8	1	0.21
SDS with 20 vol % heptane	20	2.5	0.26
CTAB with 20 vol % heptane	2	2	0.18
CTAB with 20 vol % heptane	20	20	0.34
CTAB with 20 vol % heptane plus 20 mM NaBr	2	-	0.28

Table 4.7 Variation of f with total electrolyte concentration.

Figure 4.19 **Variation of f with aqueous phase electrolyte concentration (CTAB + NaBr) for 20 vol% heptane-in-water emulsions stabilised by CTAB (2 mM). The solid line is a guide for the eye.**

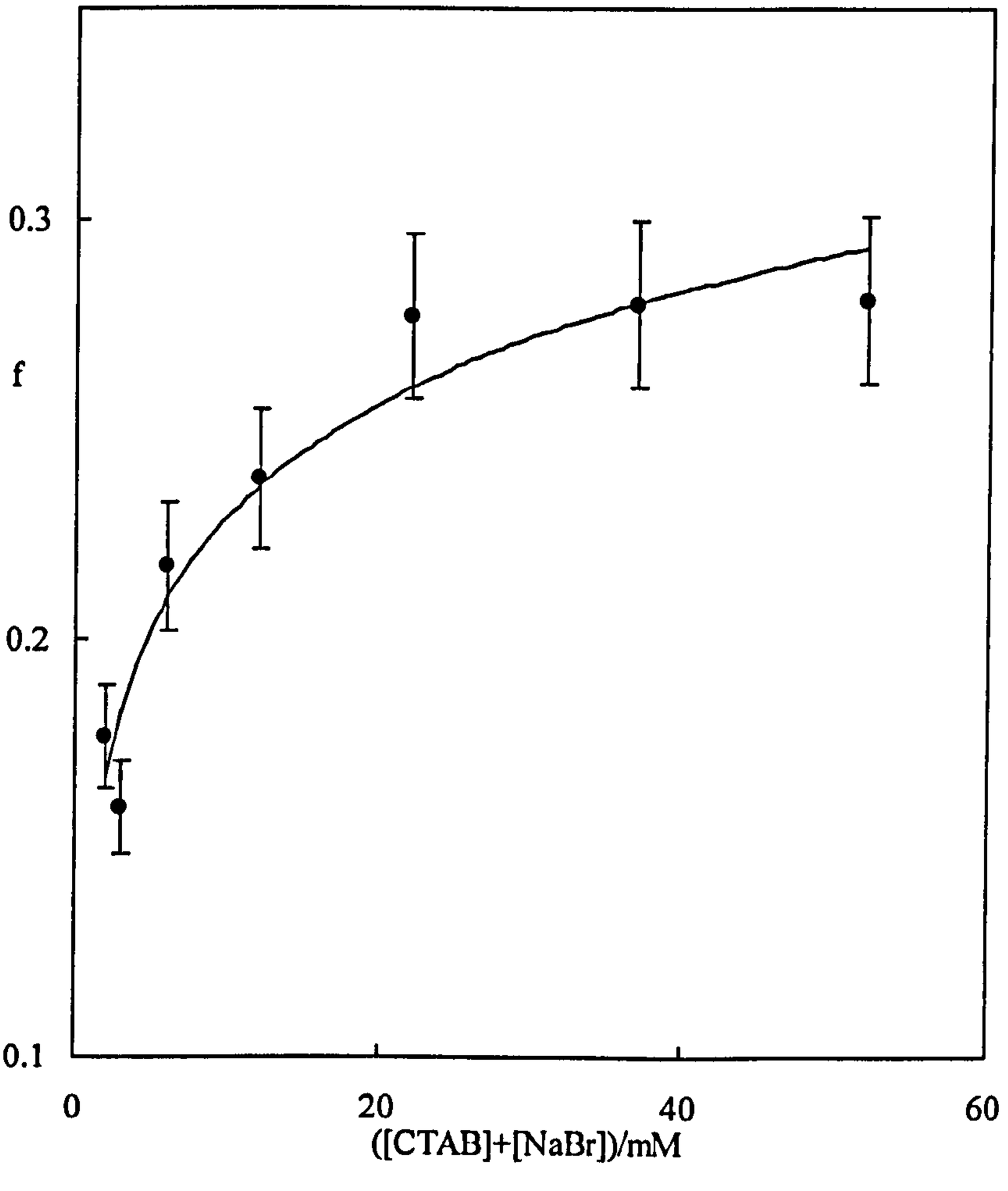

This effect has been shown to operate during oil transport between emulsion drops in compositional ripening[11]. The solubility of heptane in 20 mM SDS or CTAB is estimated to be approximately 2 orders of magnitude larger than the solubility in pure water, and hence, if micellar aided transport of oil was occurring during evaporation, the values of f in emulsions containing 20 mM SDS or CTAB are expected to be close to 1.

A more plausible explanation is that the addition of ionic surfactant acts similarly to the addition of electrolyte, that is, the water film thickness is decreased by increasing ionic strength which decreases the electrostatic repulsion across the film. Consistent with this interpretation, the last row of Table 4.7 shows that the increase in f produced by addition of 20 mM NaBr is similar to that produced by increasing the CTAB concentration from 2 to 20 mM.

4.2.4 Effect of the thickness of the stagnant vapour layer

For the same emulsion system, equation [4.7] predicts that f should increase with the stagnant vapour phase thickness h. This prediction was tested by measurement of f for a series of emulsions in which the initial total depth of emulsion in the sample tube was varied. Although h is necessarily changing slightly during the evaporation process, a constant, average value was assumed in the fitting of the mass loss curves. The variation in h during the runs is represented on the graph as the horizontal error bars. As shown in Figure 4.20, the results are in reasonable agreement with the predictions of equation [4.7] with the assumption that the water film thickness d remains independent of h and equal to 147 nm (equal to the value taken for all SDS emulsions in Figure 4.12).

Figure 4.20 Variation of f with h (averaged over the run duration) for 20 vol% heptane-in-water emulsions stabilised by 20 mM SDS. Vertical error bars indicate 10% uncertainty in f and the horizontal error bars represent the variation in h during the evaporation run. The solid line shows the calculated variation with d = 147 nm.

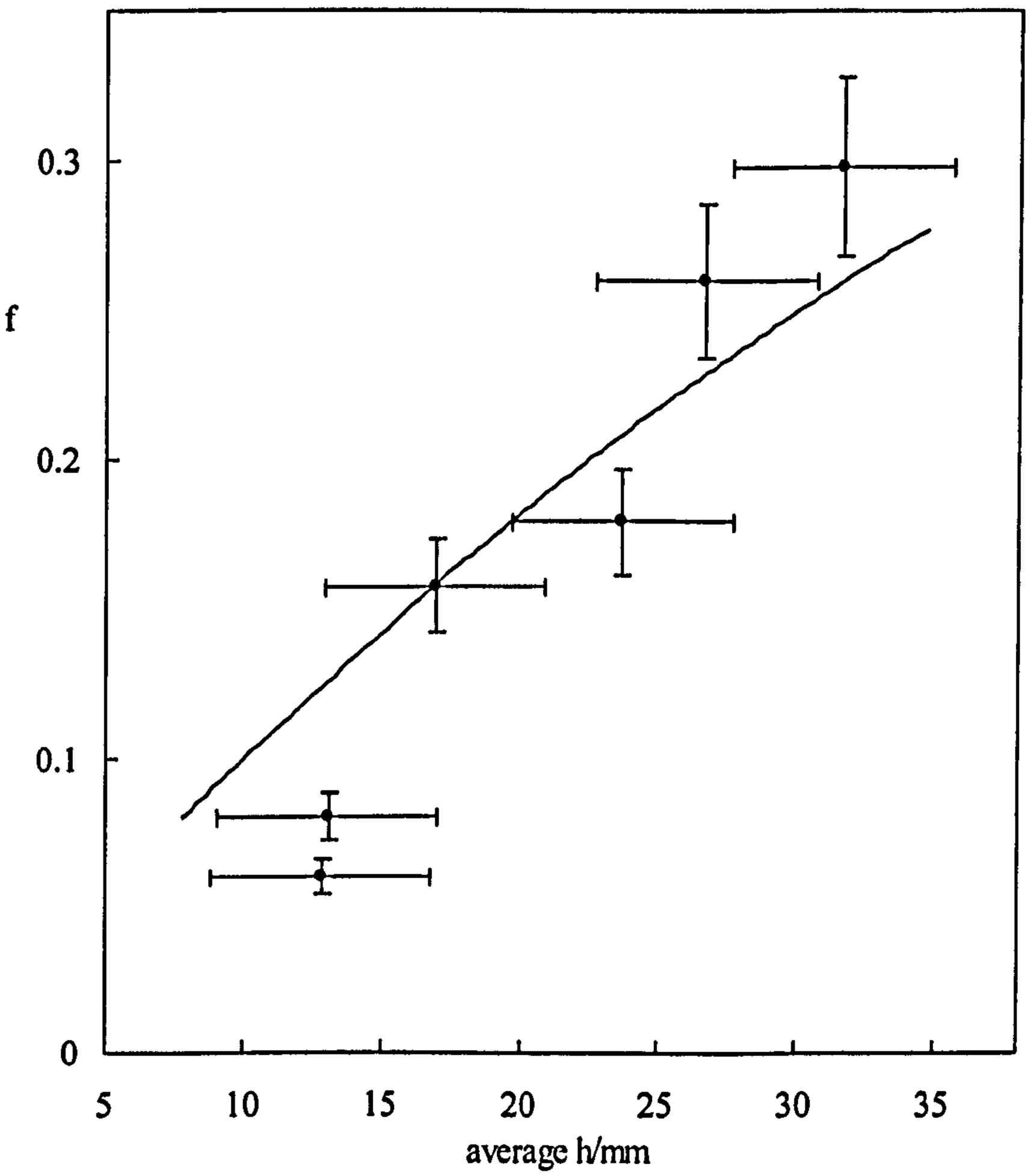

4.3 Evaporation rates of creamed w/o emulsions

The aim here is to compare the mechanism of evaporation of oil drops from creamed o/w emulsions with that of water drops from creamed w/o emulsions. The main difference between these two cases is that the surface of a w/o emulsion is not expected to have an adsorbed surfactant monolayer unlike the case for the surface of an o/w emulsion with an aqueous continuous phase. The evaporation rates of creamed w/o emulsions stabilised by Span 80 were analysed according to a model where the total evaporation rate E (expressed as the rate of mass change of the sample mass) is given by:

$$E = E_{oil} + f'.E_{water} \qquad [4.8]$$

where E_{oil} and E_{water} are the rates for pure oil and water respectively and f' reflects the magnitude of the energy barrier to transfer water from drops within the emulsion to the vapour phase. By analogy with the model used to describe the evaporation of creamed o/w emulsions, if a thin oil film is present at the upper surfaces of the w/o emulsions and the water drop evaporation occurs by water diffusion across this film, then f' is expected to correlate with the solubility of water in the oil, i.e. to decrease when the water solubility in the oil is low.

In order to fully test whether the evaporation of creamed w/o emulsions follows the same theoretical model used to describe creamed o/w emulsions, the w/o emulsions samples must meet several criteria. i) The oils used must be denser than water to ensure creaming of the water drops. ii) The emulsions must be stable with respect to coalescence. iii) The volatilities of the oils used must be less than that of water. iv) The water solubility in oil must be known and the range of oils used should be such that a

very wide range of solubility values is covered. Following literature searching, we have been able to find only very limited data on water solubility in suitable oils (chlorobenzene and dichlorobenzene) and thus have been unable to fully test the theoretical model.

Figure 4.21 shows the mass loss curves for different volume fractions in 20 mM Span 80 stabilised water-in-chlorobenzene emulsions and their respective best-fit curves. It can be seen that the model correctly predicts the effect of the water volume fraction, as it did for the effect on the variation of oil volume fraction in o/w emulsions. The fitted values for f' in different w/o emulsions are shown in Table 4.7.

Oil	ϕ_w	f'_{exp}	f'_{calc}	S^{12}/M
Chlorobenzene	0.06	0.74		3.35×10^{-3}
	0.13	0.77	0.76	
	0.24	0.80		
1,2-Dichlorobenzene	0.05	0.85	0.93	2.23×10^{-2}
	0.10	0.84		
	0.15	0.88		
1-Bromobutane	0.05	0.66		-
	0.10	0.62		

Table 4.7 Summary of f'_{exp} and f'_{calc} values (using equation [4.7]) for water-in-oil emulsions containing different oils and water volume fractions.

Figure 4.21 Mass loss curves for 6.5, 13 and 24 vol% water-in-chlorobenzene stabilised by 20 mM Span 80. The experimental data and fitted curves (corresponding to the best-fit value of f = 0.77 ± 0.03) are overlaid.

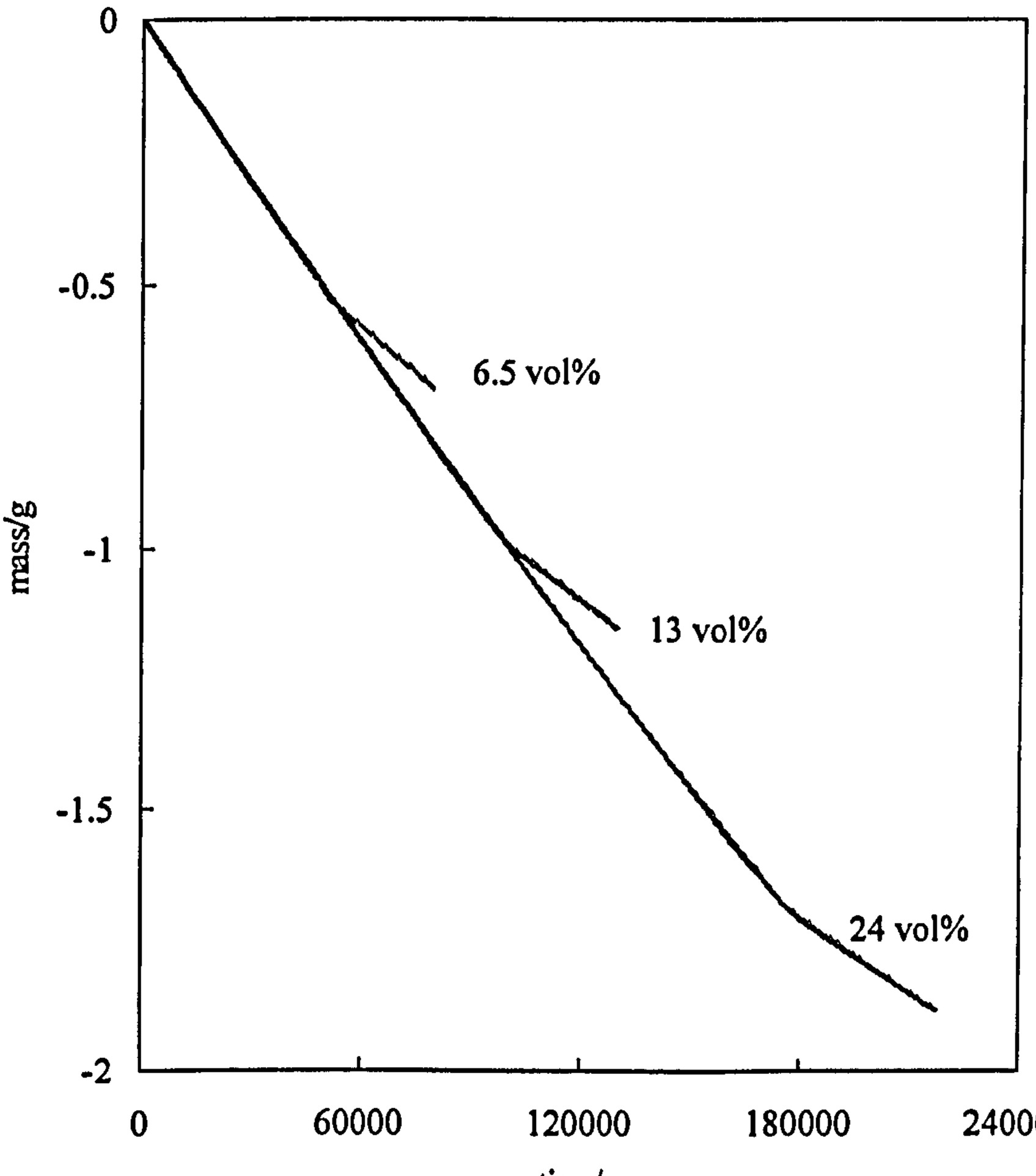

Table 4.7 shows that f' is only slightly lower than unity for both chlorobenzene and 1, 2-dichlorobenzene. Using water solubility values and the theory described for o/w emulsions, the measured f' values are approximately consistent with evaporation of water occurring by diffusion across a thin oil film at the emulsion surface and were calculated using equation [4.7]. The retardation factor is lower for 1-bromobutane but, unfortunately no water solubility data is available for this oil and hence the value cannot be compared with the theory. The overall conclusion from this work is that experimental results are consistent with the proposed mechanism but the lack of a sufficiently wide variation of water solubility in oil prevents a definitive conclusion to be reached.

4.4 Evaporation of emulsions which are unstable with respect to coalescence

The evaporation rate for an emulsion containing 20 vol% toluene-in-water and stabilised by 20 mM DGB was measured. For this emulsion, partial droplet coalescence and separation of a layer of free oil on the emulsion surface is known to occur over the timescale of the evaporation measurement[13]. In this situation, the theoretical model for stable emulsions is inappropriate and the so-called "oil layer on water model" was used to model the plot of evaporation rate versus time (obtained by numerical differentiation of the experimental mass loss curve) shown in Figure 4.22. The evaporation rate curve of the unstable emulsion is explained as follows. Initially, when stable emulsion is still present at the surface, the evaporation rate is high due to the combined loss of oil as well as water (i.e. the usual emulsion evaporation rate). After approximately 5000 s, drop coalescence has produced an oil layer covering totally the surface of the emulsion.

Figure 4.22 **Evaporation rate versus time for an initially toluene-in-water emulsion stabilised by 20 mM DBG. The experimental data (solid line) and the fitted curve (dashed line), calculated according to the oil layer model are compared.**

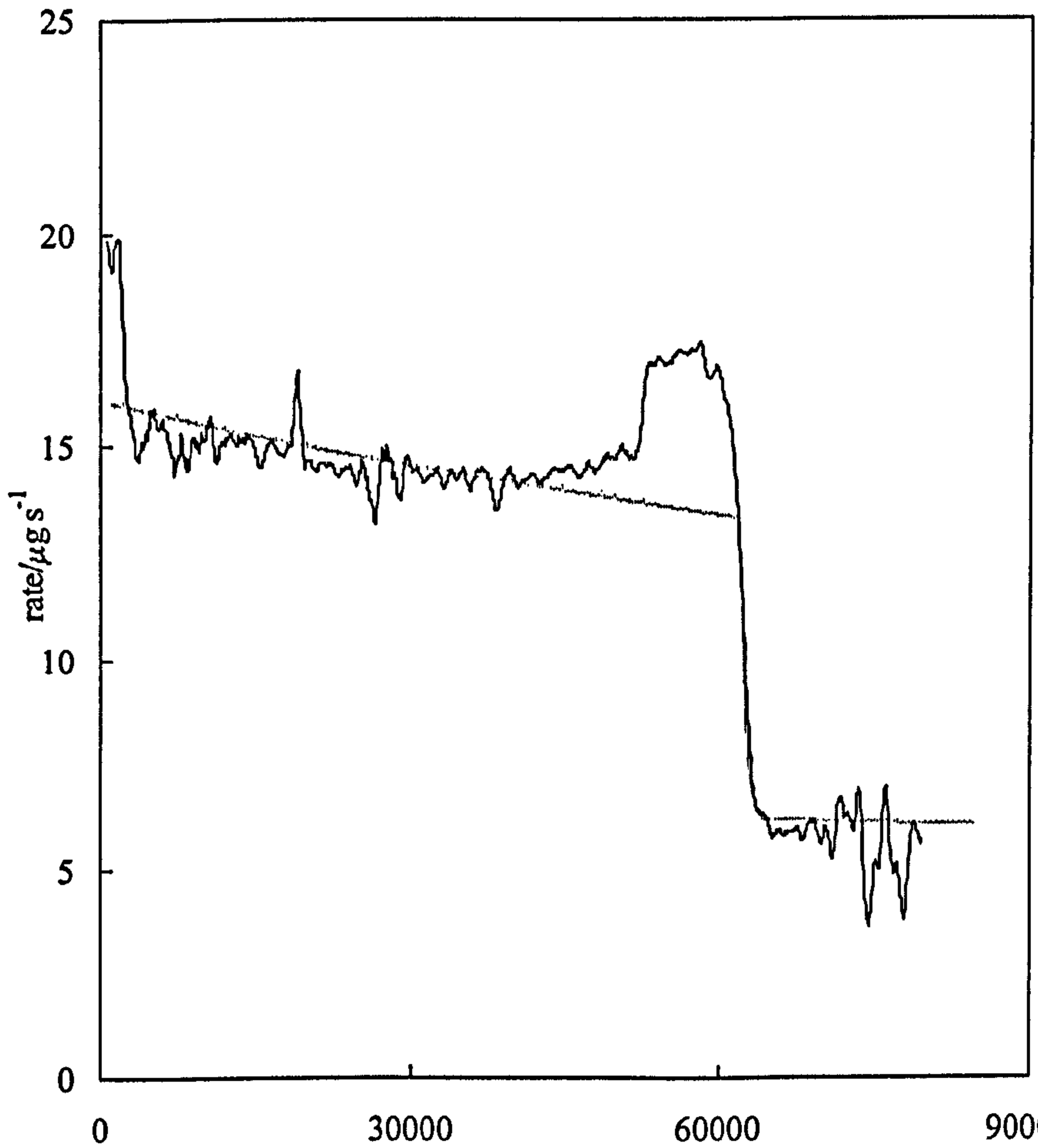

At this time, the evaporation rate corresponds to that of oil alone and agrees with the curve predicted using the model. After approximately 50000 s, the free oil layer has evaporated but residual non-coalesced emulsion drops remain. Hence, the evaporation rate rises as both the oil and water evaporate simultaneously. Finally, when all the oil has evaporated (~ 60000 s), the rate drops to that of water alone. This interesting example serves to illustrate how the evaporation rate profile can provide kinetic information on the emulsion breakdown processes.

4.5 Conclusions

- Evaporation rates of o/w emulsions with squalane (non-volatile) as oil show the same evaporation rate as pure water. This confirms that the evaporation rate of the continuous water phase is not affected by emulsification.
- The evaporation rate of emulsified oil is not significantly influenced by either the surfactant concentration or the oil volume fraction.
- Evaporation rates of dispersed oil drops are retarded relative to the rates of pure oils by factors ranging from 1 to 20.
- The evaporation rate reduction factor (f) is lower for emulsions stabilised by ionic surfactants than for emulsions stabilised by non-ionic surfactants and is lower for oils with low solubility than for oils with high solubility in water. Both observations suggest that the evaporation mechanism involves oil diffusion across a thin oil-water-vapour film present at the emulsion surface.

- Steric stabilisers such as high Mw polymers (PVA) retard the evaporation of dispersed oils more than nonionic or charged surfactants of low molar mass. The retardation observed increases as the Mw of the non-ionic stabiliser increases.
- Evaporation rates of dispersed water drops in creamed w/o emulsions are retarded as observed for oil drops in creamed o/w emulsions.

4.6 References

1 W. Thomson (Kelvin), *Phil. Mag.* 1871, **42**, 448.

2 R. Aveyard, B. P. Binks, P. D. I. Fletcher, T. G. Peck and C. E. Rutherford, *Adv. Colloid Interface Sci.*, 1994, 48, 93.

3 K. J. Beverley, Thesis in preparation, University of Hull.

4 C. McAucliffe, *Nature*, 1963, **200**, 1092.

5 S. Varapath, C. L. Fryf and J. Hamelink, *Environ. Toxicol. Chem.*,1996, **15**, 1264.

6 K. J. Beverley, J. H. Clint P. D. I. Fletcher, and S. Thubron, *Phys. Chem. Chem. Phys.*, 1999, **1**, 909.

7 W. S. Price and O. Söderman, *J. Phys. Chem.*, 2000, **104**, 5892.

8 R. A. Waggoner, F. D. Blum and J. C. Lang, *Macromolecules*, 1995, **28**, 2658.

9 V. Bergeron, M. E. Fagan and C. J. Radke, *Langmuir*, 1993, 9, 1704.

10 L. Lobo and D. T. Wasan, *Langmuir* 1993, 9, 1668.

11 B. P. Binks, J. H. Clint, P. D. I Fletcher, S. Ripon, S. D. Lubetkin and P. J. Mulqueen, *Langmuir*, 1999, **15**, 4495.

12 Honywell Burdick & Jackson, USA. See also www.bandj.com

13 R. Aveyard, B. P. Binks, J. Chen, J. Esquena and P. D. I. Fletcher, *Langmuir*, 1998, **14**, 4699.

Chapter 5

CHAPTER 5

EVAPORATION RATES OF SURFACTANT-STABILISED GELLED EMULSIONS

5.1 Introduction

In many commercial emulsion formulations, water-soluble, high-molecular weight polymers (biopolymers or hydrocolloids) and colloidal particles are often incorporated into the emulsion system. In most of the applications, they are used as thickeners to modify the rheology of the continuous phase and to confer viscosity and a finite yield stress on that phase[1]. A gel structure has been described as the association or cross-linking of long polymer chains to form a continuous three-dimensional network which immobilises a liquid phase[2]. The thickening or gelling effect causes the emulsion droplets to remain suspended in the continuous medium, and thus sedimentation/creaming of emulsion is eliminated. However, it is important to note that polymeric (or other) thickeners may not necessarily exhibit the tendency to adsorb at the water-oil interface and therefore, they may not, by themselves, prevent coalescence of droplets. Being predominantly hydrophilic, most water soluble polymers, e.g., polysaccharides show low or negligible surface activity at oil-water or air-water interfaces[3].

Prevention of oil drop creaming in o/w emulsions is expected to change the evaporation profiles since the dispersed oil drops should not be able to evaporate until they are exposed to the vapour by evaporation of the water continuous phase. For o/w emulsions, the creaming of oil drops due to gravity may be inhibited or retarded by modification of the rheology of the continuous phase. In our work, measurements of evaporation rates of o/w emulsions stabilised by SDS and gelled by water-soluble polymers (κ-carrageenan, Kelzan and Avicel) and solid colloidal particles (Veegum) have been carried out.

5.2 Creaming rates of emulsions as a function of polymer concentration

Prior to studying the evaporation rates, it was first necessary to determine the minimum gelling agent concentration required to prevent the creaming process. Figures 5.1 and 5.2 show the creaming rates as plots of l, the height of creaming layer, versus time of methylcyclohexane (MCH) - and toluene-in-water emulsions stabilised by 20 mM SDS and gelled by κ-carrageenan. In Figure 5.1, the polymer concentration was varied from 0.005 to 1 wt% (note that the polymer concentration is referred to the continuous phase throughout the Chapter). At the lowest polymer content considered here (0.005-0.01 wt%) the creaming rate is increased relative to that without polymer. For toluene-in-water emulsions (see Figure 5.2), [κ-carrageenan] is varied from 0.01 to 1 wt% and the same effect is observed. Moreover, in both cases the creaming process is totally inhibited for [κ-carrageenan] = 1 wt%.

Figure 5.1 **Creaming rates of 20 vol% methylcyclohexane-in-water emulsions stabilised by 20 mM SDS and gelled by κ-carrageenan (wt% shown in key).**

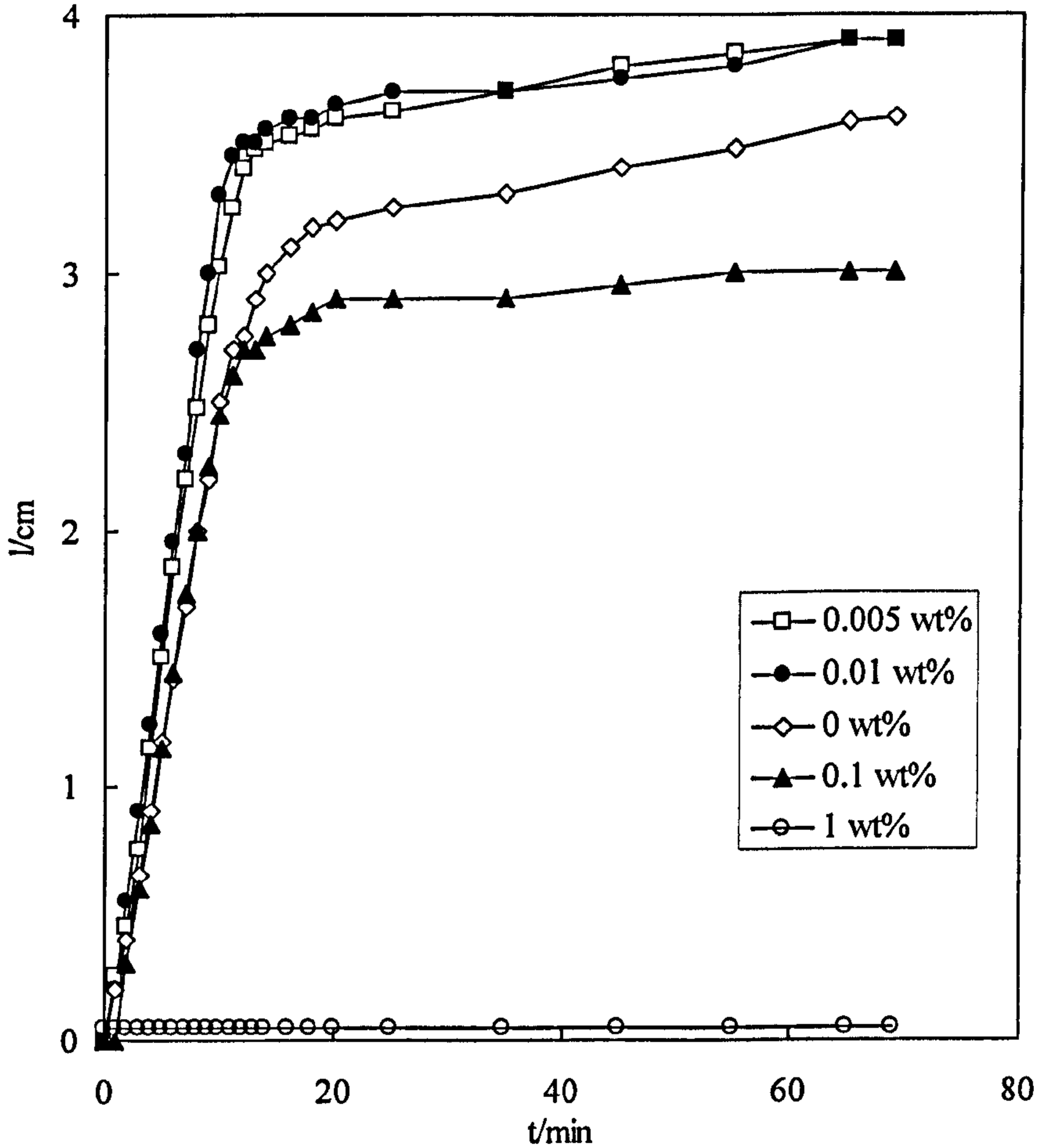

Figure 5.2 **Creaming rates of 20 vol% toluene-in-water emulsions stabilised by 20 mM SDS and gelled by κ–carrageenan.**

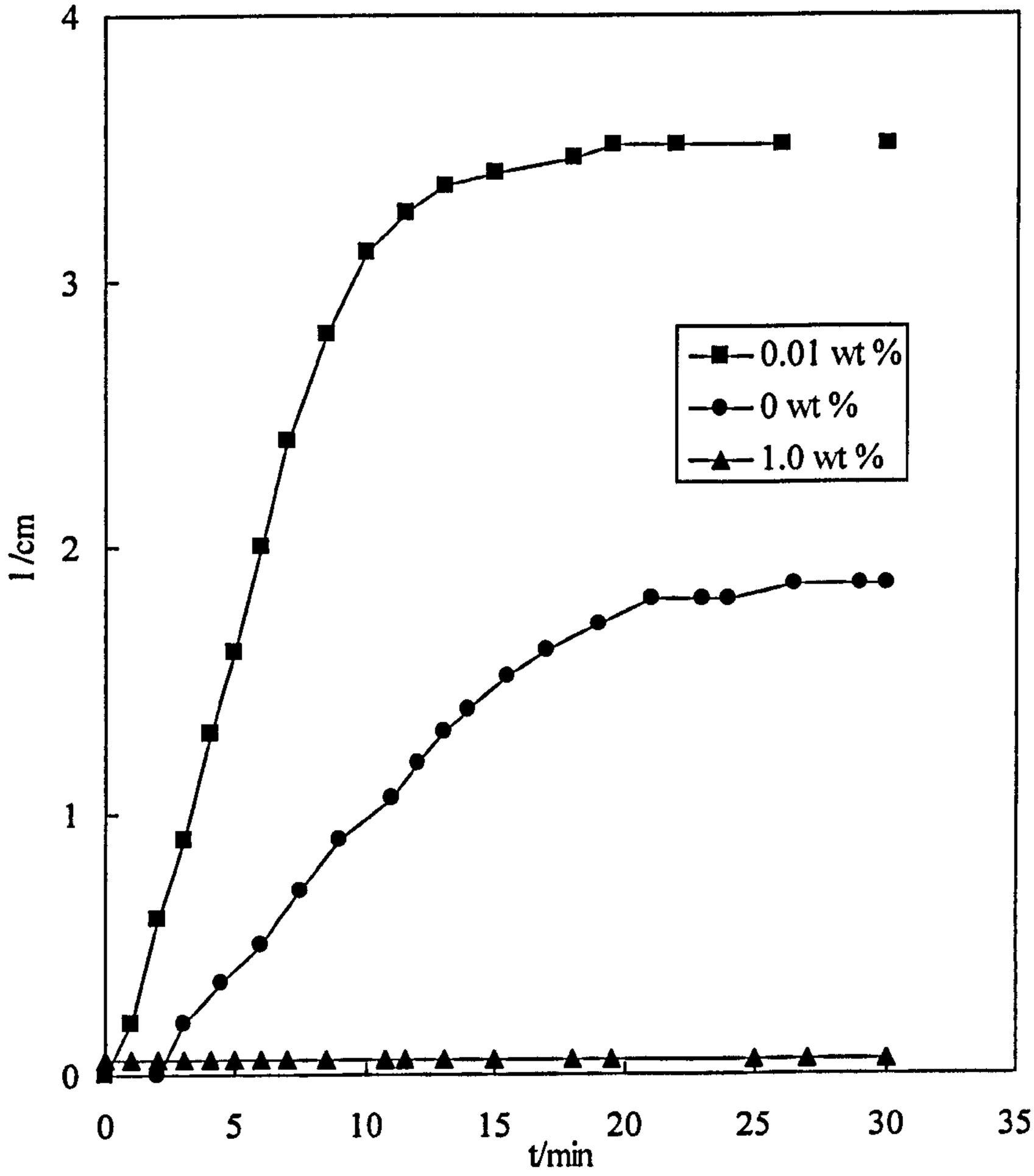

Figure 5.3 shows micrographs of 20 vol% methylcyclohexane-in-water emulsions stabilised by 20 mM SDS. In (a) no polymer is added to the emulsion and the droplets are well-distributed, whereas in (b), adding 0.01 wt% of κ-carrageenan to the aqueous continuous phase, causes the oil drops to aggregate. While high-molecular weight polymers are commonly added to improve the stability of emulsions through rheological control, their presence at low concentrations has in many instances been demonstrated to have actually the opposite effect because of the phenomenon of depletion flocculation[4]. It is well known that the presence of non-adsorbing polymers in the emulsions enhances the creaming rate of the oil layer[5]. When the surfaces of two particles approach within a distance less than the diameter of the free polymer (see Figure 5.4), the exclusion of polymer from the intervening gap is associated with an attractive force between the particles due to the tendency of the solvent to flow out from the gap under the influence of the osmotic pressure gradient. This causes an aggregation or flocculation of the droplets and hence an increase of the creaming rate is observed.

Table 5.1 shows the average drop diameter of 20 vol% methylcyclohexane-in water emulsions stabilised by 20 mM SDS and gelled by κ-carrageenan. Drop size hardly varies with polymer concentration and therefore it can be concluded that the enhanced creaming rate of those emulsions whose continuous phase contain low concentration of polymer is probably due to the depletion flocculation and probably not due to an increase of the drop size.

Figure 5.3 **Micrographs of 20 vol% methylcyclohexane-in-water emulsions stabilised by 20 mM SDS.**

a) [κ-carrageenan] = 0

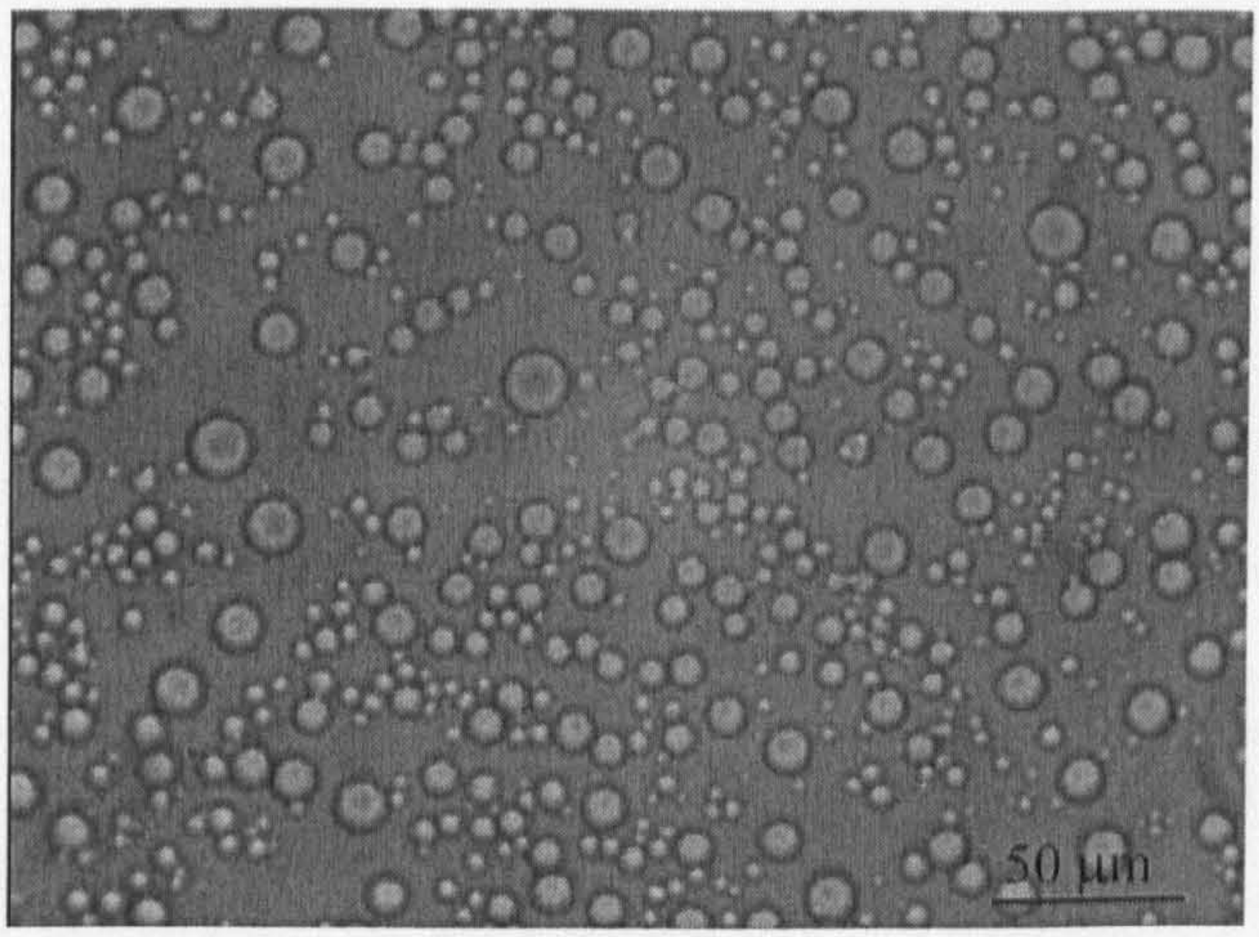

b) [κ-carrageenan] = 0.01 wt%

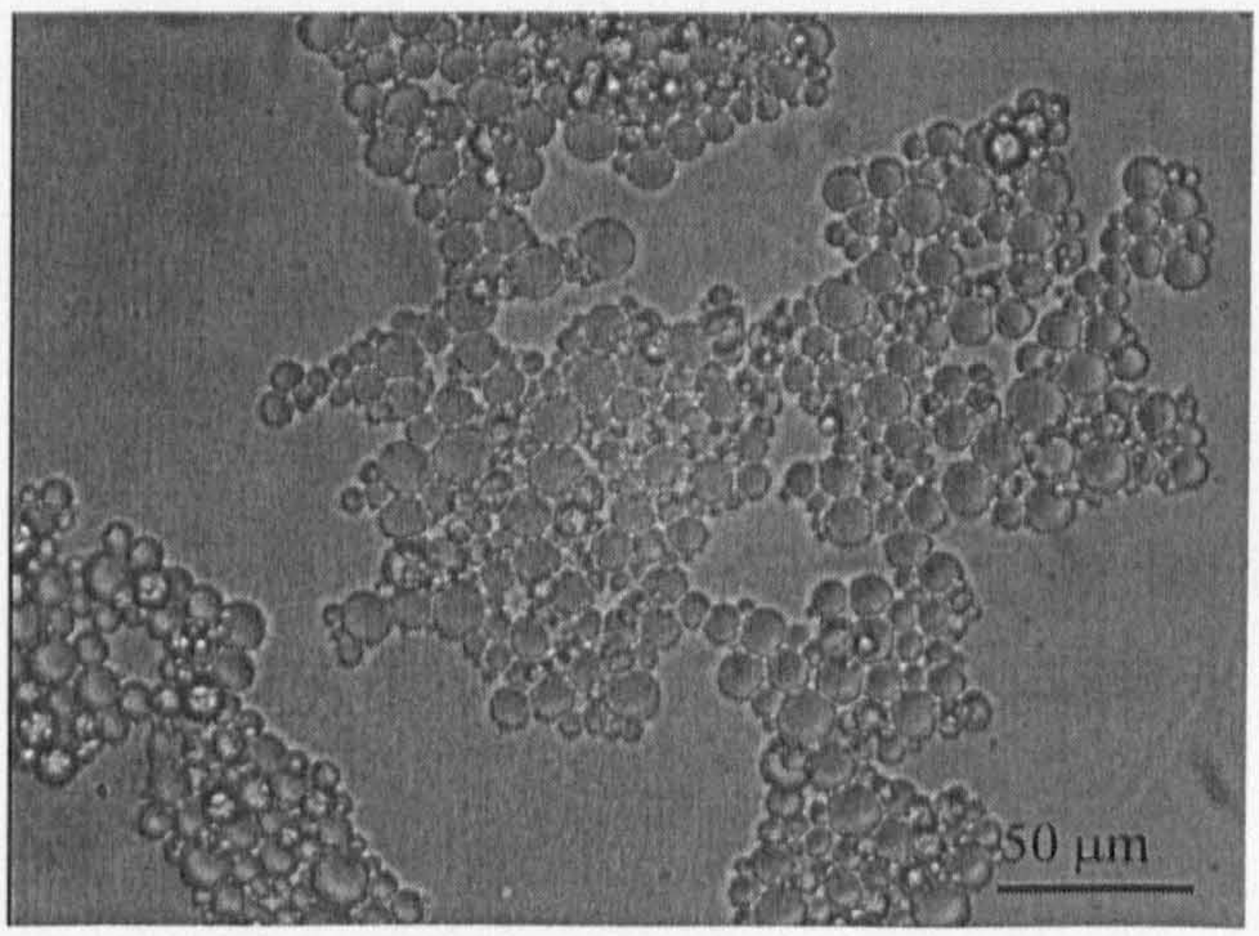

Figure 5.4 Scheme of depletion flocculation.

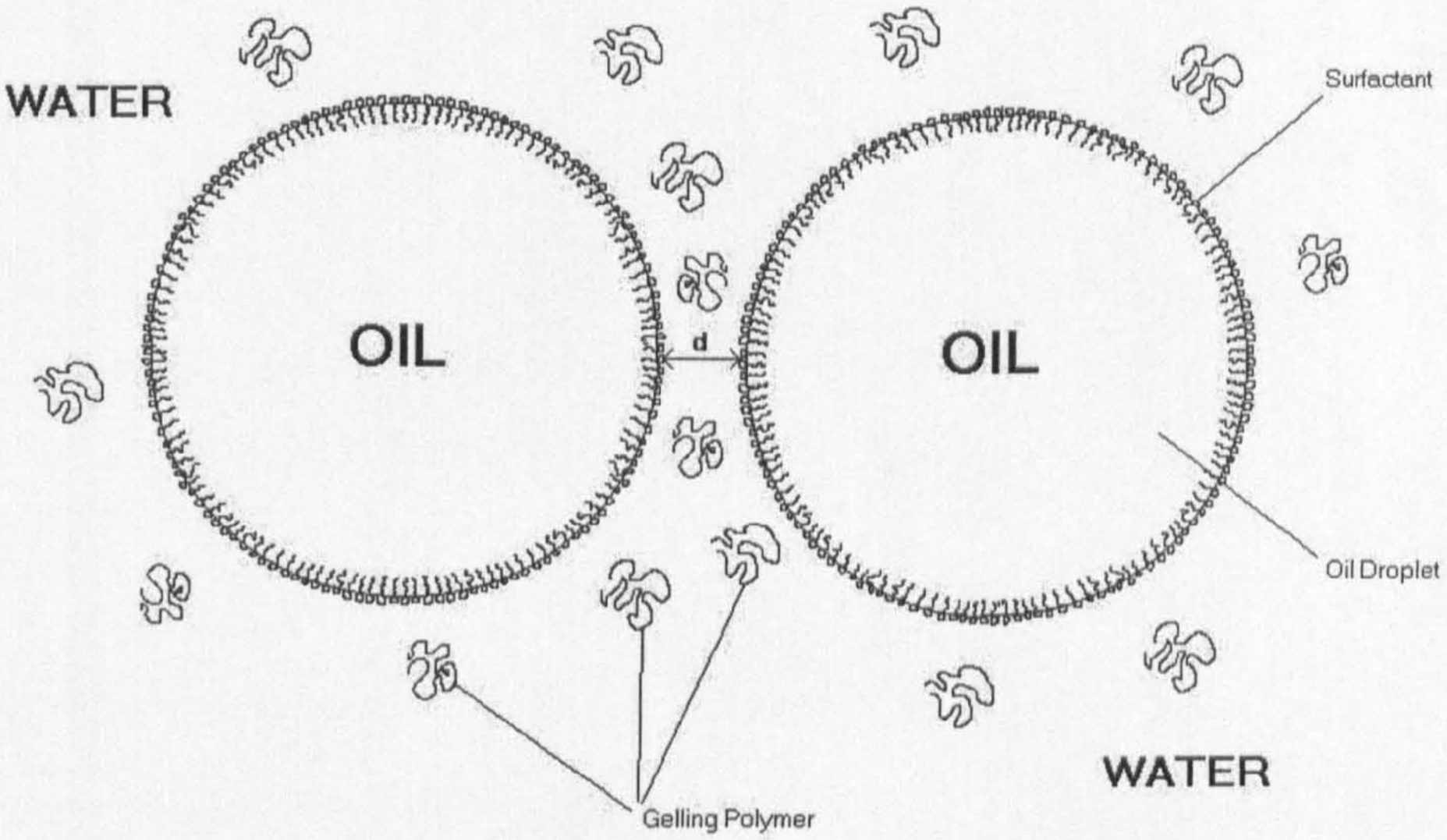

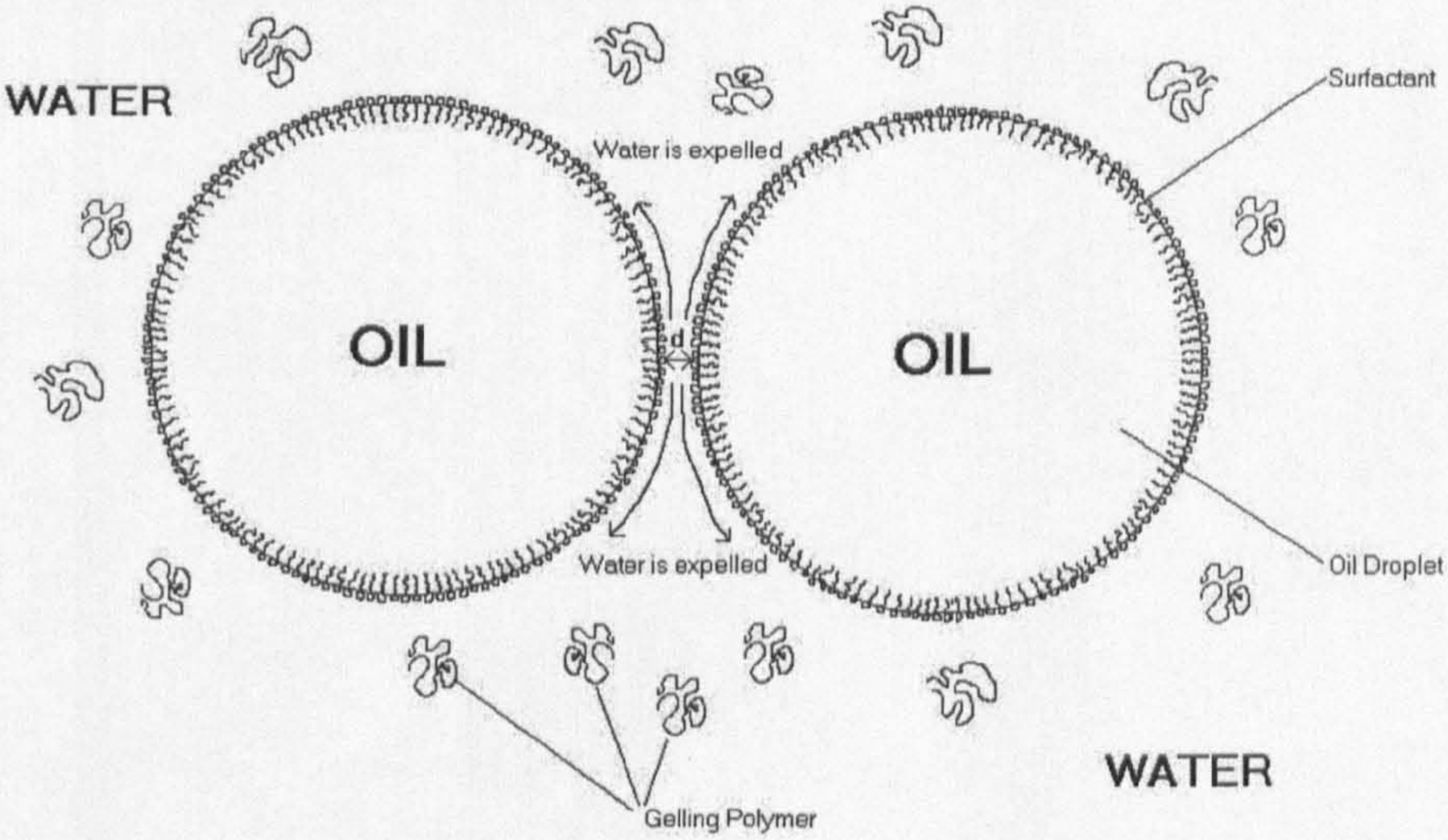

[κ-carrageenan]/ wt%	$d_{t=0}$ /μm	$d_{t=6\ days}$/μm
0	7.02	11.84
0.005	8.41	10.98
0.01	7.81	9.08
0.1	8.12	7.93

Table 5.1 **Average drop diameter at t = 0, i.e. when the rate of creaming was taken and t = 6 days later of 20 vol% MCH-in-water emulsions stabilised by 20mM SDS and gelled by κ-carrageenan.**

By comparing Figures 5.1 and 5.2, it can be seen that the minimum κ-carrageenan concentration required to prevent creaming is independent of the oil used and is approximately 1 wt%. Hence, this concentration was used in the evaporation rate measurements. Table 5.2 shows a summary of the average drop diameter of 20 vol% hexamethyldisiloxane (HMDS)-in-water emulsions stabilised by 20 mM SDS to which was added different concentrations of λ-carrageenan.

[λ-carrageenan]/ wt%	$d_{t=0}$/μm	$d_{t=6\ days}$/μm
0	9.13	10.46
0.5	8.20	9.73
0.7	7.80	7.63
0.9	9.14	9.32
1.0	9.50	9.61

Table 5.2 **Average drop diameter at t = 0, i.e. when the creaming rate was measured, and t = 6 days later for a 20 vol% HMDS-in-water emulsions stabilised by 20mM SDS and gelled by λ-carrageenan.**

Again, no effect is observed as polymer concentration is varied. These values are similar to those shown in Table 5.1, so we can conclude that the drop size is independent of the oil and carrageenan type.

It is known that κ- and λ-carrageenan form rigid and flexible gels[6] respectively and, various models have been proposed for the interaction of κ-carrageenan molecules based on helix or double helix formation. In order to choose the best gelling agent between both types of carrageenan, creaming rates of 20 vol% methylcyclohexane-in-water emulsions stabilised by such carrageenan samples have been studied. Figure 5.5 shows creaming rates of such emulsions gelled by 0.5 wt% of κ (rigid)- and λ (flexible)-carrageenan. As it was expected, due to the formation of rigid gels, the creaming rate of the emulsion gelled by κ-carrageenan is only slightly slowed down compared to that gelled by λ-carrageenan. Therefore, between both types of carrageenan, κ-carrageenan was chosen to inhibit the creaming of oil drops and then to study the evaporation rates of gelled o/w emulsions.

Figures 5.6-5.8 show the creaming rate of 20 vol% methylcyclohexane-in-water emulsions stabilised by 20 mM SDS and gelled by Kelzan (xanthan gum), Veegum (complex colloidal solid particles) and Avicel (microcrystalline cellulose). For these thickening agents, the minimum concentration needed to prevent creaming depends on the structure of the gelling agent and they are equal to 1, 2 and 3 wt% respectively.

Figure 5.5 **Comparison of creaming rates of 20 vol% MCH-in-water emulsions stabilised by 20 mM SDS and gelled by 0.5 wt% of κ- (empty circles) and λ- (filled circles) carrageenan.**

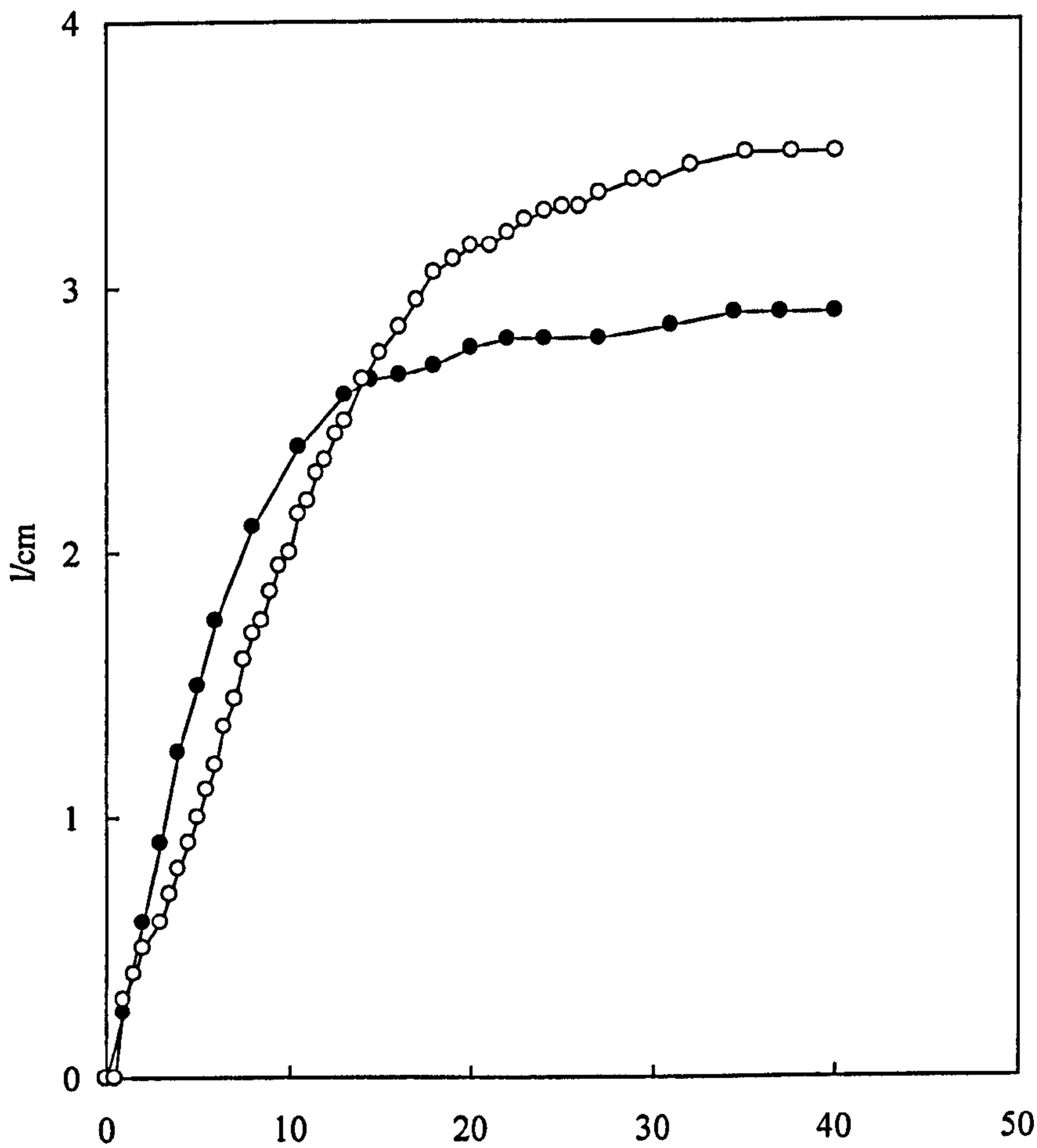

Figure 5.6 **Creaming rates of 20 vol % methylcyclohexane-in-water emulsions stabilised by 20 mM SDS and gelled by Kelzan.**

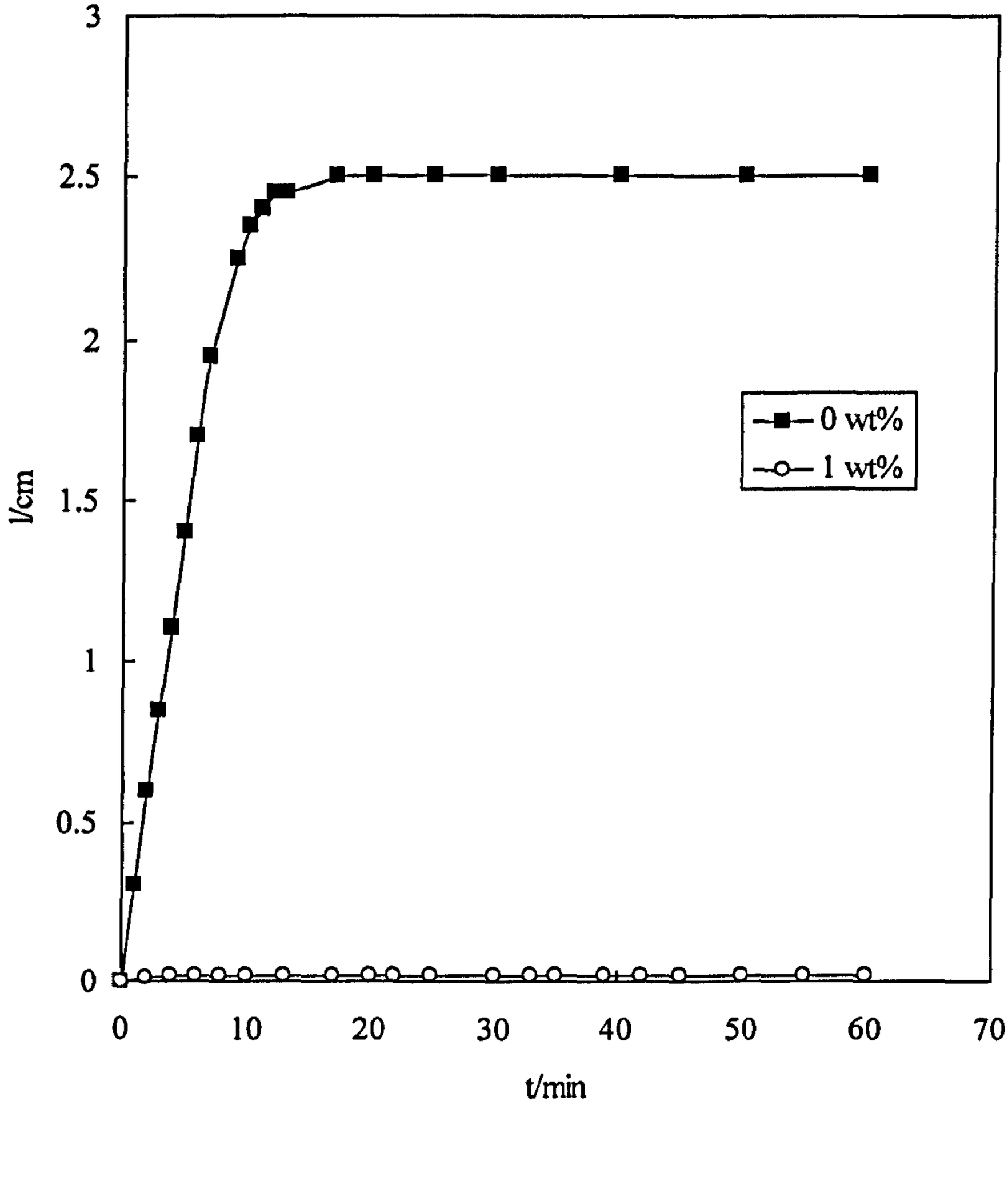

Figure 5.7 **Creaming rates of 20 vol % methylcyclohexane-in-water emulsions stabilised by 20 mM SDS and gelled by Veegum.**

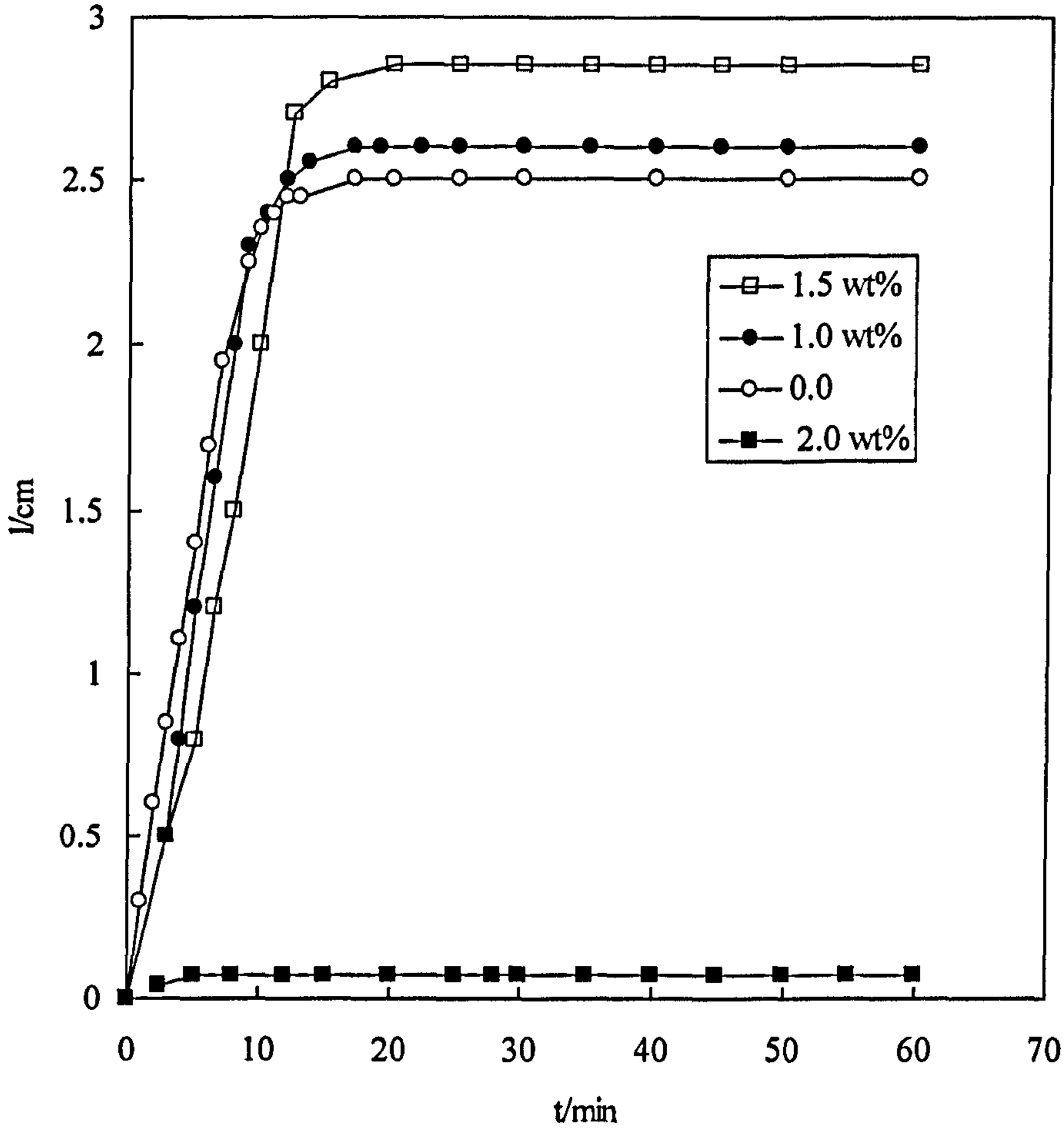

Figure 5.8 **Creaming rates of 20 vol % methylcyclohexane-in-water emulsions stabilised by 20 mM SDS and gelled by Avicel.**

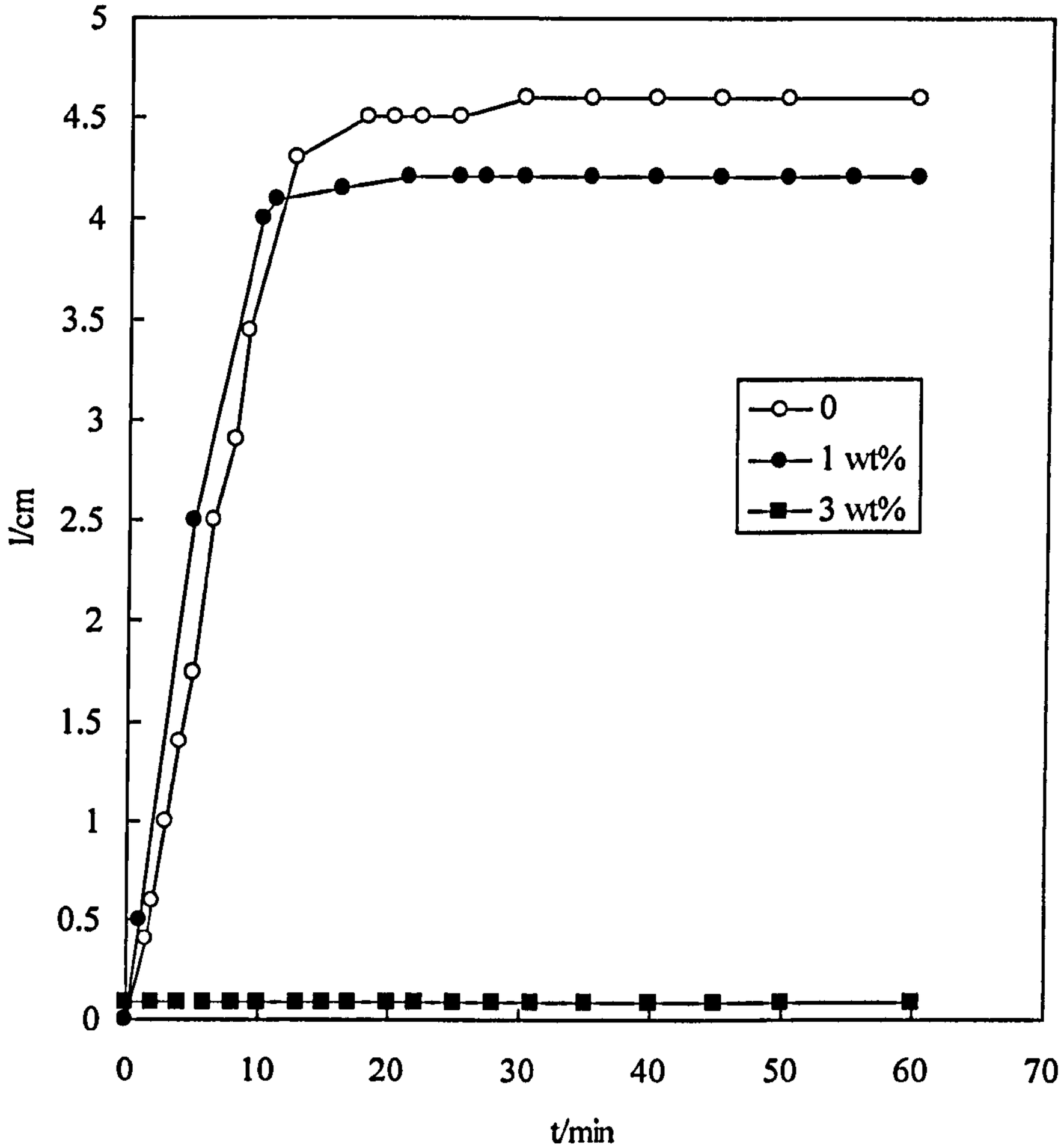

5.3 Evaporation rates of gelled emulsions

Experiments to measure evaporation rates of gelled o/w emulsions were performed by adding the required concentration of the thickening agents to each emulsion to inhibit the process of creaming. Firstly, the evaporation rates of the aqueous dispersions of gelling agent were measured. Following Raoult's law, the dispersion or dissolution of high-molecular weight polymers is not expected to affect the vapour pressure of the solvent. Consisted with this, the evaporation of highly concentrated gelled dispersions of silica particles shows a similar rate to that of pure water[7]. Figure 5.9 shows the mass loss curves of an aqueous dispersion of 1 wt% k-carrageenan together with the calculated best-fit curve. D_v is the only parameter floated (and has a value equal to that for pure water). Hence, it can be concluded that the evaporation rate of the aqueous dispersion of 1 wt% κ-carrageenan is equivalent to that of pure water. Figure 5.10 shows the mass loss curves of an aqueous dispersion of 3 wt% Avicel (m_o = 3.8 g). The experiment was carried out over 10 days (until total evaporation of the sample). Only D_v was floated and the calculated best-fit value ($D_v = 2.18 \times 10^{-5}$ m^2 s^{-1}) was again not significantly different to that for pure water. Initially, the polymer concentration was 3 wt% but as the water evaporates, the dispersion becomes more and more concentrated. At the end of the experiment, after 10 days (900000 s) and when almost all the water is lost, the mass loss rate is still approximately constant.

Figure 5.9 **Mass loss versus time plot of 1 wt% κ-carrageenan aqueous dispersion. The calculated curve, using a value of Dv for water of 2.28 x 10^{-5} m^2s^{-1}, corresponds to the evaporation of water alone. The solid line is the experimental data and the dashed line is the calculated.**

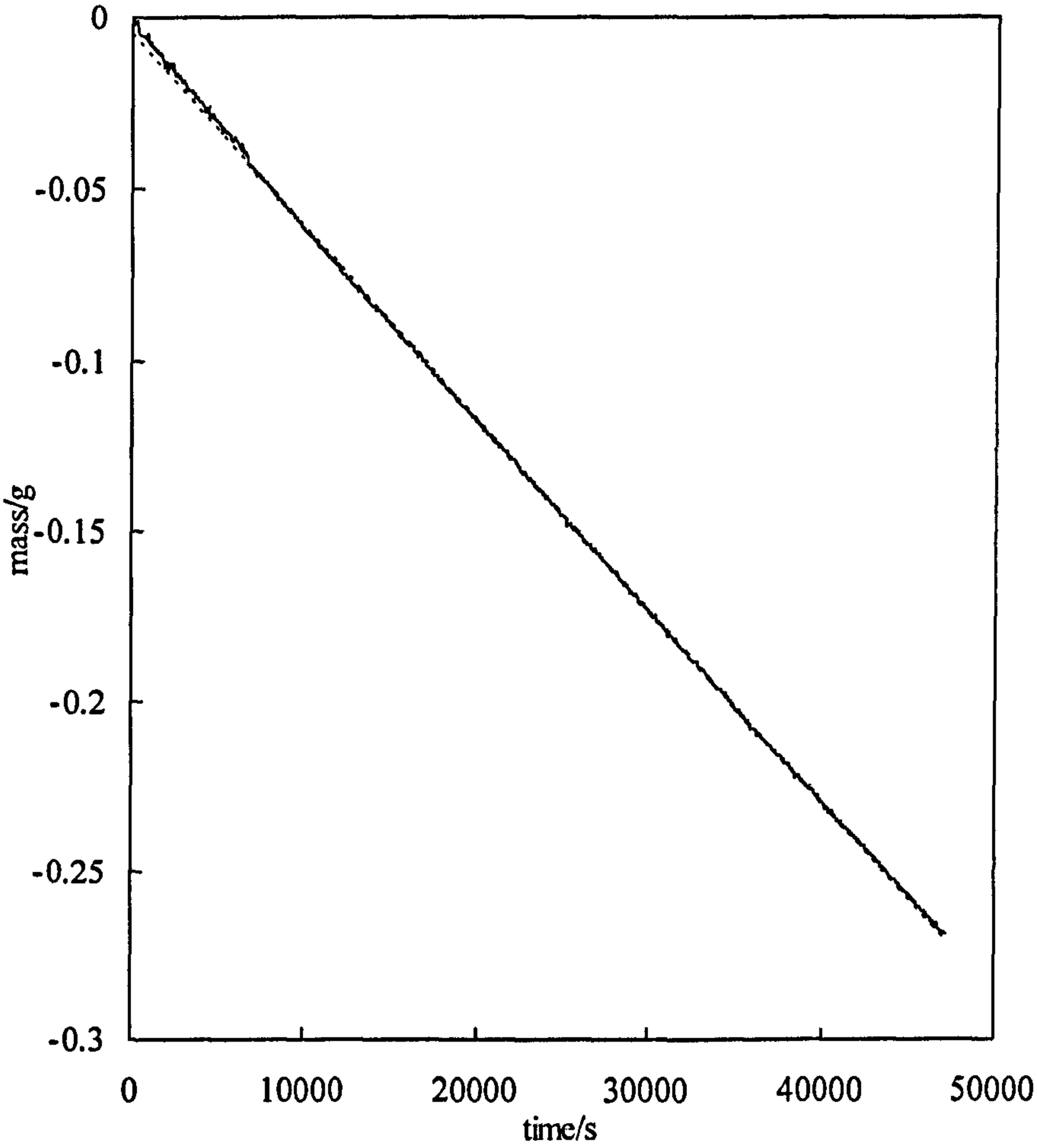

Figure 5.10 Mass loss versus time plot for a 3 wt% Avicel aqueous dispersion. The calculated curve, using a value of Dv for water of 2.18 x 10^{-5} m^2 s^{-1}, corresponds to the evaporation of water alone. The experimental data and the calculated line are compared.

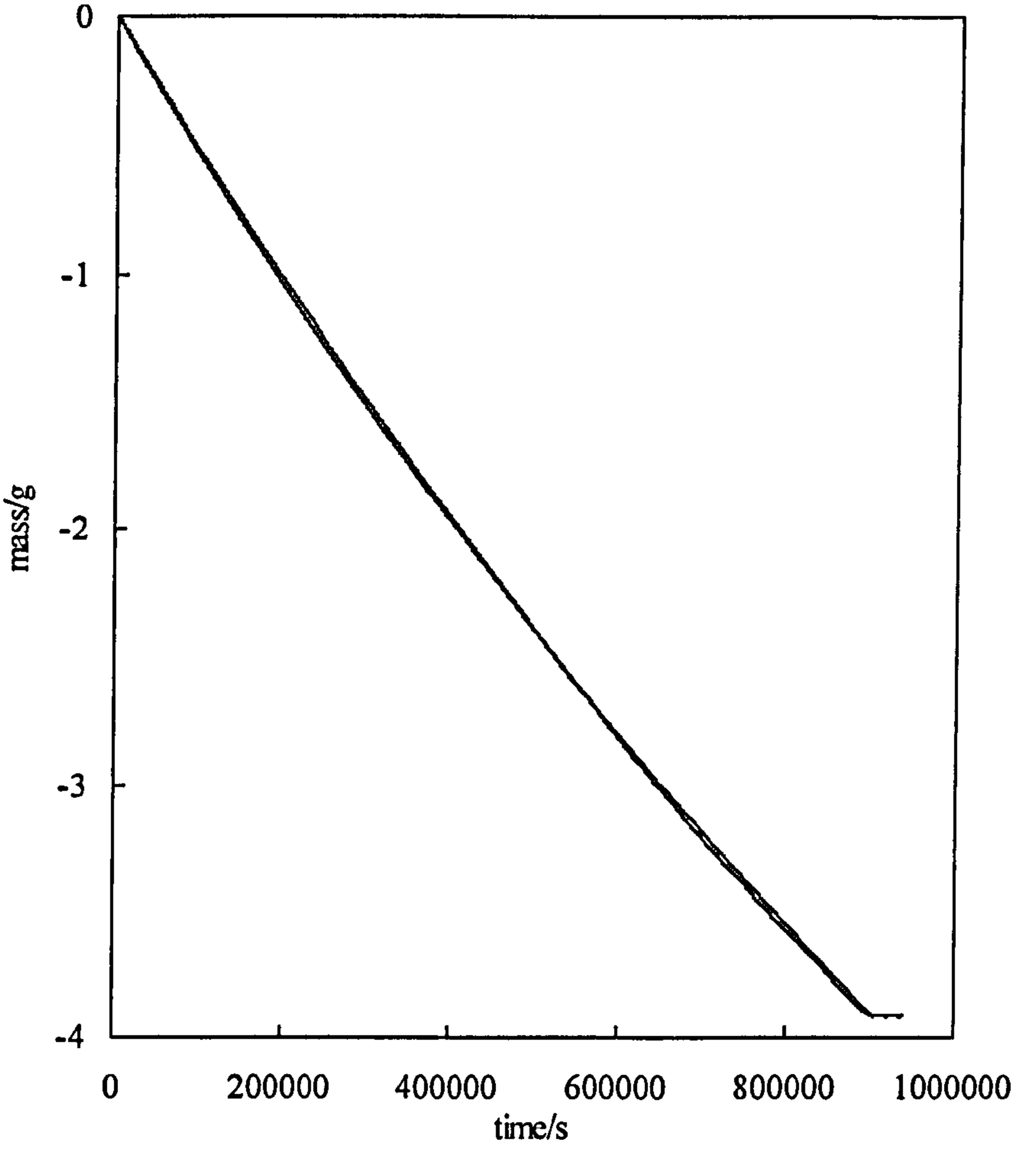

In this stage, the dispersion is very concentrated (up to 99 wt%) and very viscous but the water loss rate is constant.

Finally when all water is lost, the sample mass is only due to the remaining polymer and no further mass loss is recorded. This interesting experiment shows that the water evaporation rate (and hence the vapour pressure) is independent of the Avicel concentration, even for very concentrated aqueous dispersions (up to 99 wt%), and equal to that of bulk water.

Figure 5.11 shows the mass loss curves of pure methylcyclohexane ($\phi_o = 1$), pure water ($\phi_o = 0$) and 20-40 vol% methylcyclohexane-in-water emulsions stabilised by 20 mM SDS and gelled by 1 wt% κ-carrageenan. Gelled emulsions show intermediate mass loss rates between pure oil and pure water and as the oil volume fraction is increased, the total mass loss rate of the emulsion is more similar to that of pure oil. As the continuous phase evaporates (with the same rate as pure water), the oil drops will be uncovered at the surface which is expected to enable their evaporation (see Figure 5.12). At higher oil drop volume fractions, more of the volatile oil drops are uncovered per unit time and hence the overall mass loss increases (as observed experimentally).

In order to investigate the effect of such polymers on the evaporation of water from o/w emulsions, we have decided to use an involatile oil, squalane.

Figure 5.11 Mass loss curves for pure methylcyclohexane ($\phi_o = 1$), 20 mM SDS aqueous solution ($\phi_o = 0$) and 20-40 vol% methylcyclohexane-in-water emulsions stabilised by 20 mM SDS and gelled by 1 wt% κ-carrageenan.

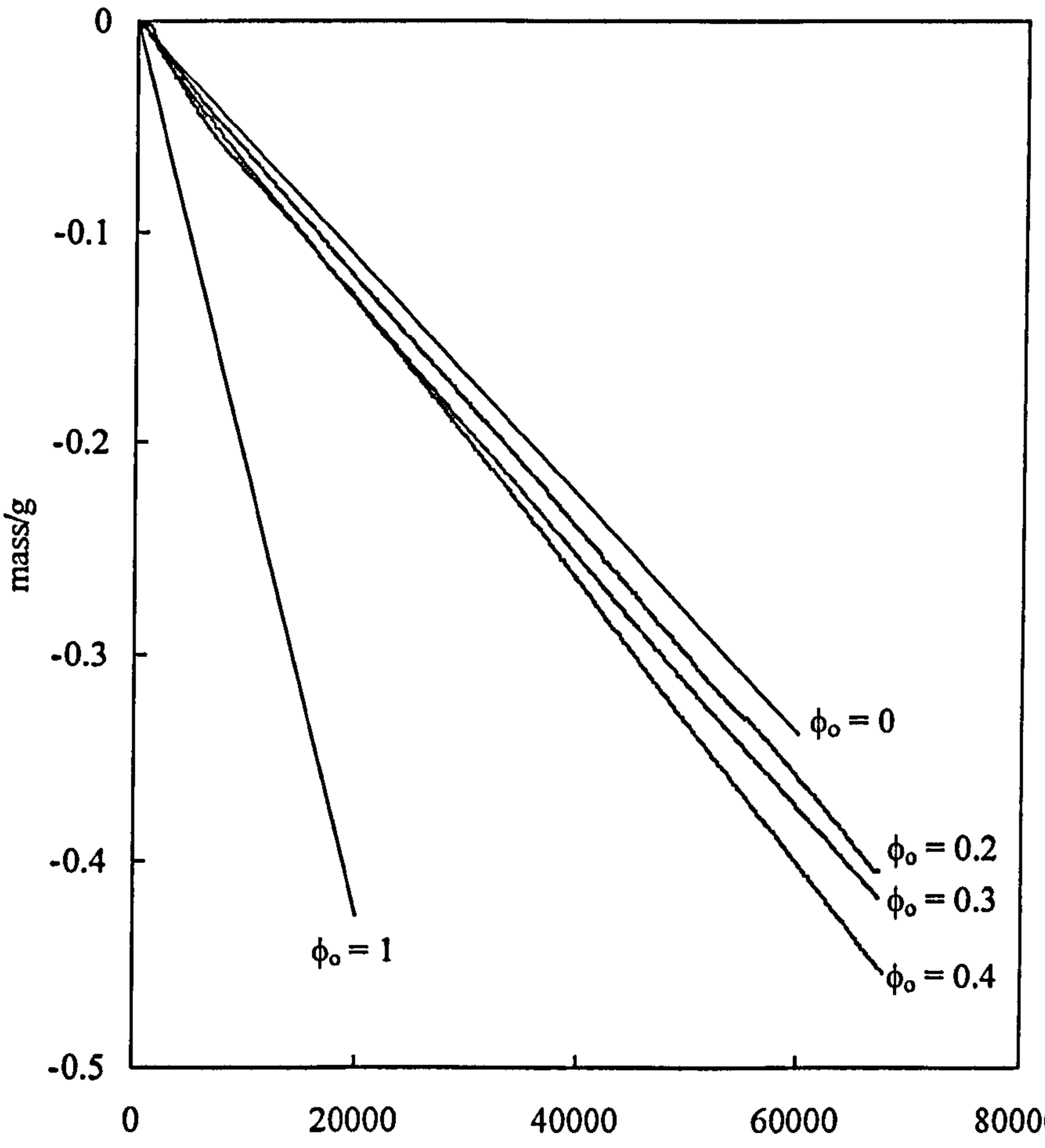

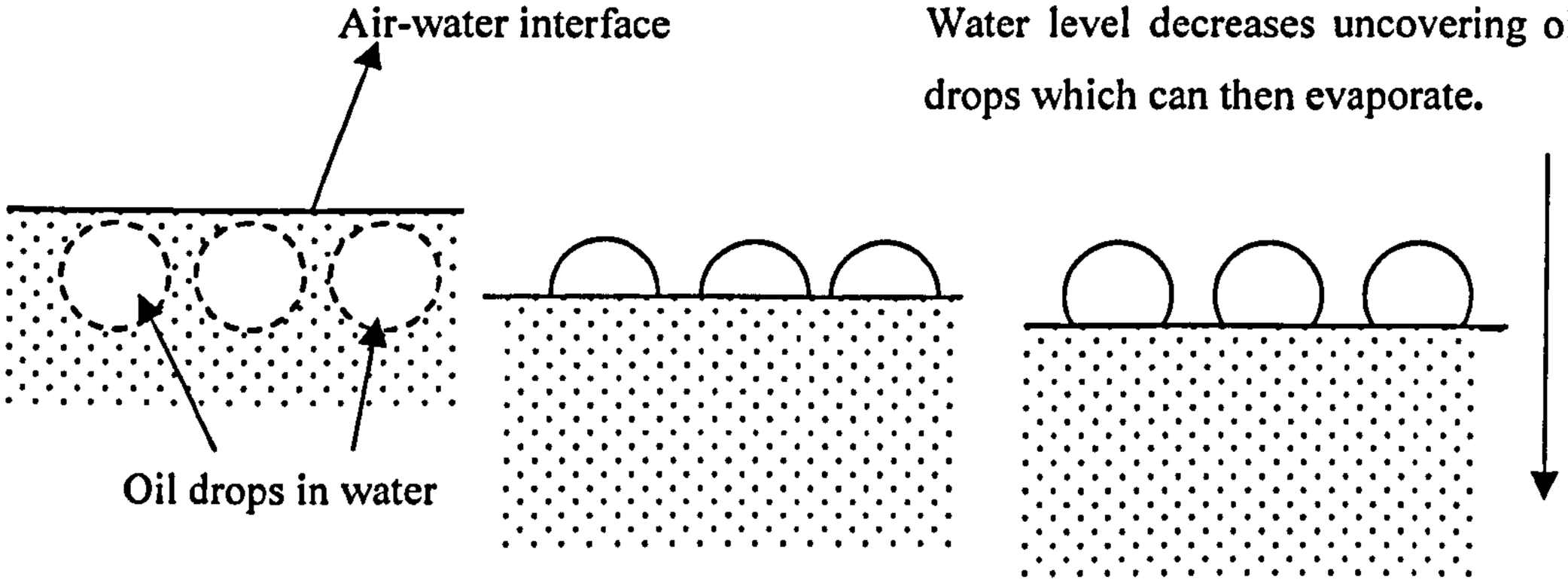

Figure 5.12 Mechanism of the evaporation of gelled emulsions.

Figures 5.13 and 5.14 show the measured mass loss curves of squalane-in-water emulsions stabilised by 20 mM SDS containing different oil volume fractions and gelled by 2 and 3 wt% of Veegum and Avicel respectively. During the mass loss measurement of such emulsions no break point is observed (as expected as the oil is involatile). Moreover, the emulsion mass loss rates are similar to the rate expected for water alone and independent of the oil volume fraction. The mass loss curves of the emulsions gelled by 2 wt% Veegum show both facts (see Figure 5.13). In this case the measured evaporation rate of the gelled emulsions is similar to that of pure water and almost independent of the oil volume fraction. For $\phi_o = 0.5$, the evaporation rate of the gelled emulsion is slightly slowed down if compared to $\phi_o = 0$ and 0.15 but this deviation may be due to an error or uncertainty in the measurement.

Figure 5.13 **Comparison between mass loss curves of squalane-in-water emulsions (ϕ_o= 0.15 and ϕ_o= 0.50) gelled by 2 wt% Veegum and 2 wt% Veegum aqueous dispersion.**

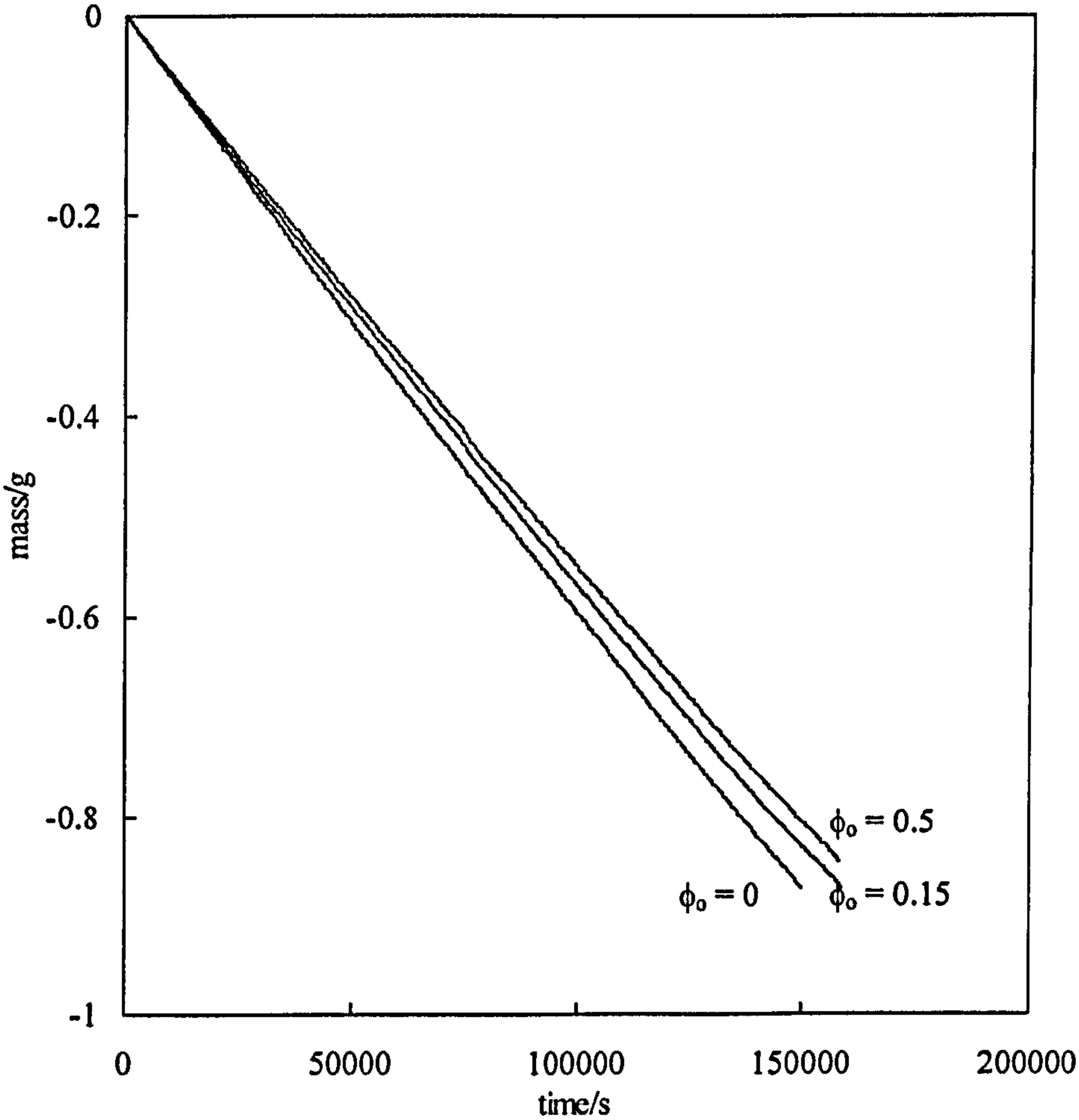

Figure 5.14 **Comparison of the mass loss curves between 50 vol% squalane-in-water emulsion stabilised by 20 mM SDS and gelled by 3 wt% Avicel and the polymer aqueous dispersion alone.**

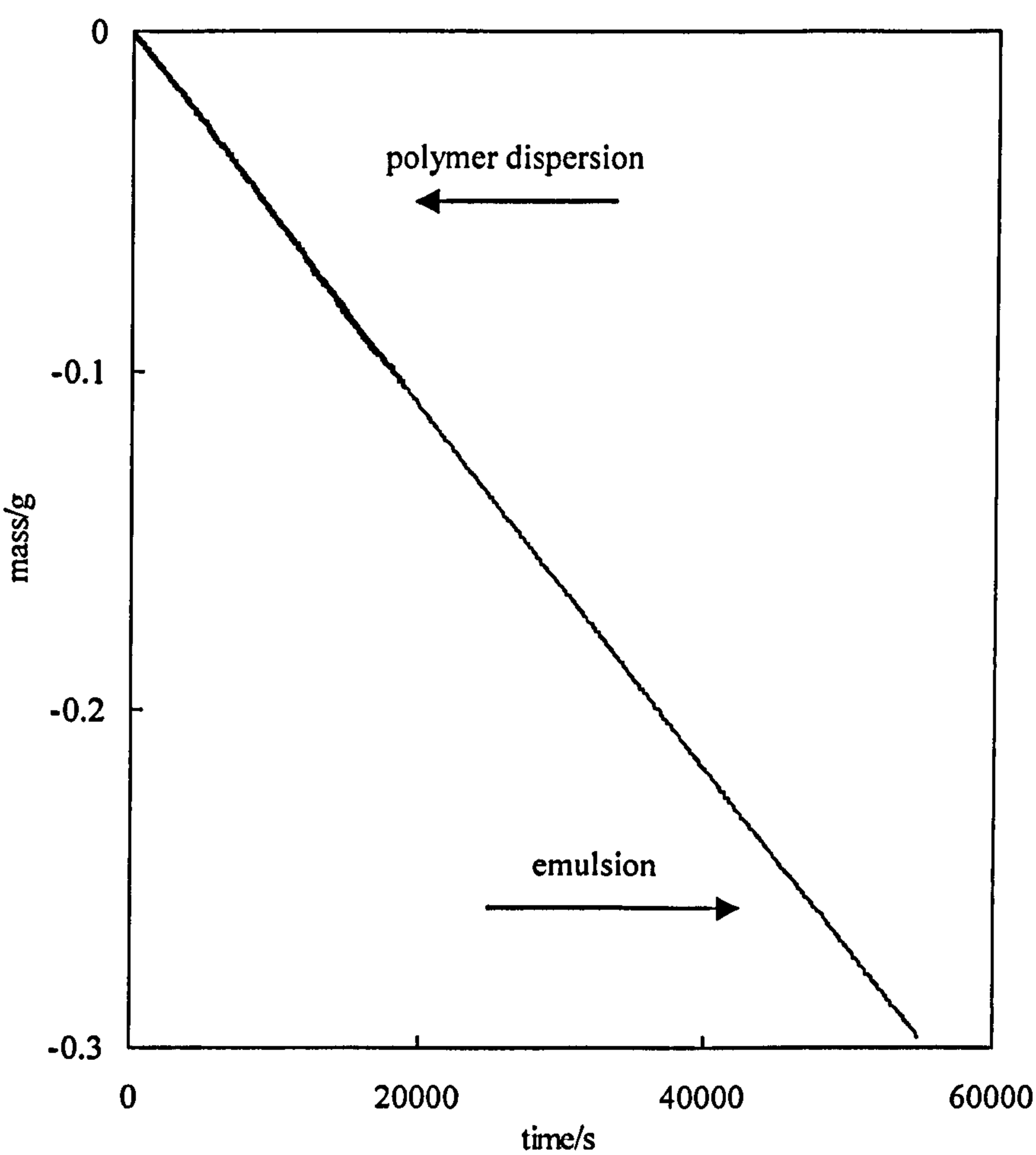

Figure 5.14 shows the comparison between the mass loss curves of an aqueous dispersion of 3 wt% Avicel and 50 vol% squalane-in–water emulsion stabilised by 3 wt% Avicel. Both curves show exactly the same slope and therefore it can be concluded that at least during the initial time, e.g., 60000 s (~20 h), squalane-in-water emulsions gelled by Avicel show no retardation of the evaporation rate of the aqueous continuous phase despite the fact that the surface is concentrating in the oil phase.

Figure 5.15 shows micrographs of the surface of a 50 vol% squalane-in-water emulsion stabilised by 20 mM SDS and gelled by 3 wt% Avicel using three different magnifications. The images were taken very carefully from the surface of the sample 36 h after the sample was left until total evaporation. As the magnification is increased, the nature of the surface is clearer. In Figure 5.15a, a general picture of the surface is shown and two different "substances" can be observed: oil dispersed droplets and darker gaps probably filled by aqueous continuous phase. In Figure 5.15b, apart from the squalane drops, which are deformed, aqueous gaps are distinguished. In Figure 5.15c, a very clear picture of the surface is shown. The edge of the image is covered by deformed and packed oil drops and in the middle, an approximately 100 μm hole appears. Inside, water insoluble, rod-like Avicel filaments are found. These insoluble filaments create "big" aqueous gaps. Hence the total oil-uncovered surface area remains big enough for the easy transport of water to the vapour phase. Hence, the mass loss of the emulsion (only due to the mass loss of the aqueous continuous phase) is equivalent to that of bulk water.

Figure 5.15 **Micrographs of the surface of a 50 vol% squalane-in-water emulsion stabilised by 20 mM SDS and gelled by 3 wt% Avicel taken 36 h after preparation.**

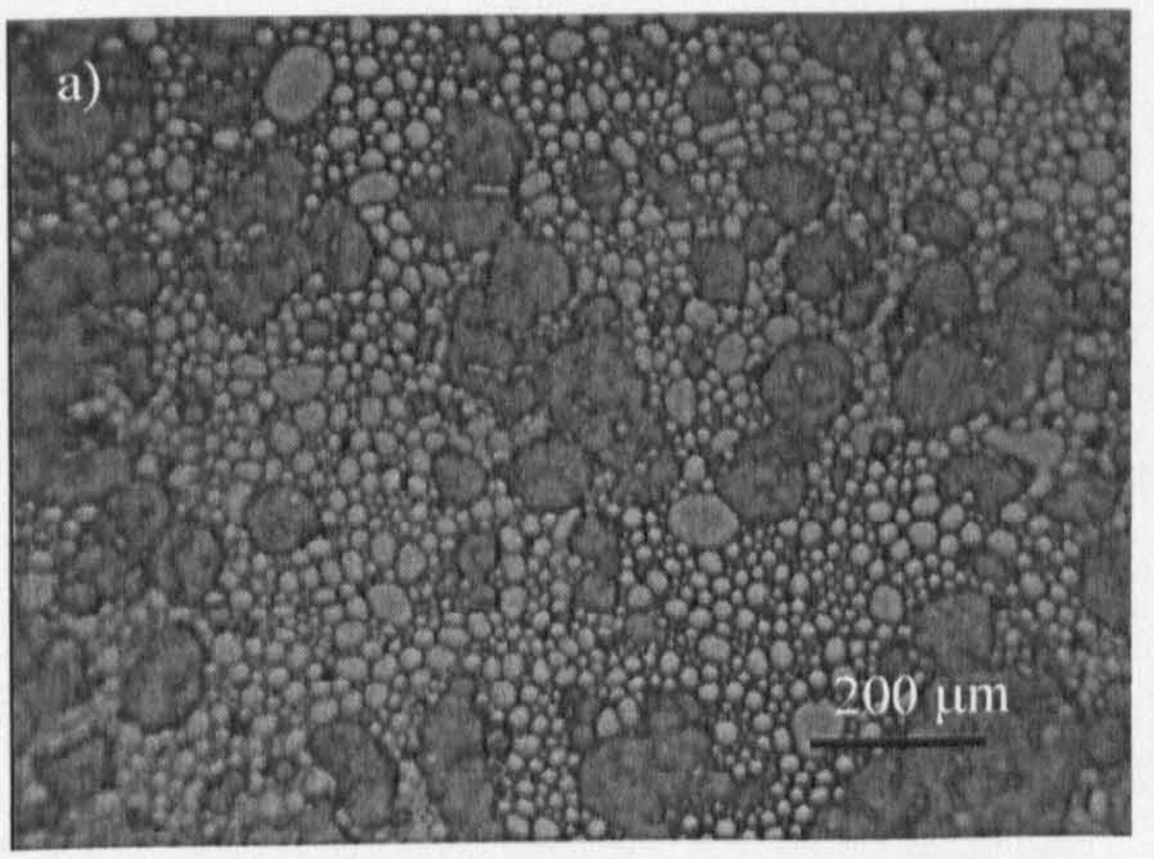

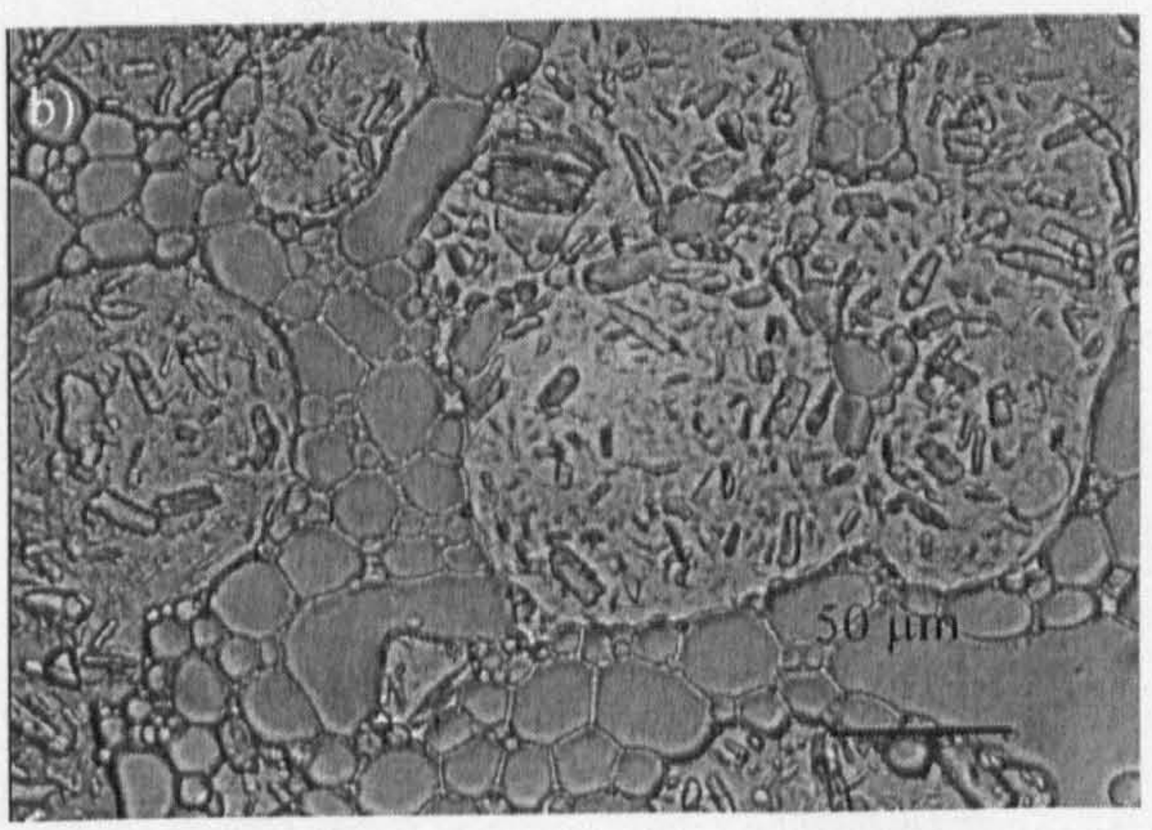

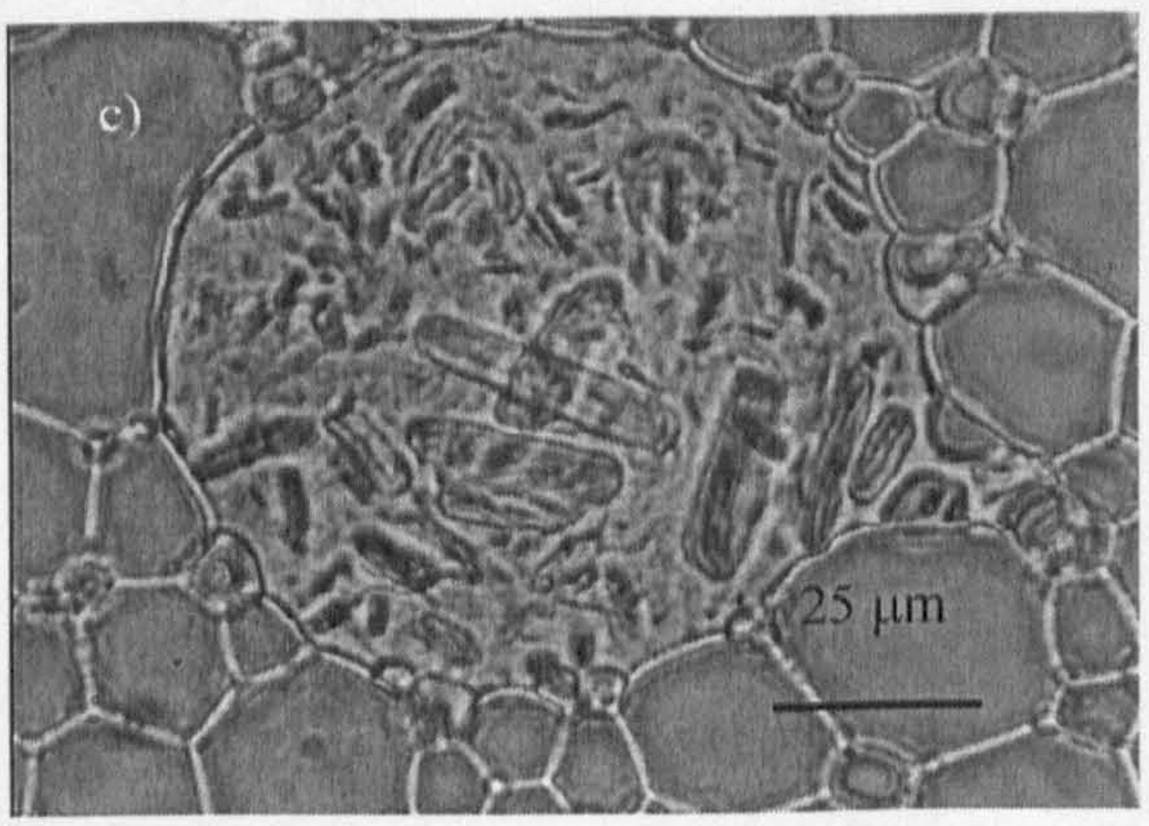

These images support the data obtained in the evaporation rate-measuring rig where (see Figure 5.14) the mass loss rate after 36 h is exactly the same as the mass loss rate of pure water.

Figure 5.16 shows the mass loss curves for squalane-in-water emulsions stabilised by 20 mM SDS and gelled by 1 wt% Kelzan. The oil volume fraction varies from 0 to 0.5. Mass loss curves of emulsions gelled by Kelzan show completely different behaviour compared to the other gelled emulsions. In this case, as the oil volume fraction is decreased, the evaporation rate of the aqueous continuous phase is increased. As the selected oil is involatile, the surface of the emulsions becomes richer gradually with the polymer and involatile oil phase while the aqueous continuous phase is evaporating. Eventually an oil layer covers the total surface area of the emulsions and completely prevents the evaporation of water. For emulsions with high oil volume fraction, it is observed that the surface is covered faster by the oil phase, inhibiting the evaporation of water at earlier times. Figure 5.17 shows micrographs of the surface of the 50 vol% squalane-in-water emulsions stabilised by 20 mM SDS and gelled by 1 wt% Kelzan. Figure 5.17a shows the surface of a fresh emulsion (t = 0). The oil drops are spherical and distributed all over the surface. After 19 h (~70000 s), (see Figure 5.17b), as the aqueous continuous phase evaporates the oil drops approach and the evaporation rate of water starts to be affected. Figure 5.17c shows the surface of the said emulsion 48 h (~175000 s) after preparation. The squalane drops are deformed and polyhedral-like in shape. The evaporation of the continuous phase is almost stopped by the presence of the oil on the top of the emulsion sample, which is evident in Figure 5.16.

Figure 5.16 **Comparison of the mass loss curves of 20 mM SDS aqueous solution, 1 wt% Kelzan aqueous dispersion and squalane-in water emulsions stabilised by 20 mM SDS and gelled by 1 wt% Kelzan.**

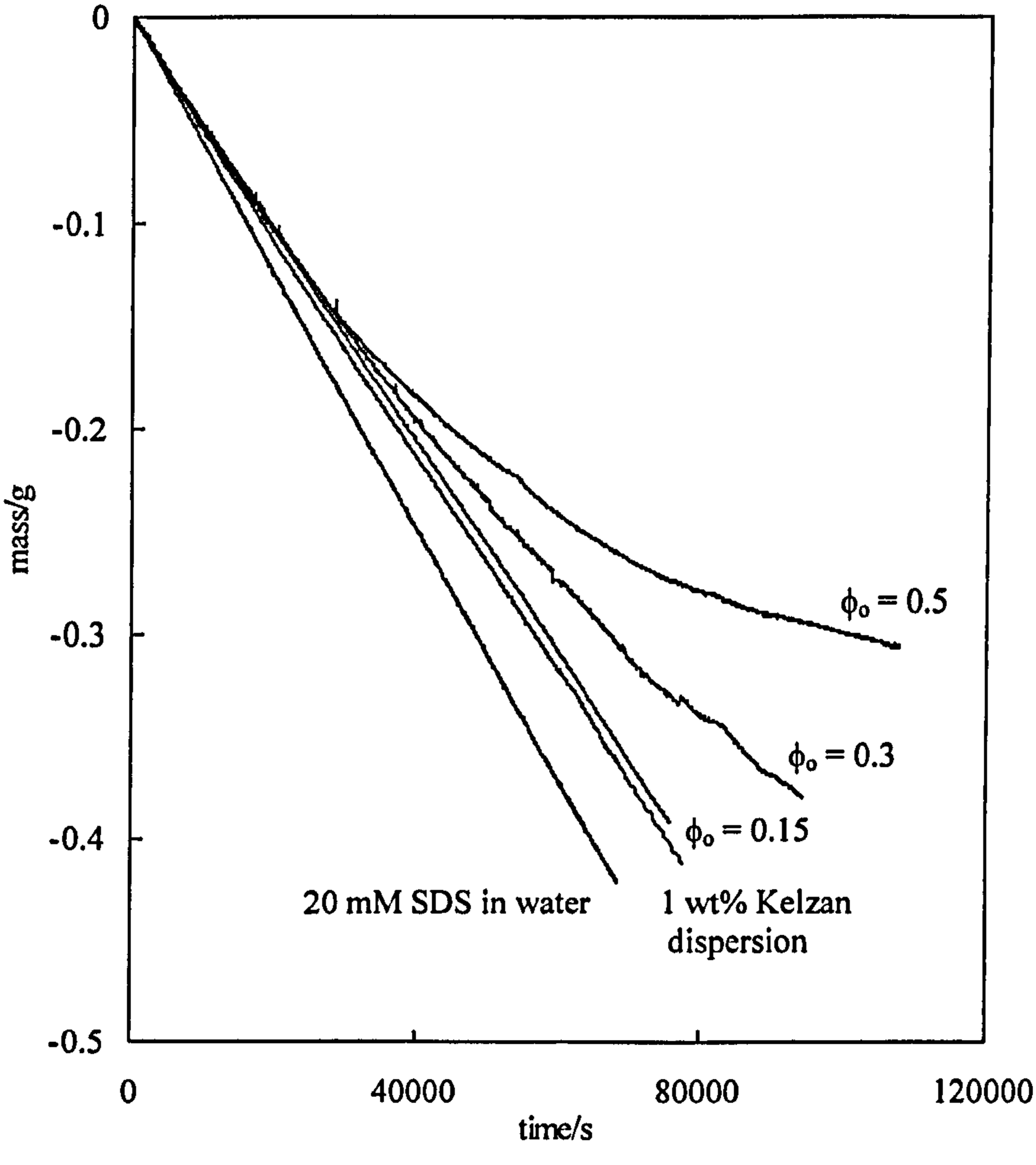

Figure 5.17 **Micrographs of the surface of a 50 vol% squalane-in-water emulsion stabilised by 20 mM SDS and gelled by 1 wt% Kelzan as a function of time.**

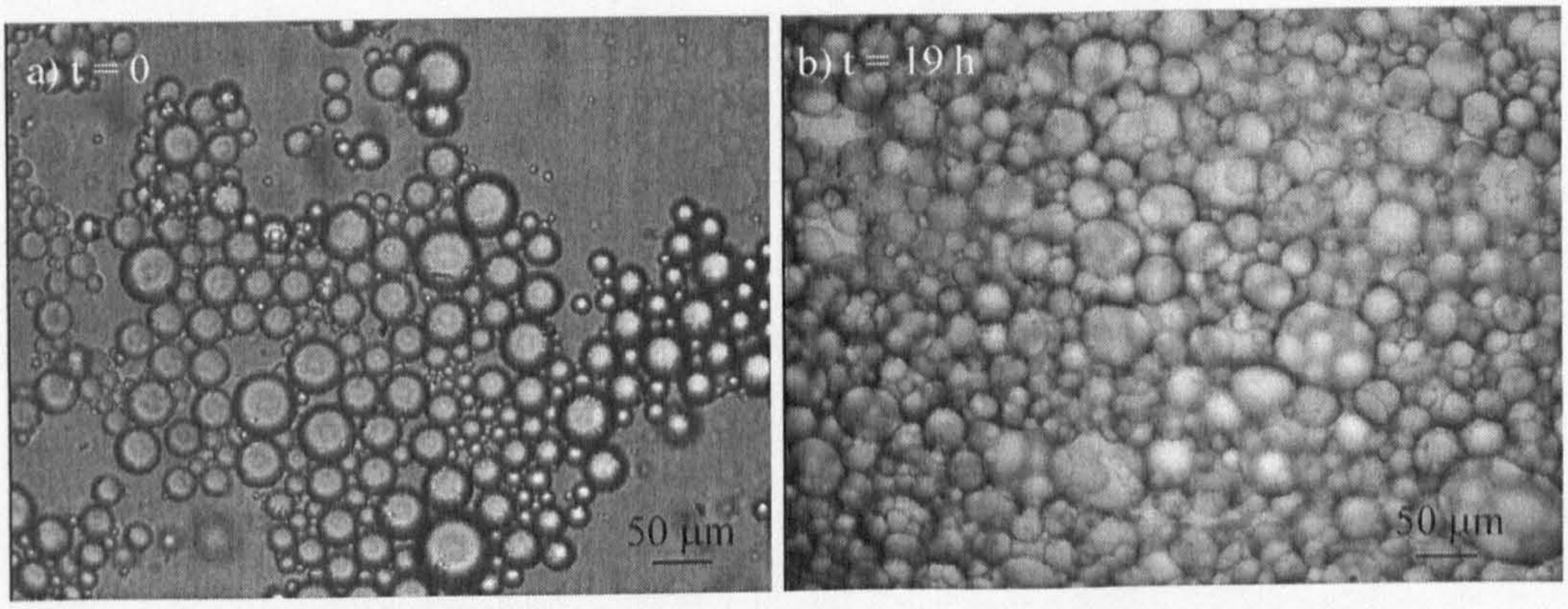

Finally, in Figure 5.17d, oil drops coalesce and form an oil layer on the top inhibiting the mass loss of the emulsion.

Complete quantitative analysis of the evaporation rates for gelled emulsions has not been undertaken as the quality and reproducibility of the mass loss curves is significantly worse than for non-gelled emulsions. We observe that evaporation of the gelled emulsions commonly leaves a "ring" of polymer residue adhering to the inner side of the sample vessel. This observation implies that the emulsion surface may stick to the sample vessel wall during evaporation which appears to cause irreproducible changes in the emulsion (and hence evaporation rate) during evaporation.

5.4 Conclusions

- Above a critical concentration, high-molecular weight polymers and solid colloidal particles inhibit the creaming process of o/w emulsions by increasing the viscosity of the aqueous continuous phase.
- The presence of non-adsorbing polymers at low concentration may accelerate the creaming by forming aggregates of oil drops by depletion flocculation.
- o/w emulsions gelled by water-insoluble polymers such as Avicel show no retardation in the water evaporation rate. This effect is related to the formation of big aqueous gaps on the surface of these gelled emulsions.

- o/w emulsions gelled by water soluble polymers such as Kelzan show retardation in the evaporation rate of the water continuous phase due to the formation of an (involatile) oil layer on the top of the emulsion.

5.5 References

1 E. Dickinson, *Gums and Stabilizers for the Food Industry*, ed. G. O. Phillips, P. A. Williams and D.J. Wedlock, IRL Press, 1988.

2 M. Glicksman, Food Hydrocolloids, vol 1, CRC Press, Boca Raton, Florida, 1982.

3 E. Dickinson and K. Pawlowsky, *J. Agric. Food Chem.* 1997, **45**, 3799.

4 E. Dickinson and S. R. Euston, *Food Polymers, Gels & Colloids*, ed. E. Dickinson, RSC Publications, Vol. 82, Cambridge, 1991.

5 E. Dickinson, M. I. Goller and D. J. Wedlock, *J. Colloid Interface Sci.*, 1995, **172**, 192.

6 A. E. Bell in "Water and Food Quality", ed. T.M. Hardman, Elsevier Applied Sci., Chapter 7, 1989

7 K. J. Beverley, J. H. Clint and P. D. I. Fletcher, *Phys. Chem. Chem. Phys.* 2000, **2**, 4173.

Chapter 6

CHAPTER 6

EVAPORATION RATES OF SURFACTANT- STABILISED HIGH INTERNAL PHASE EMULSIONS (HIPEs)

6.1 Introduction

High internal phase emulsions (HIPEs) are concentrated emulsions possessing a large volume of internal or dispersed phase. When the volume fraction of the dispersed phase in a monodisperse emulsion ϕ equals 0.74, the droplets can fit in hexagonal close packing without being deformed[1]. When ϕ exceeds this value, each droplet is deformed and thin flat films of continuous phase are formed at each point where the drops "touch". For polydisperse emulsions, the dispersed volume fraction may be higher that 0.74 as the gaps between the droplets can be filled by smaller ones. Solans *et al*[2] have reported HIPEs where the dispersed volume fraction is 0.99. HIPEs are often referred to as gel emulsions due to their high viscosity but like dilute emulsions, are thermodynamically unstable and can be broken by coalescence of dispersed droplets. As will be shown, for emulsions with such high-dispersed volume fractions, the drops may also invert or form multiple emulsions. Each film is under a compressive pressure, which is counteracted by a disjoining pressure that is developed within the film because of electrostatic, steric or other repulsive forces, so that equilibrium is maintained. As ϕ is increased is further and

further, it is plausible that a stage is reached where the disjoining pressure can no longer balance the compressive forces being exerted, and at this point the emulsion is expected to start breaking down or invert.

In this Chapter the evaporation rate of water (the continuous phase) from HIPEs containing an involatile oil (PDMS, viscosity = 300 cS) will be discussed. As will be explained in detail, the evaporation rate of water contained in the thin films separating the oil droplets depends on both the nature of the colloidal forces (repulsive and attractive) and the film thickness between two droplets. In our case, evaporation rates from emulsions stabilised by the anionic surfactants SDS will be studied. Depending on the conditions several different situations may arise: the evaporation may be controlled either by diffusion in the vapour phase of water or by the diffusion of water in the network thin films in the emulsion. On the other hand, in the presence of NaBr in the continuous phase, the repulsive electrostatic forces between SDS monolayers are expected to disappear due to a screening effect. In this case, compression of the drops may lead to coalescence and the formation of a macroscopic oil film at the surface of the sample.

In the case of HIPEs, the most likely emulsion-breaking mechanism is coalescence. As explained in Chapter 2, coalescence is the combining of two droplets to form a single larger droplet. Coalescence involves a thinning of the continuous phase film between the droplets until all the continuous phase has been expelled and two drops merge. The time needed for coalescence to happen will depend on the stability of the

emulsions, which depends on the colloidal forces present within the thin film of thickness d formed between the drops. Figure 6.1 shows how two drops merge into a bigger one. The coalescence mechanism is not yet well understood but is thought to be related to the preferred curvature and rigidity of the stabilising surfactant monolayer[3,4].

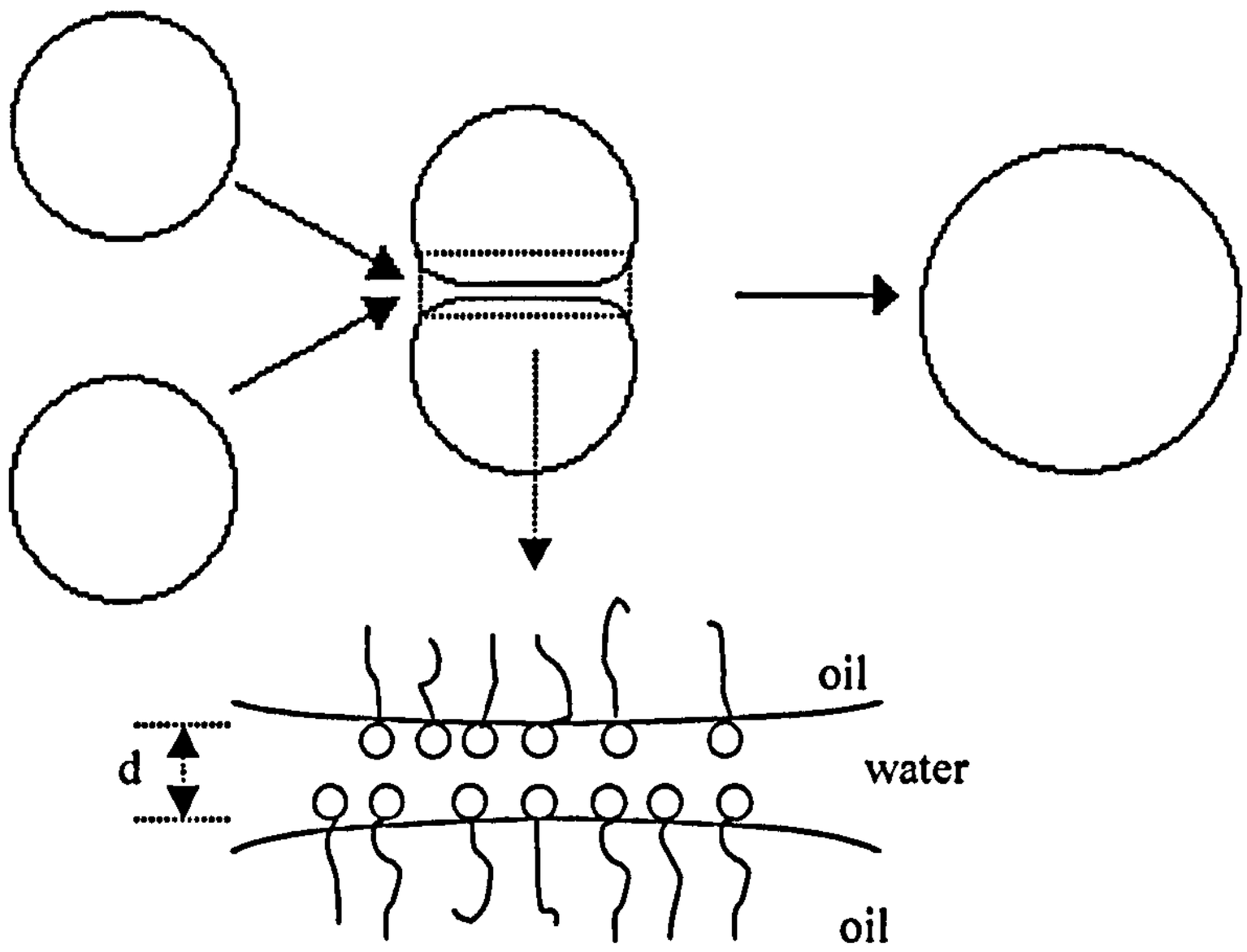

Figure 6.1 Droplet coalescence.

The interactions between two interfaces (oil drops in this case) can be quantified as an excess pressure per unit film area or disjoining pressure, Π, versus the separation distance, i.e. the film thickness, d. The disjoining pressure is defined as positive when it resists film thinning, i.e., the net forces between two oil droplets stabilised by surfactant monolayers are repulsive.

The vapour pressure P of water confined in the thin water films separating the oil drops is affected by the disjoining pressure operating between the drop surfaces according to[5],

$$P = P_o \exp\left(-\frac{\Pi v}{kT}\right) \qquad [6.1]$$

where P_o is the vapour pressure of bulk water, v is the molecular volume of water and k is the Boltzmann constant. From equation [6.1], it can be seen that a positive disjoining pressure (i.e. a repulsive force between oil drops) causes a decrease in water vapour pressure and, a corresponding decrease in evaporation rate. For the emulsions used in this work, which are stabilised by the anionic surfactant SDS, we assume that the total disjoining pressure decays exponentially with film thickness d according to

$$\Pi = \Pi_o \exp(-d/d_o) \qquad [6.2]$$

where Π_o is the disjoining pressure corresponding to contact between emulsion drop surfaces (i.e. d = 0) and d_o is the decay length. This form of exponential force law is expected for electrostatic repulsive forces for which the decay distance d_o is equal to the Debye length[6].

For undeformed drops, the total surface area per unit volume exposed by the oil droplets, A_o is given by:

$$A_o = \left[\frac{m_t - m_w}{\rho_o}\right] \times \left[\frac{1}{4/3\,\pi r_o^3}\right] \times \left[4\pi r_0^2\right] = \frac{(m_t - m_w)}{\rho_o} \cdot \frac{3}{r_o} \qquad [6.3]$$

where m_t is the total mass, m_w is the water mass and ρ_o and r_o are the density and the average radius of the oil drops. For emulsions containing drops with a mean non-deformed spherical radius r, the average water film thickness d is

$$d = \frac{2v_w}{A_o} \approx \frac{2\phi_w r_o}{3(1-\phi_w)} \qquad [6.4]$$

where all parameters are known. We assume that the mean drop diameter does not change during the evaporation. Since the oil is involatile, as water mass loss is recorded, ϕ_w is always known and d is easily calculated. It should be noted that the value of d is only expected to be uniform throughout the emulsion if the water is uniformly distributed. If water diffusion in the emulsion is slow relative to the water evaporation rate, then a water concentration gradient will develop in the emulsions (a hence a gradient in d).

Equations [3.14], [6.1] and [6.4] combined with the assumption that the disjoining pressure varies with d, can be used to predict evaporation mass loss versus time curves for concentrated emulsions. Use of equation [6.2] corresponding to electrostatic repulsion between the emulsions drop surfaces, enables the sensitivity of the water evaporation rates to strength and range of electrostatic repulsive inter-droplets forces (i.e. through variation of Π_o and d_o) to be explored. Apart from model parameters relating to the colloidal forces, all other input parameters (P, D_v, h, r_o, A, etc) are easily measured independently.

Figure 6.2 shows a series of simulated mass loss curves corresponding to water evaporation at 25 °C from 3.0 g o/w emulsions samples initially containing 20 vol% of water. Figure 6.2a shows the effect of changing the magnitude of repulsive disjoining pressure through variation of Π_0.

Figure 6.2 **Simulated water mass loss curves for o/w emulsions containing 80 vol% of dispersed drops of involatile oil. Unless stated otherwise, r = 4 μm, $\Pi_0 = 3 \times 10^8$ Pa and $d_0 = 50$ nm. In Figure 6.2a, the right hand scale shows the film thickness corresponding to the mass loss indicated on the left hand scale.**

a) Variation of Π_0

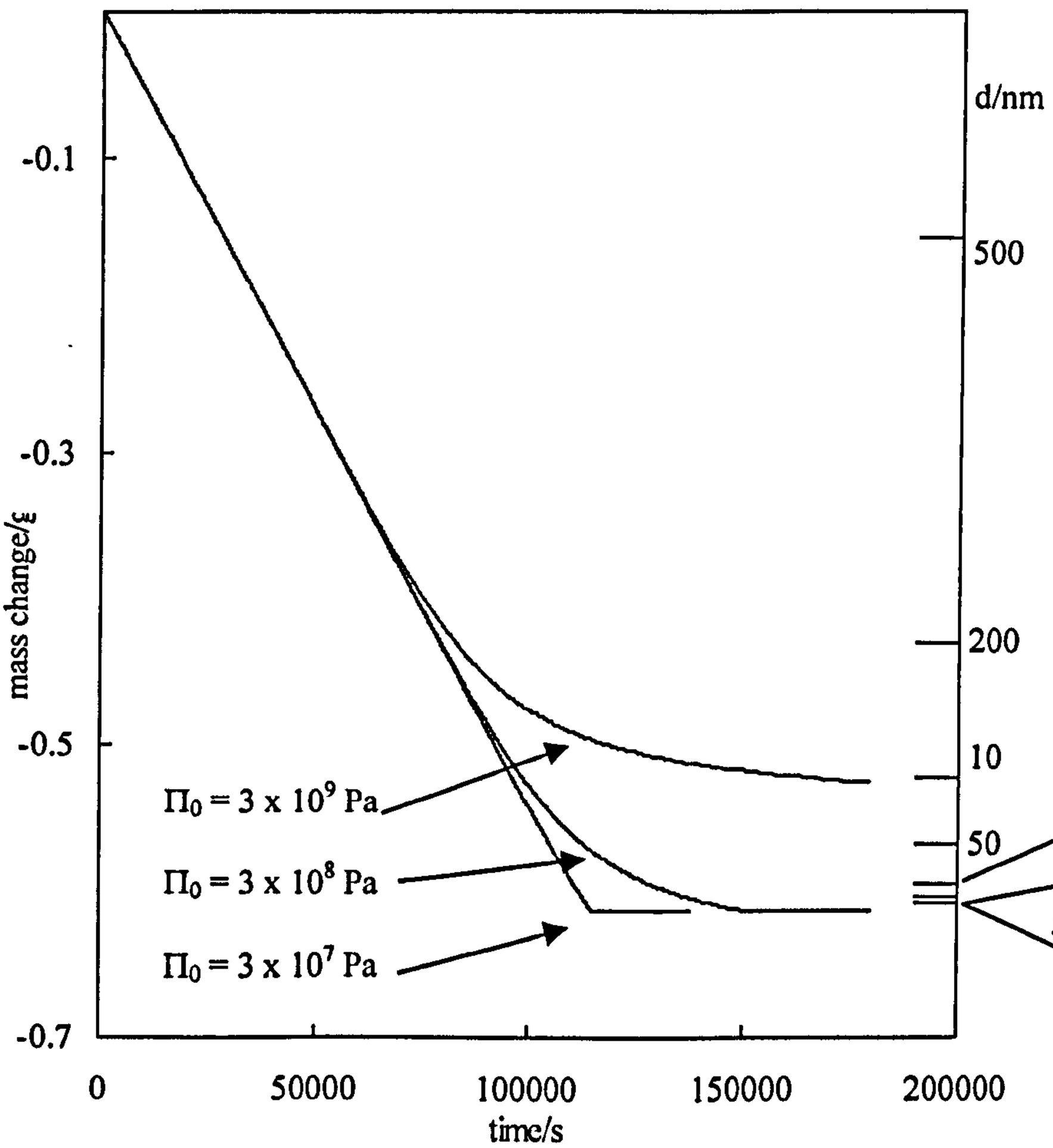

When repulsive forces are weak (i.e. when Π_0 is low), the mass loss curves show a sharp kink corresponding to the point at which all the water initially present is lost. Stronger repulsion acts to reduce the water pressure and slow the evaporation before all the water is lost, i.e. the kink is "smoothed". A repulsive disjoining pressure of the order of 10^7 Pa is required to produce measurable reduction in vapour pressure (and hence evaporation rate) of about 10%. For this magnitude of repulsive interaction to give an observable "smoothing" of the sharply kinked mass loss curve, the disjoining pressure must operate over a film thickness of at least 20 nm (see right scale of Figure 6.2a). Both the magnitude and the range of repulsion required to significantly affect the evaporative mass loss curves are much higher than experimentally measured values. For o/w emulsions stabilised by SDS at a concentration equal to the cmc, the disjoining pressure decays exponentially from approximately 4×10^6 Pa at d = 2.5 nm to 2×10^5 Pa at d = 5 nm[7]. Figure 6.2b shows the influence of the range d_0 of electrostatic repulsive forces. Short range forces (e.g. d_0 = 5 nm) give a strongly kinked mass loss curve since virtually all the available water must be lost before the films are thin enough to be affected by the colloidal forces. Longer range forces give smoother curves. Figure 6.2c shows the influence of emulsion drop radius. When all the other parameters are kept constant, the largest drop size produces the lowest film surface area and hence the thickest film, weakest inter-droplet repulsion and the most linked mass loss curve. Overall, comparison of the calculated curves and the disjoining pressure isotherms of ref. (11) shows that emulsion stabilised by SDS possess interactions of too low a magnitude and range to produce a significant smoothing of the mass loss curves from the limiting kinked shape corresponding to negligible interaction.

b) Variation of d_0

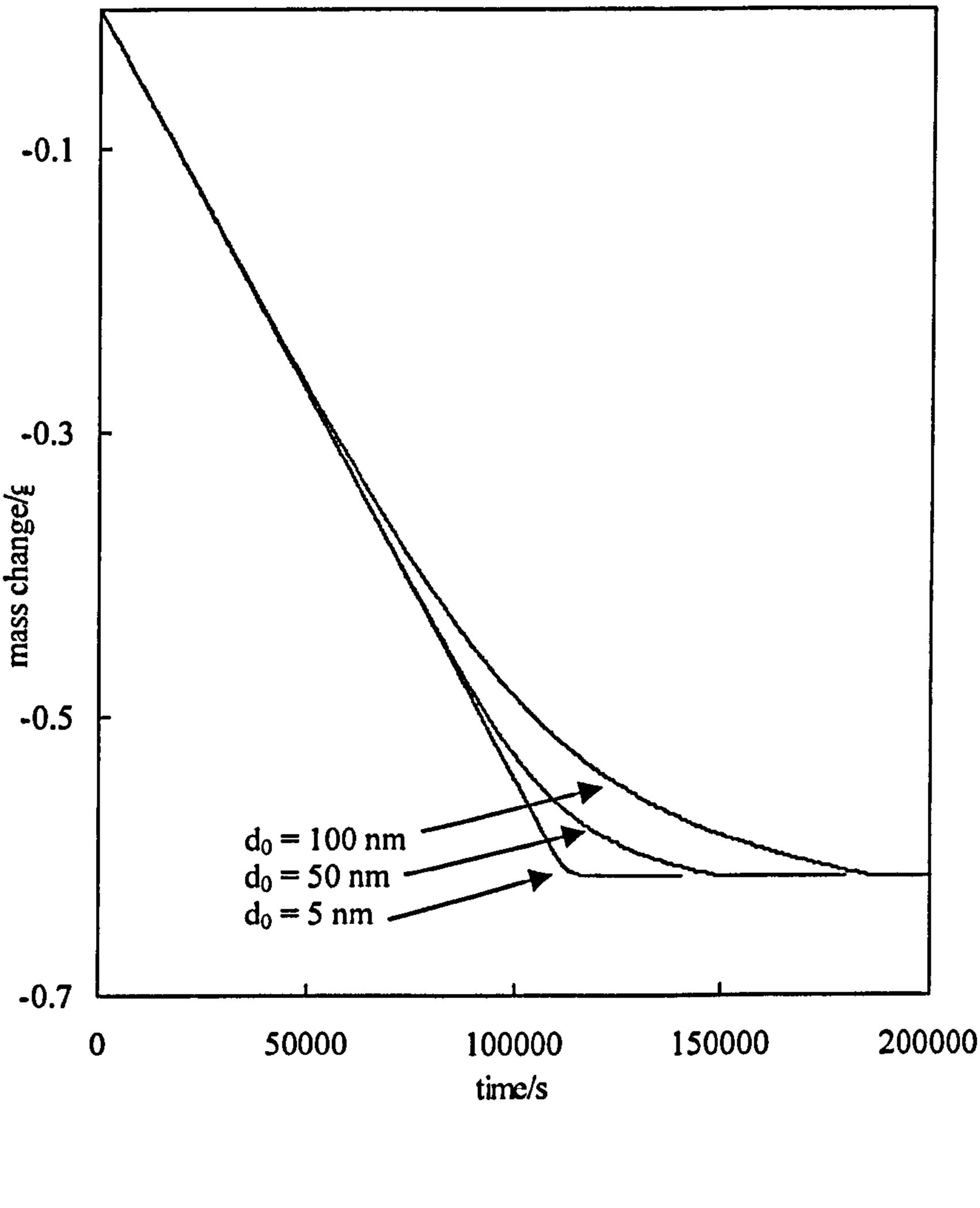

c) Variation of r

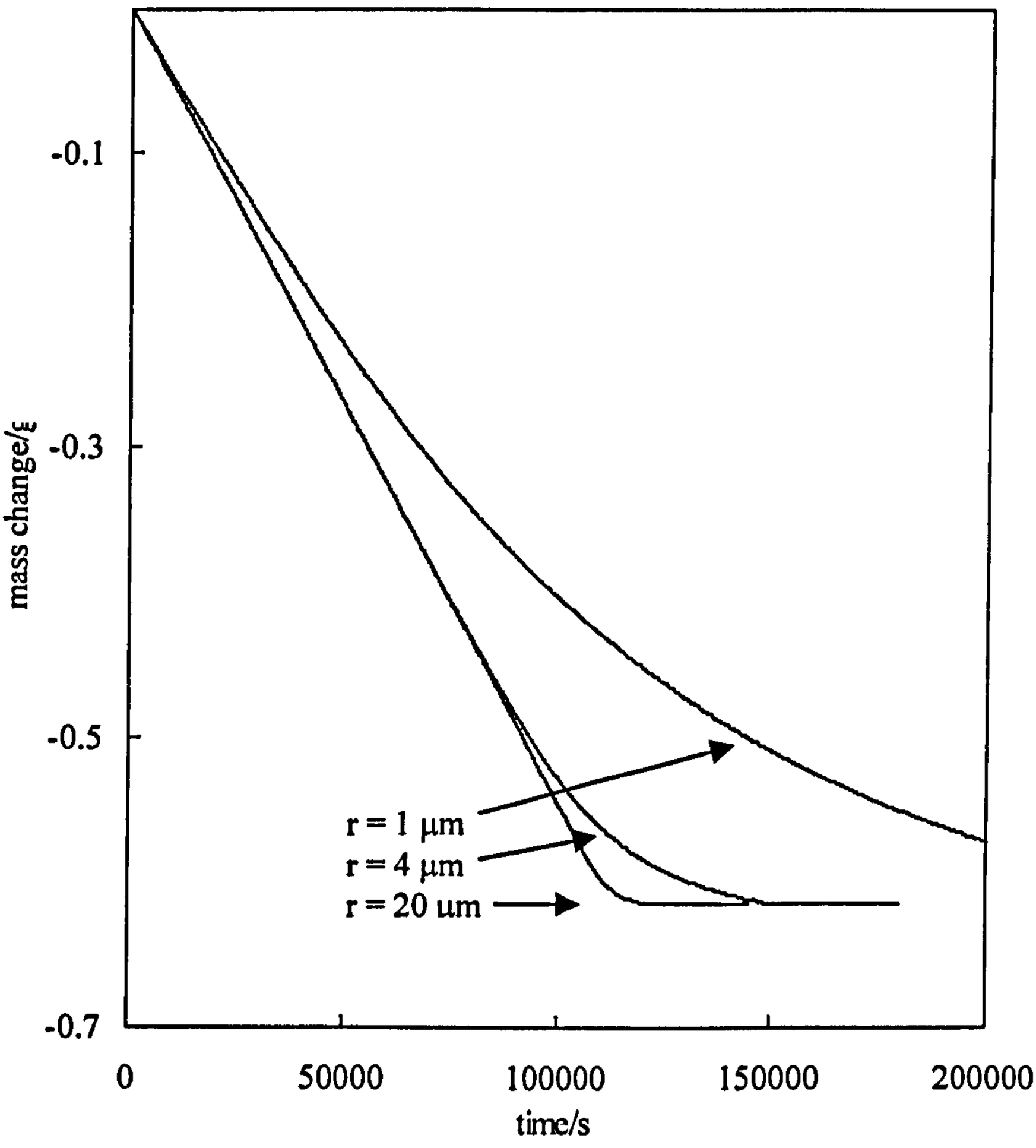

6.2 Phase behaviour of PDMS/w/NaBr emulsions

6.2.1 Absence of NaBr

One way to identify whether an emulsion is o/w or w/o, is to measure the conductivity of the system. Emulsions where the continuous phase is water (o/w) show high conductivity if compared with the conductivity showed by oil continuous phase emulsions (w/o). Starting from a PDMS-in-water emulsion stabilised by 20 mM SDS we found that, in the absence of salt, the conductivity drops drastically from 68 to 0.57 μS cm^{-1} when the oil volume fraction of the emulsion is varied from 0.9 to 0.93. It can be said therefore that PDMS/w emulsions invert from o/w to w/o in that range, at $\phi_o = 0.92$ (see Figure 6.3). This is the first time that phase inversion from o/w to w/o emulsions stabilised by SDS in the absence of co-surfactant has been reported.

Figure 6.4 shows micrographs of PDMS-water emulsions stabilised by 20 mM SDS, for (a) $\phi_o = 0.7$ (o/w), (b) $\phi_o = 0.8$ (o/w), (c) $\phi_o = 0.92$ (around phase inversion) and (d) $\phi_o = 0.95$ (w/o). For the lowest oil volume fraction considered here, $\phi_o = 0.7$ (below the theoretical hexagonal close packing limit of 0.74), the drops are fairly spherical. For $\phi_o = 0.8$ drops are no longer spherical and are distorted. When, ϕ_o is increased up to 0.92, phase inversion occurs and the emulsion turns from o/w to w/o. In this case, during such a transition, the formation of o/w/o multiple emulsions were found (Figure 6.4c). Finally, when $\phi_o = 0.95$, the inversion is complete. Figure 6.4d, shows a highly diluted water-in-PDMS emulsion stabilised by 20 mM SDS, where the volume of the dispersed phase, ϕ_w, is 0.05.

Figure 6.3 **Conductivity of PDMS-water emulsions stabilised by 20 mM SDS as a function of oil volume fraction at 25 °C. The line represents the phase inversion threshold.**

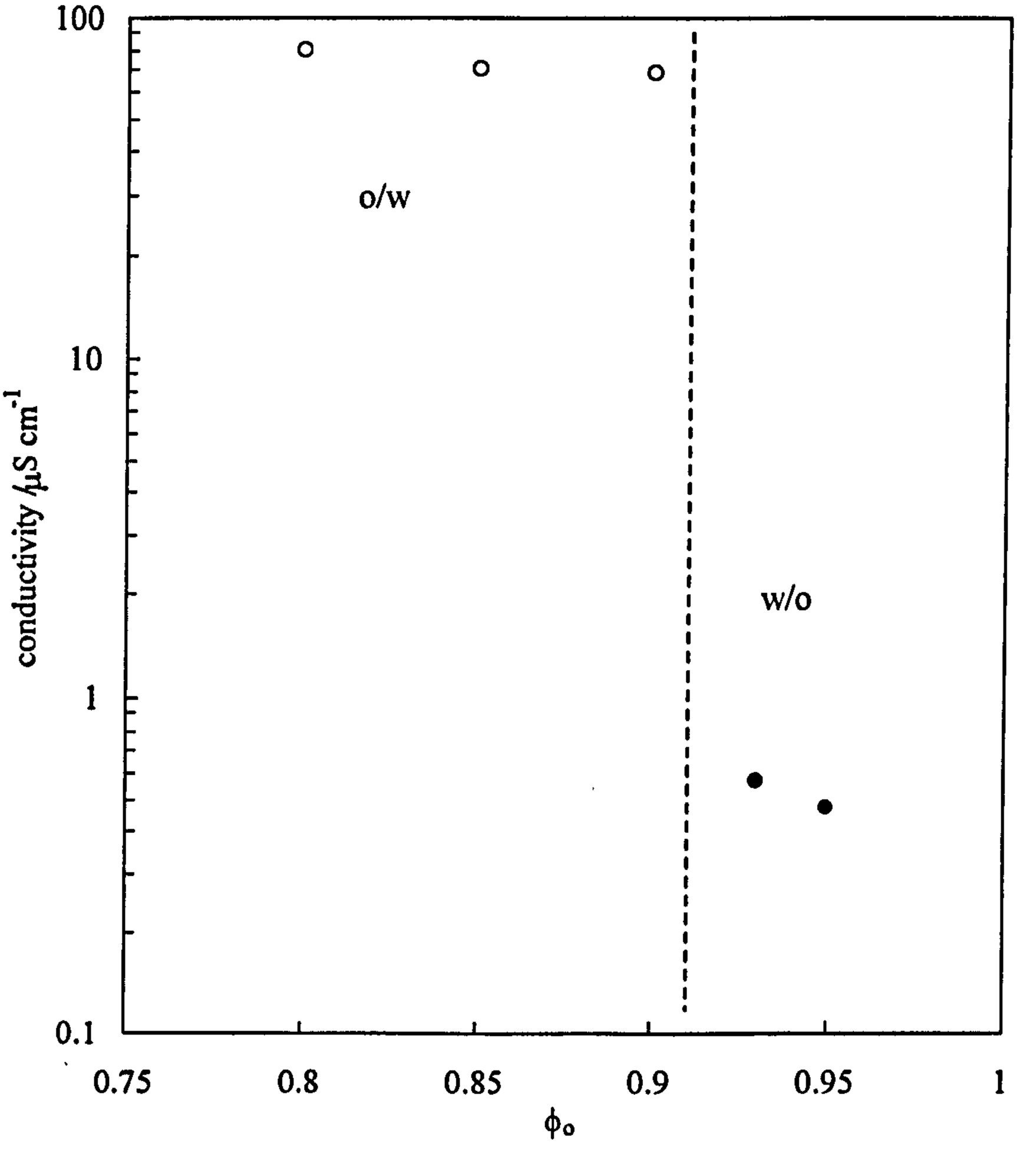

Figure 6.4 **Micrographs of PDMS-water emulsions stabilised by 20 mM SDS for (a) ϕ_o = 0.7 (o/w), (b) ϕ_o = 0.8 (o/w), (c) ϕ_o = 0.92 (around phase inversion) and (d) ϕ_o = 0.95 (w/o).**

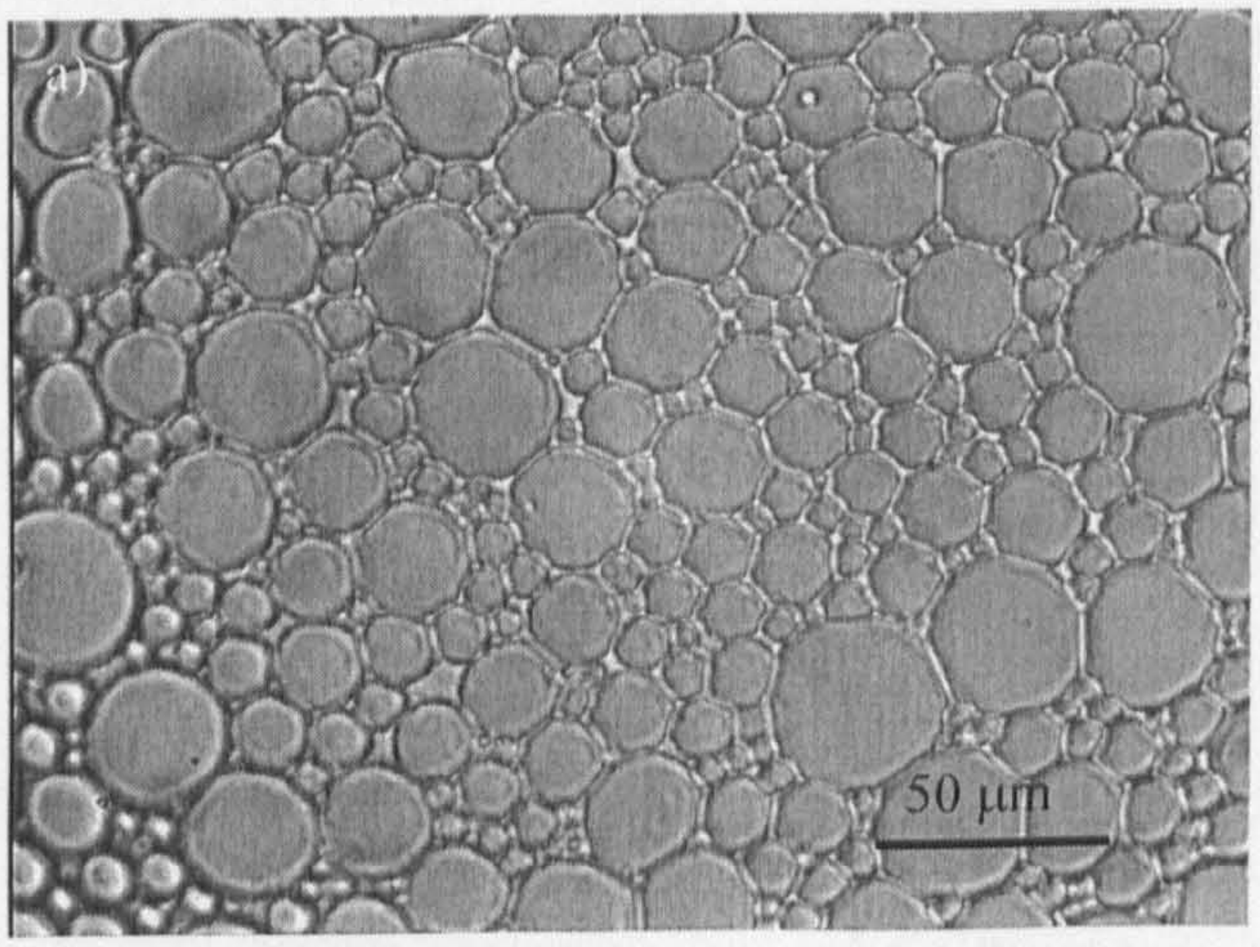

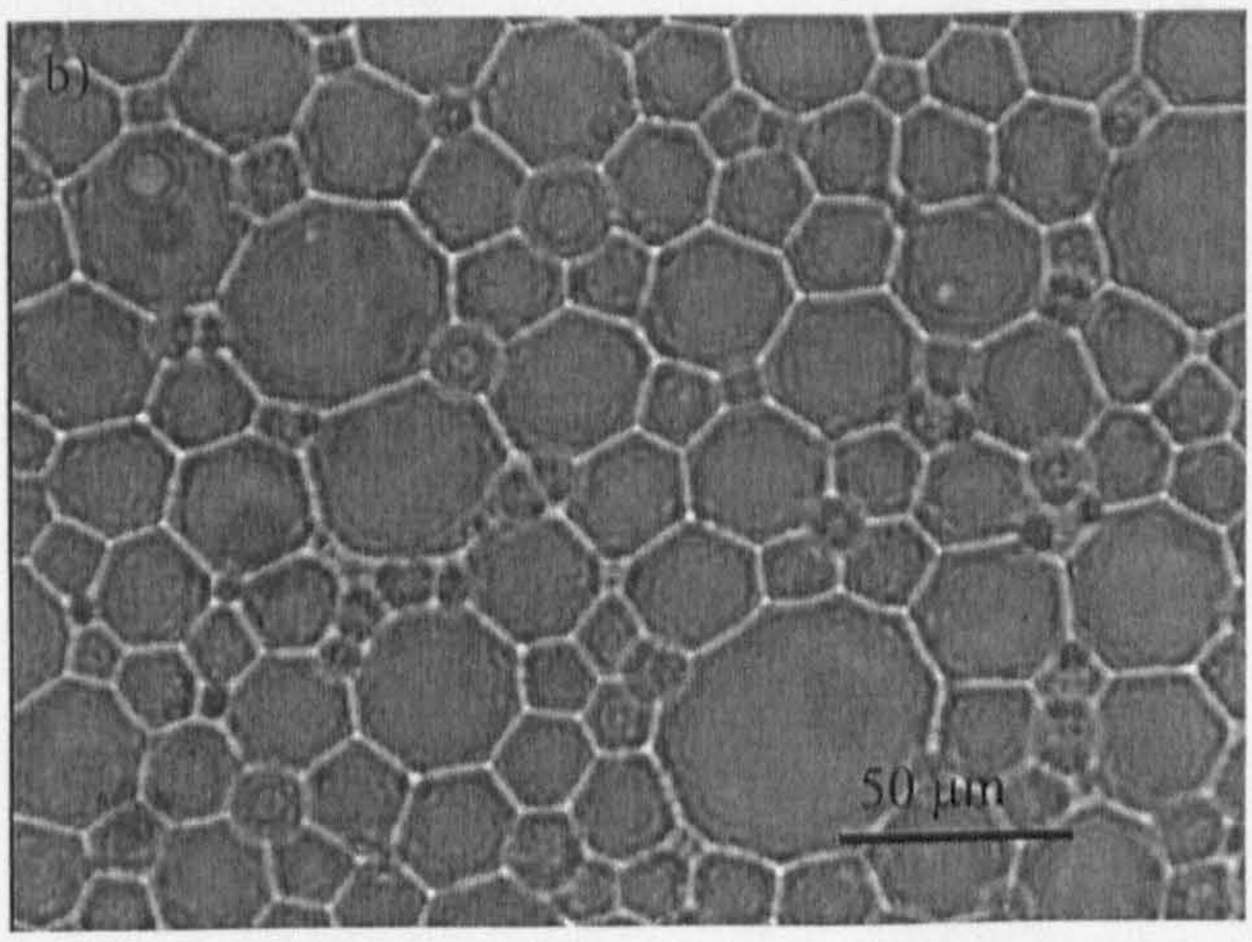

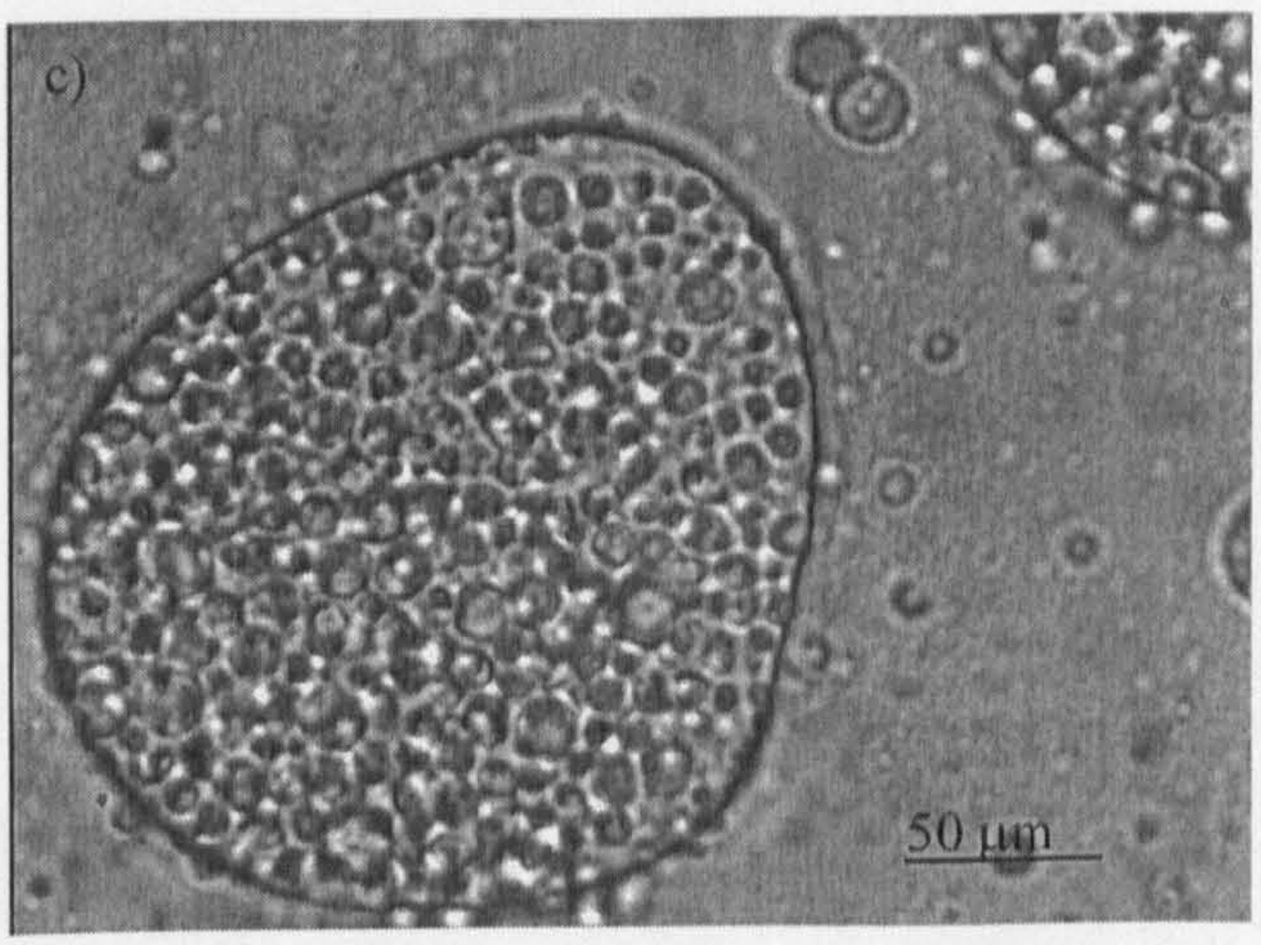
c)
50 µm

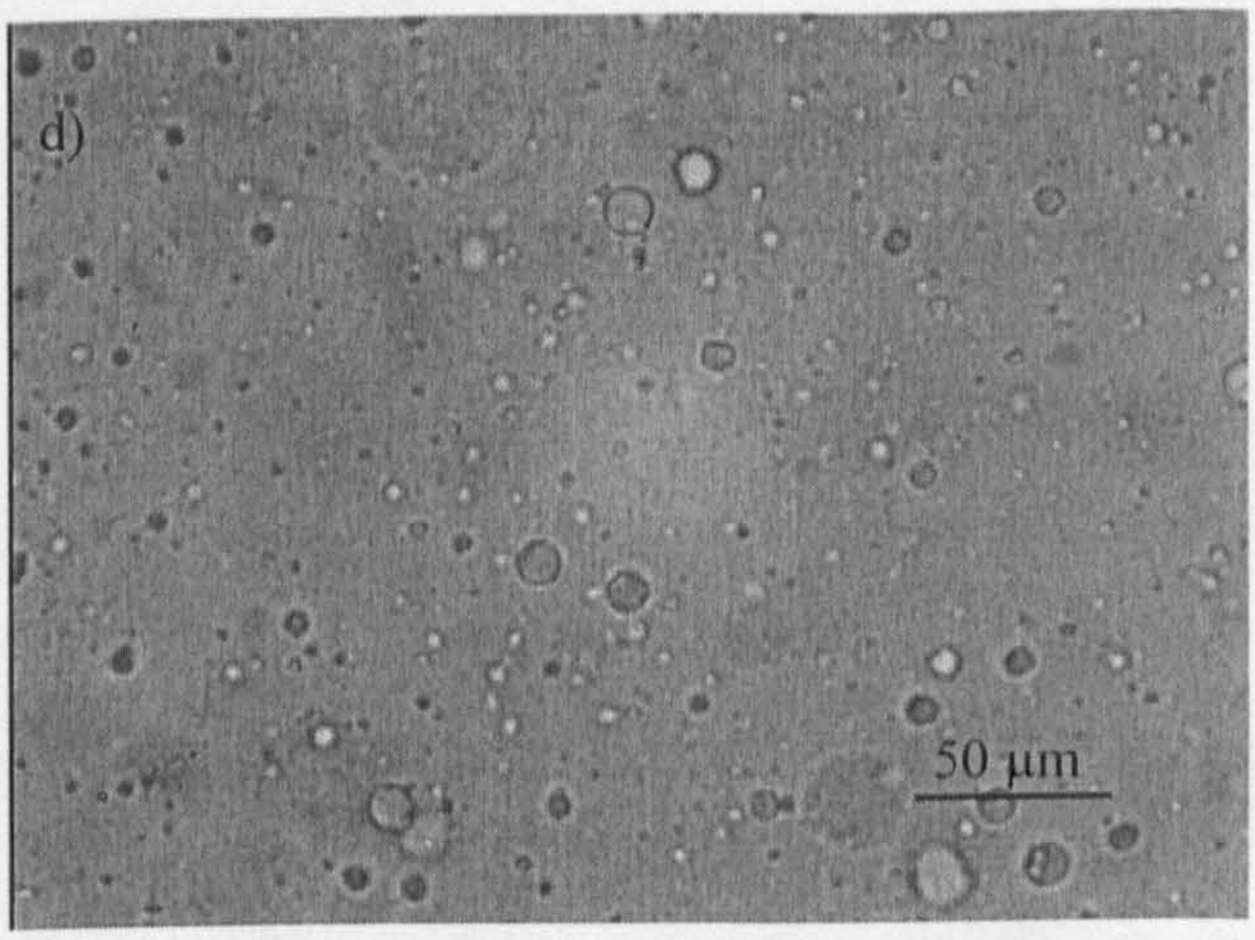
d)
50 µm

6.3.2 *Addition of NaBr*

It is well known that the presence of electrolyte may trigger phase inversion in emulsions[8,9]. When salt is added into the emulsion, the apparent cross-sectional area of the head group is reduced because of the screening of the repulsive forces between charged head groups. When the head group area is smaller than the cross-sectional area of the tail group, the curvature of the monolayer changes and the surfactant chains pass from the inside (o/w) to the outside (w/o) part of the drop (see also Chapter 1).

Figure 6.5 represents the phase diagram of PDMS-w emulsions stabilised by 20 mM SDS in the presence of NaBr. Starting from an o/w emulsion and for oil volume fractions up to 0.85, the NaBr concentration needed to cause a phase inversion is constant and approximately 0.35 M. It the absence of NaBr, as shown before, PDMS-in-water emulsions invert to water-in-PDMS emulsions when ϕ_o = 0.92. Figure 6.6 shows micrographs of a series of PDMS-water emulsions stabilised by 20 mM SDS and containing 0.3 M NaBr in the continuous phase as a function of the oil volume fraction. The presence of salt does not affect quantitatively the structure of the emulsions. However, as shown in Figure 6.5, for PDMS-in-water emulsions stabilised by 20 mM SDS and [NaBr] = 0.3 M, the ϕ_o at which the phase inversion (o/w to w/o) occurs is shifted from 0.93 to approximately ϕ_o= 0.9. In section 6.3.2, the evaporation rates of PDMS-in-water emulsions stabilised by 20 mM SDS in the presence of NaBr will be shown and the critical oil volume fraction needed for phase inversion for batch-homogenised emulsions and for emulsions in the evaporation rig will be discussed.

Figure 6.5 **Phase inversion map for batch emulsions containing PDMS, aqueous NaBr and stabilised by 20 mM SDS. Open circles correspond to w/o emulsions whereas filled circles correspond to o/w emulsions. The dashed line corresponds to the phase inversion threshold.**

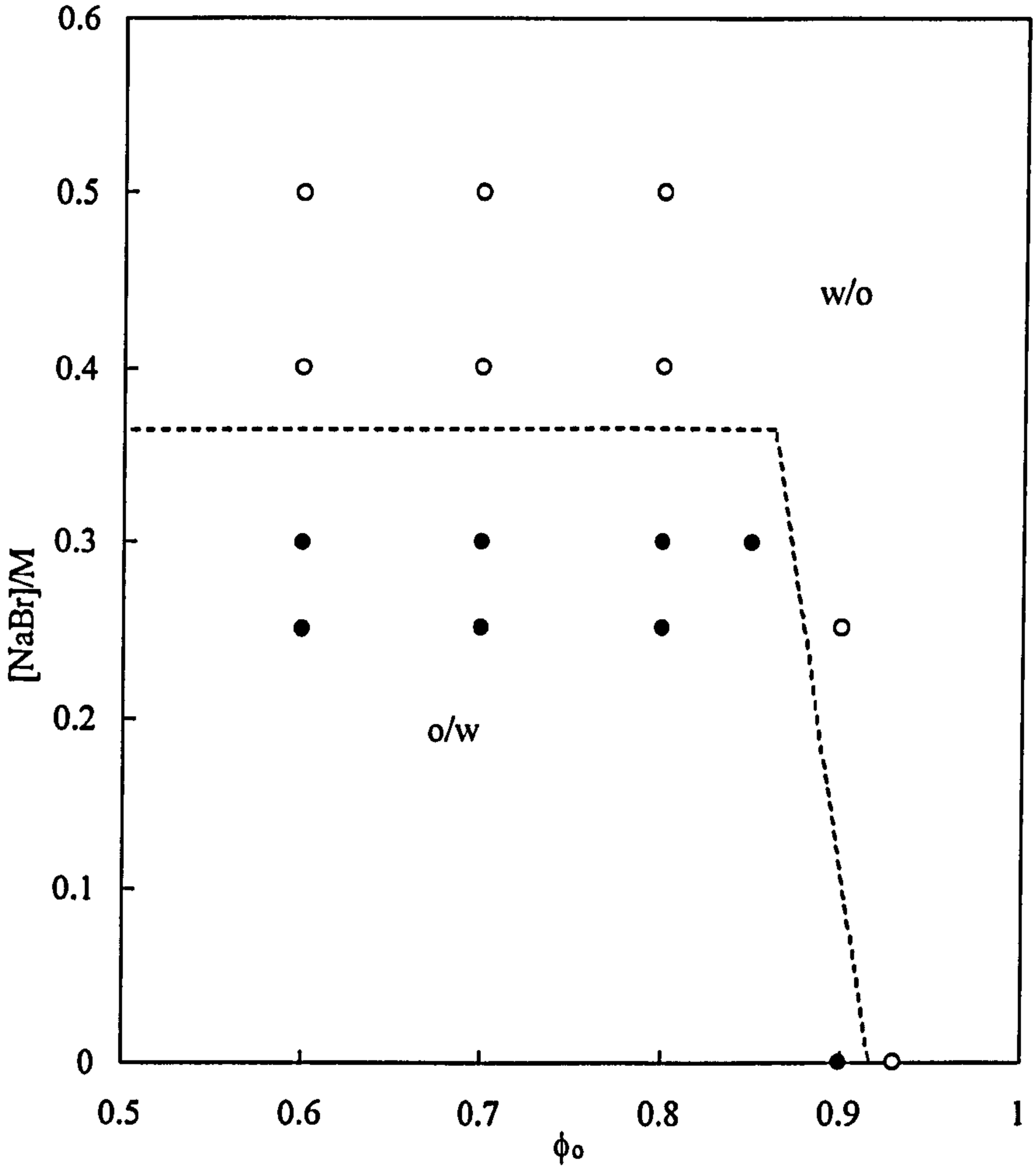

Figure 6.6 **Micrographs of PDMS-water emulsions stabilised by 20 mM SDS and added 0.3 M NaBr for (a) ϕ_o = 0.7 (o/w), (b) ϕ_o = 0.8 (o/w), (c) ϕ_o = 0.9 (around phase inversion) and (d) ϕ_o = 0.99 (w/o).**

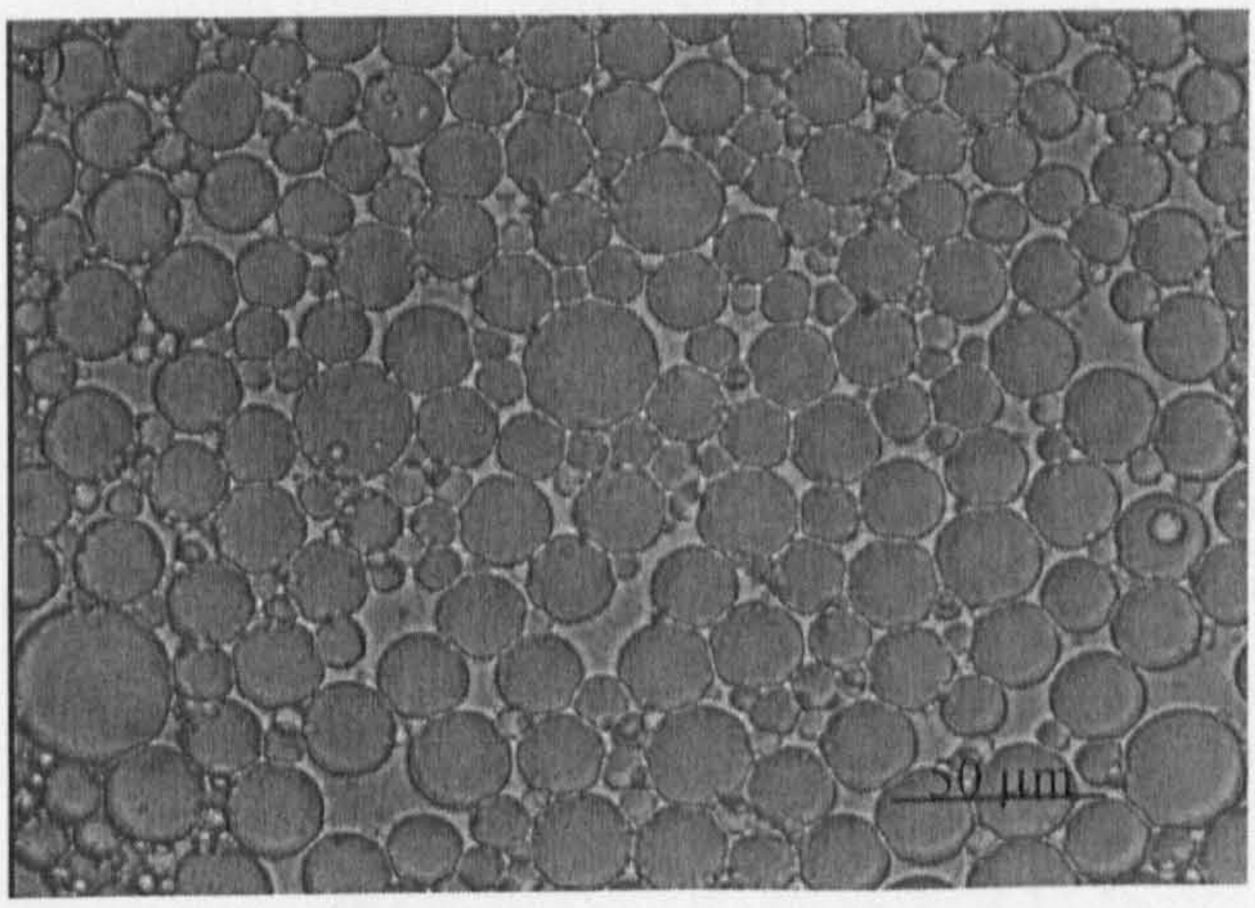

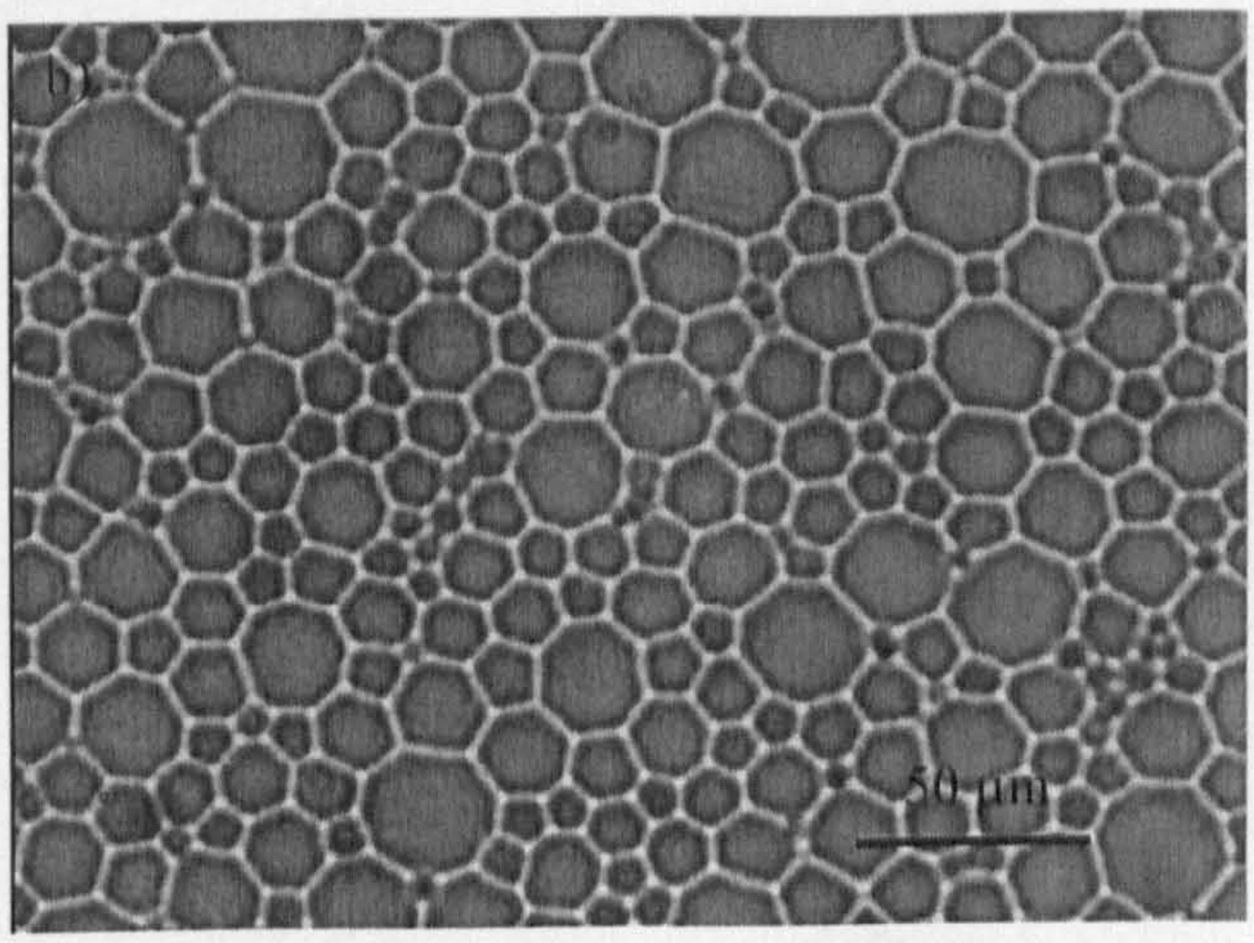

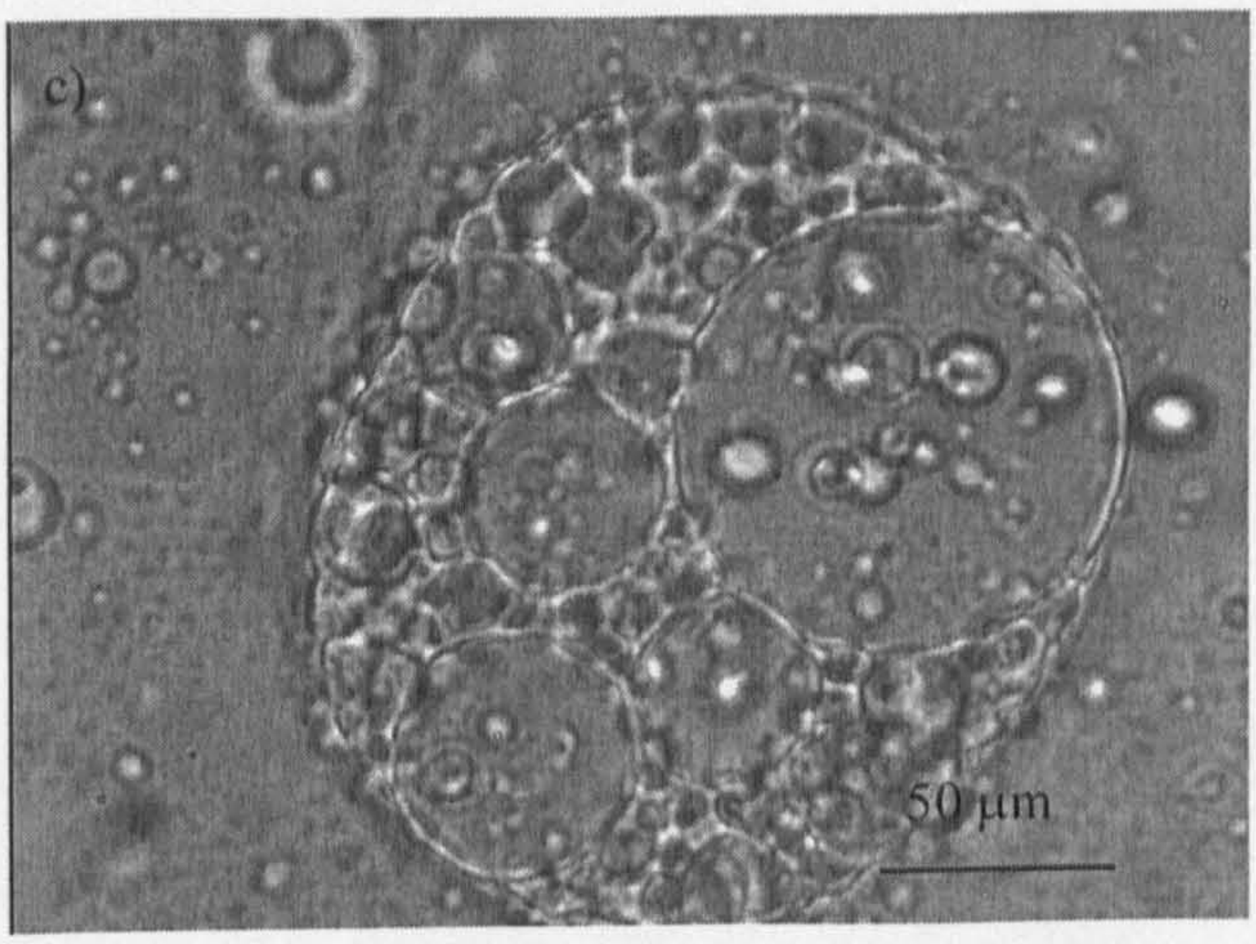
c)
50 µm

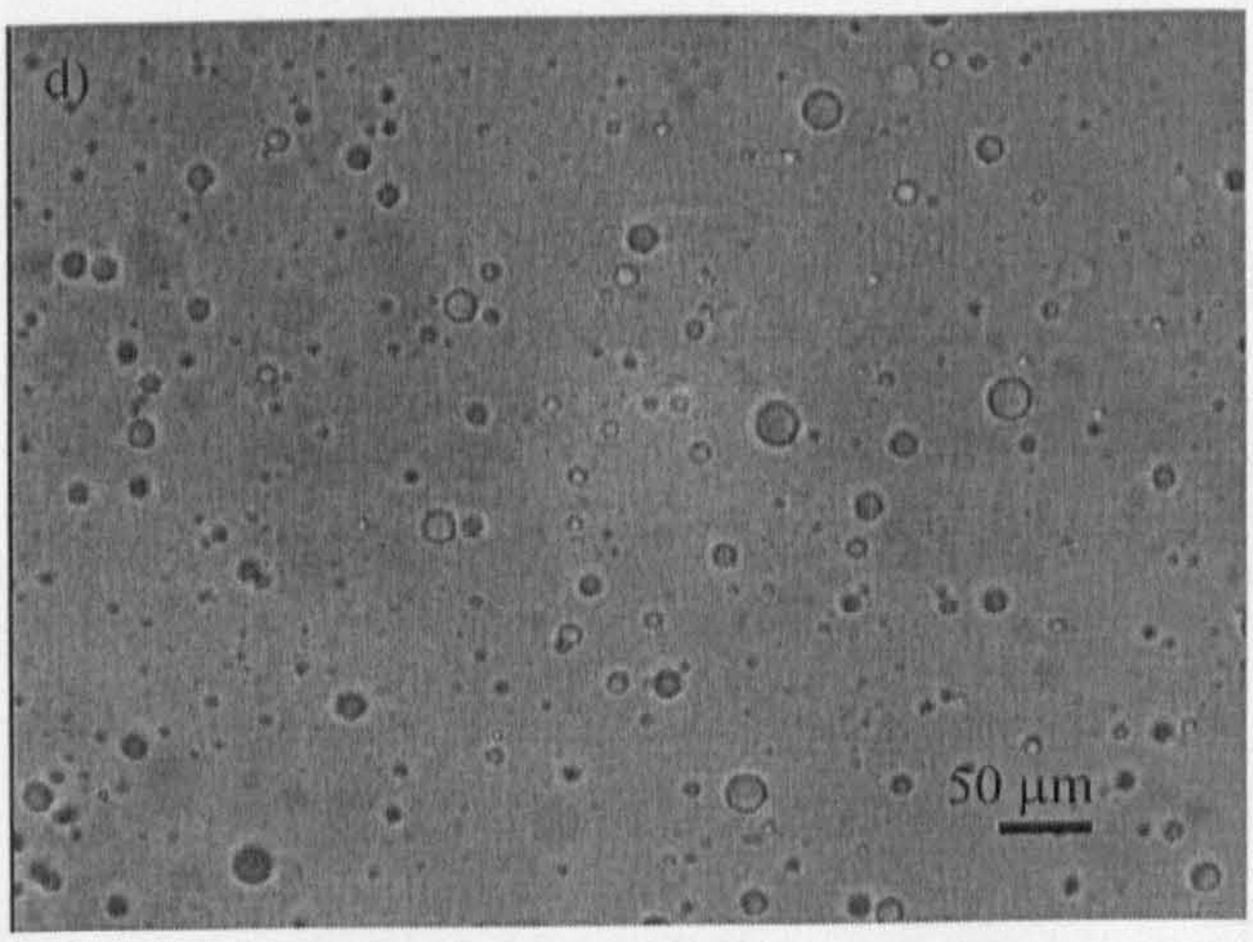
d)
50 µm

6.3 Evaporation rates of HIPEs

6.3.1 Effect of initial sample mass

Firstly, the way in which the evaporation rate of water is influenced by the initial emulsion sample mass will be discussed. Figure 6.7 shows experimental water mass loss curves for a series of emulsions with initial water volume fractions of 0.1, 0.2 and 0.3 and an initial total mass of approximately 3.0 g for each emulsion. The average oil droplet radius was 4.0 μm in all cases. All experimental curves were fitted simultaneously using equations [3.14] and [6.1-6.3] to obtain the apparent best-fit values of $\Pi_o = 3.0 \times 10^8$ Pa and $d_o = 110$ nm. The model proposed here assumes that the evaporation rate limiting step is the vapour diffusion of the water across a stagnant vapour layer above the emulsion. Notice that this is the rate controlling step for pure liquids (see Chapter 3) and for the continuous phase in creamed emulsions (see Chapter 4). The fits shown in Figure 6.7, suggest that this so-called "vapour diffusion control" model does not apply to our experimental data. Firstly, the quality of the fit is not particularly good. Secondly, the best-fit value of Π_0 of 3.0×10^8 Pa is much larger than the disjoining pressure measured in comparable systems[10] and than the value of critical disjoining pressure required to induce droplet coalescence in comparable emulsion systems[11]. Thirdly, the best-fit value of $d_0 = 110$ nm is much larger than the Debye length estimated for the electrolyte concentration in the emulsion samples (20 mM SDS in the aqueous phase corresponds to a Debye length of around 2 nm). These comparisons strongly suggest that the smooth slowing down of evaporation rates observed in Figure 6.7 before all water is lost is not due to a decrease in the vapour pressure of the water as a result of thin film compression.

Figure 6.7 **Mass loss curves of PDMS-in-water emulsions stabilised by 20 mM SDS (m_0 = 3.0 g). The experimental data (solid) is compared with the calculated (dashed) best fit curve and the different ϕ_o are shown in the graph.**

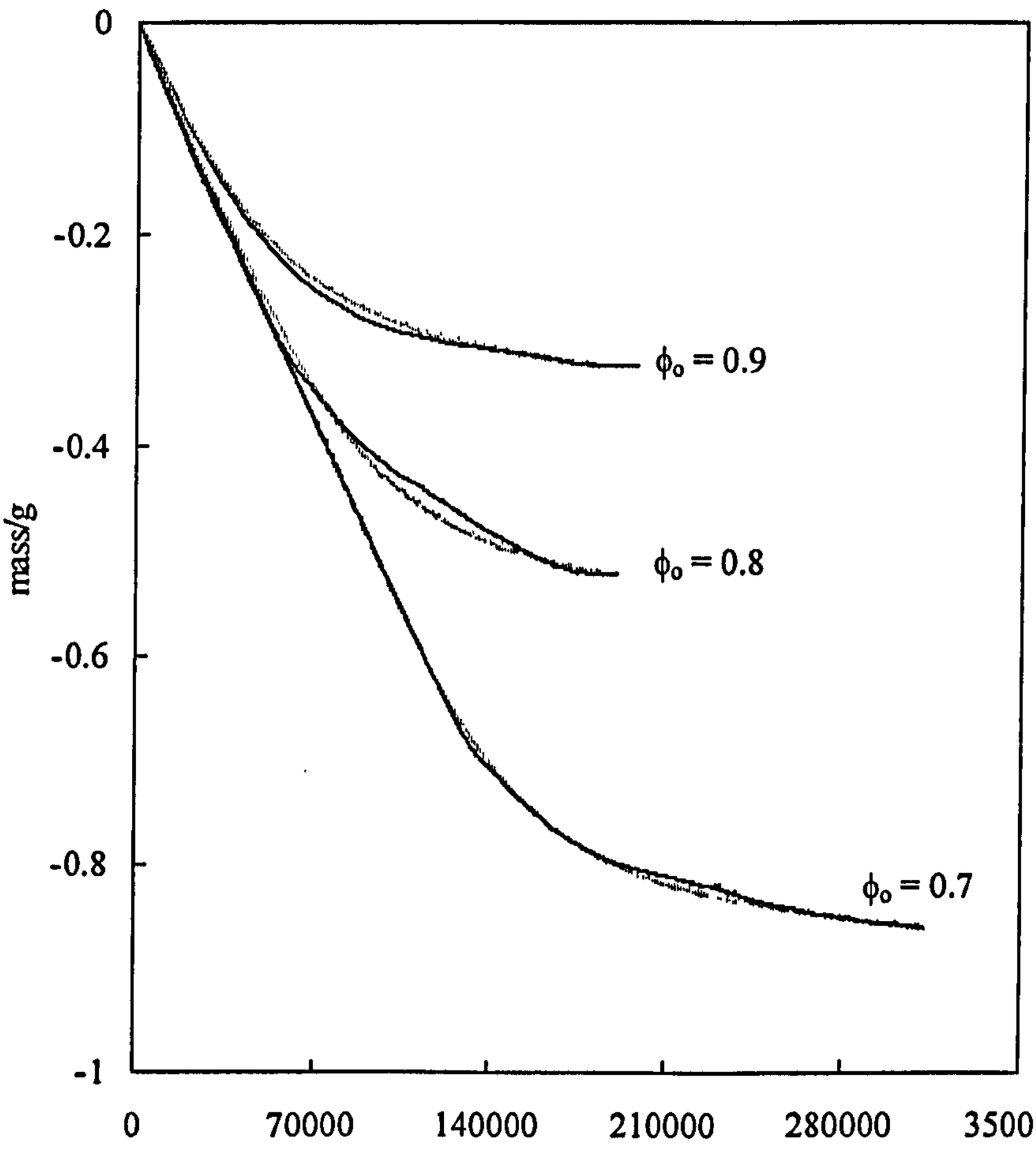

Therefore, we propose that in this case, where the initial emulsion mass is 3.0 g (equal to the half of the total volume of the sample tube), the vapour diffusion is not the water evaporation rate limiting step. The experimental data and the impossibility of fitting these curves with the "vapour diffusion" model, suggest that the formation of a network of nm size water films in the emulsions may form a water concentration gradient within the emulsion. So, the water evaporation rate may be limited by the diffusion of the water in the liquid (through the "channels", see Figure 6.8) instead of in the vapour.

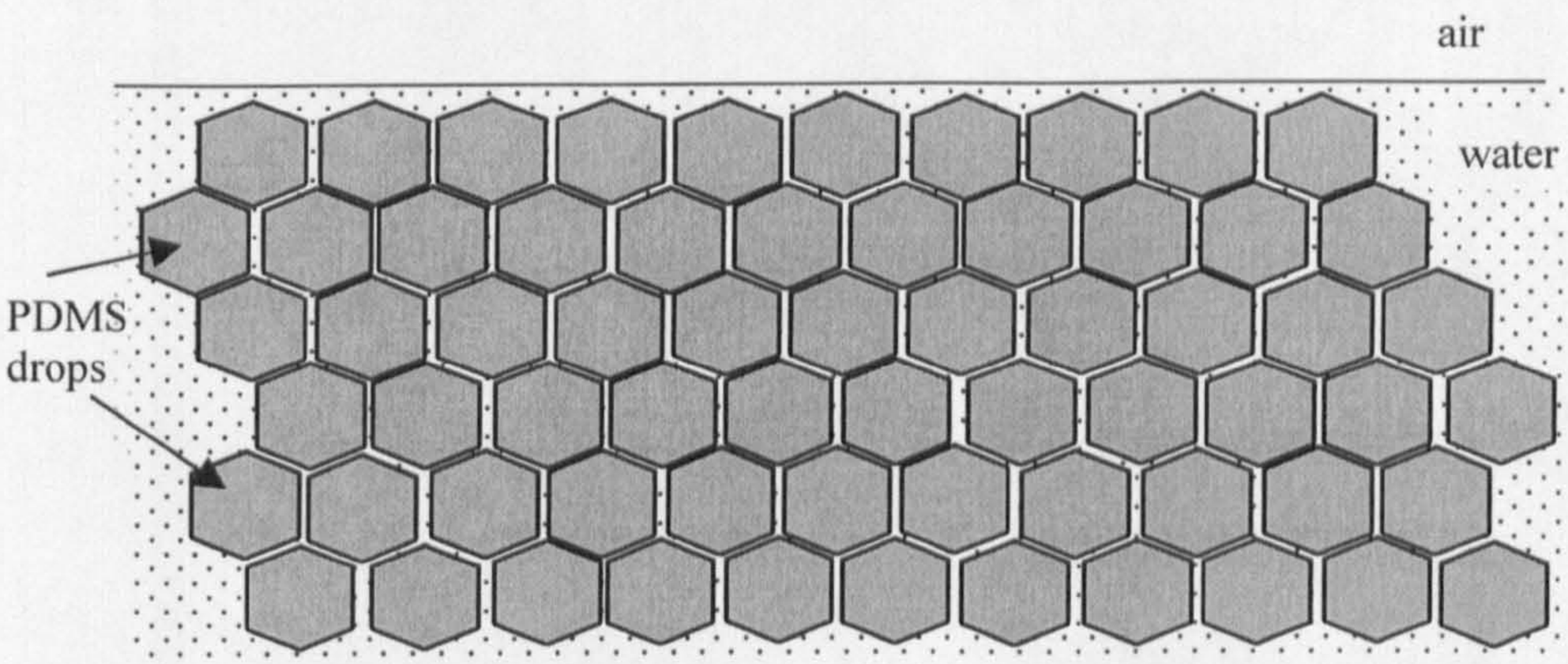

Figure 6.8 Schema of a HIPE. The evaporation rate of water may be limited by the diffusion of water through the nm size films.

In order to confirm that the evaporation rate of water is controlled by the diffusion of the water in the thin films, mass loss curves of several PDMS-in-water emulsions stabilised by 20 mM SDS where the initial sample mass was 0.5 g were measured. In this case, as the thickness of the stagnant layer, h, is increased, the mass transport rate in the vapour space was decreased. As the emulsion depth is decreased, water diffusion rates in

the emulsion are expected to increase. Both these effects should favour a switch from "liquid diffusion control" to "vapour diffusion control". If vapour diffusion were rate limiting, then the mass loss curve shapes and best-fit values of Π_0 and d_0 should be identical for different h values. Figure 6.9 shows plots of water loss versus time measured for a series of 0.5 g emulsions samples with initial water volume fraction of 0.1, 0.2 and 0.3. For this series, the initial value of h was 36.5 mm, compared to 26.7 mm when 3.0 g of emulsions sample were used. Comparing corresponding plots in Figures 6.7 and 6.9, it is shown that increasing h causes the mass loss curves to become significantly more "kinked" and this is reflected in the best-fit value of d_o = 12 nm, (compared with 110 nm for the data of Figure 6.7). The best fit value of Π_0 is virtually unchanged at 2.7 x 10^8 Pa. The observed change in shape of the mass loss curves at different h clearly confirms that the liquid phase transport is rate limiting (at least partially) and hence that a water concentration gradient is generated during evaporation. The fact that virtually all the available water is lost by evaporation suggests that oil droplet coalescence to produce a macroscopic oil film at the emulsion surface apparently does not occur, except possibly in the final stage of water loss. This type of behaviour has been observed in drying studies of concentrated o/w emulsion films by Bouchama et al.[12], albeit without controlled gas flow (and knowledge of the thickness of the stagnant vapour space) as used in this study.

Figure 6.10 shows micrographs of an emulsion containing 80 vol% PDMS and stabilised by 20 mM SDS as a function of time. 3 g of the sample were left in an open vessel on a bench and images with the optical microscope were taken every 24 h.

Figure 6.9 **Mass loss curves of PMDS-in-water emulsions stabilised by 20 mM SDS (m_0 = 0.5 g). The experimental data (solid curve) is compared with the calculated (dashed curve) best fit.**

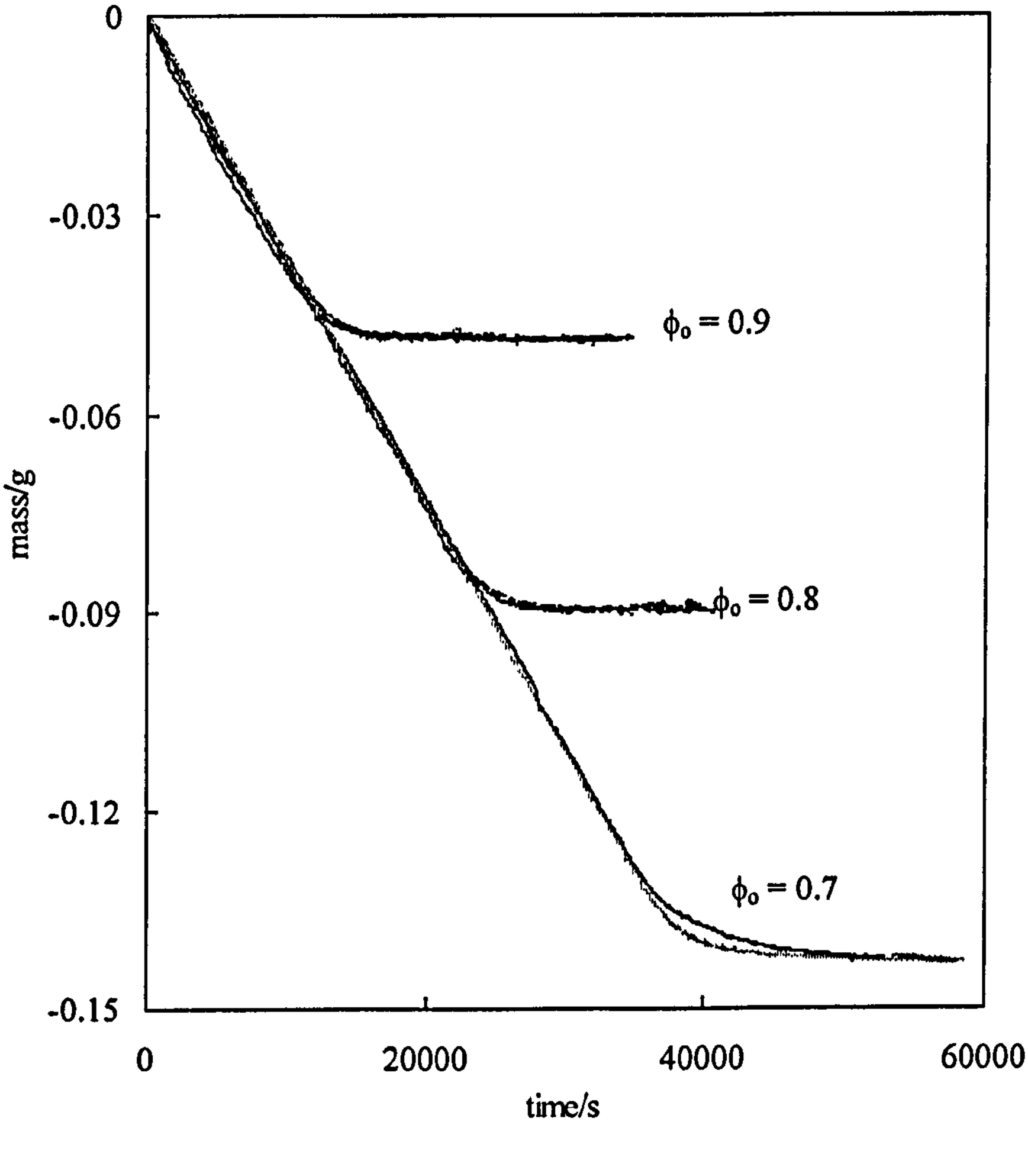

Figure 6.10 **Micrographs of a 80 vol% PDMS-in-water emulsion stabilised by 20 mM SDS as a function of time a) t = 0, b) t = 1 day, c) t = 4 days and d) t = 5 days.**

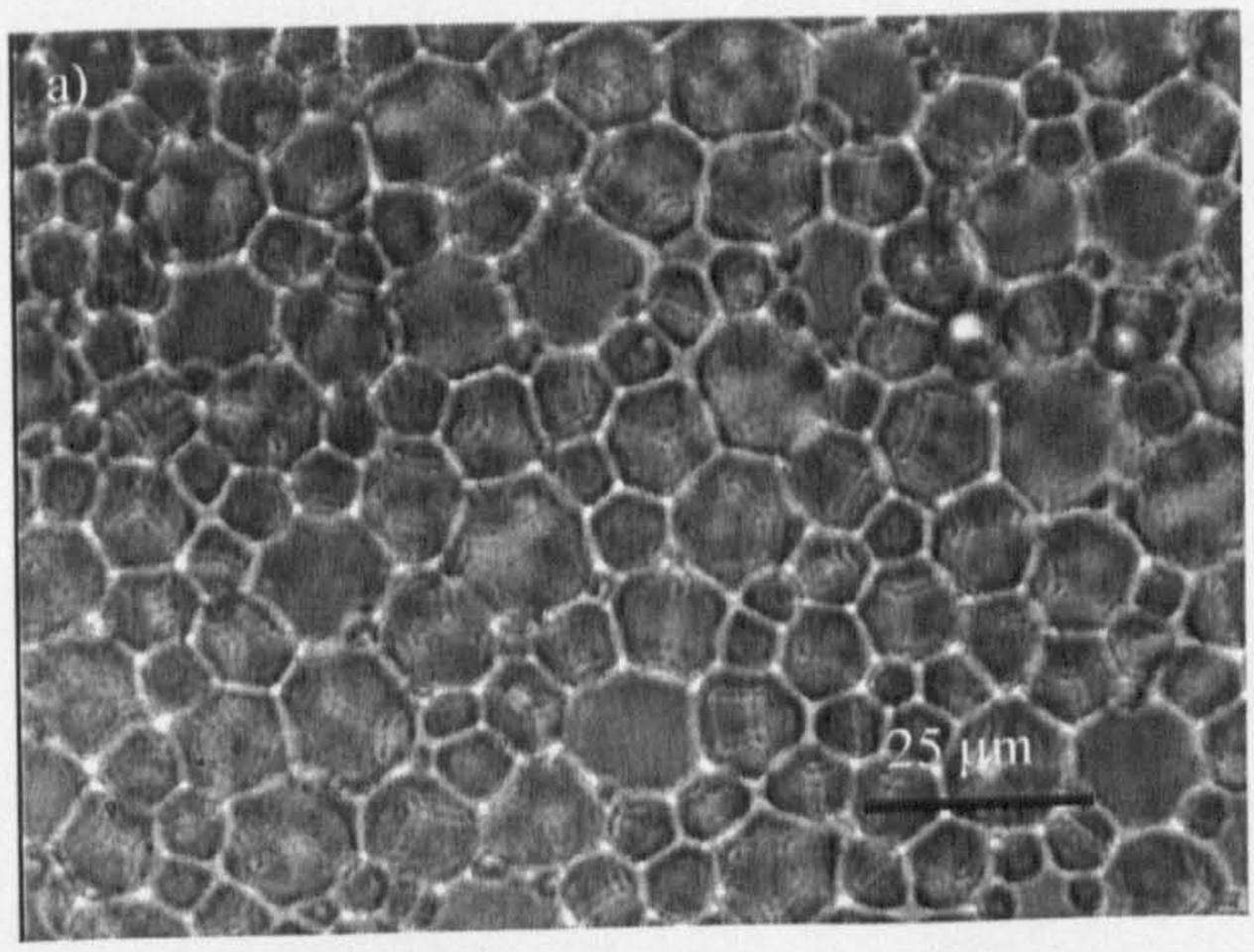

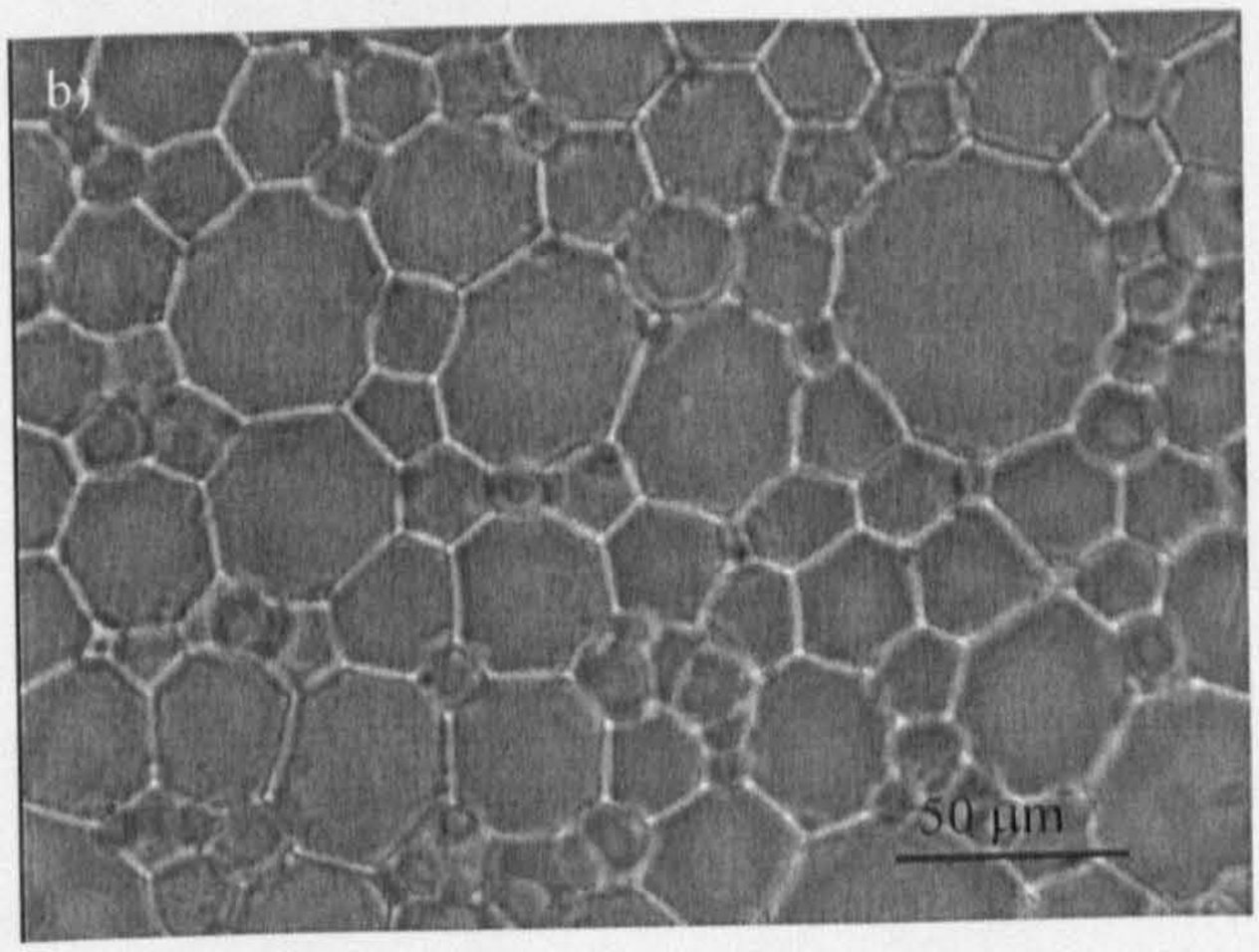

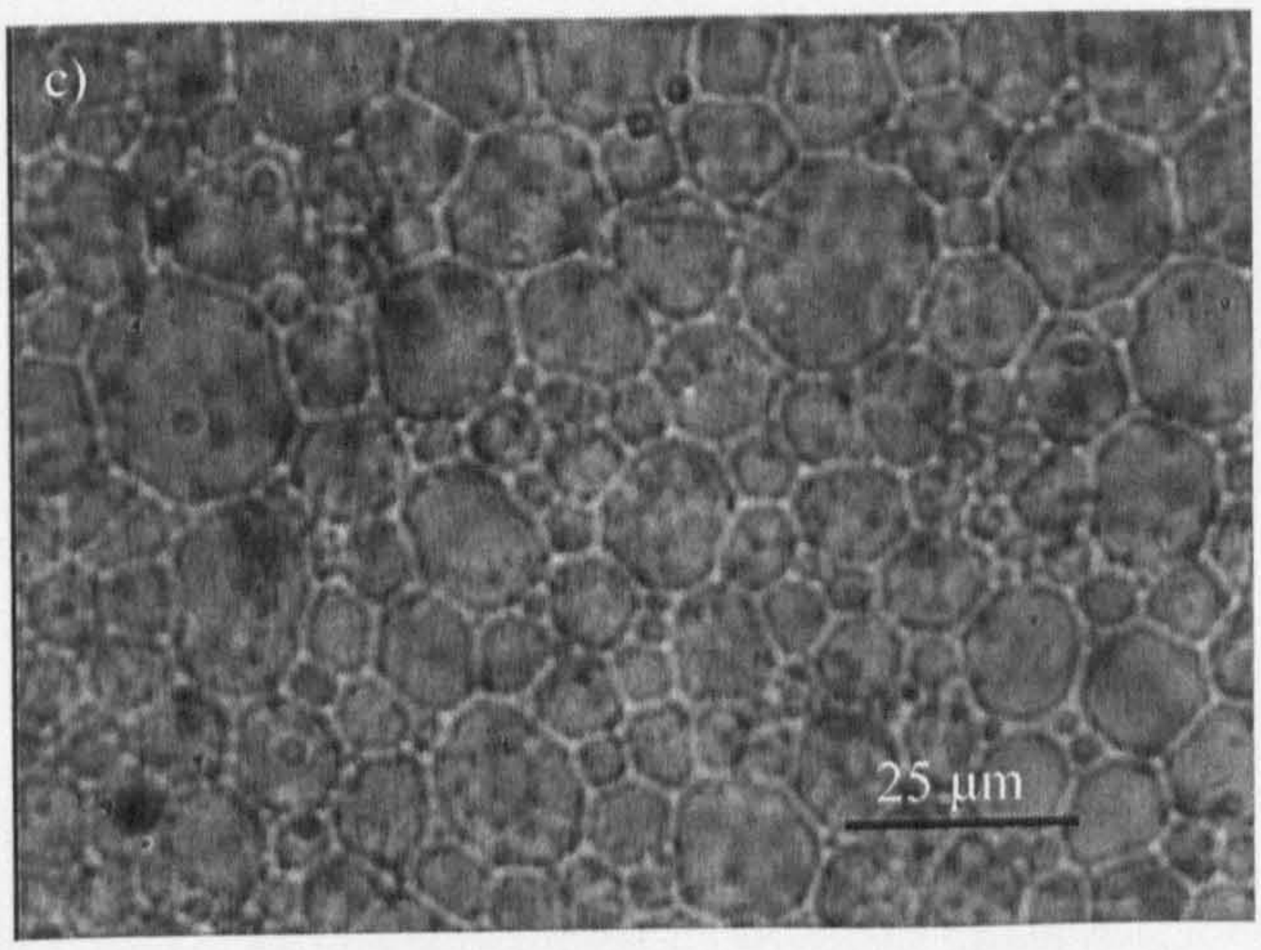
c)
25 µm

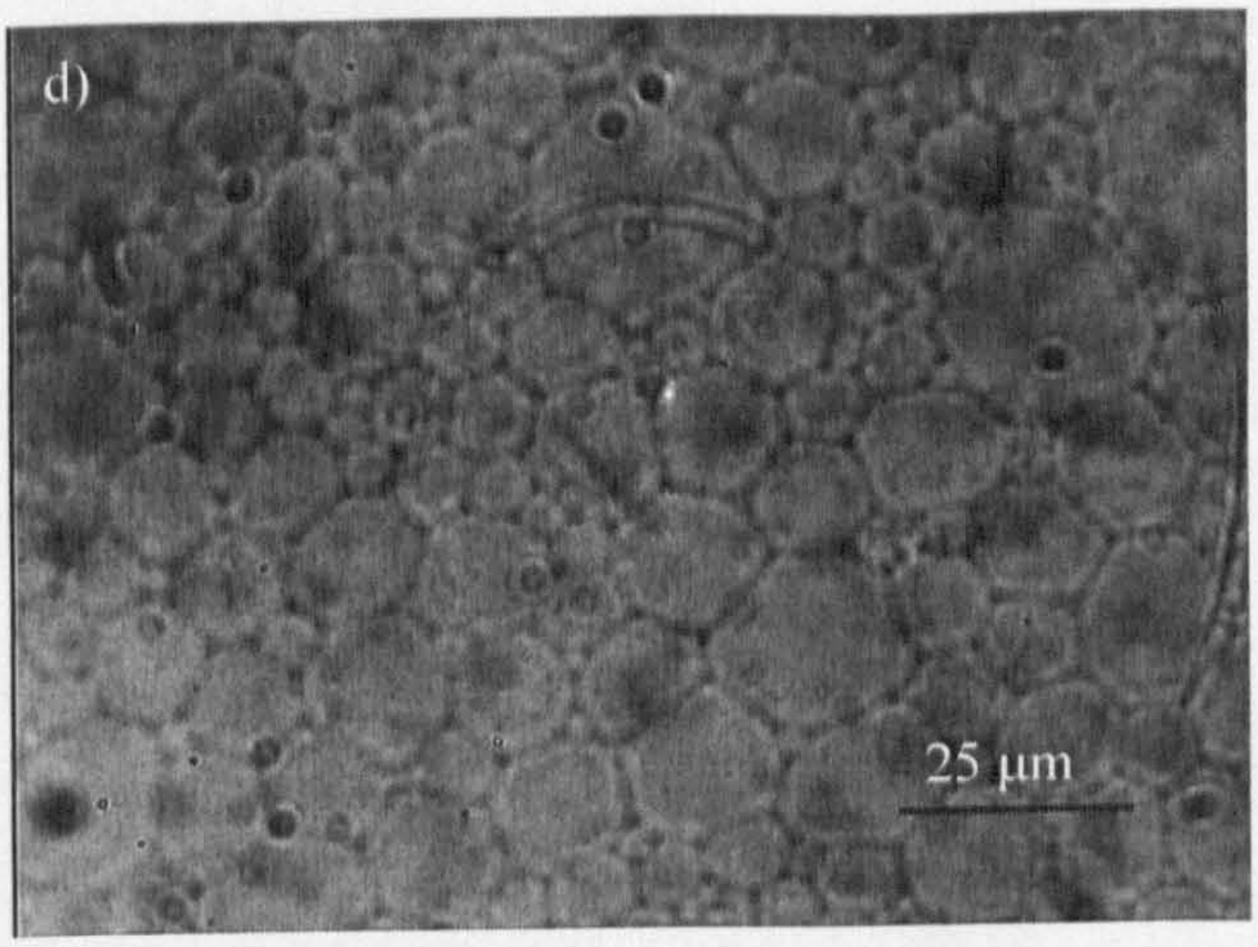
d)
25 µm

During the first 4 days (Figures 6.10a-c) no effect in the thickness of the water films between the PDMS droplets is observed. In this stage the evaporation rate of water is expected to be constant and equal to that of bulk water. Figure 6.10d shows a micrograph of that emulsion taken after 5 days. In this case, as most of the water is evaporated and the water films or channels surrounding the oil drops are becoming extremely thin. No coalescence is observed yet.

6.3.2 Effect of NaBr

In the introduction of this Chapter, the way in which two drops may merge has been described. The process of coalescence in the presence of NaBr is expected to be faster as salt ions screen the electrostatic repulsion between the surfactant monolayers that are stabilising the oil drops. The lack of such repulsions will compress the drops further and therefore coalescence of oil drops is expected to happen in earlier stages of the evaporation if compared with that of the emulsions in the absence of NaBr. Figures 6.7 and 6.9 show that in absence of salt, the mass loss of water is rather complete. In either case, the corresponding total volume of water which was lost were approximately 0.3 g, 0.6 g and 0.9 g when the initial mass was $m_0 = 3.0$ g, being $\phi_w = 0.1$, 0.2 and 0.3 respectively and 0.05 g, 0.1 g and 0.15 g when $m_0 = 0.5$ g being $\phi_w = 0.1$, 0.2 and 0.3 respectively. For emulsions which are initially o/w, water loss by evaporation increases both [NaBr] and ϕ_o (and [SDS]) and is therefore expected to trigger phase inversion and production of an oil film which serves to prevent further water evaporation. Figure 6.11 shows mass loss curves of a series of emulsions ($m_0 = 0.5$ g) initially containing 30 vol% water and the [NaBr] indicated in the legend.

Figure 6.11 Mass loss of 70 vol% PDMS-in-water emulsions stabilised by 20 mM SDS and containing different initial NaBr concentrations (shown in legend). The initial mass of each emulsion was 0.5 g. The horizontal dashed line corresponds to the plateau value expected for complete water loss.

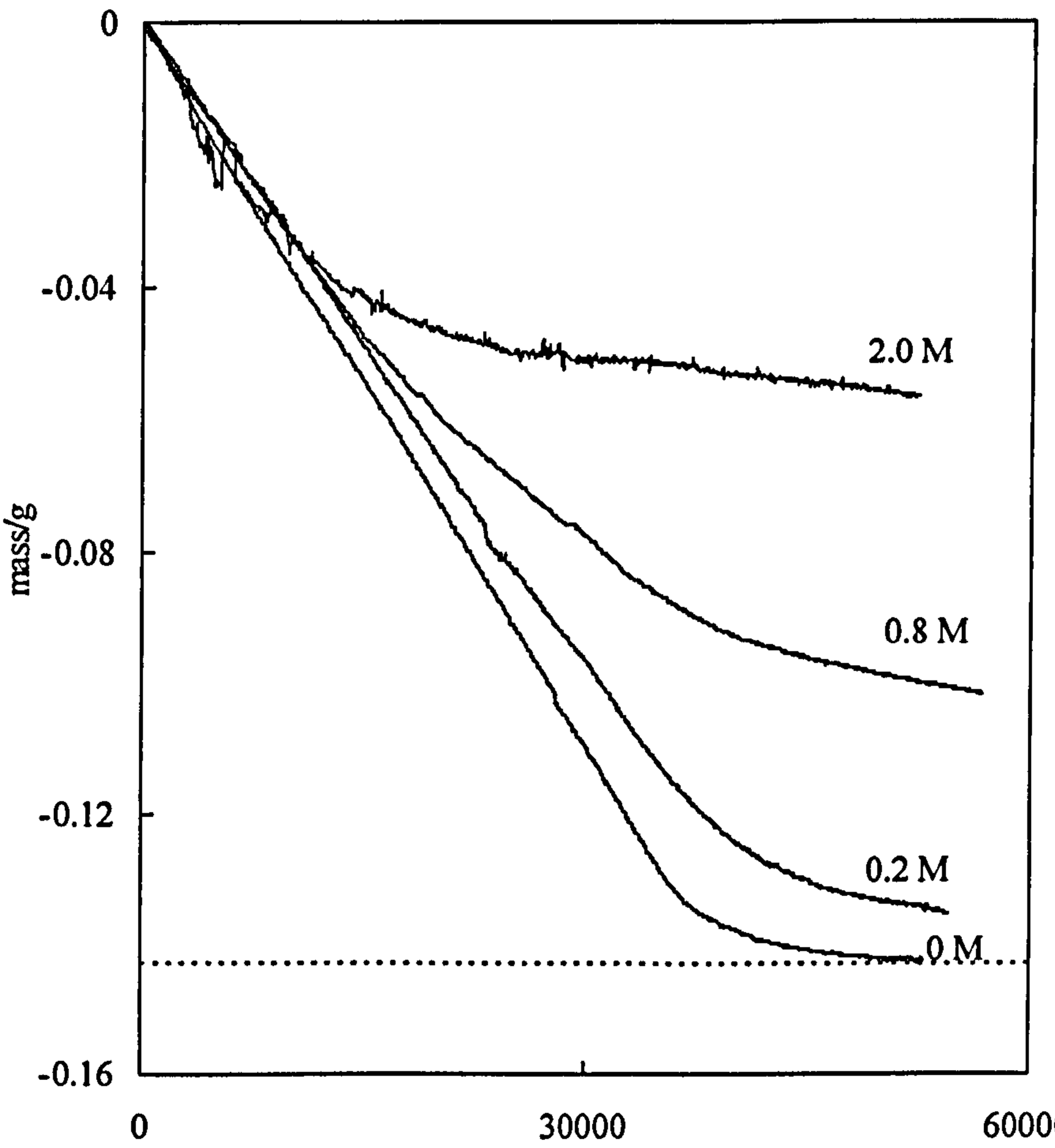

The emulsion samples were prepared by addition of the required volume of a concentrated aqueous NaBr solution to an aliquot of an o/w emulsion prepared with zero NaBr. For emulsions containing zero added NaBr, all water content (approx. 0.15 g) is lost before mass loss ceases. As the NaBr is increased, the evaporation slows and stops well before all the water initially present is lost. This behaviour is not expected if the only effect of NaBr addition is to reduce the range of the electrostatic repulsion between droplets. If this were the case, loss of all the water present would be expected as well, but probably at a different rate. The most likely explanation, (qualitatively consistent with the observation) is that addition of NaBr induces oil droplet coalescence and the formation of a water-impermeable film which prevents water loss.

In the absence of added NaBr, the batch-homogenised emulsions invert from o/w to w/o at ϕ_o of 0.92, i.e. at ϕ_w of 0.08. From Figures 6.7 and 6.9, water evaporation ceases when ϕ_w reduces to less than approximately 0.01. Clearly, water evaporation retardation does not occur at the same composition as phase inversion in the batch-homogenised emulsions. This may be related to the difference in SDS concentration induced by water evaporation or the lack of homogenisation as the emulsion composition alters by the evaporation.

We have seen that adding salt to the emulsion triggers coalescence. On the other hand it has been shown (see Figure 4.18) that the water evaporation rates of electrolyte aqueous solutions slow down slightly as NaBr concentration is increased. Figure 6.12 shows both effects together.

Figure 6.12 **Mass loss curves of (a) 20 mM SDS aqueous solution, (b) 80 vol% PDMS-in-water emulsion stabilised by 20 mM SDS, (c) 1 M NaBr aqueous solution and (d) 80 vol% PDMS-in-water emulsion stabilised by 20 mM SDS containing 1 M NaBr.**

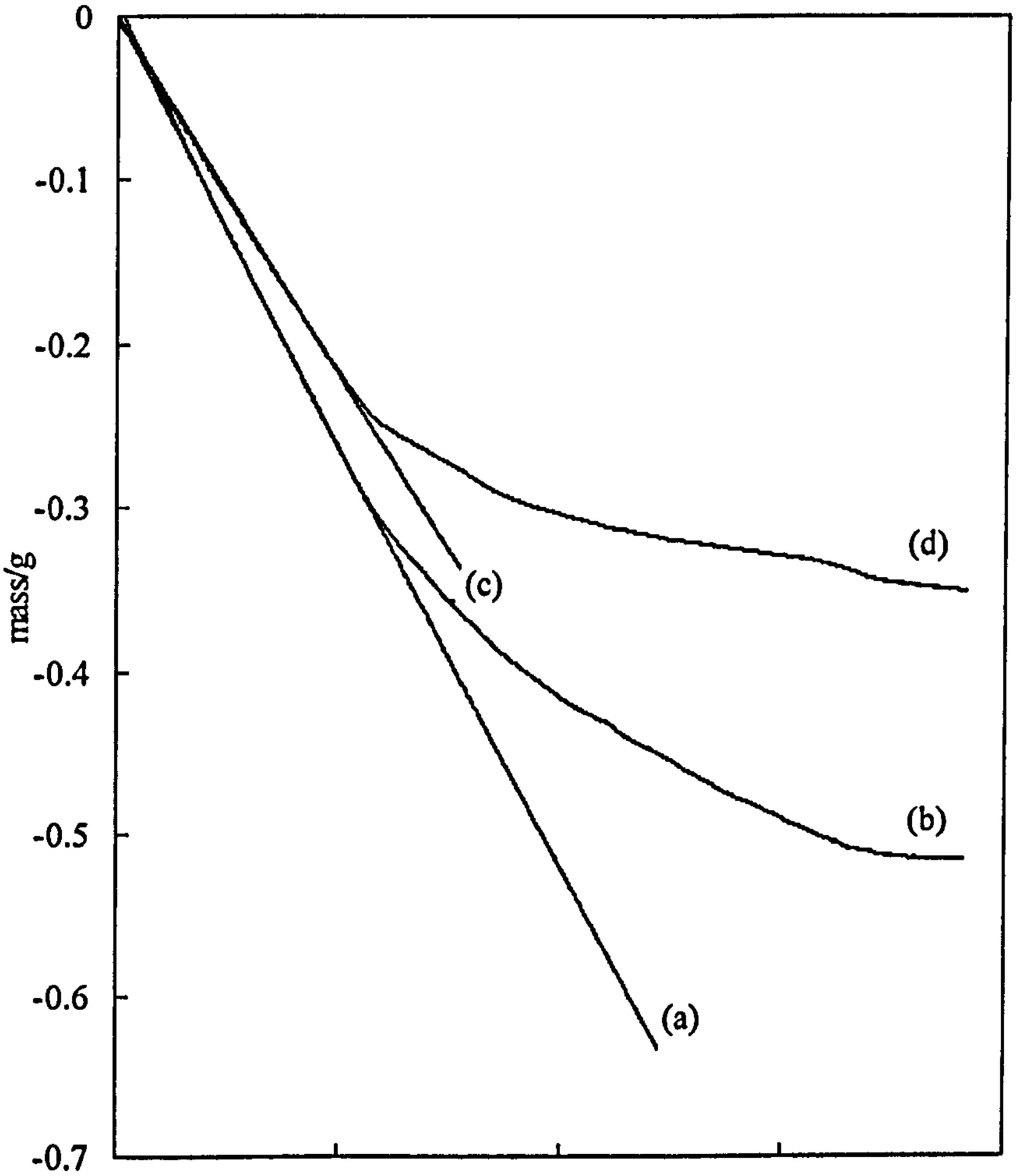

Curve 6.12a represents the mass loss rate of 3.0 g of 20 mM SDS aqueous solution (which is exactly the same to that of pure water). Curve 6.12b corresponds to the mass loss rate of 3.0 g of 80 vol% PDMS-in-water emulsion stabilised by 20 mM SDS. Both 6.12a and 6.12b show the same initial rate which corresponds to the evaporation rate of 20 mM SDS solution. Obviously 6.12a is straight for the time period shown here, whereas 6.12b first slows down due to the "diffusion control" and then levels off when all the water is lost. Curve 6.12c represents the mass loss of 3 g of 1M NaBr aqueous solution. The rate is constant but slowed compared to that of 20 mM SDS aqueous solution. Finally curve 6.12d corresponds to the evaporation rate of approx. 3 g of 80 vol% PDMS-in-water emulsion stabilised by 20 mM SDS and containing 1 M NaBr. The initial rate of 6.12d, which represents the evaporation rate of the aqueous continuous phase (20 mM SDS + 1M NaBr), is identical to that of 6.12c. In 6.12d the levelling off is after 50,000 s (same as in (b) but less water loss is required before a macroscopic oil layer is formed).

6.5 Conclusions

- When mass transfer across the stagnant vapour controls the evaporation rate of water, the evaporation can be slowed down by repulsive interaction between droplets.
- Water evaporation from o/w HIPES may be limited by diffusion in the network of water films within the emulsion. In this situation, water loss by evaporation from the emulsion surface leads to a gradient in water concentration.

- Addition of NaBr to the emulsion triggers compression of the oil drops leading to coalescence. Using involatile oils in o/w HIPEs with added NaBr, the evaporation of water is stopped before all the water present is lost, by the formation of an oil layer on the top of the emulsion.

6.6 References

1 K. J. Lissant, *J. Colloid Interface Sci.*, 1966, **22**, 462.

2 R. Pons, I. Carrera, P. Erra, H. Kunieda and C. Solans, *Colloids Surf. A*, 1994, **91**, 259.

3 P. D. I. Fletcher and D. I. Horsup, *J. Chem. Soc. Faraday Trans.*, 1992, **88**, 855.

4 A. S. Kabalnov, Coalescence in Emulsions, in *Modern Aspects of Emulsion Science*, Ed. B. P. Binks, RSC, 1998, pp. 205-260.

5 B. V. Derjaguin, N. V. Churaev and V. M. Muller, *Surface Forces*, Plenum Press (Consultants Bureau), New York, 1987.

6 See for example, R. J. Hunter, *Foundations of Colloid Science*, vol. 1, Clarendon Press, Oxford, 1991.

7 O. Sonneville-Aubrun, V. Bergeron, T. Gulik-Krywicki, B. Jonsson, H. Wennerstrom, P. Linder and B. Cabane, *Langmuir*, 2000, **16**, 1566.

8 J. N. Israelachvili, D. J. Mitchell and B. W. Ninham, *J. Chem. Soc., Faraday Trans. II*, 1976, **72**, 1525.

9 R. Aveyard, B. P. Binks and J. Mead, *J. Chem. Soc., Faraday Trans. I.* 1986, **82**, 1755.

10 See for example B. P. Binks, W-G-Cho and P. D. I. Fletcher, *Langmuir*, 1997, **13**, 7180 and references therein.

11 J. Bibette, *Langmuir*, 1991, **8**, 3178.

12 F. Bouchama, G. Estramil, A.J.E. Autin and G.J.M Koper, *Colloids Surf. A*, 2002, **210**, 120.

Chapter 7

CHAPTER 7

EVAPORATION STUDIES OF SOLID PARTICLE-STABILISED EMULSIONS

7.1 Introduction

In the introduction of this thesis, the way in which emulsions may be stabilised solely by colloidal particles (Pickering emulsions) has been shown. Following the study of the evaporation rates from a wide range of different emulsions, in the present Chapter the evaporation rates of silica particle dispersions and emulsions stabilised by such particles will be discussed. Moreover, we have found that the solid residues left behind after the evaporation of both oil and water from Pickering emulsions, show very interesting porous microstructures which are related to the properties of the parent emulsions. Related macroporous inorganic materials have been shown to possess a unique set of properties including high specific stiffness, high damping capacity, high thermal shock resistance and high surface area[1,2]. The possibility arises that, depending on exactly how oil and water are lost, solid-stabilised emulsions can be used as templates for the initial ordering of particles around the drops and the subsequent formation of new porous solid phases.

7.2 Evaporation rates of colloidal aqueous dispersions

Before the study of the evaporation rates of solid-stabilised emulsions, we first measured the effect of the particles on the evaporation rate of the aqueous continuous phase. Several groups have studied the effect of adsorbed surfactant monolayers on the retardation of the evaporation rate of water[3,4] and the evaporation rates of solid dispersions have only been studied by our group in Hull[5]. Results show that close-packed surfactant monolayers adsorbed at the air-water interface may retard the evaporation rate of water but that highly concentrated particle dispersions (gels) do not affect such rates.

Figure 7.1 shows the mass loss curves of a series of aqueous dispersions of hydrophilic particles (79.9 % SiOH) as a function of particle concentration. The best way to discuss the particle effect is to compare the slopes or gradients of such curves. The mass loss rate of water under the usual conditions followed during this thesis is $5.7 \pm 0.3 \times 10^{-6}$ g s^{-1}. For this series of curves, the gradients are 5.42×10^{-6}, 5.07×10^{-6} and 4.81×10^{-6} for pure water, 1 wt% dispersion and 4 wt% dispersion respectively. The difference between the extremes is approximately 10 %, double the estimated uncertainty of 5% assumed in our experiments. This measurable but small difference in the evaporation rate of water is probably due to a decrease in the vapour pressure of water as the particle concentration is increased. Figure 7.2 shows mass loss curves of pure water and 1 wt% aqueous dispersions of silica particles where the % SiOH at the surface of the silica particles was varied.

Figure 7.1 Mass loss curves of aqueous dispersions of hydrophilic silica particles (79.9 % SiOH). Particle concentrations are shown in the graph.

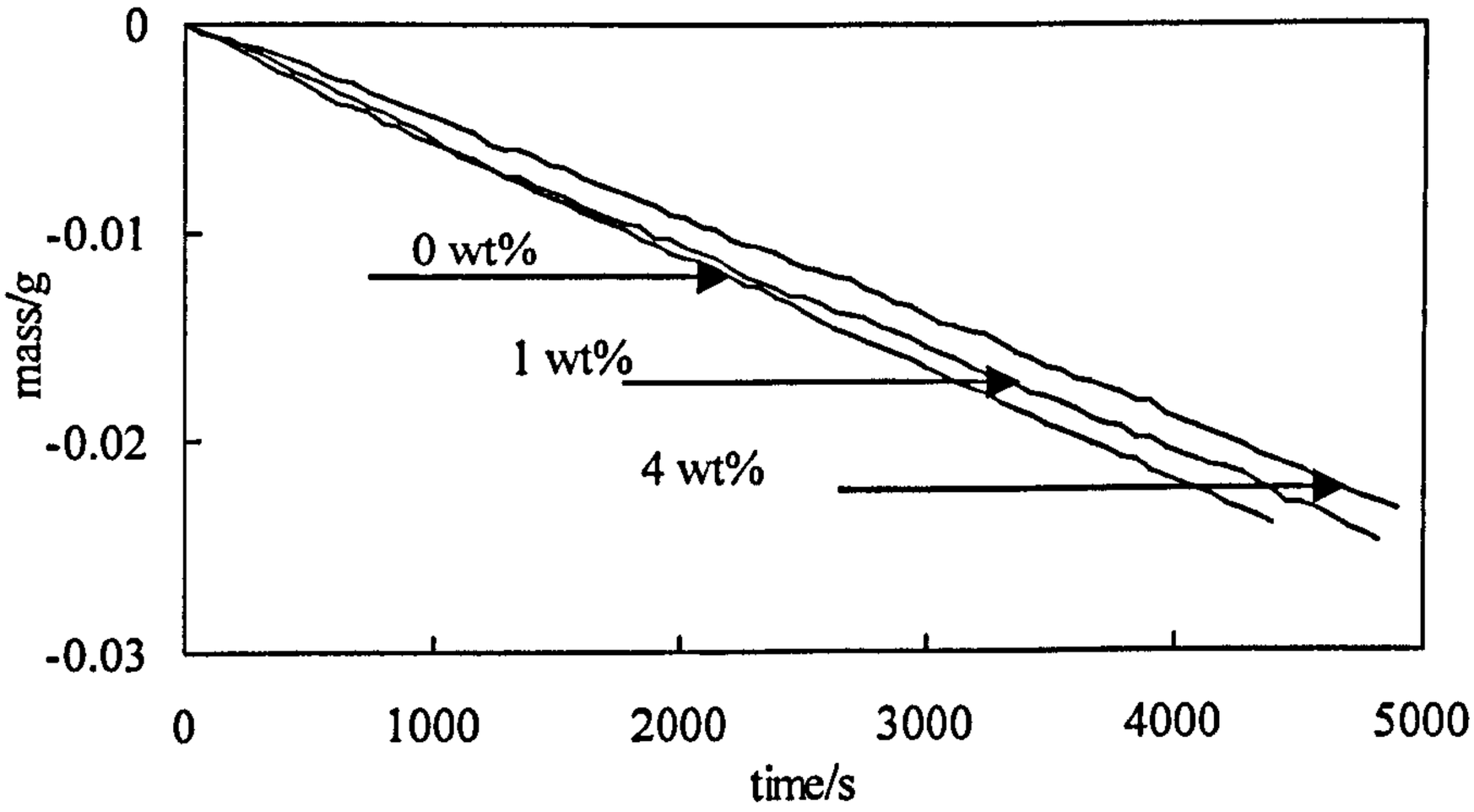

Figure 7.2 Mass loss curves of pure water and aqueous dispersions of silica particles with surface SiOH groups ranging from 18 to 57% (see legend).

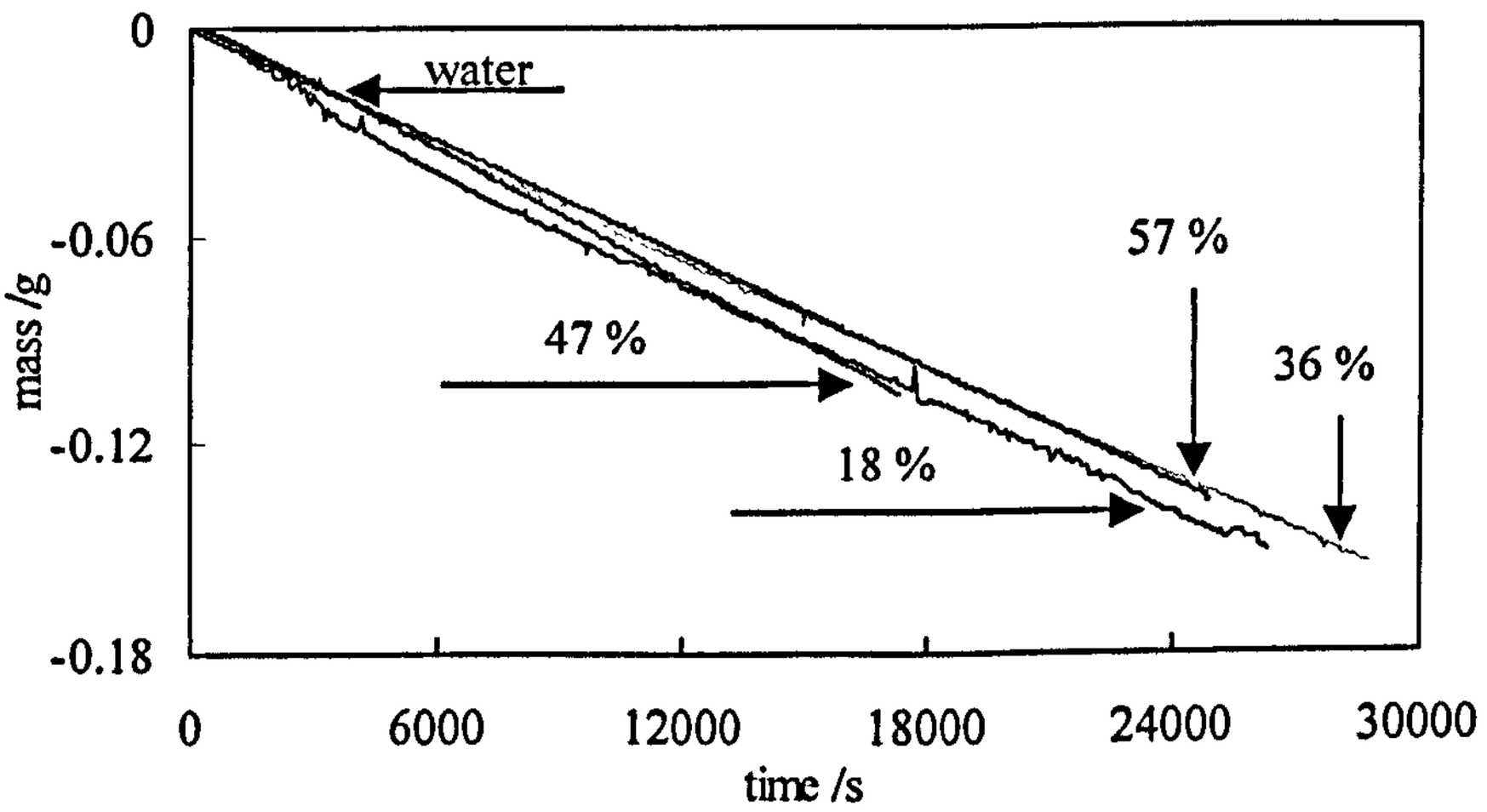

The SiOH content of the particles used in this study varied from 18 % (most hydrophobic) to 57.0 % (least hydrophobic). All curves show analogous mass loss rates (within the measuring error) and similar to that of water. Figures 7.1 and Figure 7.2 show that aqueous dispersions of neither hydrophilic nor hydrophobic particles show significant retardation in the evaporation rate if compared to that of pure water.

Figure 7.3 shows a plot of the mass loss versus time of three different systems. One of the curves represents the mass loss of pure water. A second curve shows the mass loss rate of 1 wt% silica particles (47 %SiOH) dispersed in water. The third one represents the mass loss rate of an aqueous sample with the same type of particles initially dispersed in 1ml of pentane (1 wt%) and then left on the top of the aqueous sample. It is not very clear if pentane spreads spontaneously or form lenses on water[6], but enough volume of a dispersion of particles in pentane was added on the top of the aqueous sample to assure a homogeneous covering of the sample surface by the particles. After the evaporation of the pentane (a few minutes), the particles are expected to totally cover the surface of the sample. The results shown in Figure 7.3 suggest that the particle covering is not highly packed and that the water molecules do not find a physical barrier before they are transported to the vapour phase.

Finally, as no silica particle dispersion (in bulk or surface) reduced the evaporation of water, the mass loss of water with a particle-stabilised emulsion on the top of the water was studied. In our group in Hull we have observed[7] (and further results will

be shown later) that the solid residues left behind after the evaporation of emulsions stabilised by particles may form fairly hard structures.

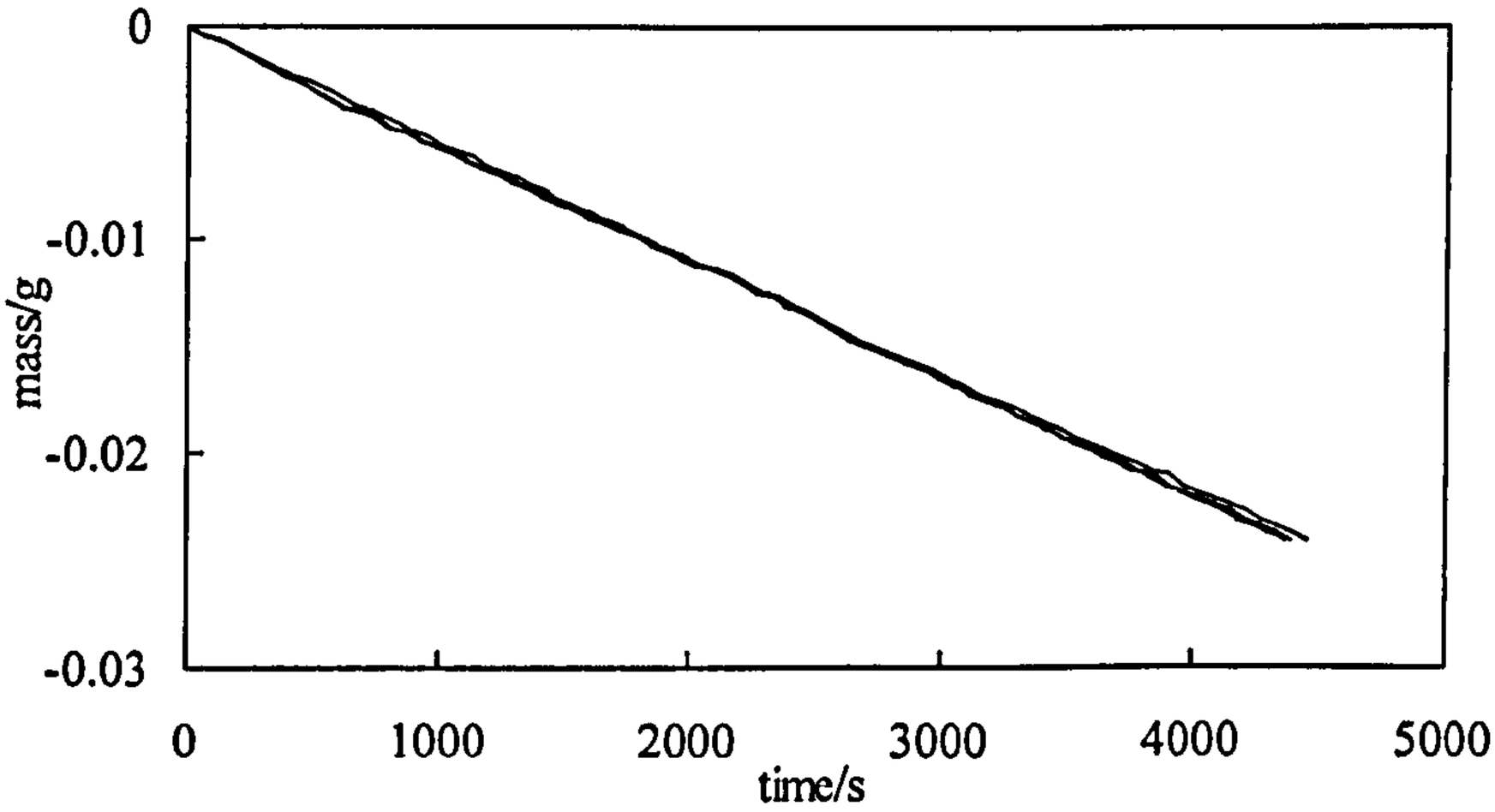

Figure 7.3 Mass loss curves of pure water, an aqueous dispersion of 1 wt% silica particles (47 % SiOH) and pure water with 1 wt% of such particles deposited at the water/air interface from a suspension in pentane.

A 50 vol% toluene-in-water emulsion stabilised by 6 wt% of 87 % SiOH silica (dispersed initially) in water and 2 wt% of 47 % SiOH silica (dispersed initially in toluene) was prepared and left on the top of a sample of pure water. Figure 7.4 shows the mass loss curve of pure water, toluene (both dashed lines to be compared) and the complex colloidal system. In the initial stage of the evaporation of the complex, the mass loss of toluene and water (from the emulsion) is measured (the rate is approximately the sum of both mass loss rates) and after approximately 45,000 s (12 hours), since toluene is evaporated, only mass loss of the remaining water is recorded. The mass loss rate of

remaining aqueous sample is the same to that of pure water. Therefore, it can be said that the microstructured "tablet" formed (by evaporation of the emulsion) on the top of the aqueous sample does not seem to retard the mass loss rate of water. This is mainly due to the fact the tablet remained wet and fragile during the run.

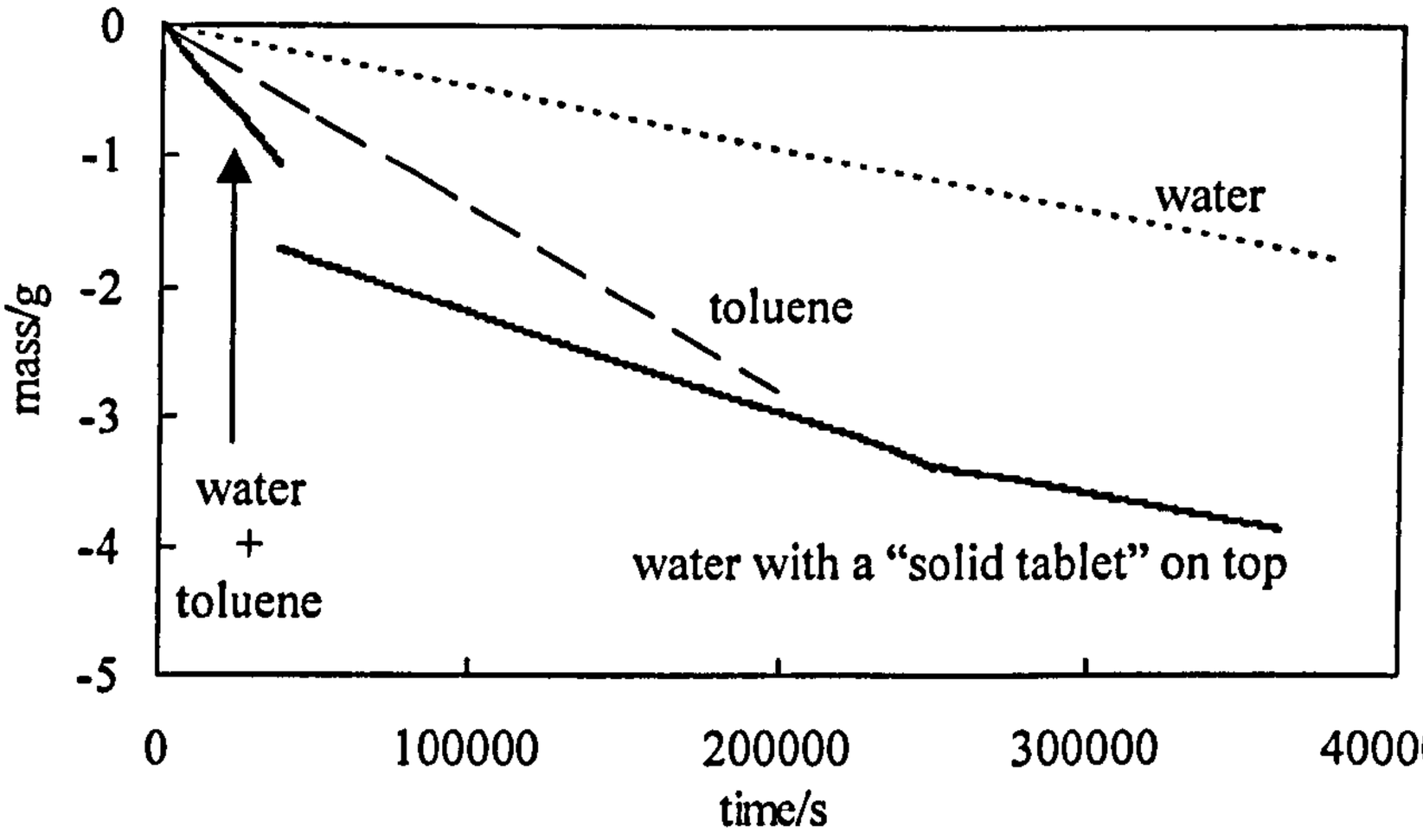

Figure 7.4 **Mass loss curves of pure water, pure toluene and water with a solid tablet on top formed from the evaporation of a 50 vol% toluene in-water emulsion.**

7.3 Evaporation rates of particle-stabilised emulsions

One of the aims of the study of the evaporation rates of Pickering emulsions was to compare these with emulsions stabilised by surfactants under the same conditions. The particle concentration used to stabilise emulsions was generally 1 wt% dispersed in the continuous phase and for these emulsions, within a few minutes creaming was complete.

Figure 7.5 compares the mass loss curves of 10 vol% methylcyclohexane-in-water emulsions stabilised by a) 1 wt% silica particles (76 % SiOH) and b) 20 mM SDS. As we discussed in Chapter 4, mass loss curves of creamed emulsions stabilised by surfactants show a two-stage decay, the first gradient being due to the mass loss of both oil and water followed by a second less steep curve, which is due only to the mass loss of water. For the 10 vol% methylcyclohexane-in-water emulsion stabilised by 20 mM SDS, after approximately 30000 s (~8 h) all the oil is lost and the mass loss recorded in the second stage is due solely to water mass loss. In contrast, the plot of mass loss versus time for the 10 vol% MCH-in-water emulsion stabilised by 1 wt% silica particles (76 % SiOH) shows a virtually constant gradient for over 250000 s (3 days). This observation (and the comparison with pure water and MCH mass loss rates) suggests that the recorded mass loss over the run, is due to the simultaneous mass loss of both oil (retarded relative to bulk water) and water. Therefore, it can be said that during the first 30000 s, the mass loss curve of the solid-stabilised emulsion is slowed down compared to that of the surfactant-stabilised emulsions. For particle aqueous dispersions, no retardation was observed in the evaporation rate if compared to that of water, so we suggest that the observed retardation in the evaporation rate of the emulsions is only affecting to the dispersed oil drops. On one hand, solid particles have much higher energy of attachment (to the o-w interface) than surfactants, and the other hand, because of the steric repulsion, the thickness of the water film in the case of solid-stabilised emulsions is much thicker. Both physical barriers may slow down the evaporation rate of the oil drops.

Figure 7.5 **Comparison between the mass loss curves of 10 vol% methyl-cyclohexane-in-water emulsions stabilised by a) 1 wt% solid silica particles (76 % SiOH) and b) 20 mM SDS.**

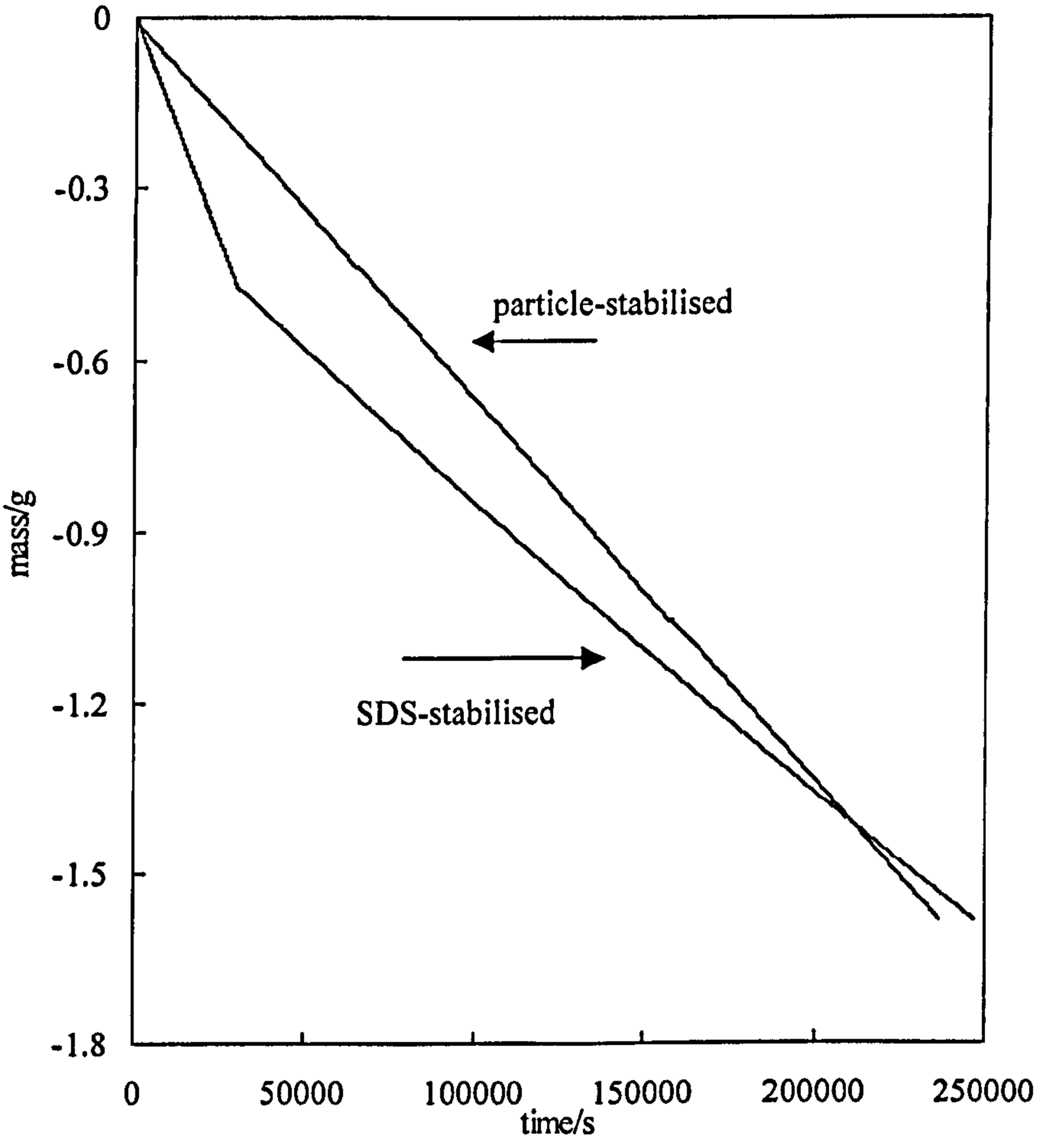

After 30000 s, curve a) still represents the mass loss of both oil and water whereas in curve b), as all the oil is lost, the mass loss of water is only recorded. When the theoretical model to fit mass loss curves of creamed emulsions stabilised by surfactants was applied the f values ≈ 0.

Evaporation rates of emulsions stabilised by solid silica particles were initially measured for samples contained in a cylindrical glass sample tube. Evaporation rate measurements were found to be relatively irreproducible due to the formation of residue "rings" adhering to the vessel walls. In an attempt to prevent residue adhesion, the following runs were carried out in Teflon (PTFE) vessels. In this case, the particle residues showed little adhesion to the inner vessel walls but they did not settle at the bottom of the sample tube either. The particle residues formed a cylindrical column of thickness equal to 2 mm or so. Figure 7.6 shows a typical solid structure formed following the evaporation of a solid-stabilised emulsion (containing toluene) in the Teflon vessel. As the shape and the volume of the solid residue were irreproducible, the cross-sectional area of the tube was also unknown and therefore the mass loss data was impossible to analyse in detail.

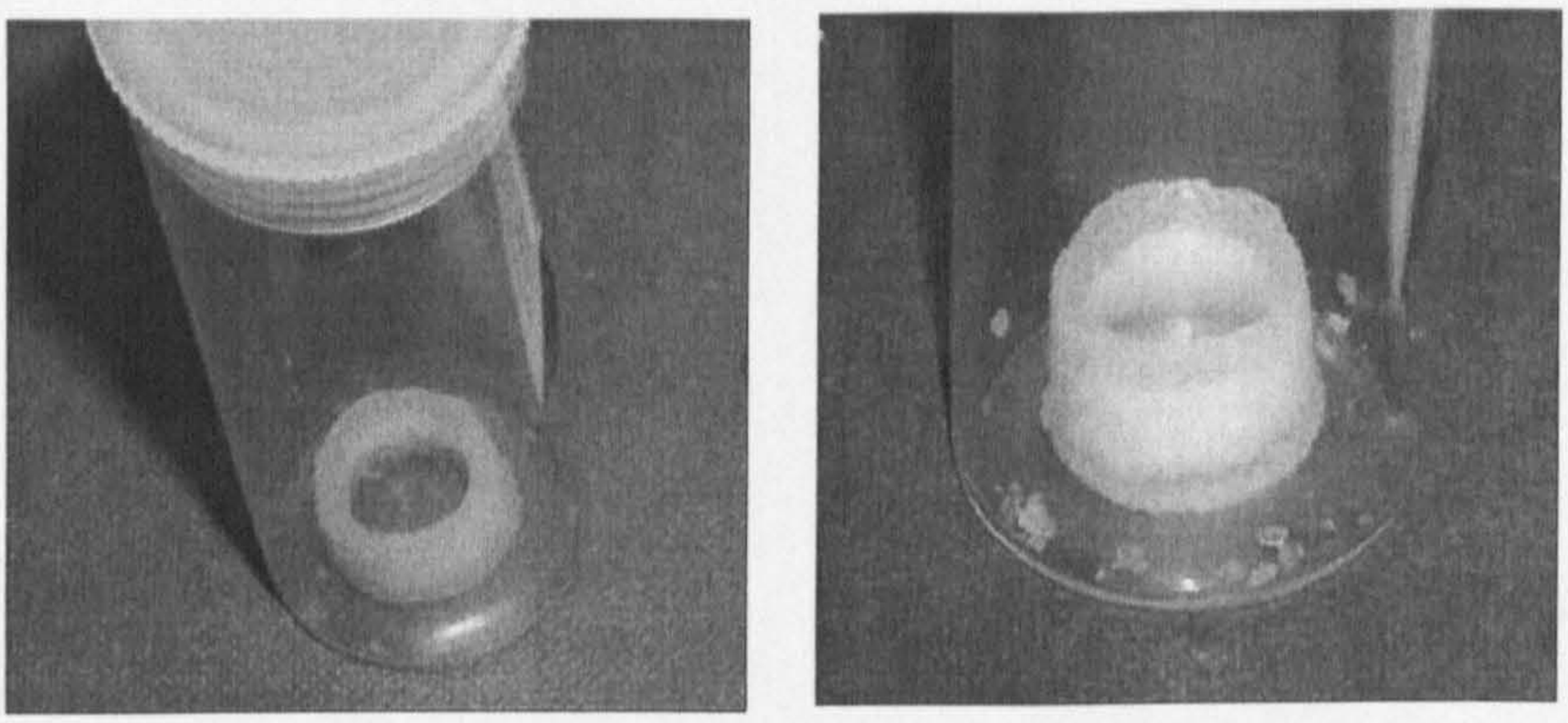

Figure 7.6 **Solid residues after total evaporation (from a PTFE tube) of 10 vol% toluene-in-water emulsion stabilised by silica particles (76% SiOH). Different images of the same sample are shown.**

7.4 Solid phases following evaporation of particle-stabilised emulsions

Following liquid evaporation, solid stabilised emulsions have been observed to form solid residues with a porous structure[7]. The type of microstructure is probably related to the conditions (oil type, oil content, particle type, particle concentration and emulsion type) of the initial emulsion. Emulsions varying all those parameters were prepared and approximately 4 ml of each emulsion was left in open glass tubes at room temperature until the volatile species were completely evaporated (up to 3 weeks). Images of the dried residues were obtained using SEM.

Figure 7.7 shows an example of a solid residue left behind after the evaporation of an o/w emulsion stabilised by hydrophilic particles. In (a) an example of these porous

inorganic materials can be observed. The cavities are formed after the evaporation of the dispersed phase of the emulsion and hence the pore size is probably related to the drop size of such emulsions. The size of the cavities shown in Figure 7.7 is approximately 5-10 μm. In (b) a further magnification of Figure 7.7a is shown. In this image the way in which the cavities are formed is revealed. As discussed in Chapter 1, solid silica nanoparticles adsorb at the oil/water interface and stabilise the emulsions. Using low temperature scanning electron microscopy[8] it has been observed that particles adopt different configurations (flocs or close packed layers) at the oil-water interface depending on the nature of the oil. Notice that the cavities are held by the network which is produced by the particles that were dispersed in the continuous phase before the evaporation started.

Figure 7.7 **a) Macroporous structure left behind after total evaporation of the volatile species from an emulsion stabilised by silica particles. b) Magnification of the rectangle drawn in a).**

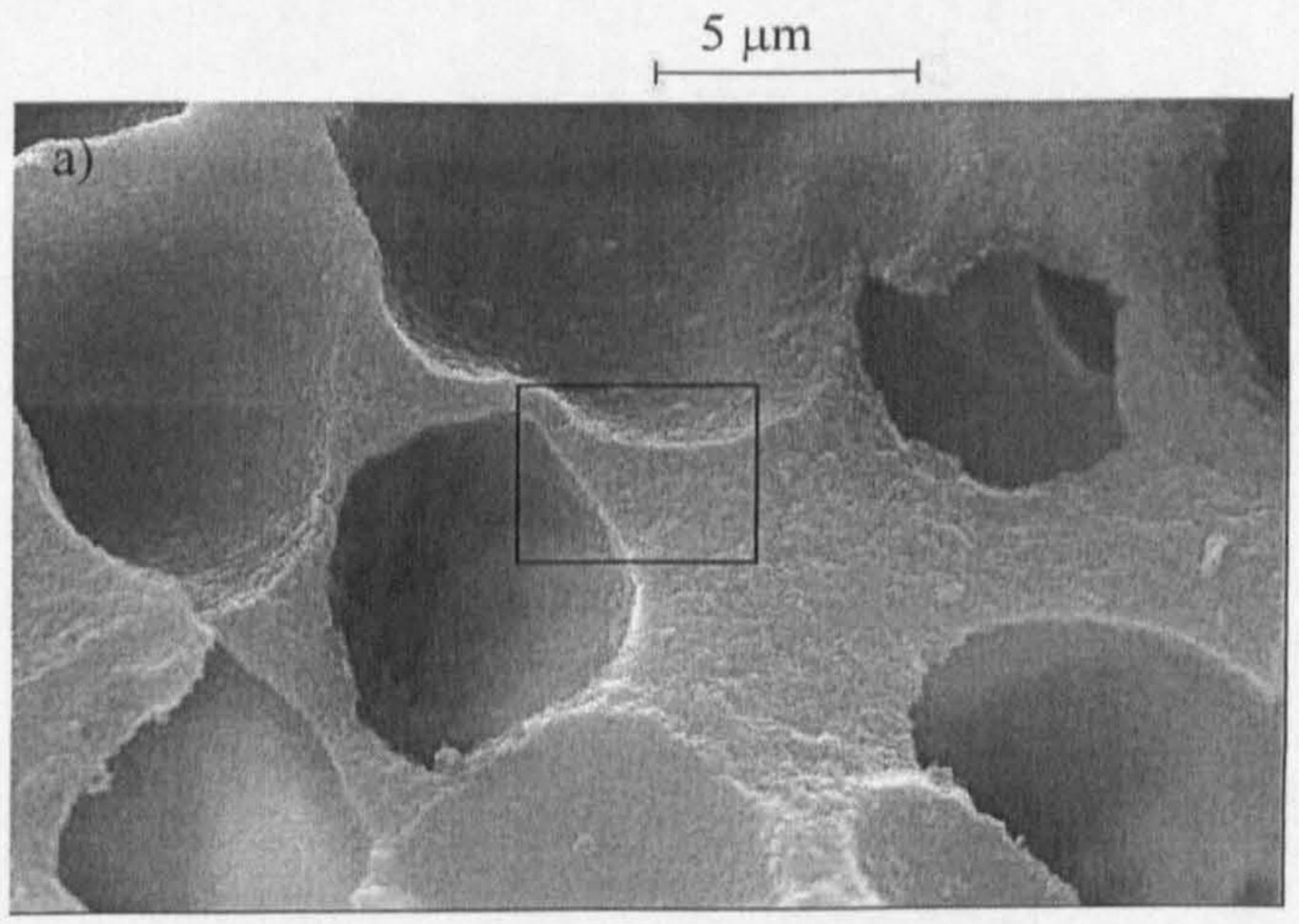

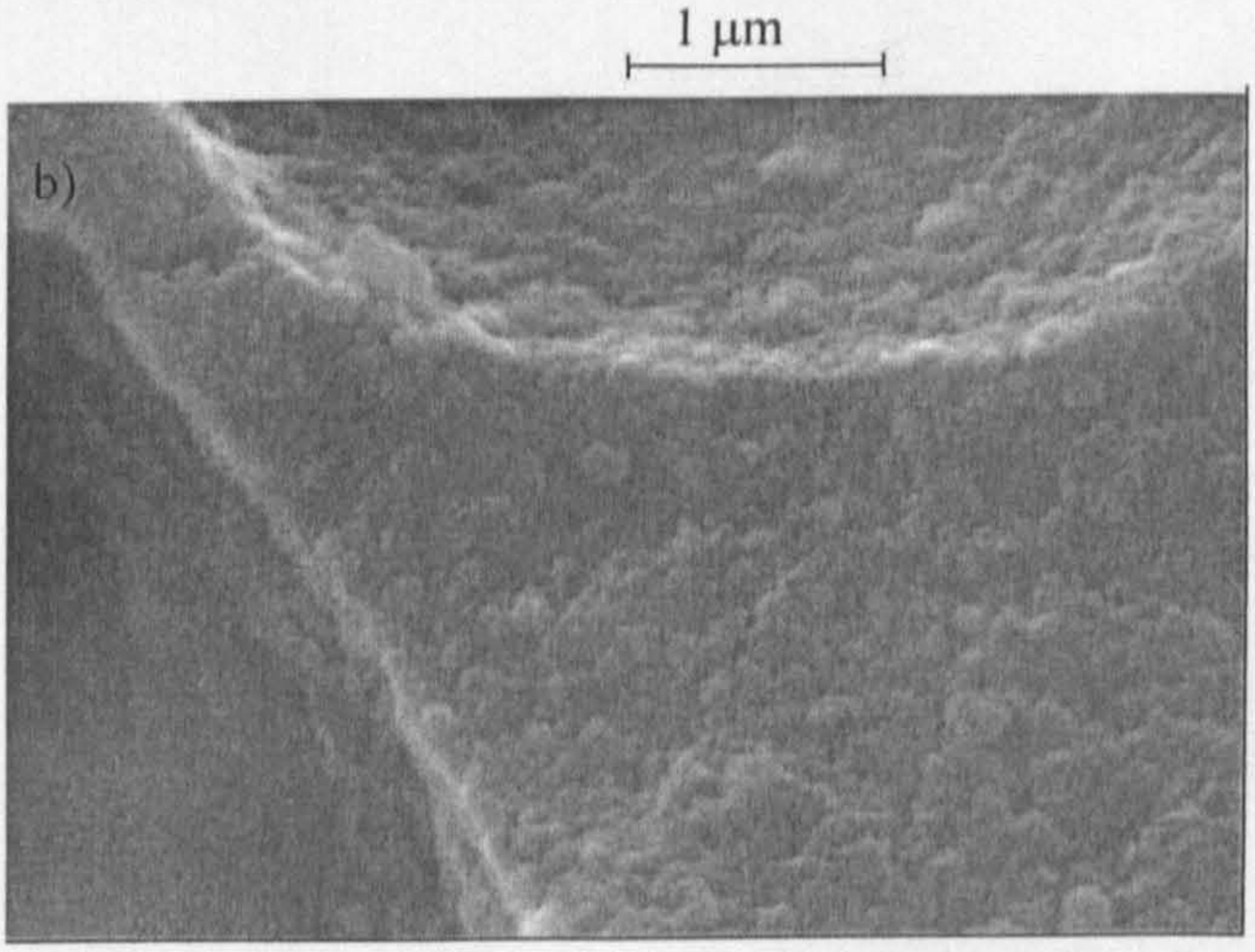

7.4.1 Effect of oil type

First of all the oil type in both o/w and w/o emulsions was studied and to do that, different oils with a relatively wide range of vapour pressure were chosen. Figure 7.8 shows SEM images of solid residues obtained after evaporation of 10 vol% o/w emulsions stabilised by 1 wt% hydrophilic silica particles (76 % SiOH) in which the oils were a) hexane (P = 19812 Pa), b) HMDS (P = 4887 Pa) and c) decane (P = 180 Pa). Solid structures obtained after the evaporation of o/w emulsions prepared by oils with vapour pressures 5-6 times higher than water (P_w = 3167 Pa), such as pentane (not shown) or hexane (Figure 7.8a) show "knobbly" structures. On the other hand, emulsions prepared with oils with vapour pressures of the same order of magnitude as that of water or less (150-6500 Pa), such as HMDS (Figure 7.8b) or long chain alkanes (Figure7.8c), show a sponge-like microstructure. It appears that the porosity of the structure is related to the vapour pressure of the oil. Highly volatile oils do not stay long enough in the emulsion to form stable cavities, whereas after evaporation of emulsions with oils with vapour pressure similar to or lower than that of water, stable pores are formed and remain as cavities.

In Figure 7.9 SEM images of solid residues left behind after the evaporation of 10 vol% w/o emulsions stabilised by 1 wt% (47 % SiOH) are shown. The oils used in the present study were chlorobenzene (Figure 7.9a), methylcyclohexane, perfluoroheptane, perfluoropentane (Figure 7.9b) and toluene (Figure 7.9c).

Figure 7.8 **SEM images of solid residues obtained from the evaporation of 10 vol% oil-in-water emulsions stabilised by 1 wt% silica particles (76% SiOH), the oil phase being a) hexane, b) HMDS and c) decane.**

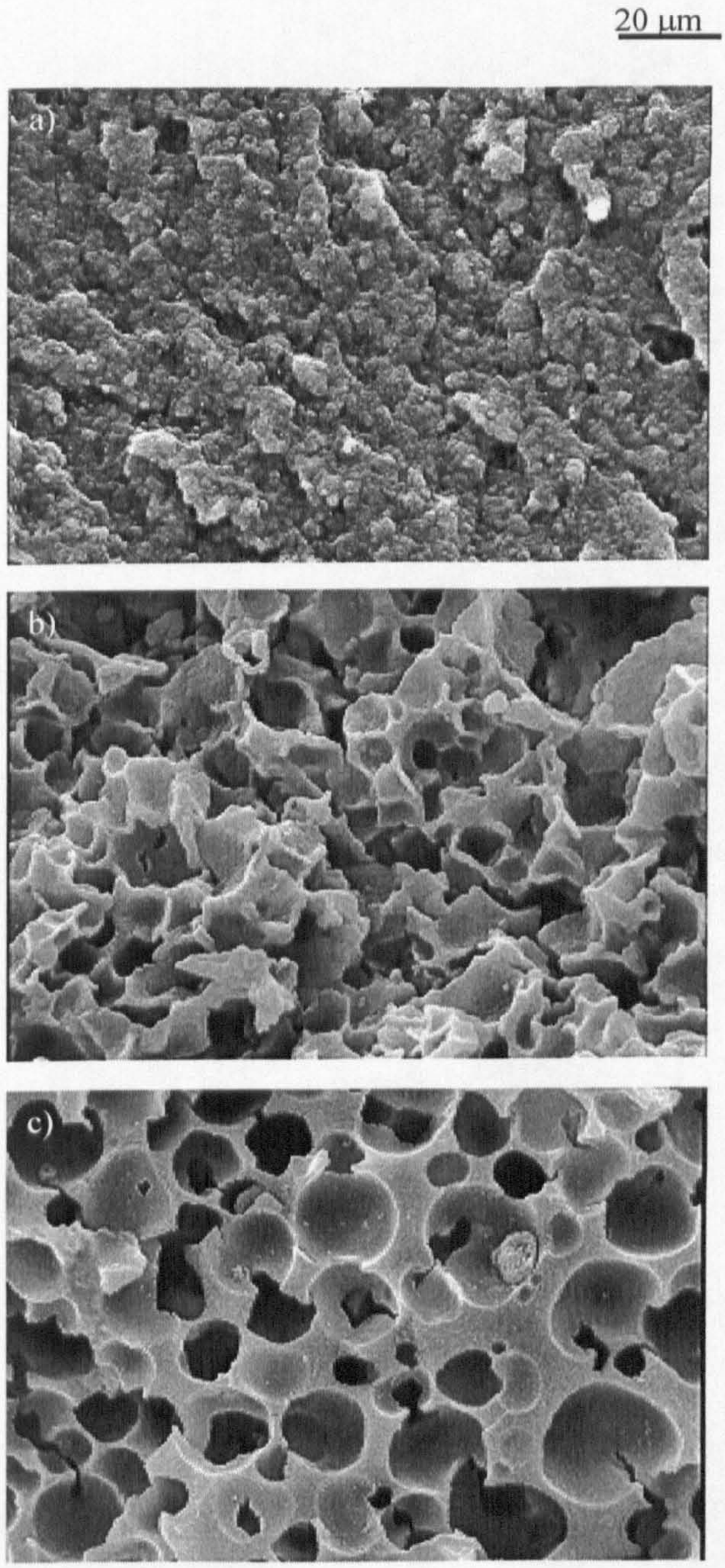

Figure 7.9 **SEM images of 10 vol% w/o emulsions stabilised by 1 wt% silica particles (47 % SiOH) the oils being a) chlorobenzene, b) perfluoropentane and c) toluene.**

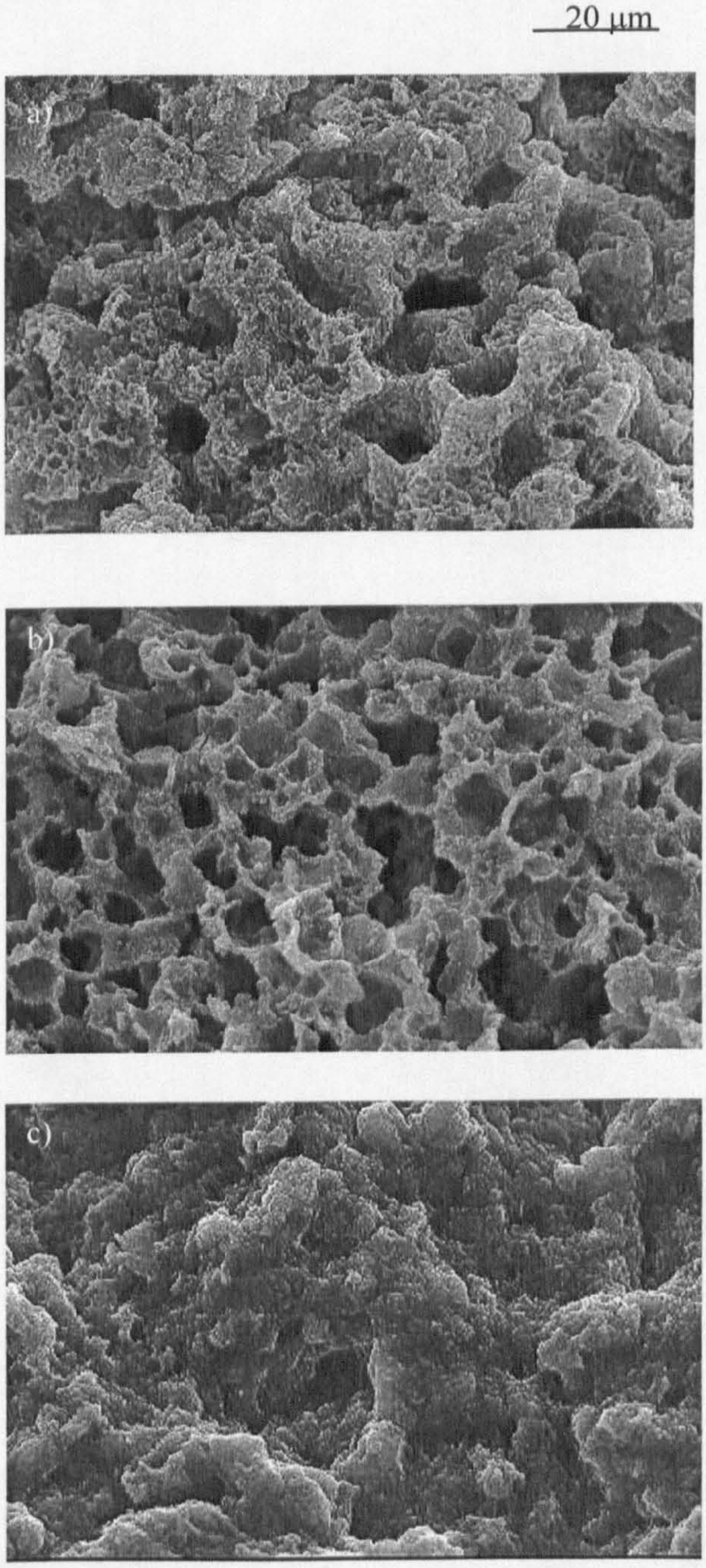

Solid residues from w/o emulsions prepared with very volatile oils such as short chain perfluorocarbons (P = 1-8 x 10^4 Pa) show porous microstructures, whereas in the case of w/o emulsions prepared by oils with similar or lower vapour pressure to that of water ($P_{chlorobenzene}$ = 1554 Pa), solid residues show a "knobbly" appearance. It should be noted that chlorobenzene and perfluoropentane are denser than water and thus, in these emulsions, the water drops creamed. This case is similar to o/w emulsions where oil drops are less dense than water and hence also cream. When toluene is used as oil in w/o emulsions, water drops sediment and no porous structure is observed. All these SEM images suggest that the porosity of the structure seems to be related to emulsion type, emulsions stability (creaming or sedimentation) and the relative vapour pressures of the oil and water.

7.4.2 Effect of oil volume fraction

Figure 7.10 shows SEM images of the solid residues remaining after the evaporation of methylcyclohexane-in-water emulsions containing different oil volume fractions and stabilised by 1 wt% silica particles (76% SiOH). All microstructures show "sponge-like" arrangements. The oil volume fraction is increased from 0.2 to 0.6 and the increase in pore size is clear. The mean drop size of the initial emulsion (summarised in Table 7.1) is represented to scale by the white circle shown in the bottom right corner of each image.

Figure 7.10 **SEM images of solid residues obtained after the evaporation of methylcyclohexane-in-water emulsions stabilised by 1 wt% 76 % SiOH for oil volume fractions in the emulsions, ϕ_o, a) 0.2, b) 0.4 and c) 0.6.**

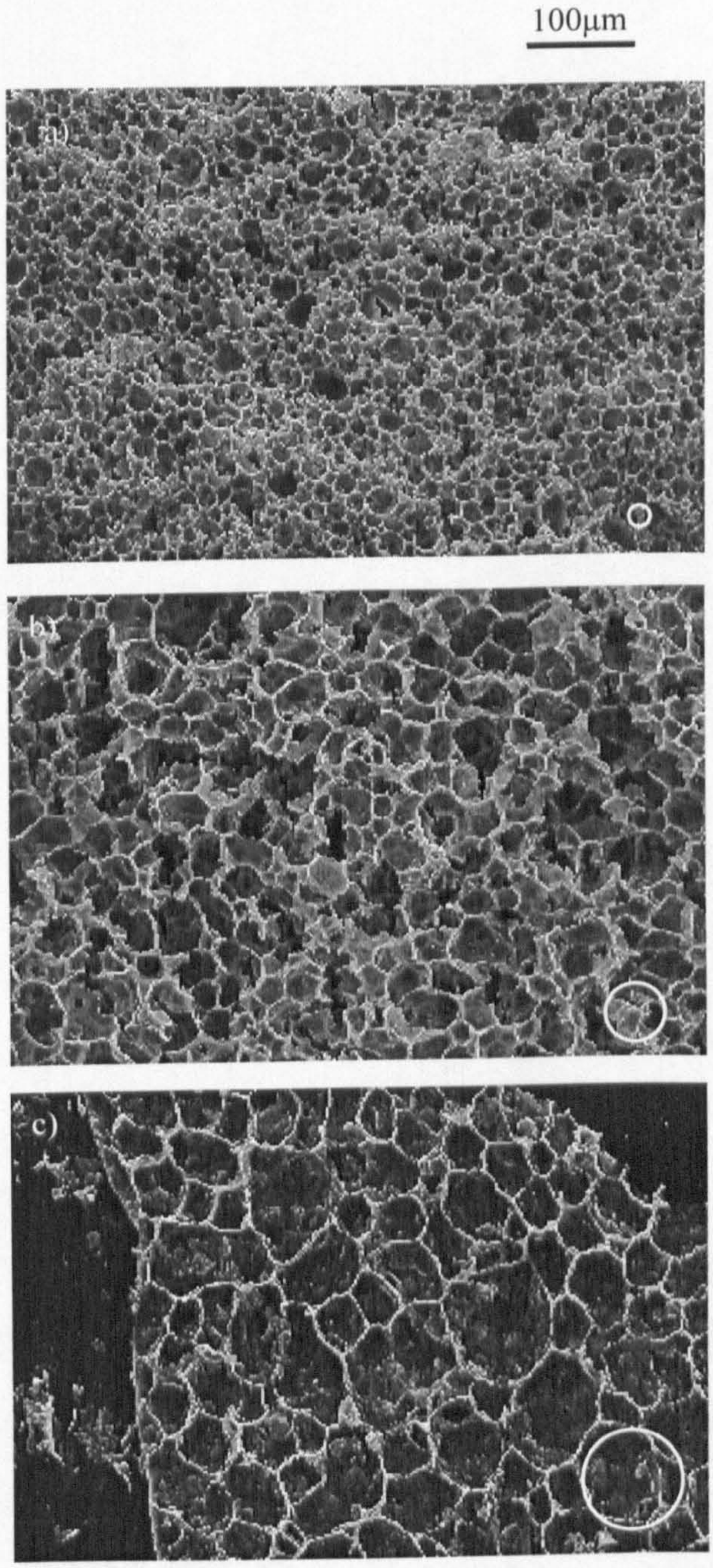

ϕ_o	$d_{(t=0)}$ / μm	$d_{(t=24\ h)}$ / μm
0.1	35.5	35.55
0.2	22.3	21.4
0.4	59.6	43.6
0.6	100.3	87.3

Table 7.1 Summary of the average drop diameter of the oil drops in methylcyclohexane-in-water emulsions stabilised by 1 wt% (76 % SiOH) for t = 0 and t = 24 h after preparation.

Comparison of the mean drop diameters of the parent emulsions (white circles) and the cavity sizes observed in Figure 7.10 (and later in this Chapter) shows that there is a close correlation between them, i.e., the solid residues contain cavities of a similar size distribution to the original drop sizes. Hence, it is clear that the residue morphology can be "tuned" to a desired feature size by adjustment of the drop size of the original emulsion.

7.4.3 Effect of particle hydrophobicity

Phase inversion of emulsions may be achieved by different means. In general, transitional inversion[9] occurs when, at fixed volume fraction of oil and water, the HLB of the system (temperature or electrolyte concentration) is changed. In surfactant-stabilised emulsions this can be achieved, for example, by increasing the concentration of either hydrophobic or hydrophilic groups in the system. For emulsions stabilised by solid particles, the change in HLB may be achieved by varying the particle wettability[10]. Water-toluene emulsions stabilised by particles with up to ~50 % SiOH groups

(hydrophobic) form w/o emulsions, where more hydrophilic particles prefer form o/w emulsions[10].

Figure 7.11 shows the conductivity of water-toluene emulsions stabilised by silica particles of different wettability (hydrophobicity) initially dispersed in toluene. For hydrophobic particles (approx. up to 50 % SiOH), the conductivity is very low indicative of w/o emulsions and rises sharply for o/w emulsions when particles with higher hydrophilic group content are used as stabilisers. Notice that for this specific system, and close to the phase inversion, the conductivity is low even for emulsions stabilised by relatively hydrophilic particles (55 % SiOH). In all cases the emulsion type was confirmed using the "the drop test" method.

Figures 7.12a-7.12f show images obtained after total evaporation of 50 vol% toluene containing silica-stabilised emulsions where particles of a wide range of hydrophobicity (from 36 to 87 % SiOH) were used as stabilisers. Solid phases from w/o emulsions (before phase inversion) and o/w emulsions (immediately after inversion) show filled structures (7.12a-c). Solid phases of residues of o/w particle-stabilised emulsions away from inversion show porous structure (7.12d-e) and finally, emulsions stabilised by highly hydrophilic particles (87 % SiOH) were unstable and the residues show filled structures (7.12f). This series of SEM images illustrates that stable toluene-in-water emulsions leave porous microstructures, whereas water-in-toluene emulsions and emulsions close to phase inversion (57 % SiOH) show filled structures.

Figure 7.11 **Conductivity of water-toluene emulsions (ϕ_w = 0.5) stabilised by silica particles of different wettability initially dispersed in toluene.**

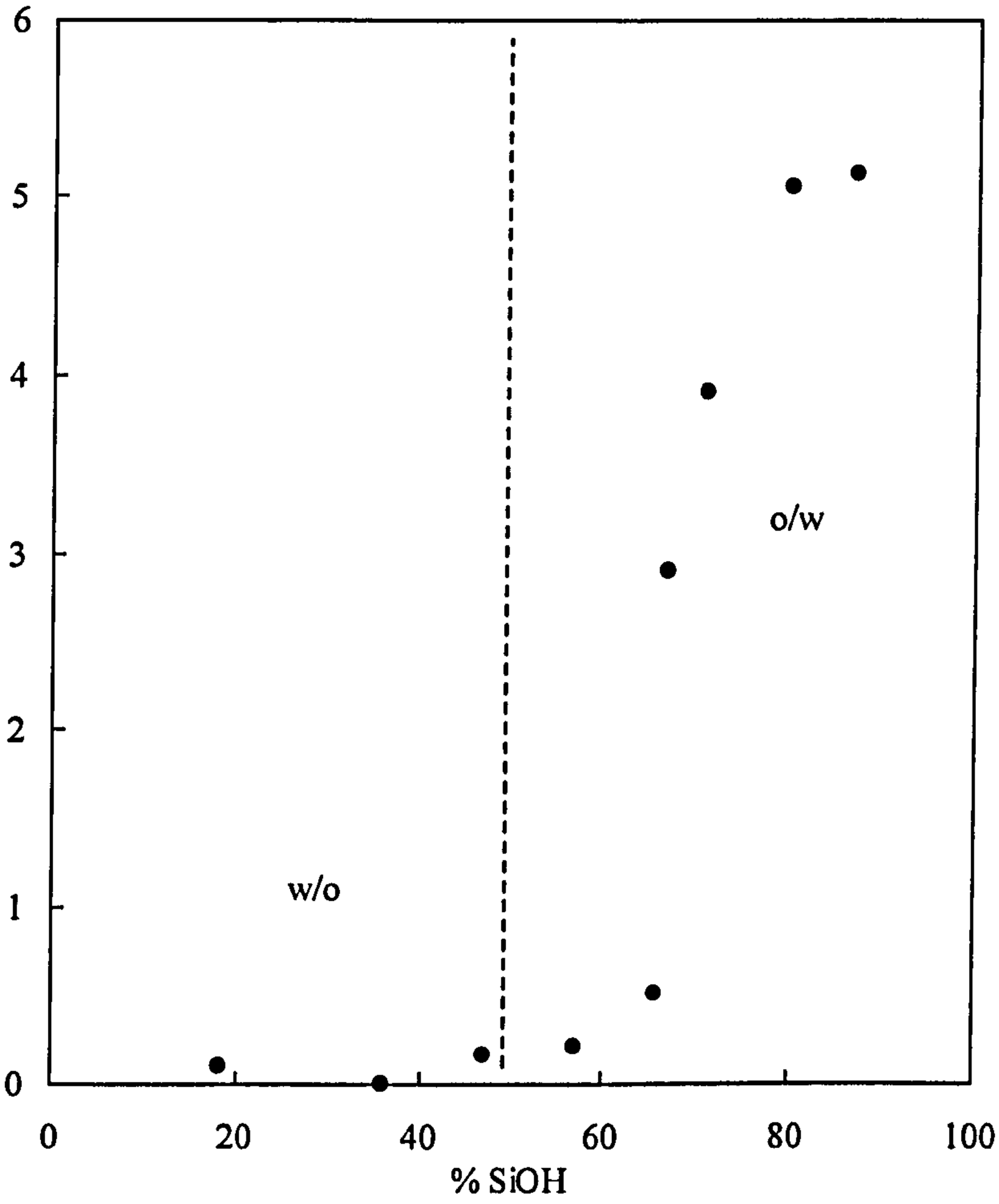

Figure 7.12 SEM images of solid residues obtained after the evaporation of 50 vol% water-toluene emulsions stabilised by silica particles with the following % SiOH: a) 36 %, b) 47 %, c) 57 %, d) 71 %, e) 79.9 %, and f) 87 %.

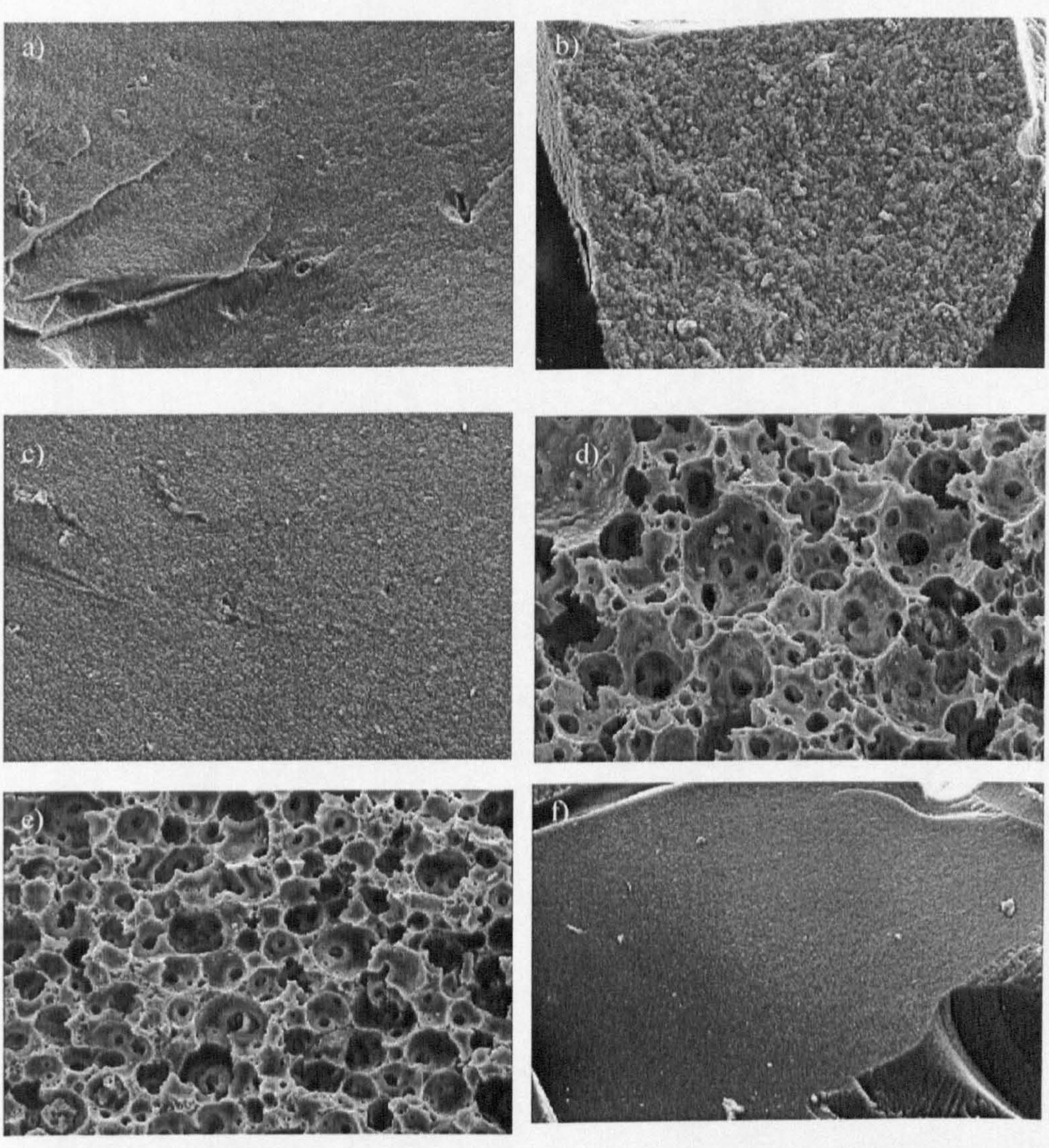

Although it is not totally clear, this is probably due to the relative evaporation rates ratio of toluene and water and the configuration of particles at the toluene/water interface.

7.4.4 Effect of particle concentration

Figures 7.13a-c show SEM images of solid residues left behind after the evaporation of 10 vol% methylcyclohexane-in-water emulsions stabilised by 1, 2 and 4 wt% of 76 % SiOH silica particles. All structures show a "sponge-like" structure. Clearly, the pore size of the microstructure is decreased as particle concentration is increased. Figures 7.14a-b show the same effect by using 10 vol% decane-in-water emulsions stabilised by 1 and 4 wt% of 76 % SiOH as initial emulsion. The mean pore size is in all cases similar to the mean drop size of the initial emulsions. The mean drop diameters of the 10 vol% methylcyclohexane- and 10 vol% decane-in-water emulsions stabilised by different concentration of silica particles (76 % SiOH) are summarised in Table 7.2.

Oil	[particle] / wt %	$d_{(t=0)}$ / μm	$d_{(t=24\ h)}$ / μm
methylcyclohexane	1	35.50	35.55
	2	16.5	16.5
	4	14.2	14.8
decane	1	32.1	29.8
	4	13.1	13.0

Table 7.2 Summary of mean drop diameter of 10 vol% methylcyclohexane- and 10 vol% decane-in-water emulsions stabilised by 76 % SiOH.

Figure 7.13 **SEM images of solid residues obtained after the evaporation of 10 vol% methylcyclohexane-in-water emulsions stabilised by a) 1 wt% b) 2 wt% and c) 4 wt% silica particles (76 % SiOH). The white circle shows (to scale) the average drop size of the parent emulsion.**

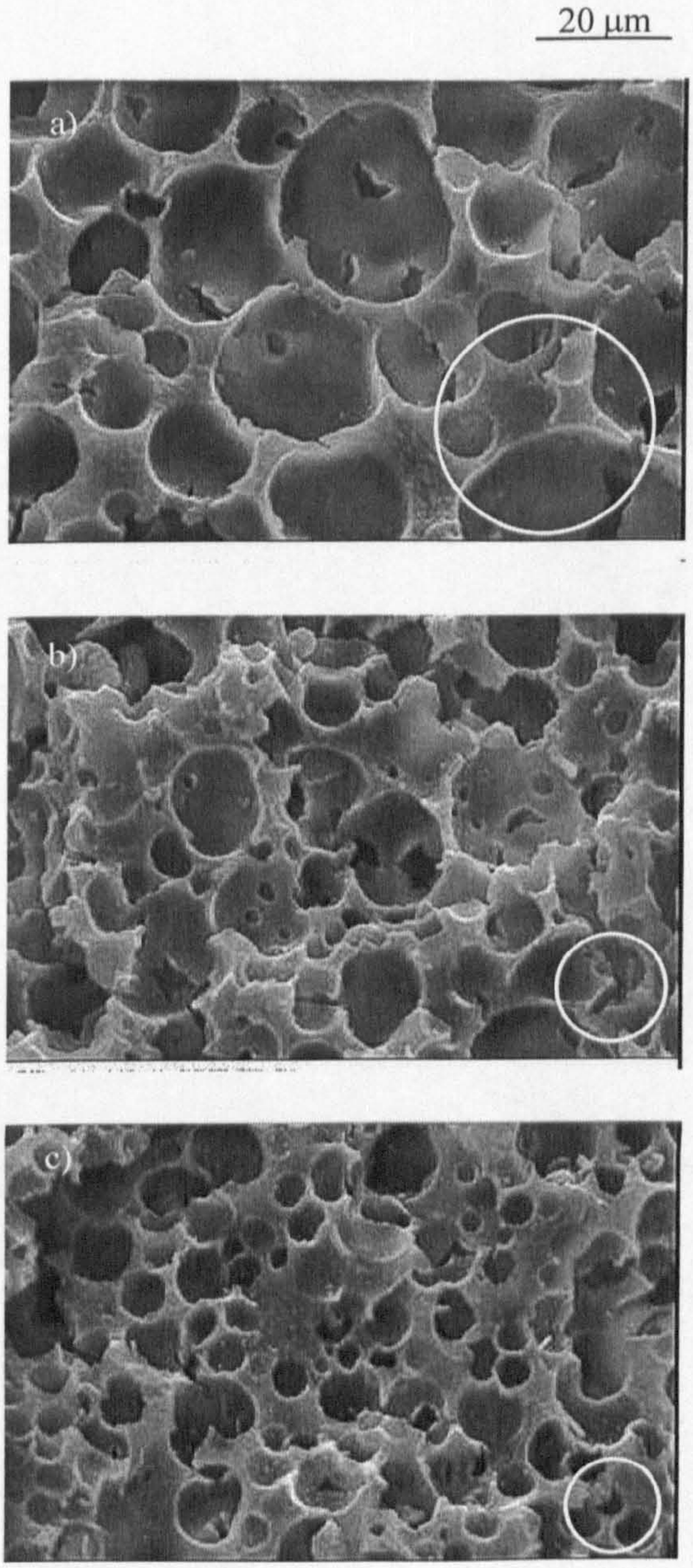

Figure 7.14 **SEM images of solid residues obtained after the evaporation of 10 vol% decane-in-water emulsions stabilised by a) 1 wt% and b) 4 wt% silica particles (76% SiOH). The white circle shows (to scale) the average drop size of the parent emulsion.**

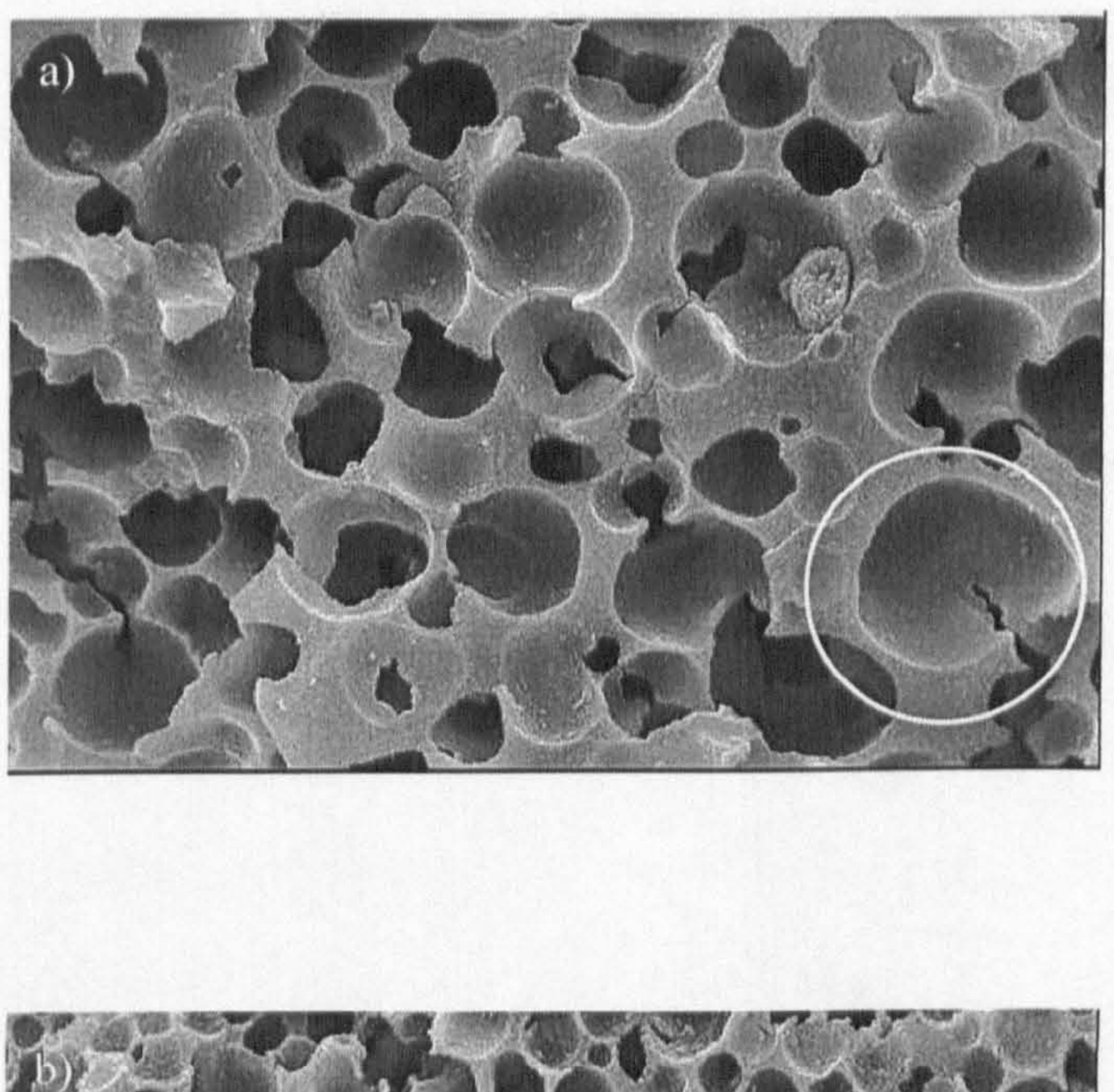

Clearly, as the particle concentration is increased, the drop and pore sizes are decreased. Note as well, that in most cases the pores are smaller than the drops because some oil is lost before the cavity is finally structured.

Figures 7.15 and 7.16 show the particle concentration effect on the microstructures of the solid residues obtained after the evaporation of 10 vol% water-in-HMDS and 10 vol% water-in-hexane emulsions stabilised by 47 % SiOH particles respectively. In both cases a) represents [particle] = 1 wt% and b) [particle] = 4 wt%. SEM images of w/o emulsions with 1 wt% particles show a "knobbly" structure similar to that observed in several cases before, but as the particle concentration is increased a better defined porous structure is formed.

7.4.5 Effect of oil-water ratio

Phase inversion of emulsions, from o/w to w/o and vice versa, can be achieved by changing the oil/water volume ratio. This is known as catastrophic inversion since it is accompanied by dramatic changes in properties of the emulsions, including viscosity and drop size[11]. It is known that toluene-water emulsions stabilised by hydrophilic silica invert at a volume fraction of water around 0.7[11]. Figure 7.17 shows the conductivity of water-toluene emulsions stabilised by 47 % SiOH silica particles as a function of the volume fraction of water. The particle concentration was 1 wt% in the emulsions (initially 2 wt% dispersed in toluene) and was kept fixed. In agreement with the literature value, the catastrophic inversion happens at a volume fraction of water around 0.7.

Figure 7.15 **SEM images of 10 vol% water-in-HMDS emulsions stabilised by a) 1 wt% and b) 4 wt% silica particles (47 % SiOH).**

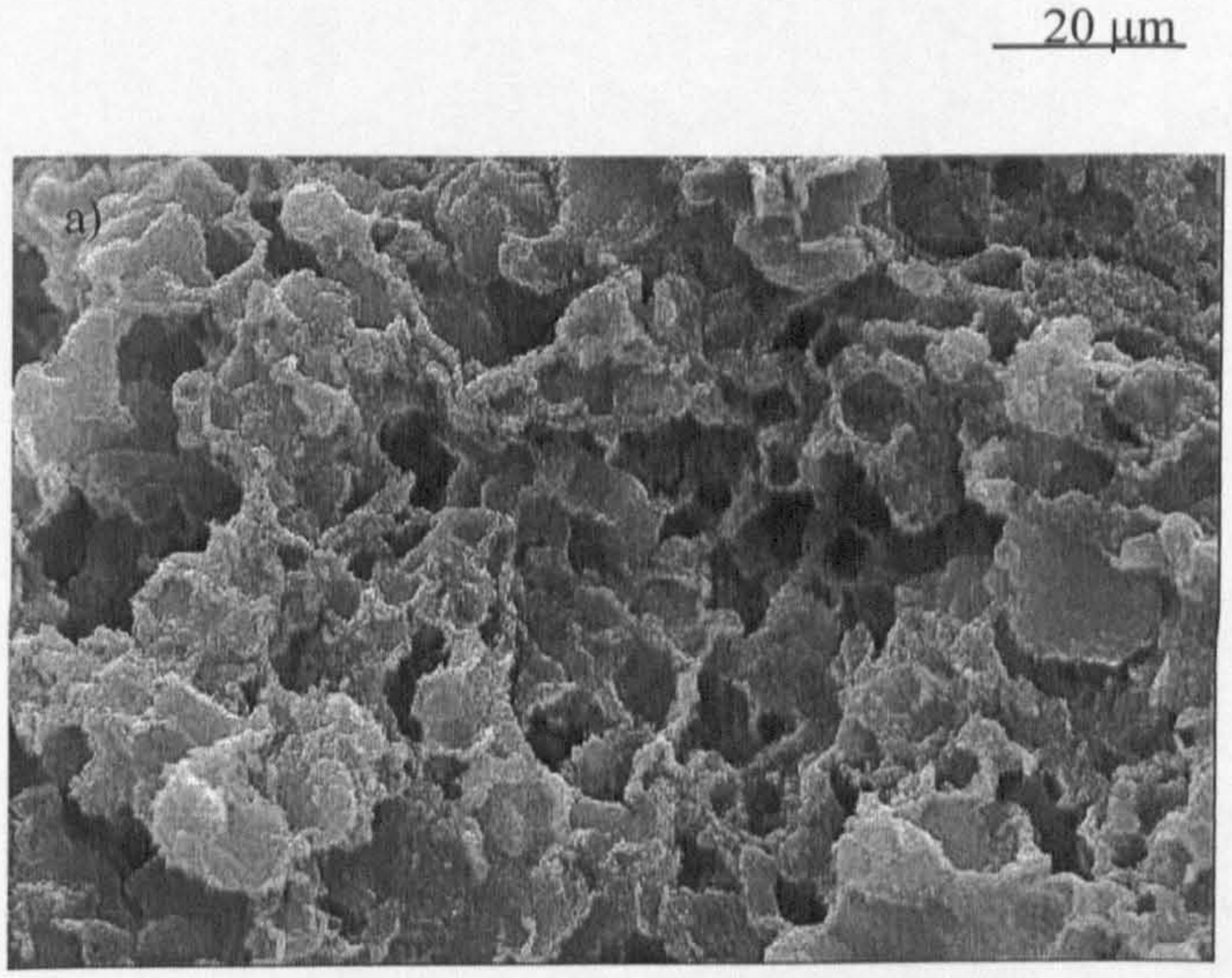

Figure 7.16 **SEM images of 10 vol% water-in-hexane emulsions stabilised by a) 1 wt% and b) 4 wt% silica particles (47 % SiOH).**

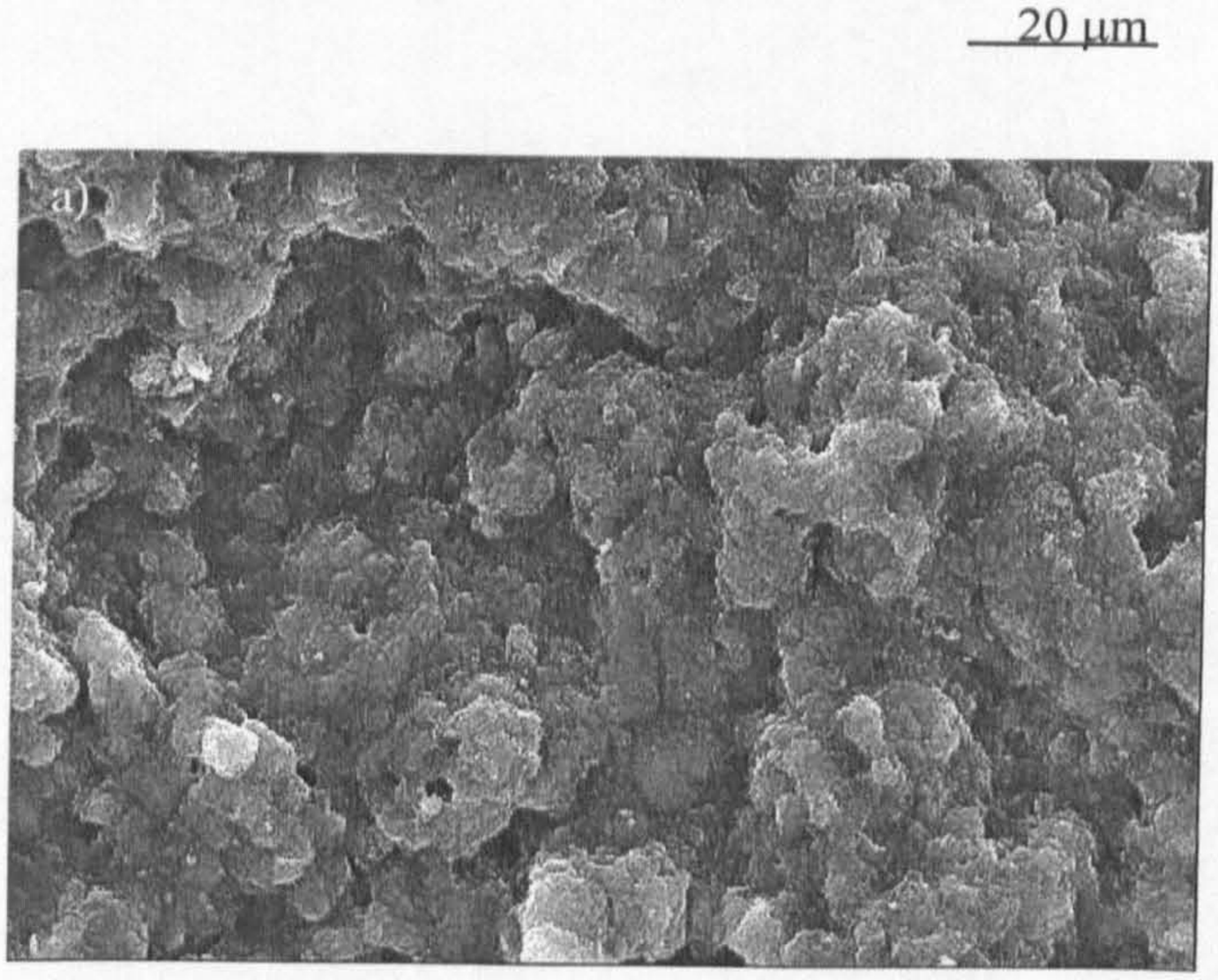

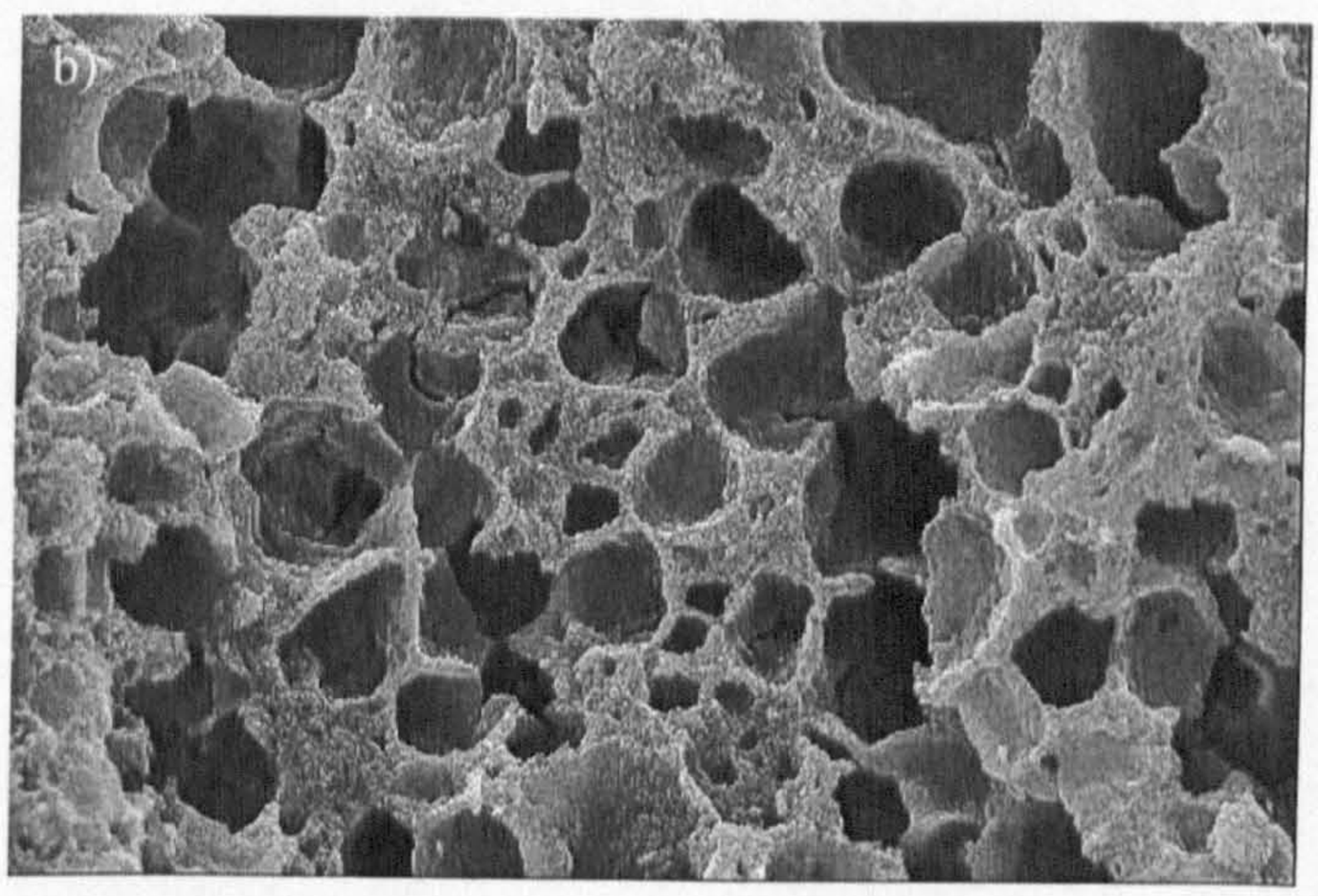

For lower ϕ_w, the emulsion type is w/o (low conductivity), whereas for $\phi_w > 0.7$ the emulsion is an o/w (high conductivity). Figures 7.18a-d show SEM images of the solid residues obtained after the evaporation of the emulsions with different ϕ_w (0.3, 0.5, 0.7 and 0.9). For the lower water volume fraction (Figures 7.18a-b), SEM images show the characteristic microstructures seen after evaporation of w/o emulsions. For $\phi_w = 0.7$, close to phase inversion, the microstructure (Figure 7.18c) is sheet-like as observed during the transitional inversion (Figure 7.12c). For the o/w emulsion at high volume fraction, the SEM shows the "sponge-like" microstructure again (Figure 7.18d), characteristic of most o/w emulsions.

Figure 7.17 **Conductivity of water-toluene emulsions stabilised by 1 wt% 76 % SiOH silica particles as a function of the volume fraction of water.**

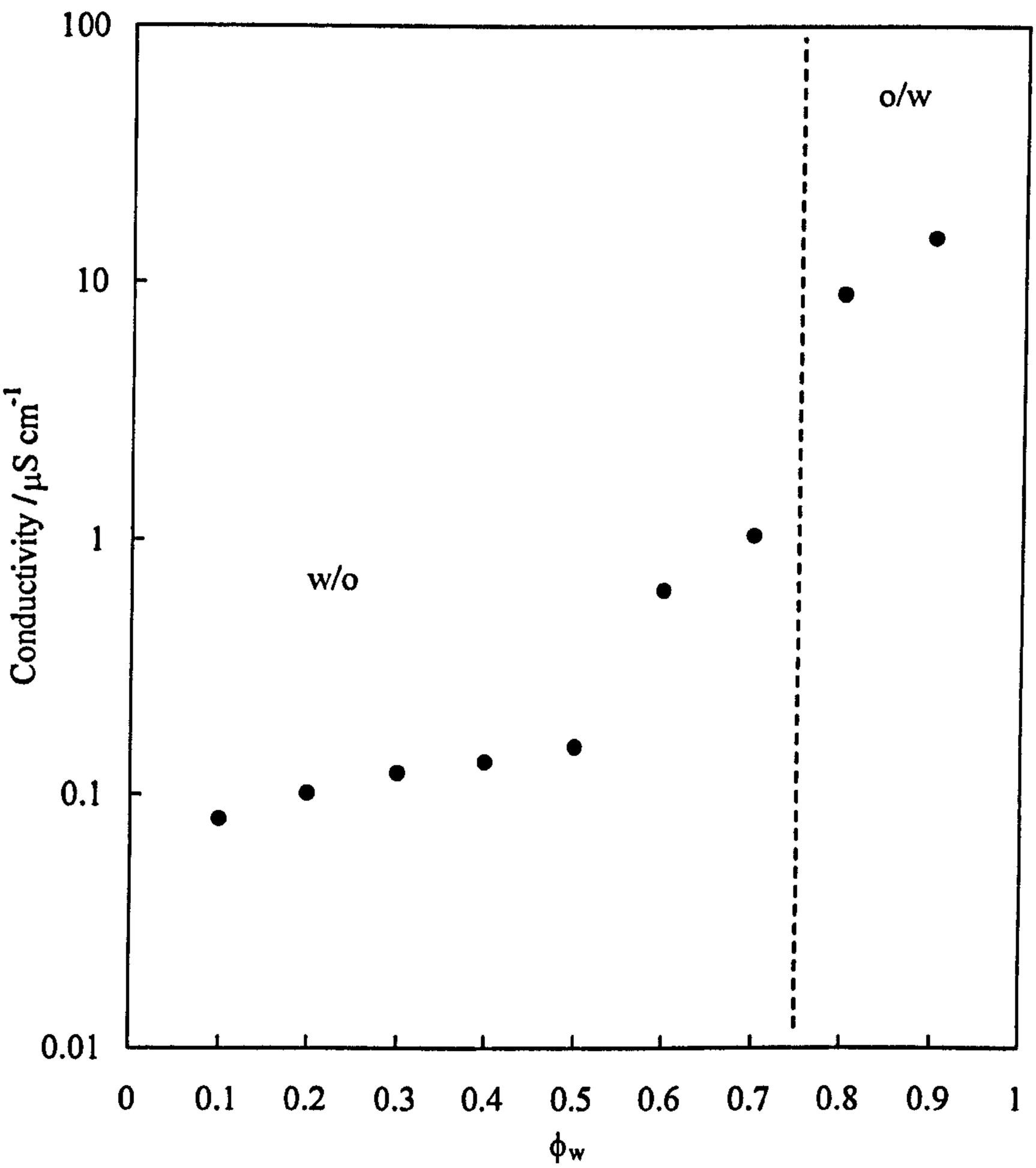

Figure 7.18 **SEM images of toluene-water emulsions stabilised by 1 wt% 47% SiOH for a) $\phi_w = 0.3$ (w/o), b) $\phi_w = 0.5$ (w/o), c) $\phi_w = 0.7$ (inversion point) and d) $\phi_w = 0.9$ (o/w).**

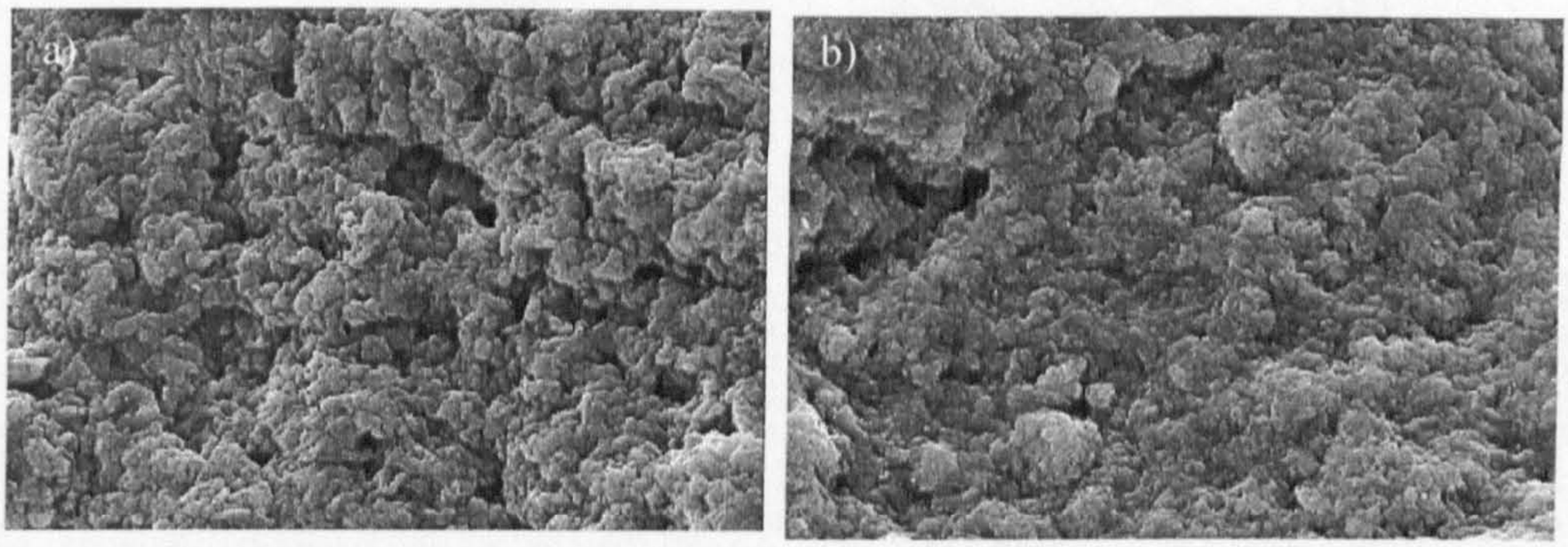

System	Emulsion type	d[a] (drop)/μm	d (pore)/μm
1 wt% 76% SiOH, MCH	o/w (0.1)[b]	18.5	17.55
1 wt% 76% SiOH, MCH	o/w (0.2)	22.3	20.23
1 wt% 76% SiOH, MCH	o/w (0.6)	100.3	87.36
1wt% 76 % SiOH, decane	o/w (0.1)	32.1	16.00
1wt% 76 % SiOH, dodecane	o/w (0.1)	31.6	13.16
4wt% 76 % SiOH, decane	o/w (0.1)	13.1	10.91
4wt% 76 % SiOH, dodecane	o/w (0.1)	14.9	10.55
1wt% 76 % SiOH, heptane	o/w (0.1)	33.7	18.73
2wt% 76 % SiOH, MCH	o/w (0.1)	16.5	14.22
4wt% 76 % SiOH, MCH	o/w (0.1)	14.2	8.42
1 wt% 47 % SiOH, perfluoropentane	w/o (0.1)	8.6	8.21
1 wt% 47 % SiOH, perfluoroheptane	w/o (0.1)	6.0	4.86
4 wt% 47 % SiOH, hexane	w/o (0.1)	13.8	11.73
4wt% 47 % SiOH, HMDS	w/o (0.1)	9.3	9.6

Table 7.3 **Comparison between drop size of particle-stabilised emulsions and pore size from microporous structures obtained after evaporation of the previous emulsions. a = volume mean diameter measured by the Mastersizer (o/w) and optical microscope (w/o). b = Number in brackets refers to dispersed phase volume fraction.**

In order to understand better the relation between the oil used in the emulsions and the type of microstructure of the solid residue obtained, Table 7.3 summarises the average drop size of the initial emulsions and the mean pore size of the microstructure (only the porous ones) left behind after the evaporation of the previous respective

emulsions. The mean pore size was determined as the arithmetical mean of 15 pores taken randomly. With some exceptions, both mean sizes are very similar with generally the mean pore size being slightly smaller than the mean drop size. As mentioned above, this may be due to the shrinkage of the pores while the oils evaporate. In case of the emulsions containing oils of low volatility (decane, dodecane) the mean pore size is much smaller that the initial drop size. This is maybe because pores containing highly volatile oils (such as methylcyclohexane) stop shrinking at an earlier stage of the evaporation process as compared with pores containing low-volatility oils where the process of pore shrinking continues for longer as the oil loss also takes longer.

7.4.6 Monodisperse porous silica materials

Finally, we have tried to make macroporous materials with uniform pore sizes from monodisperse emulsions. Only two ways of making monodisperse solid-stabilised emulsions have been reported in the literature[12,13]. The monodisperse emulsions shown in the present work have been made following the experimental protocol explained in ref. (13). Starting from an 10 vol% methylcyclohexane-in-water emulsion stabilised by 4 wt% 76 % SiOH (emulsified at 13,000 rpm for 2 minutes), oil was then added sequentially (from $\phi_o = 0.1$ to $\phi_o = 0.6$ in 6 steps), rehomogenizing for 30 s after each addition. Figure 7.19 shows the average drop diameter and the span of the distribution of a set of emulsions as a function of the oil volume fraction.

Figure 7.19 **Mean drop average diameter d, and span, of methylcyclohexane-in-water emulsions stabilised by 4 wt% silica particles (76 % SiOH) where the oil volume fraction was increased progressively.**

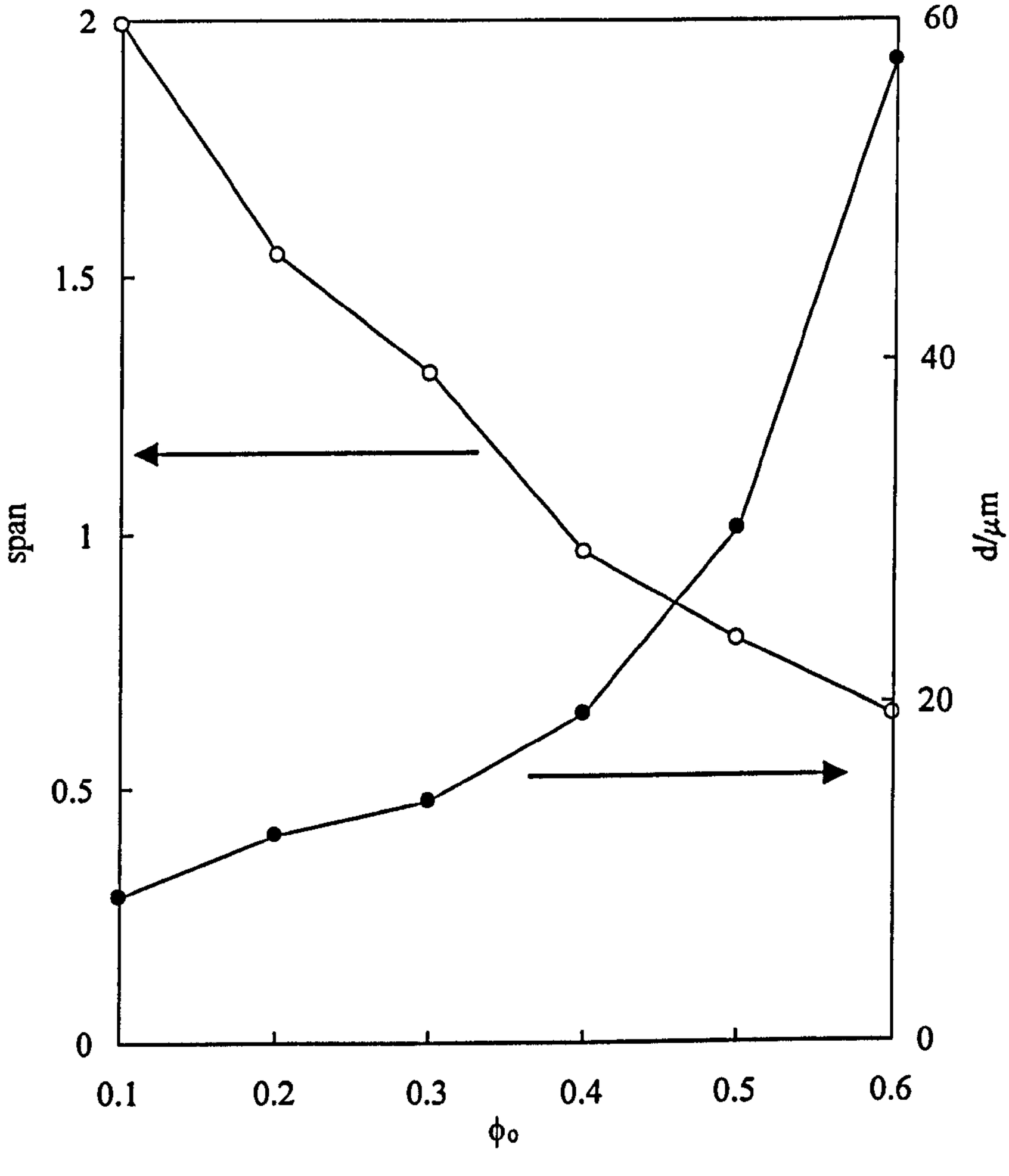

The span of a distribution is calculated from the percentiles using[14]

$$\text{Span} = \frac{d[v,0.5] - d[v0.1]}{d[v,0.5]} \qquad [7.1]$$

where d[v,p] is the volume average diameter at fraction p and thus, the span gives a measure of the width of the volume distribution relative to the median diameter, d[v,0.5]. The drop diameter (filled points) increases gradually from 8.62 to 57 μm with an associated decrease in the span (open points) from two to around 0.6. The mechanism responsible for such behaviour is not very well understood. Figure 7.20a-b show SEM images of another set of emulsions stabilised by 4 wt% 76 % SiOH and containing 60 vol% methylcyclohexane which was added a) in one step, previous to the emulsification and b) adding a known volume of oil stepwise and rehomogenizing between any two steps. Although the "monodispersity" in this case is not particularly good, it is clear that the pore size distribution is narrower in b) than in a) and the pore walls look stiffer.

Figure 7.20 SEM images of the solid residues obtained after the evaporation of 60 vol% methylcyclohexane-in-water emulsions stabilised by 4 wt% 76 % SiOH. a) Preparing the final emulsion in one step and b) preparing the emulsion adding the oil stepwise and rehomogenizing between any two steps. The white circle shows (to scale) the average drop size of the parent emulsion.

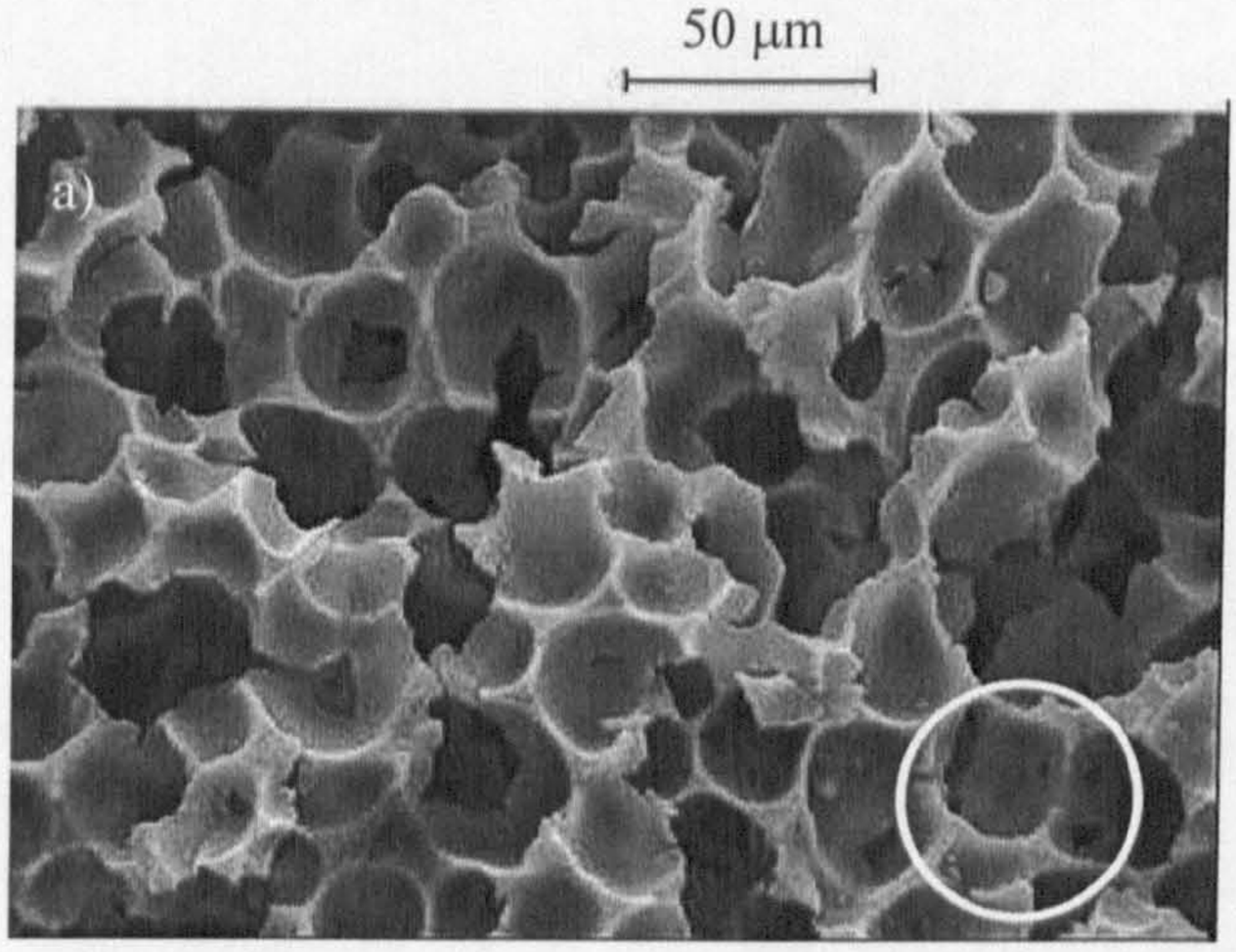

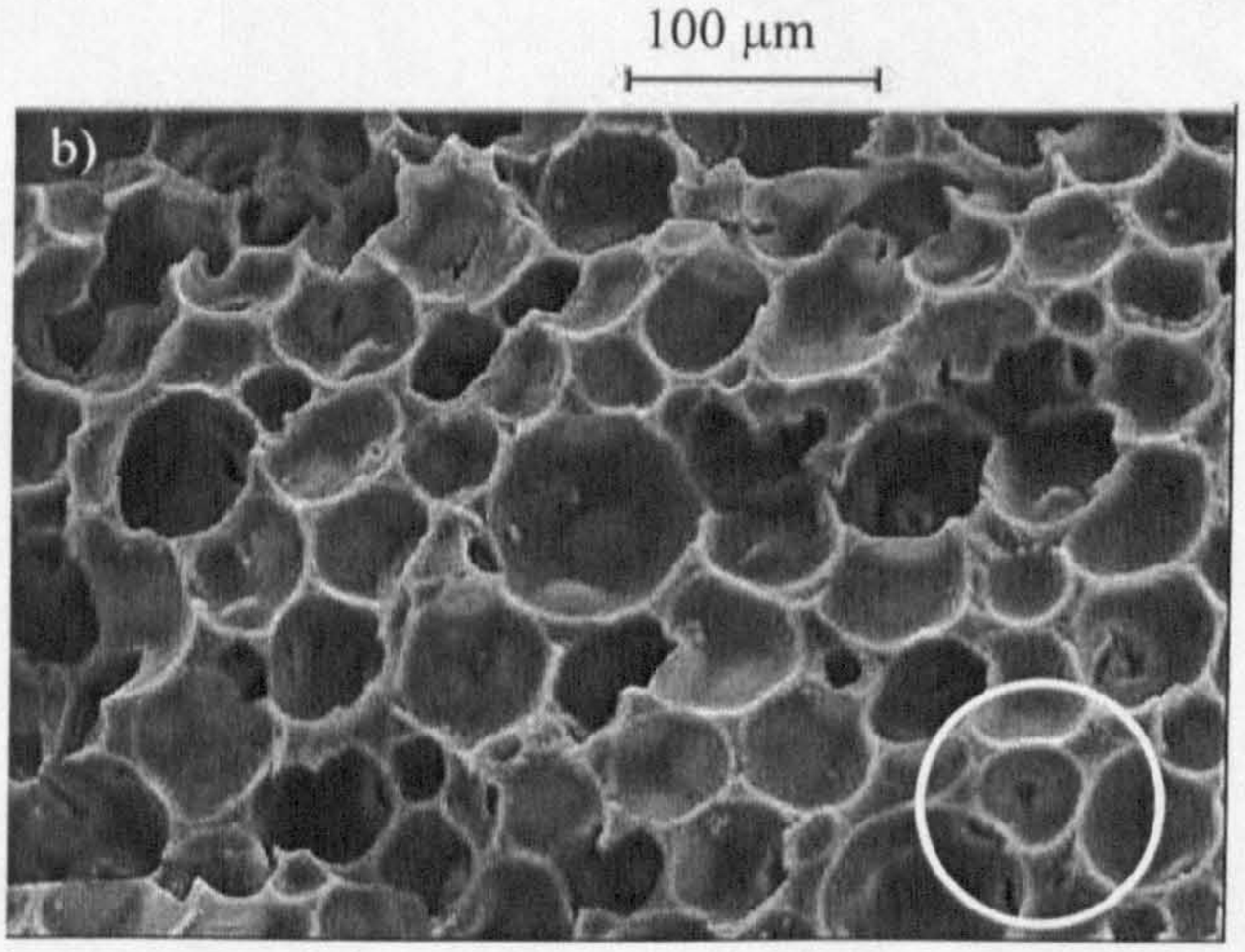

7.5 Conclusions

- Evaporation rates of aqueous particle dispersions are the same as that of pure water.
- Mass loss plots of solid-stabilised o/w creamed emulsions show a curve with virtually constant gradient in comparison with the two-stage decay of surfactant-stabilised emulsions under the same conditions. In Pickering emulsions, the dispersed oil mass loss rate seems to be further retarded relative to surfactant-stabilised emulsions. This is probably due to the high attachment energy and high steric repulsion associated with the particles.
- Solid residues left after evaporation of o/w emulsions containing volatile oils (relative to water) show a "knobbly" microstructure. When oils with similar or lower vapour pressure to that of water were used, "sponge-like" structures were obtained.
- For emulsions containing volatile oils, the mean drop diameter is similar to the mean pore diameter, whereas when oils with low vapour pressure are used, the pores are much smaller.
- After evaporation from monodisperse emulsions, reasonably monodisperse porous structures may be obtained.
- 50 vol% toluene/water emulsions stabilised by silica particles invert from o/w to w/o and vice versa when the Si-OH content at the particle surface is 47 % (transitional inversion).
- Toluene/water emulsions stabilised by 47 % Si-OH silica particles invert from o/w to w/o and vice versa when $\phi_w = 0.7$.

7.6 References

1 A. Imhof and D.J. Pine, *Nature*, 1997, **389**, 948.

2 A. Imhof and D.J. Pine, *Adv. Mater.*, 1998, **10**, 697.

3 C. E. Mc Namee, G.T. Barnes, I.R. Gentle, J.B. Peng, R. Steitz and R. Probet, *J. Colloid Interface Sci.*, 1998, **207**, 258.

4 P. C. Schultz, R.M. Minardi, M.E. Gshaider de Ferrera and B. Vuano, *Colloid Polym. Sci.*, 1998, **276**, 92.

5 K. J. Beverley, J. H. Clint and P. D. I. Fletcher, *Phys. Chem. Chem. Phys.*, 2000, **2**, 4173.

6 C. del Cerro and G.J. Jameson, *J. Colloid Interface Sci.*, 1970, **34**, 473.

7 B. P. Binks, *Adv. Mater.*, 2002, **14**, 1824.

8 B. P. Binks and M. Kirkland, *Phys. Chem. Chem. Phys.*, 2002, **4**, 3727.

9 J. Salager in *Encyclopedia of Emulsion Technology*, Ed. P. Becher, Marcel Decker, New York, 1988, Vol. 3, p 79.

10 B. P. Binks and S. O. Lumsdon, *Langmuir*, 2000, **16**, 8622.

11 B. P. Binks and S. O. Lumsdon, *Langmuir*, 2000, **16**, 2539.

12 J. Giermanska-Kahn, V. Schmitt, B. P. Binks and F. Leal-Calderon, *Langmuir*, 2002, **18**, 2515.

13 B. P. Binks and J. A. Rodrigues, *Langmuir*, 2003, **12**, 4905.

14 See for example Malvern Manual or www.Malvern.co.uk

Chapter 8

CHAPTER 8

SUMMARY OF THE MAIN CONCLUSIONS AND FUTURE WORK

8.1 Summary of the main conclusions

In this thesis evaporation rates from emulsions stabilised by surfactants and nanometer size particles have been studied. Moreover, we have found that the solid residues left behind after the evaporation of the latter emulsions show macroporous structure depending on the properties of the initial emulsions.

A gravimetric technique has been used to study the evaporation rates of simple liquids and emulsions. We have proposed different models to understand the evaporation mechanisms of different type of emulsions including creamed emulsions, gelled emulsions and HIPEs. For pure liquids, we have verified that diffusion of the vapour through the stagnant layer of gas above the sample is the rate limiting step and we have determined the diffusion coefficients of water and organic solvents in the vapour phase.

In creamed o/w emulsions stabilised by surfactants we showed that the evaporation rate of the continuous aqueous phase is the same as that of bulk water. The

evaporation rate of the oil dispersed phase is retarded up to 20 times if compared to that of bulk oil. The retardation factor depends, among other parameters, on the solubility of the oil in water. Therefore we can conclude that the oil transport from the emulsion to the vapour phase occurs by diffusion through the thin asymmetric oil-water-air film present at the emulsion surface.

In emulsions gelled by thickening agents like polymers or colloidal particles, we have shown that the evaporation rate of the aqueous continuous phase does not depend on the concentration of the thickening agents. In contrast, the evaporation of the dispersed oil phase does depend on the polymer type. Emulsions containing volatile oils and gelled by κ-carrageenan show similar mass loss rates to that of bulk water. Emulsions containing involatile oils and gelled by Veegum and Avicel also show the same mass loss rate to that of pure water. Emulsions containing involatile oils and gelled by Kelzan, show a retardation of the evaporation rate of water which is due to the formation of an oil layer at the surface.

In high internal phase emulsions (HIPEs) containing dispersed involatile oils, three major cases have been studied. When the thickness of the stagnant layer above the emulsion sample is relatively large compared to the thickness of the sample, the evaporation rate is controlled by the diffusion of the liquid in the vapour. When the sample height is small compared to the stagnant layer thickness, the evaporation rate of the continuous phase is controlled by the diffusion of such phase in the nm size thin-film network formed as the oil drops get closer. In both cases all water is lost.

presence of salt in the emulsion triggers coalescence and a macroscopic oil layer is observed on the top of the sample. As the salt concentration is increased, the formation of the oil layer happens at earlier stages inhibiting a further mass loss of the sample.

In emulsions stabilised by solid particles, the mass loss curve shows a simple curve with constant gradient. This gradient is less steep than that shown in the mass loss rate curves of emulsions stabilised by surfactants. The large steric repulsions which are present in Pickering emulsions and the high attachment energy of the particles to the o-w interface may act to slow down the evaporation of the oil drops. In addition, the solid residues left behind after the evaporation of emulsions stabilised by nm-size silica particles show a range of different types of microstructures. Depending on the conditions under which the emulsions were prepared, i.e., oil type, particle type, etc., the solids may show macroporous structures with pore size distribution similar to the initial emulsion drop size distribution.

8.2 Future work

In addition to the work discussed in this thesis, some possible further work is suggested:

In many applications involving fragrance release, evaporation of the volatile components occur rapidly resulting in time dependent changes in the vapour composition, and hence perceived odour as evaporation proceeds. In order to engineer a system in

which the vapour composition remains constant ("the first smell is the same as the last") it is necessary that the rate-limiting step of evaporation does not involve the vapour pressures of the volatile components. A possible strategy to achieve this is to prepare emulsion drops containing mixtures of the volatile species which are immobilised within a gelled continuous phase. Emulsions may be gelled using suitable polymers (see Chapter 5) and the variation of the vapour composition during the course of the evaporation could be assessed by GLC.

Moreover, it is of interest to know the last localization of involatile species after the evaporation of the volatile liquids from an emulsion. Observing SEM, optical and fluorescence microscope images of solid residues obtained from Pickering emulsions containing oil-soluble (in o/w emulsions) and water-soluble (in w/o emulsions) dyes (fluorescent) would probably show the preferred location of the dyes after the complete evaporation of such emulsions.

Appendices

Appendix I

Tables of experimental results

This section contains the data used to produce some of the figures contained in this thesis. The results are tabulated according to the figure number which is referred to within the Chapter.

AI.1 Data from Chapter 2

Table A2.6 Calibration data of measured gas flow rate versus flow meter reading for flowmeters 1 and 2.

Flowmeter 1

Flow rates/ units	Flow rate/dm^3 min^{-1}
0	0
2.5	0.659
3	0.821
4	1.068
5	1.267
6	1.483
7	1.760
8	1.974
9	2.172

Flowmeter 2

Flow rates/ units	Flow rate/dm^3 min^{-1}
0	0
1.4	1.470
2	2.059
3	3.170
4.5	4.389
6	5.764

AI.2 Data from Chapter 4

Table A4.12 Variation of the oil evaporation factor f with X for o/w emulsions stabilised by DBG, CTAB and SDS.

CTAB		DBG		SDS	
X	f	X	f	X	f
177.224	0.99	384.48	1.03	112.43	0.93
5.017	0.587	1.096	0.52	2.907	0.54
0.509	0.34	1.017	0.65	0.298	0.26
0.137	0.1506	0.245	0.113	0.145	0.08
0.074	0.071	6.031	0.93	0.188	0.158
0.068	0.0625	0.709	0.56	0.263	0.179
2.421	0.6			0.351	0.298
0.311	0.233			0.142	0.0599
154.034	0.86			0.331	0.3847
				0.068	0.0776
				1.357	0.58
				0.180	0.1
				116.38	0.9515
				90.067	0.96

Table A4.14 Variation of the oil evaporation factor f with X/(h/d) for o/w emulsions stabilised by low and high Mw PVA

Low Mw PVA		High Mw PVA	
X/(h/d)	f	X/(h/d)	f
8.62×10^{-6}	0.19	4.84×10^{-4}	0.75
1.91×10^{-6}	0.062	1.78×10^{-5}	0.15
5.88×10^{-4}	0.79	1.64×10^{-6}	0.0001
5.25×10^{-4}	0.71	1.62×10^{-6}	0.02
1.77×10^{-5}	0.24	8.65×10^{-6}	0.11
5.25×10^{-4}	0.8	6.00×10^{-4}	0.8
1.86×10^{-5}	0.21	6.00×10^{-4}	0.82
8.62×10^{-6}	0.19	1.62×10^{-6}	0.029

Table A4.16 Cube of the volume average drop diameter versus time for 20 vol% o/w emulsions containing either toluene or heptane and stabilised by 20 mM SDS.

toluene		heptane	
t/h	**$d^3/\mu m^3$**	**t/h**	**$d^3/\mu m^3$**
1.00	274	0.00	187
9.00	1083	1.16	115
23.00	4012	20.00	234
31.75	7100	24.00	781
48.00	16175	29.00	958
55.00	20458	44.50	638
		47.00	783
		68.00	1154

Table A4.19 Variation of f with aqueous phase electrolyte concentration (CTAB + NaBr) for 20 vol% heptane-in-water emulsions stabilised by CTAB (2 mM).

C/mM	f
2	0.177
3	0.160
6	0.217
12	0.238
22	0.277
37	0.280
52	0.281

Table A4.20 Variation of f with h for 20 vol% heptane-in-water emulsions stabilised by 20 mM SDS.

h/mm	f
26.71	0.26
13.04	0.08
16.92	0.158
23.69	0.179
31.64	0.298
12.80	0.0599

AI.3 Data from Chapter 5

Table A5.1 Creaming rates of 20 vol% methylcyclohexane-in-water emulsions stabilised by 20 mM SDS and gelled by κ-carrageenan (concentration in brackets).

t/min	l/cm (0.005 wt%)	l/cm (0.01 wt%)	l/cm (0.1 wt%)	l/cm (0 wt%)	l/cm (1 wt%)
0	0	0	0	0	0.05
1	0.25	0.2	0	0.2	0.05
2	0.45	0.55	0.3	0.4	0.05
3	0.75	0.9	0.6	0.65	0.05
4	1.15	1.25	0.85	0.9	0.05
5	1.51	1.6	1.15	1.175	0.05
6	1.85	1.95	1.45	1.425	0.05
7	2.2	2.3	1.75	1.7	0.05
8	2.475	2.7	2	2	0.05
9	2.8	3	2.25	2.2	0.05
10	3.025	3.3	2.45	2.5	0.05
11	3.25	3.45	2.6	2.7	0.05
12	3.4	3.5	2.7	2.75	0.05
13	3.475	3.5	2.7	2.9	0.05
14	3.5	3.55	2.75	3	0.05
16	3.525	3.6	2.8	3.1	0.05
18	3.55	3.6	2.85	3.175	0.05
20	3.6	3.65	2.9	3.2	0.05
25	3.625	3.7	2.9	3.25	0.05
35	3.7	3.7	2.9	3.3	0.05
45	3.8	3.75	2.95	3.4	0.05
55	3.85	3.8	3	3.475	0.05
65	3.9	3.9	3	3.575	0.05
69	3.9	3.9	3	3.6	0.05

A5.2 Creaming rates of 20 vol% toluene-in-water emulsions stabilised by 20 mM SDS and gelled by κ–carrageenan (concentration in brackets).

t/min	l/cm (0 wt%)	t/min	l/cm (0.01 wt%)	t/min	l/cm (1 wt%)
0	0	0	0	0	0.06
2	0	1	0.2	1	0.06
3	0.2	2	0.6	2	0.06
4.5	0.35	3	0.9	3	0.06
6	0.5	4	1.3	4	0.06
7.5	0.7	5	1.6	5	0.06
9	0.9	6	2	6	0.06
11	1.05	7	2.4	7	0.06
12	1.18	8.5	2.8	8.5	0.06
13	1.3	10	3.1	10.8	0.06
14	1.38	11.5	3.25	11.5	0.06
15.5	1.5	13	3.35	13	0.06
17	1.6	15	3.4	15	0.06
19	1.7	18	3.45	18	0.06
21	1.8	19.5	3.5	19.5	0.06
23	1.8	22	3.5	25	0.06
24	1.8	26	3.5	27	0.06
26.5	1.85	30	3.5	30	0.06
29	1.85				
30	1.85				

Table A5.5 Comparison of creaming rates of 20 vol% MCH-in-water emulsions stabilised by 20 mM SDS and gelled by 0.5 wt% of κ- and λ-carrageenan.

κ-carrageenan		λ-carrageenan	
t/min	l/cm	t/min	l/cm
0	0	0	0
0.5	0	1	0.25
1	0.3	2	0.6
1.5	0.4	3	0.9
2	0.5	4	1.25
3	0.6	5	1.5
3.5	0.7	6	1.75
4	0.8	8	2.1

4.5	0.9	10.5	2.4
5	1	13	2.6
5.5	1.1	14.5	2.65
6	1.2	16	2.67
6.5	1.35	18	2.7
7	1.45	20	2.77
7.5	1.6	22	2.8
8	1.7	24	2.8
8.5	1.75	27	2.8
9	1.85	31	2.85
9.5	1.95	34.5	2.9
10	2	37	2.9
10.5	2.15	40	2.9
11	2.2		
11.5	2.3		
12	2.35		
12.5	2.45		
13	2.5		
14	2.65		
15	2.75		
16	2.85		
17	2.95		
18	3.05		
19	3.1		
20	3.15		
21	3.15		
22	3.2		
23	3.25		
24	3.28		
25	3.3		
26	3.3		
27	3.35		
29	3.4		
30	3.4		
32	3.45		
35	3.5		
37.5	3.5		
40	3.5		

Table A5.6 Creaming rates of 20vol % methylcyclohexane-in-water emulsions stabilised by 20 mM SDS and gelled by Kelzan.

[Kelzan] = 1 wt%		Kelzan] = 0	
t/min	**l/cm**	**t/min**	**l/cm**
0	0	0	0
2	0	1	0.3
4	0	2	0.6
6	0	3	0.85
8	0	4	1.1
10	0	5	1.4
13	0	6	1.7
17	0	7	1.95
20	0	9	2.25
22	0	10	2.35
25	0	11	2.4
30	0	12	2.45
33	0	13	2.45
35	0	17	2.5
39	0	20	2.5
42	0	25	2.5
45	0	30	2.5
50	0	40	2.5
55	0	50	2.5
60	0	60	2.5

Table A5.7 Creaming rates of 20 vol% methylcyclohexane-in-water emulsions stabilised by 20 mM SDS and gelled by Veegum.

[V] = 0 wt%		[V] = 1 wt%		[V] = 2 wt%		[V] = 1.5 wt%	
t/min	**l/ cm**	**t/min**	**l/ cm**	**t/min**	**l/ cm**	**t/min**	**l/ cm**
0	0	0	0	0	0	0	0
1	0.3	3	0.5			3	0.5
2	0.6	4	0.8	2.5	0.04	5	0.8
3	0.85	5	1.2	5	0.07	6.5	1.2
4	1.1	6.5	1.6	8	0.07	8	1.5
5	1.4	8	2	12	0.07	10	2
6	1.7	9	2.3	15	0.07	12.5	2.7
7	1.95	10.5	2.4	20	0.07	15	2.8
9	2.25	12	2.5	25	0.07	20	2.85
10	2.35	13.5	2.6	28	0.07	25	2.85
11	2.4	17	2.6	30	0.07	30	2.85
12	2.45	19	2.6	35	0.07	35	2.85
13	2.45	22	2.6	40	0.07	40	2.85
17	2.5	25	2.6	45	0.07	45	2.85
20	2.5	30	2.6	50	0.07	50	2.85
25	2.5	35	2.6	55	0.07	60	2.85
30	2.5	40	2.6	60	0.07		
40	2.5	45	2.6				
50	2.5	50	2.6				
60	2.5	60	2.6				

Table A5.8 Creaming rates of 20 vol% methylcyclohexane-in-water emulsions stabilised by 20 mM SDS and gelled by Avicel.

[Avicel] = 0		[Avicel] = 1 wt%		[Avicel] = 2.0 wt%	
t/min	**l/cm**	**t/min**	**l/cm**	**t/min**	**l/cm**
0	0	0	0	0	0.08
1.5	0.4	1	0.5	2	0.08
2	0.6	5	2.5	4	0.08
3	1	10	4		0.08
4	1.4	11	4.1	6	0.08
5	1.75	16	4.15	8	0.08
6.5	2.5	21	4.2	10	0.08
8	2.9	25	4.2	13	0.08
9	3.45	27	4.2	15	0.08
12.5	4.3	30	4.2	17	0.08
18	4.5	35	4.2	20	0.08
20	4.5	40	4.2	22	0.08
22	4.5	45	4.2	25	0.08
25	4.5	50	4.2	28	0.08
30	4.6	55	4.2	31	0.08
35	4.6	60	4.2	35	0.08
40	4.6			40	0.08
45	4.6			45	0.08
50	4.6			50	0.08
60	4.6			60	0.08

AI.4 Data from Chapter 6

Table A6.2 Conductivity of PDMS-water emulsions stabilised by 20 mM SDS as a function of oil volume fraction at 25 °C.

ϕ_o	κ/ μS cm^{-1}
0.8	80
0.85	70.1
0.9	68
0.93	0.57
0.95	0.47

Table A6.4 Effect of salt concentration on the oil volume fraction at inversion of PDMS-water emulsions stabilised by 20 mM SDS.

w/o		o/w	
ϕ_o	[NaBr]/M	ϕ_o	[NaBr]/M
0.7	0.5	0.7	0.25
0.8	0.5	0.8	0.25
0.7	0.4	0.9	0
0.8	0.4	0.6	0.25
0.9	0.25	0.6	0.3
0.6	0.5	0.7	0.3
0.6	0.4	0.8	0.3
0.93	0	0.85	0.3

AI.5 Data from Chapter 7:

Table A6.1 Conductivity of water-toluene emulsions ($\phi_w = 0.5$) stabilised by silica particles of different wettability and initially dispersed in toluene.

$\kappa/\mu S\ cm^{-1}$	%SiOH
0.1	18.3
0	36
0.16	47
0.21	57
0.51	65.7
2.9	67
3.9	71
5.05	79.9
5.12	87

Table A6.2 Conductivity of water-toluene emulsions stabilised by 76 % SiOH silica particles as a function of the volume fraction of water.

$\kappa/\mu S\ cm^{-1}$	ϕ_w
14.2	0.9
8.7	0.8
1.01	0.7
0.61	0.6
0.15	0.5
0.13	0.4
0.12	0.3
0.1	0.2
0.08	0.1

Table A6.3 Drop size distribution and span of the distribution of the methylcyclohexane-in-water emulsion stabilised by 4 wt% 76 % SiOH as a function of the oil volume fraction (added continually).

ϕ_o	span	d/μm
0.1	1.99	8.62
0.2	1.54	12.36
0.3	1.31	14.34
0.4	0.96	19.38
0.5	0.79	30.13
0.6	0.64	57.59

Appendix II

Refractive index and vapour pressure of the liquids

Table AII.1 Refractive index of the liquid used in this work

Liquid	Refractive index @ 20°C
water	1.3330
benzene	1.5011
o-xylene	1.5055
toluene	1.4961
Methylcyclohexane	1.4533
Cyclopentane	1.4065
n-hexane	1.3749
n-heptane	1.3876
n-octane	1.3974
n-decane	1.4097
n-dodecane	1.4195
HMDS	1.3748 (25°C)
PDMS	1.4030
Squalane	1.4990

Tables AII.2 Vapour pressure of some liquids used in this thesis.

from MJ Hunter, EL Warrick, JF Hyde and CC Currie, JACS, 1946, 68, 2284

Open chain dimethyl siloxanes (n times) with trimethyl siloxy end groups

n = 0, 0.65 cSt

temp/°C	VP/Torr	(1/T)/K^{-1}	ln(VP/Torr)
0	8.59	0.003661	2.150599
20	27.8	0.003411	3.325036
40	76.1	0.003193	4.332048
60	186.1	0.003002	5.226284
80	400	0.002832	5.991465
99.5	760	0.002683	6.633318

temp/°C	VP/Torr	VP/Pa
25	36.6548	4886.898

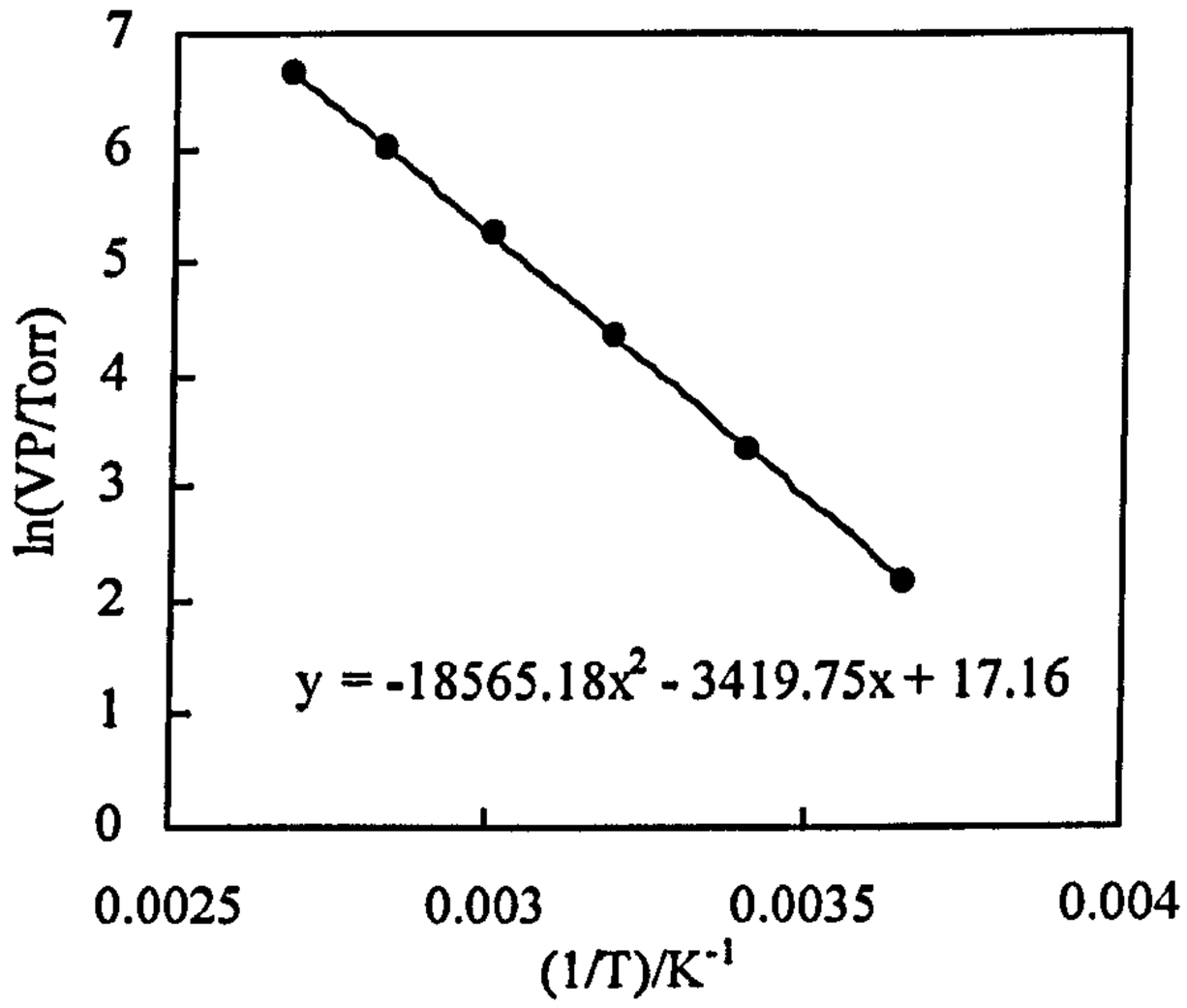

from ref Ind & Eng Chem, 1947, 39, p517

Ethylbenzene

temp/°C	VP/Torr	(1/T)/K^{-1}	ln(VP/Torr)
-9.8	1	0.003797	0.000000
13.9	5	0.003484	1.609438
25.9	10	0.003344	2.302585
38.6	20	0.003208	2.995732
52.8	40	0.003068	3.688879
61.8	60	0.002986	4.094345
74.1	100	0.002880	4.605170
92.7	200	0.002733	5.298317
113.8	400	0.002584	5.991465
136.2	760	0.002443	6.633318

temp/°C	VP/Torr	VP/Pa
25	9.5885	1278.36121

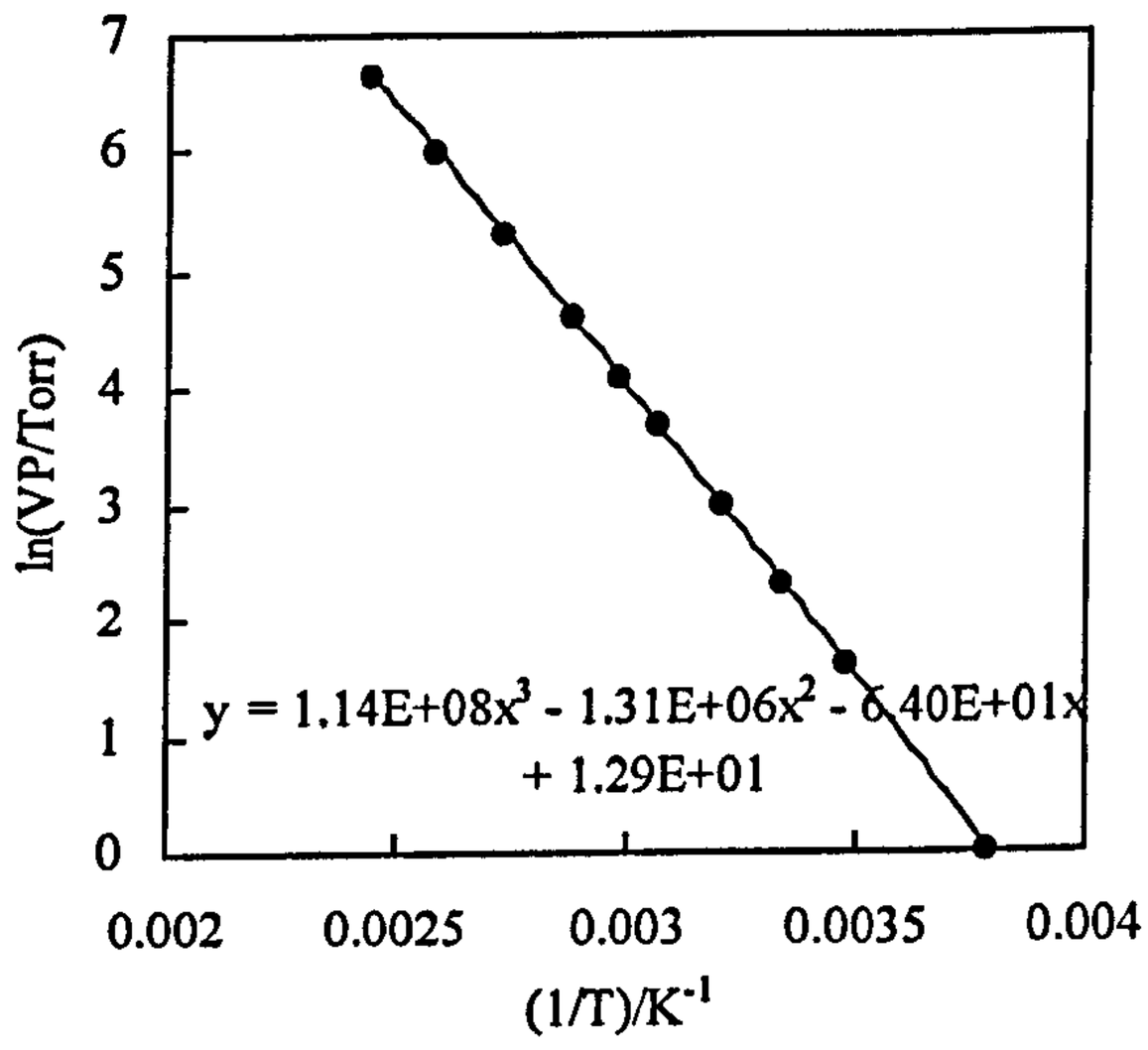

from ref Ind & Eng Chem, 1947, 39, p517

o-Xylene

temp/°C	VP/Torr	(1/T)/K^{-1}	ln(VP/Torr)
-3.8	1	0.003713	0.000000
20.2	5	0.003409	1.609438
32.1	10	0.003276	2.302585
45.1	20	0.003142	2.995732
59.5	40	0.003006	3.688879
68.8	60	0.002924	4.094345
81.3	100	0.002821	4.605170
100.2	200	0.002678	5.298317
121.7	400	0.002533	5.991465
144.4	760	0.002395	6.633318

temp/°C	VP/Torr	VP/Pa
25	6.67604	890.064987

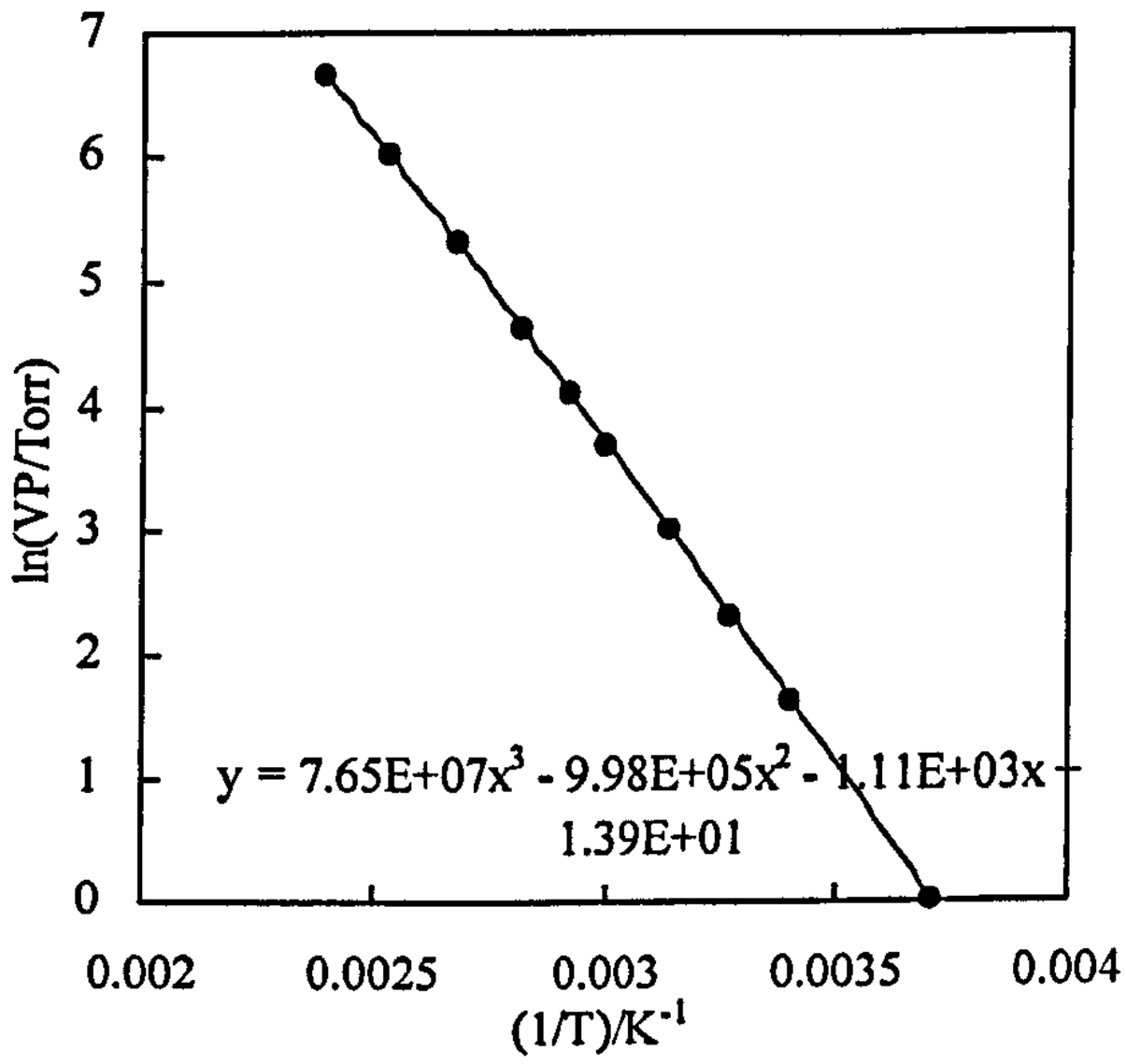

from ref Ind & Eng Chem, 1947, 39, p517

Methylcyclohexane

temp/°C	VP/Torr	(1/T)/K^{-1}	ln(VP/Torr)
-35.9	1	0.004215	0.000000
-14	5	0.003859	1.609438
-3.2	10	0.003704	2.302585
8.7	20	0.003548	2.995732
22	40	0.003388	3.688879
30.5	60	0.003293	4.094345
42.1	100	0.003172	4.605170
59.6	200	0.003005	5.298317
79.6	400	0.002835	5.991465
100.9	760	0.002673	6.633318

temp/°C	VP/Torr	VP/Pa
25	46.1412	6151.649080

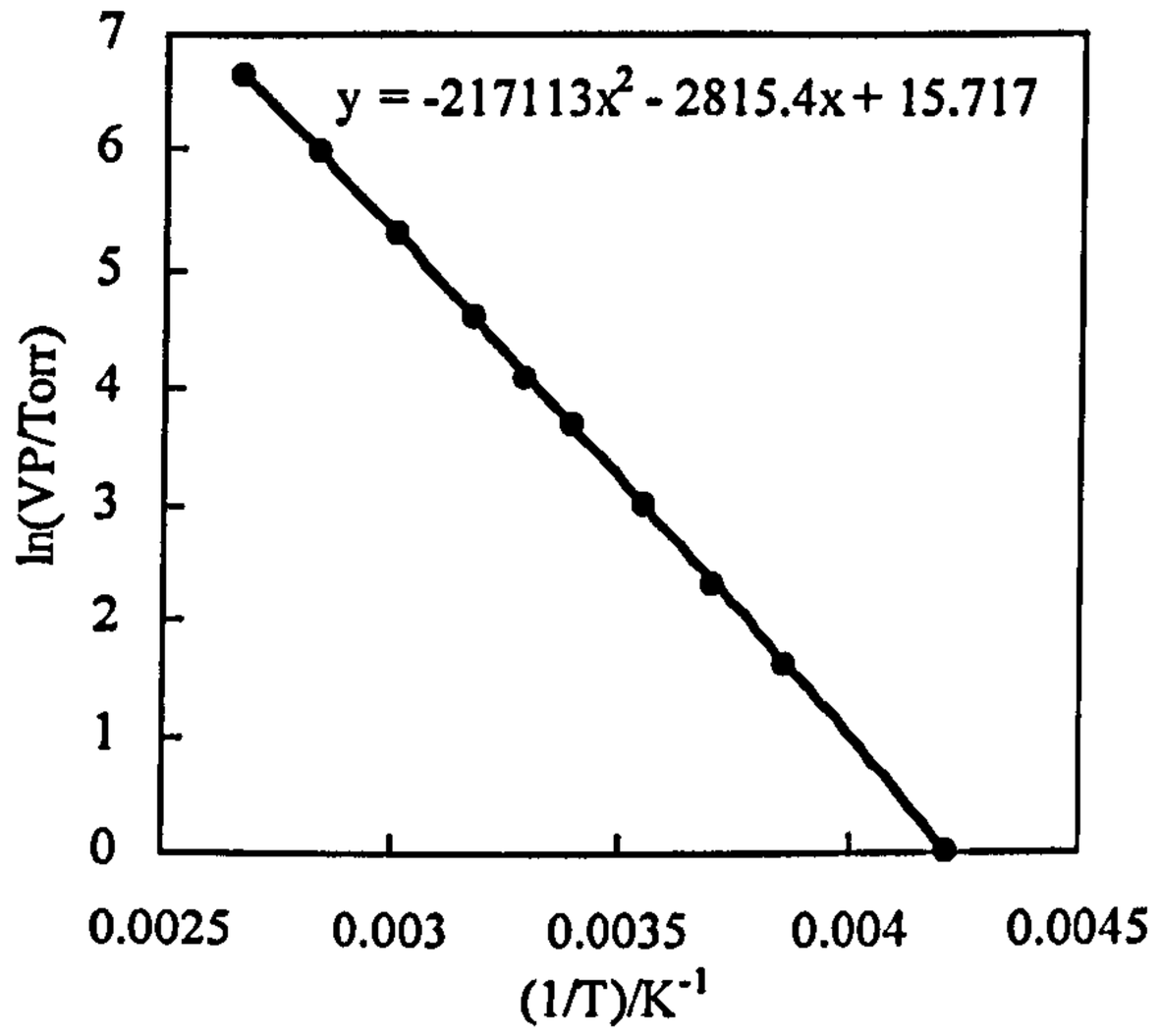

from ref Ind & Eng Chem, 1947, 39, p517

1-Bromobutane

temp/°C	VP/Torr	(1/T)/K^{-1}	ln(VP/Torr)
-33	1	0.004164	0.000000
-11.2	5	0.003818	1.609438
-0.3	10	0.003665	2.302585
11.6	20	0.003512	2.995732
24.8	40	0.003356	3.688879
33.4	60	0.003262	4.094345
44.7	100	0.003146	4.605170
62	200	0.002984	5.298317
81.7	400	0.002818	5.991465
101.6	760	0.002668	6.633318

temp/°C	VP/Torr	VP/Pa
25	40.1743	5356.132399

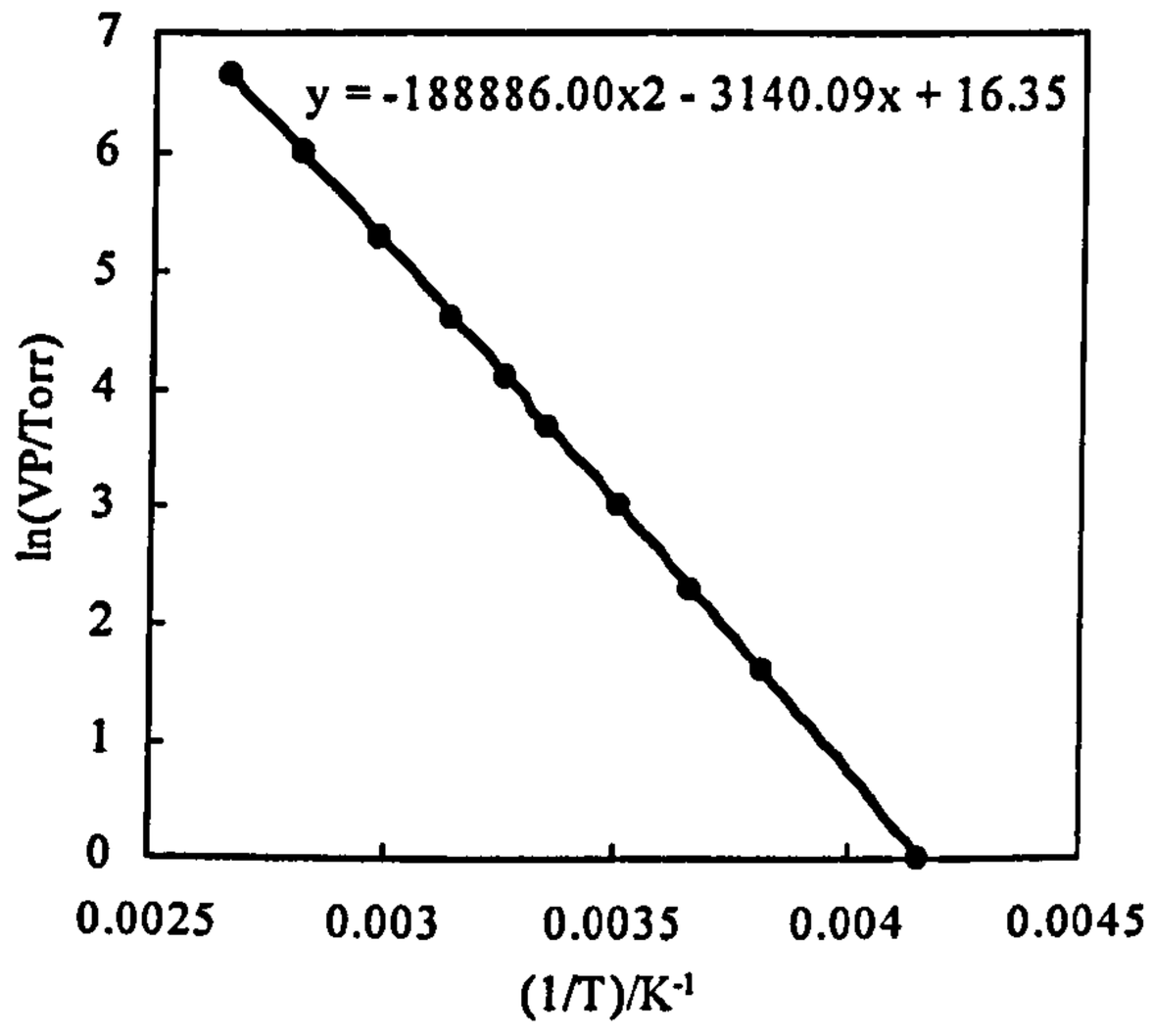

Chlorobenzene

temp/°C	VP/Torr	(1/T)/K^{-1}	ln(VP/Torr)
-13	1	0.003507	0.000000
10.6	5	0.003524	1.609438
22.2	10	0.003386	2.302585
35.5	20	0.003240	2.995732
49.7	40	0.003097	3.688879
58.3	60	0.003017	4.094345
70.7	100	0.002908	4.605170
89.4	200	0.002758	5.298317
110	400	0.002610	5.991465
132.2	760	0.002467	6.633318

temp/°C	VP/Torr	VP/Pa
25	11.6612	1554.701759

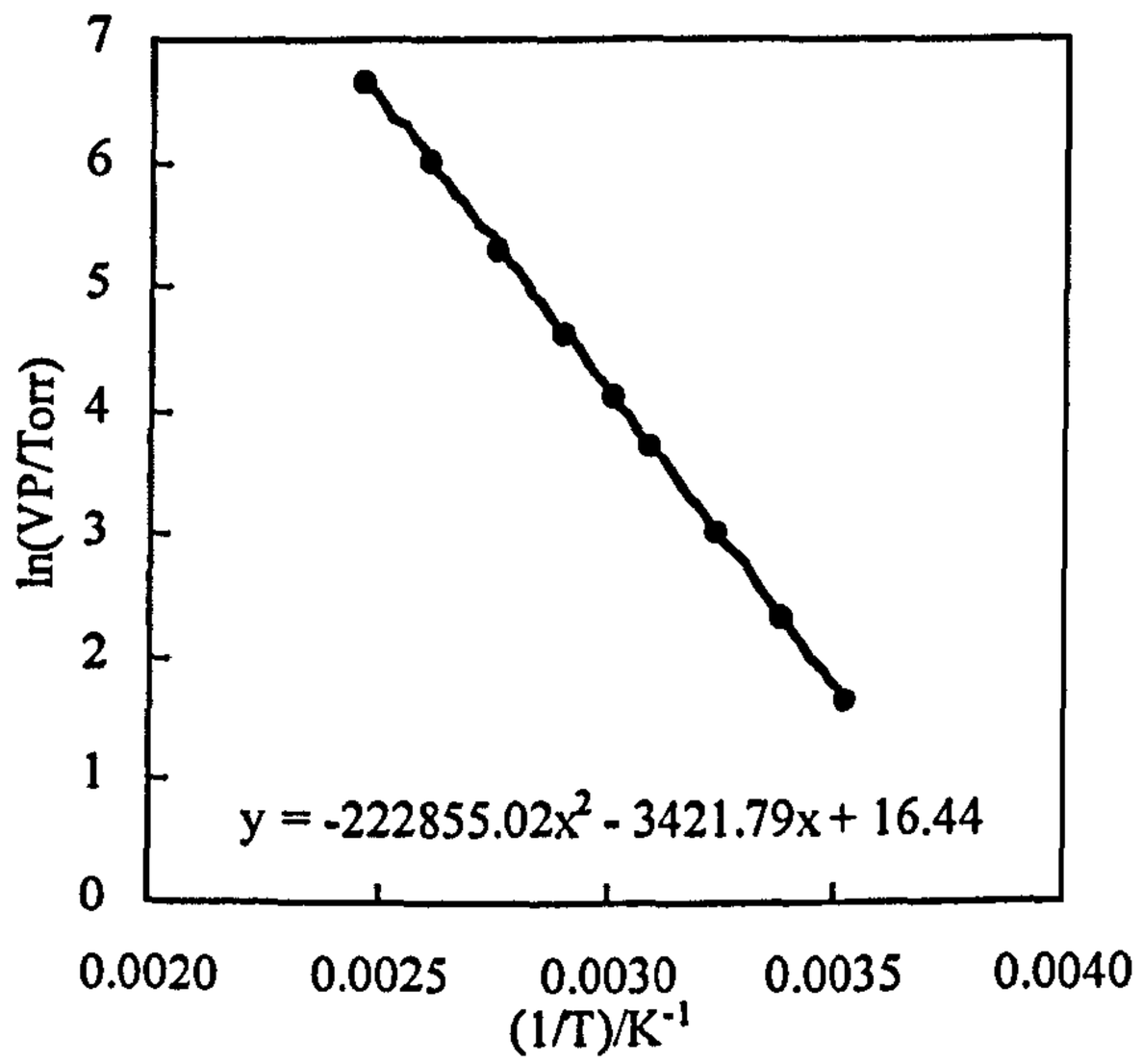

1,2-Dichlorobenzene

temp/°C	VP/Torr	(1/T)/K^{-1}	ln(VP/Torr)
20	1	0.003143	0.000000
46	5	0.003133	1.609438
59.1	10	0.003010	2.302585
73.4	20	0.002886	2.995732
89.4	40	0.002758	3.688879
99.5	60	0.002683	4.094345
112.9	100	0.002590	4.605170
133.4	200	0.002460	5.298317
155.8	400	0.002331	5.991465
179	760	0.002212	6.633318

temp/°C	VP/Torr	VP/Pa
25	4.43976	591.918795

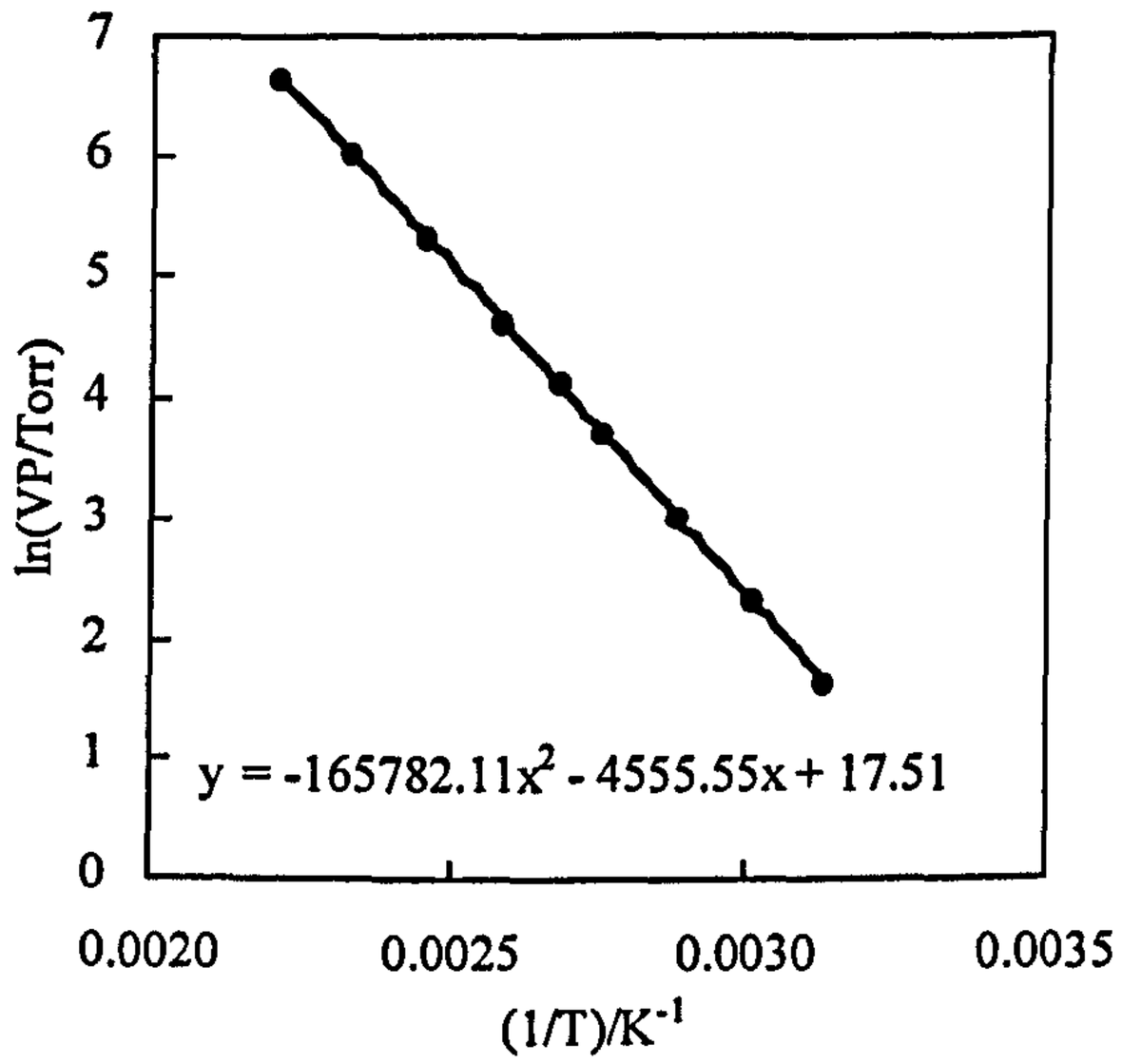

Appendix III

VBA program codes

Appendix III.1 VBA program code enabling the automatic data logging from the Precisa balance using WinWedge.

The EXCEL file used to run the data logging and plotting is PRELOG.xls, which contains the correct VBA module to automatically run Software Wedge.

```
Public Const MyPort$ = "Com2"
Sub getdata()
    Range("a11", "b2000").Value = ""
    Static RowPointer As Long, ColPointer As Long
    RowPointer = 11: ColPointer = 1
    dt = [$C$11]
    time0 = Timer
    timelast = Timer
100 timec = Timer
    STO$ = INKEY$
    If STO$ = Chr$(27) Then GoTo 300
    If (timec - timelast) > dt Then GoTo 200 Else GoTo 100
200 ChannelNum = DDEInitiate("WinWedge", "Com2")
    Application.DDEExecute ChannelNum, "[SENDOUT('P0',13,10)]"
    Application.Wait Now + TimeValue("00:00:01")
    F1 = DDERequest(ChannelNum, "Field(1)")
WedgeData$ = F1(1)
DDETerminate ChannelNum
Sheets("Sheet1").Cells(RowPointer, ColPointer).Formula = (Timer - time0)
Sheets("Sheet1").Cells(RowPointer, ColPointer + 1).Formula = WedgeData$
RowPointer = RowPointer + 1
timelast = Timer
GoTo 100
```

```
300 RowPointer = 11
    ColPointer = 1
End Sub

Sub Auto_Open()
    Toolbars("Standard").Visible = False
    Toolbars("Formatting").Visible = False
    On Error GoTo ErrorHandler
    AppActivate "Software Wedge-" + MyPort$
    On Error GoTo 0
    AppActivate Application.Caption
    Exit Sub
ErrorHandler:
    RetVal = Shell("C:\WINWEDGE\WINWEDGE.EXE
C:\WINWEDGE\Precisa.SW1", 4)
    If RetVal = 0 Then
    Beep
    MsgBox ("Cannot find WinWedge.Exe")
    Exit Sub
    Else
    Application.Wait Now + 0.00002
    End If
    Resume Next
End Sub

Sub Auto_Close()
    Toolbars("Standard").Visible = True
    Toolbars("Formatting").Visible = True
    On Error Resume Next
    chan = DDEInitiate("WinWedge", MyPort$)
    DDEExecute chan, "[Appexit]"
End Sub
```

Appendix III.2 VBA program code used to fit mass loss curves for creamed o/w emulsion samples.

```
Function tmcalc(m, f, ro, rmo, difo, po, zo, moi, rw, rmw, difw, pw, zw, mwi)
A = [c6]
ht = [d6]
R = [a6]
T = [b6]
m = m / 1000
alpha = rmw * difw * pw * zw
beta = rmo * difo * po * zo * f
mo = moi + ((beta * m) / (alpha + beta))
mw = mwi + m - ((beta * m) / (alpha + beta))
b = (R * T) / (A ^ 2 * (alpha + beta))
c = moi / ro
d = beta / (2 * ro * (alpha + beta))
e = mwi / rw
j = 1 / (2 * rw)
g = beta / (2 * rw * (alpha + beta))
h = A * ht
i = (R * T) / (alpha * rw * A ^ 2)
x = -(moi * (alpha + beta)) / (beta)
tc = (b * x) * (c + (d * x) + e + (j * x) - (g * x) - h)

'calculates the time taken for emulsion to lose m when oil is present
If mo < 1E-23 Then GoTo 100
tmcalc = (b * m) * (c + (d * m) + e + (j * m) - (g * m) - h)
GoTo 500

'calculates the time taken for emulsion to lose m when oil has been depleted
100 tmcalc = i * ((m * moi) + (m * mwi) + (m ^ 2 / 2) - (m * ht * rw * A) - (x * moi) -
(x * mwi) - (x ^ 2 / 2) + (x * ht * rw * A)) + tc
500 End Function
```

AppendixIII.3 VBA program code used to fit mass loss curves for layered systems.

```
Function tmcalc(m, f, ro, rmo, difo, po, zo, moi, rw, rmw, difw, pw, zw, mwi)
A = [c6]
ht = [d6]
R = [a6]
T = [b6]
m = m / 1000
alpha = rmw * difw * pw * zw
beta = rmo * difo * po * zo * f
mo = moi + ((beta * m) / (alpha + beta))
mw = mwi + m - ((beta * m) / (alpha + beta))
b = (R * T) / (A ^ 2 * (alpha + beta))
c = moi / ro
d = beta / (2 * ro * (alpha + beta))
e = mwi / rw
j = 1 / (2 * rw)
g = beta / (2 * rw * (alpha + beta))
h = A * ht
i = (R * T) / (alpha * rw * A ^ 2)
x = -(moi * (alpha + beta)) / (beta)
tc = (b * x) * (c + (d * x) + e + (j * x) - (g * x) - h)

'calculates the time taken for emulsion to lose m when oil is present
If mo < 1E-23 Then GoTo 100
tmcalc = (b * m) * (c + (d * m) + e + (j * m) - (g * m) - h)
GoTo 500

'calculates the time taken for emulsion to lose m when oil has been depleted
100 tmcalc = i * ((m * moi) + (m * mwi) + (m ^ 2 / 2) - (m * ht * rw * A) - (x * moi) -
(x * mwi) - (x ^ 2 / 2) + (x * ht * rw * A)) + tc
500 End Function
```

Appendix IV

Configuring a Precisa 125 Balance to a 486 PC using Software WinWedge with Excel to log and plot mass versus time curves.

Cable requirements

In order to connect the balance and the computer it is necessary to have a cable (25 pin female to 25 pin male) connected from COM2 port to the PC to the RS232 connector of the balance. The pins used in cable connections are shown in the following table:

Male pin number (balance)	Female pin number (PC)
2	3
3	2
6	20
7	7

Balance settings

balance unit	Unit1g
calibration	cal ext
Baud rate	9600 bdr
parity	PAr odd
Print	Print UST
combined print function	Prt-ALL on
delayed printout	Prt-dEL off
Good laboratory practise	Glp-off
last digit	LASt d on
Auto zero	A-Zero oFF
Date setting	SEt D+T

Anti-theft coding	SetPrO TEC
Auto standby mode	A-Stby off
Menu latch	Latch off
Status point	StAtUS Prt